The Formation of Molecular Hydrogen in the Interstellar Medium

FARAHJABEEN ISLAM

Thesis submitted for the degree of Doctor of Philosophy

University College London

2009

I, Farahjabeen Islam, confirm that the work presented in this thesis is my own. Where information has been derived from other sources, I confirm that this has been indicated in the thesis.

For my family and for Ben

Abstract

H_2 is the most abundant molecule in the interstellar medium and forms on the surface of interstellar dust grains. Laboratory studies have been conducted of HD formation on a dust grain analogue, which is a highly-oriented pyrolytic graphite surface held at 15 K, under ultra-high vacuum. The molecules desorb from the surface in a distribution of ro-vibrational states, which are probed using Resonance Enhanced Multi-Photon Ionization Spectroscopy. HD in a particular ro-vibrational state is ionized using laser photons detected by a time-of-flight mass spectrometer. The HD^+ ion yields are then data processed to obtain the relative rotational populations of HD formed within one vibrational level and an average rotational temperature can be found. In this thesis, HD formed in vibrational states $v = 3 – 7$ have been studied. This carries on from previous studies of HD and H_2 in the $v = 1$ and 2 states. Within each vibrational level, the most populated rotational state was found to be $J = 1$ or 2. The most populated vibrational state was found to be $v = 4$.

The HD experimental results were extrapolated to give the relative ro-vibrational population distribution of nascent H_2, which provides a new model for the formation pumping of H_2. This new formation pumping model has been implemented into a radiative transfer code, written by Casu and Cecchi-Pestellini, which takes into account formation, radiative and collisional pumping mechanisms to calculate the total population distribution of H_2 in an interstellar cloud and to generate H_2 spectra. The sensitivity of the H_2 spectra to the physical conditions of interstellar dark clouds, such as cloud density and temperature, has been investigated. H_2 spectra generated using the new experimentally-derived formation pumping model has also been compared to H_2 spectra generated using other established, theoretically-derived formation pumping models.

Contents

List of Tables

List of Figures

Chapter One

Chapter Two

Chapter Three

Chapter Four

Chapter Five

Chapter One

Introduction

Hydrogen, in its different forms, is of paramount importance to astronomy because it is the most abundant element in the Universe. Hydrogen comprises approximately 90% of the Universe by number density or about 75% of the Universe by mass [1]. The spectral lines of hydrogen are prominent in a great variety of astronomical objects and the role of hydrogen in astrochemistry has been a subject of much study. Astronomers have discovered spectral lines from H^+, H-atoms, H_2 molecules, H_2^+ and H_3^+ in vast clouds of gas and dust in the space between stars, known as the interstellar medium (ISM) [2]. It is from these clouds that stars, solar systems, and ultimately, planets like the Earth have formed; thus the chemistry of interstellar clouds has major consequences for astronomy.

By far the most abundant molecule found in the ISM is H_2. It has long been known that most of the H_2 detected in the ISM must form on the surface of interstellar dust grains [1, 3-6]. However, many aspects concerning the formation of H_2 still remain a mystery. What is the formation mechanism for the recombination of H-atoms on an interstellar dust grain? Is the nascent H_2 molecule formed with significant internal and kinetic energy and can it be detected? Does the formation process cause heating of the dust grain? The answers to these questions could have a significant impact on the chemistry of the ISM. The work presented in this thesis investigates these questions using a combination of laboratory experiments and astrophysical modelling.

1.1 Interstellar Clouds

At first glance with the naked eye, the space between the stars seems to be empty. Observations with telescopes have shown that this is not the case: in the 18th century, Charles Messier stumbled across faint smudges of light in the sky when looking for comets. We now know that these are actually nebulae or interstellar clouds, where gas and dust are so close to a star that the gas becomes hot and radiates and the dust reflects light. One such interstellar cloud of gas and dust is the Iris Nebula, or NGC 7023, shown in Figure 1.1. This image of spectacular beauty occurs because interstellar dust grains are very small – about the same size as visual wavelengths – leading to blue light being scattered more efficiently than red light to produce the glowing blue vista below.

Figure 1.1 The Iris Nebula, or NGC 7023, which is about 6 light years across and 1400 light years away, is located in the constellation Cepheus. Gas and dust surrounds a massive, hot, young star. Filaments glow with red photoluminescence as invisible ultraviolet starlight is converted to visible red light by dust grains. The nebula is mostly blue, characteristic of reflection of starlight from dust grains, hence NGC 7023 is known as a reflection nebula.

Credit: Jean-Charles Cuillandre (CFHT). Image taken from Astronomy Picture of the Day [7], http://apod.nasa.gov/apod/ap051229.html

Spectroscopic observations provide much of the information that we know about interstellar gas. The atoms, ions and molecules in the gas may emit or absorb radiation corresponding to transitions between their various energy levels; thus by analysing light from the Iris Nebula we can determine its chemical composition. Rotational effects within the Galaxy can also be used to calculate the mass of interstellar matter. Interstellar gas is found to have a mean density of about 1 atom cm^{-3} [1]. As aforementioned, the gas is mainly comprised of 90% hydrogen by number density, as well as about 10% helium. Less than 0.1% of the atoms in the interstellar gas are carbon, nitrogen, oxygen or other heavier elements. Dust grains make up about 1% of the interstellar cloud by mass, such that the gas-to-dust ratio is 10^{12} by number density. This gas-to-dust ratio appears to be constant throughout the Galaxy in all regions in the ISM.

Regions in the ISM are loosely defined in a number of ways. For a definitive study of the classification of interstellar clouds see Snow and McCall [8]. The major volume of the ISM is comprised of tenuous plasma, known as 'coronal' gas, and is mainly heated by supernovae shocks [9]. It is too hot to contain molecules at a temperature of $T \sim 10^6$ K and has a number density of hydrogen nuclei of $n_H \sim 10^3$ m^{-3}. Chemically important regions can be classified into those where neutral hydrogen, in molecular or atomic form, is the most predominant species (HI regions) or where the hydrogen is ionized due to starlight (HII regions).

Another useful classification is to make a distinction between HI regions: diffuse clouds, where T ~ 100 K, $n_H \sim 100$ cm^{-3}; dark clouds, where T ~ 10 K, $n_H \sim 10^4$ cm^{-3}; and translucent clouds, which are an intermediate cloud type between the two extremes. The material within the clouds is not distributed uniformly, but is 'clumpy' such that clouds vary greatly in size and density. Clumpiness is due to matter in the clouds gravitating towards each other. Consequently these clumps themselves will be clumpy and turbulent, thus the values given for temperature and number density of hydrogen are not definitive. Together, interstellar clouds constitute only a few percent of the volume of the ISM, yet contain most of its mass [9]. Diffuse clouds mainly consist of atomic hydrogen because they are the least dense and thus fully exposed to starlight, which readily dissociates any hydrogen molecules [1]. Dark clouds are relatively dense, hence are not penetrated by ultraviolet (UV) radiation. Dark clouds

are the regions in which most molecules in the ISM are found, and hence are also known as molecular clouds. The chemistry of diffuse and dark clouds will be discussed in Section 1.8. The whole of the ISM is suffused by the cosmic microwave background radiation left over from the Big Bang and also by cosmic rays consisting of high energy protons and electrons from various origins such as rotating neutron stars and supernovae. The Milky Way Galaxy also contains a weak, ordered, large-scale magnetic field of ~ 0.1 nT [1]. The diffuse and dark cloud densities may be related in an evolutionary sequence as part of the stellar lifecycle: diffuse clouds collapse to become dark clouds, which themselves collapse until nuclear fusion is ignited to form stars. These stars interact with the ISM *via* their stellar winds and radiation until ultimately star-death occurs and the stars yield their metal-rich content back to the ISM. An image of the stellar nursery, or 'active star forming region', IC 1396 can be seen in Figure 1.2. Dark regions can be seen to interact with glowing HII regions, where UV photons from hot young stars, born within the folds of the dense, dark regions, ionize hydrogen atoms. As the electrons and atoms recombine they radiate; hence IC 1396 is also known as an emission nebula.

Figure 1.2 IC 1396 in the constellation Cepheus. This image was taken in H-Alpha emission, in the red part of the visible spectrum.

Credit: Nick Wright (CfA), IPHAS collaboration. Image taken from Astronomy Picture of the Day [10], http://apod.nasa.gov/apod/ap050930.html

1.2 Hydrogen in the Early Universe

Around 3×10^5 years after the Big Bang, protons and electrons formed the first hydrogen and helium atoms in a period of time known as the Recombination Era. Ever since then, hydrogen in its atomic and molecular forms has played a leading role in shaping the Universe. The early Universe was then extremely hot, at temperatures above 1000 K. Hydrogen atoms were able to radiate away some of this heat after being ionized, providing an important cooling mechanism so that gases could begin to collapse under gravity to form the first stars (Population III stars) and galaxies. Cooling mechanisms are essential to allow gravitational collapse because the pressure of hot gas resists further contraction unless heat can be emitted in the form of radiation, both in the early Universe and in the ISM.

Once neutral atomic hydrogen was present in the Universe, radiative reactions led to the formation of molecular ions such as H_2^+ and HD. H_2 was first formed *via* ion-molecule exchange reactions involving protons and electrons, with typical reaction schemes shown below:

$$\begin{aligned} H + e^- &\rightarrow H^- + h\nu \\ H^- + H &\rightarrow H_2 + e^- \end{aligned} \qquad 1.1$$

or

$$\begin{aligned} H + H^+ &\rightarrow H_2^+ + h\nu \\ H_2^+ + H &\rightarrow H_2 + H^+ \end{aligned} \qquad 1.2$$

Collisions of H_2 with atomic hydrogen ensued, leading to the excitation of H_2 in vibrational levels above $v = 0$. At the high temperatures of the early Universe, vibrational levels were easily populated. These excited molecules could then emit radiation through vibrational transitions and allow the gas to cool. H_2 is also an effective coolant for gases at T ~ 100 K, where collisions result in rotational excitation, followed by emission. Hence H_2 cooling mechanisms also take place in the ISM and remain of great importance to the present day.

1.3 Observations of Interstellar Molecular Hydrogen

Molecular hydrogen was expected to be abundant in the ISM as far back as the 1930s by Sir Arthur Eddington, long before it was actually discovered [8]. The problem with observing molecular hydrogen in the ISM arises from the fact that H_2 is symmetric and homonuclear, thus it possesses no "electric-dipole allowed" vibrational or rotational transitions. Electric-quadrupole transitions may occur in the infra-red (IR) but the probability of these are very small, with the Einstein A coefficient of the 2 – 0 rotational transition being 3×10^{-11} s^{-1}. This corresponds to a lifetime against radiative emission of over 1000 years [2]. Hence, although the first molecules were detected in the 1930s, namely CH, CH^+ and CN, the H_2 molecule was not observed despite its much greater abundance [8].

H_2 in the ISM could not be successfully observed until the advent of space telescopes as many of the IR and UV transitions cannot be seen from ground-based telescopes due to telluric lines, which are caused by absorption from molecules in the Earth's atmosphere [8, 11]. Finally in 1970, using rocket-based spectroscopy, Carruthers detected strong H_2 absorption in ξ Persei, having observed far-UV electronic transitions of H_2 in the Lyman and Werner bands lying below 111.5 nm [12]. Subsequently in 1972, the *Copernicus* orbital observatory was launched in order to detect interstellar H_2 absorption, again *via* UV spectrometry [13]. In this study, H_2 was discovered in more than 100 lines-of-sight towards diffuse regions. H_2 was found to possess significant rotational excitation, with the temperature of the gas determined to be 81 ± 13 K.

Ground based telescopes first observed emission from H_2 in 1976 [14, 15]. These observations were of the IR quadrupole emissions of H_2 at 2.2 – 2.4 μm, in a region of the spectrum not obscured by telluric lines. The rotational temperature of H_2 determined from these IR observations was found to be $T \sim 2000$ K. The satellite telescope, Far Ultraviolet Spectroscopic Explorer (FUSE, 1999 – 2007) [16], found molecular hydrogen in ro-vibrationally excited states using a broader UV wavelength than *Copernicus* in a wide range of astrophysical environments, such as reflection nebula and circumstellar gas [8]. Ro-vibrationally excited H_2 has also been found *via* observations at mid-UV wavelengths using spectrographs on the Hubble Space

Telescope (HST) [17]. The mechanisms for populating H_2 in such highly excited states, often called pumping mechanisms, are mainly *via* UV and collisional excitation in the ISM and are discussed in Section 1.7.

It is much more difficult to detect H_2 in dark clouds as there is no UV pumping to populate Lyman and Werner bands, hence the only method of direct observation is from IR emission due to ro-vibrational transitions. As stated previously, IR lines are difficult to observe from Earth due to telluric lines and due to H_2 having no dipole moment. Thus, ro-vibrational transitions are very weak in the cold bulk of dark clouds. Therefore, alternative means of determining the H_2 abundance have been developed other than direct observations. Many of these techniques involve using a tracer species: molecules, or dust, which are easier to detect than H_2 and then to infer the molecular hydrogen abundance by some proportionality relation [1, 18]. The main tracer of molecular gas is CO, which is the next most abundant molecule after H_2 and possesses a dipole moment of $\mu = 0.11$ Debye. CO is rotationally excited by collisions with H_2 molecules and is easily observed at radio and submillimetre wavelengths with ground-based telescopes. In clouds where both H_2 and CO molecules can be observed, the H_2:CO ratio is typically $n(H_2) = 10^5\, n(CO)$ [1], thus the abundance of H_2 can be inferred *via* observations of CO.

1.4 The "Formation Problem" for Molecular Hydrogen

The high abundance of H_2 in the ISM posed some problems for astronomers. Photolysis of H_2 readily occurs such that 10 % of all absorption events of interstellar radiation by H_2 results in the destruction of the H_2 molecule. From rate calculations of these reactions, it can be determined that a H_2 molecule in a diffuse cloud will have a lifetime of ~1000 years, which is very short on an astrophysical timescale [19]. Thus there must be an efficient mechanism for the formation of H_2 in the ISM to account for the high abundance.

In the early Universe, H_2 was formed *via* electron and proton catalysed reactions as explained in Section 1.2. However, in diffuse and dark interstellar clouds, protons and electrons are sparse, with proton and electron fractions $x_{H+} = x_{e-} = 10^{-4} - 10^{-7}$ [20].

Hence proton and electron catalysed formation of H_2 is very slow and can only account for 1 in 1000 H_2 molecules [19]. The direct radiative association of hydrogen atoms, shown in 1.3 below, is also highly inefficient. Although this process is perfectly adequate in atmospheric conditions, the low pressures in the ISM dramatically decreases the contact time between H-atoms, such that the period of vibrational oscillation in the molecule is typically only 10^{-13} s, in comparison to a transition probability of $\sim 10^{-8}$ s^{-1}. There is not sufficient contact time for the excited hydrogen molecule to radiate away its binding energy of 4.5 eV before it is likely to dissociate. This means that the efficiency of molecular hydrogen formation is too low to account for observations: only one in 10^5 collisions would result in the formation of molecular hydrogen [3].

$$H + H \rightarrow H_2 + h\nu \qquad 1.3$$

A three body reaction, shown in 1.4 below, would be much more efficient for H_2 formation as the third body, M, could remove the excess energy from H_2^*. However, in the ISM, the low pressures mean that the likelihood of three bodies colliding is negligible, hence this reaction is unimportant below H-atom densities of $\sim 10^8$ cm^{-3} [1]. Such high densities do not arise in diffuse and dark clouds, although do occur in circumstellar environments.

$$H + H + M \rightarrow H_2^* + M \rightarrow H_2 + M^* \qquad 1.4$$

Hence the widely accepted theory is that H_2 molecules must be formed through heterogeneous catalysis on the surface of dust grains in the ISM [3, 5, 11, 14, 21-80]. This formation channel was suggested by van de Hulst in 1948, then first modelled by Gould and Salpeter in 1963 [5]. This formation mechanism is thought to be highly efficient, such that almost all H-atoms adsorbed onto a dust grain leave as part of a H_2 molecule [5, 81]. It is this formation process that is under investigation in this thesis.

1.5 Formation of Molecular Hydrogen on Surfaces

The formation process can be considered in a series of steps: an H-atom adsorbs on the surface of a dust grain; diffuses across the surface; reacts with another H-atom; possibly undergoes processing on the surface; and then finally, an H_2 molecule desorbs. The formation of the molecule releases a binding energy of 4.5 eV. This binding energy is partitioned between various modes: the internal energy of the molecule; the translational or kinetic energy of the molecule and heat that flows into the surface of the dust grain. If the nascent molecule leaves the grain with some internal energy, such that its rotational or vibrational levels are excited above v, J = 0, 0 or 1, then this excitation process is known as formation pumping and is discussed in Section 1.7.1.

At the low temperatures involved in the ISM, sticking probabilities are taken to be unity, meaning that any hydrogen atoms colliding with a dust grain will freeze out on its surface [14, 42]. An H-atom adsorbs to a dust grain surface either due to van der Waals forces, which is known as physisorption, or by the formation of chemical bonds, which is known as chemisorption. The mobility of an adsorbed atom depends on the strength of the bond to the surface. The adsorbed hydrogen atom then moves around the surface *via* thermal hopping or quantum tunnelling [39] as shown by Figure 1.3. The mass of the species is important in this movement around the grain, which may imply that the formation of HD will differ from the formation of H_2, as the mobility of the heavier D-atom will be restricted in comparison to the H-atom.

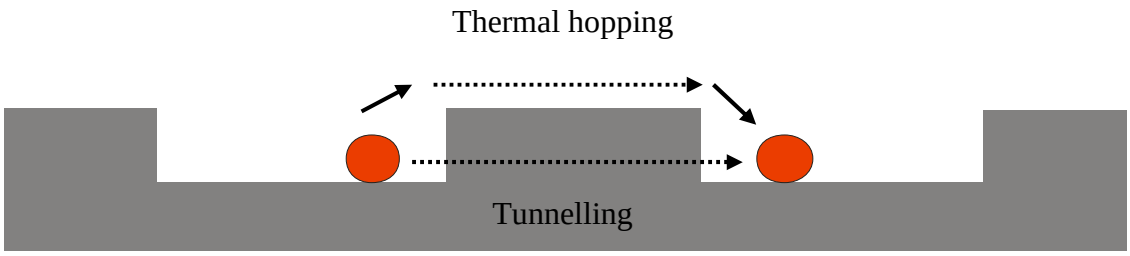

Figure 1.3 Possible methods for an H-atom to diffuse across the surface of a dust grain to move from one adsorption site to another adsorption site.

There are two main pathways in which molecular hydrogen can be formed, namely the Eley-Rideal (ER) mechanism and the Langmuir-Hinshelwood (LH) mechanism, which are shown below in Figure 1.4:

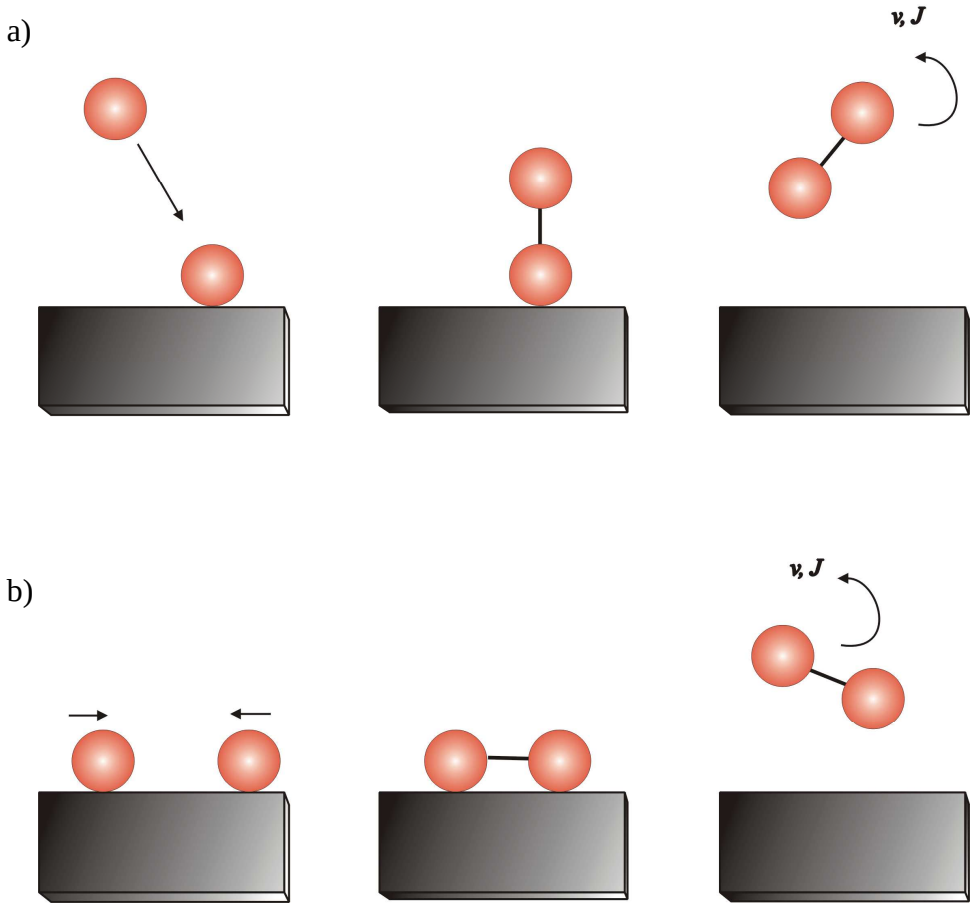

Figure 1.4 The two possible formation mechanisms for H_2 on a surface.
(a) shows the ER mechanism whilst (b) shows the LH mechanism.

The ER mechanism is the simpler process, where one H-atom is adsorbed onto the surface and reacts with another still in the gas phase. The molecular hydrogen may then desorb from the surface:

$$H(ads) + H(g) \rightarrow H_2(ads) \rightarrow H_2(g) \qquad 1.5$$

The LH process requires two H-atoms to be adsorbed; H_2 is synthesized on the surface and then possibly desorbs:

$$H(ads) + H(ads) \rightarrow H_2(ads) \rightarrow H_2(g) \qquad 1.6$$

The ER and LH mechanisms are two extremes. The real formation process may be better described by the 'hot atom' mechanism (HA) [56], which is intermediate to the ER and LH mechanisms. In the HA mechanism, one H-atom is adsorbed, and is bound to the surface. However, the second H-atom, although trapped on the surface, does not become thermalized with the surface before it reacts with the fully adsorbed, already thermalized, first H-atom to form H_2. All three of these mechanisms have been studied theoretically [14, 41, 42, 50, 52-54, 56, 58, 60, 65-67, 82-85], with most work done on the ER mechanism as it is the easiest to model. However, in interstellar conditions, the LH mechanism is thought to dominate, since at such low pressures, there will be very low coverage of H-atoms. There will be so few adatoms on the surface that it is unlikely that a gas phase atom will collide with a pre-adsorbed atom on impact with the dust grain.

1.5.1 Theoretical Studies of Molecular Hydrogen Formation

As aforementioned, Gould and Salpeter [5] developed the first theoretical model of H_2 formation in the ISM in 1963. They modelled a 'dirty-ice' surface and found that between temperatures of 10 – 20 K, the formation of H_2 must have recombination efficiency between 0.1 and 1. Hollenbach and Salpeter [45, 86] extended the treatment to model dust grains as irregular surfaces and to include H-atoms bound to defects. They found that in fact, at low temperatures, below a critical temperature of 40 – 50 K, recombination efficiency is ~1.

Cazaux and Tielens [38, 39] found that H_2 can form efficiently on dust at T = 6 – 300 K. A physisorbed H-atom was found to recombine efficiently with a chemisorbed H-atom up to ~ 100 K. At higher temperatures, the residence time of physisorbed atoms on the surface was too short to react and form H_2, hence at high temperature regions of the ISM, two chemisorbed H-atoms are required to form molecular hydrogen. The reaction between two chemisorbed H-atoms was found to be less efficient than the reaction between a physisorbed and chemisorbed atom [38].

An investigation into the adsorption of hydrogen onto a coronene-like model of graphite was made by Jeloaica and Sidis [87] using density functional theory (DFT).

They found a significant barrier to the chemisorption of H-atoms of ~ 0.2 eV. This barrier was later confirmed by experiment by Zecho *et al.* on a highly-oriented pyrolitic graphite (HOPG) surface [88]. Jeloaica and Sidis [87] observed that chemisorption of a hydrogen atom required surface relaxation and was found to only occur on atop sites, directly above a surface carbon atom. However, physisorption of hydrogen atoms was site independent and there was high mobility of hydrogen atoms around the surface. The ER mechanism for H_2 formation was compatible with both chemisorbed or physisorbed hydrogen atoms. However, the LH mechanism was only possible with physisorption, since any chemisorbed atoms could not freely diffuse around the surface.

As previously described, the H_2 binding energy is redistributed between the internal energy of the molecule, the translational energy of the molecule and energy taken up by the dust grain surface. The dust grains in the ISM may be formed of carbonaceous or silicate material and this is likely to have an effect on this energy partition. A recent study on chemisorption and physisorption by Goumans *et al.* [89] has shown that H_2 formed on a olivine surface, $(Fe,Mg)_2SiO_4$, should be much less ro-vibrationally excited than H_2 formed on a graphite surface. The nature of dust grains will be described in Section 1.6.

Takahashi *et al.* [62, 63] used classical molecular dynamics to study the formation of H_2 on water ice surfaces *via* both the ER and LH mechanisms. The nascent H_2 molecules were found to be highly ro-vibrationally excited with significant population of the $v = 5 – 8$ levels. The energy partition was calculated as follows: 70 – 79% of the H-H binding energy was converted to vibrational energy of the nascent molecule; 10 – 15 % into rotational energy; 7 – 12 % into translational energy and only 3 – 5 % was absorbed by the ice. Takahashi *et al.* conclude that as H_2 is formed in such highly excited states, IR emissions may be observable in regions without a source of UV or dynamical excitation.

In 2000, Farebrother *et al.* [14] investigated H_2 formation proceeding *via* the ER mechanism, by using time-independent scattering calculations on a potential energy surface (PES) using DFT. The results indicated that the probability of forming H_2 on the graphite surface was high, which was in agreement with classical, empirical

studies of interstellar clouds [57, 58]. The study by Farebrother *et al.* [14] also predicted vibrational excitation of the nascent H_2 molecule. For the collision energies considered, it was predicted that the vibrational distribution of the formed H_2 molecules would peak about $v = 2$. The same group then investigated further [50] using a more 3D approach, where plane-wave DFT was used to calculate the PES. It was found that the most likely vibrational states were $v = 3 – 5$. Most of the molecules were found to be highly rotationally excited, with J states up to $J = 20$ populated. The rotational states with the highest population would be $J = 8 – 11$.

In 2001, Meijer *et al.* [42] performed calculations of H_2 formation on a graphite surface, by employing a time-dependent wave packet method. The presence of spectator H-atoms was included. The H-atoms, in the form of a monolayer physisorbed onto the graphite surface, did not associate to form molecules, but had an effect on the reaction dynamics. A significant redistribution of the energy was seen to occur, even without the excitation of the spectator H-atoms. The excited vibrational states of nascent H_2 molecules were now found to extend to $v = 2$ and $v = 3$. Thus, the spectator-graphite bond may be an important reservoir of energy, which can be released or retained during the desorption of H_2 from the surface.

In a further study investigating the LH mechanism in 2007, Kerkeni and Clary [85] studied the recombination of H-atoms on a graphene slab. This study also used DFT in order to build a PES. Reaction probabilities were calculated for H-H collision energies of 1 – 15 meV, thought to be relevant to the ISM. Kerkeni and Clary found that the reaction is barrier-less and that the vibrational excitation of H_2 molecules peaks at $v = 8$, with significant populations at $v = 5$ and $v = 4$.

Work from the Sidis group predicts varying amounts of formation pumping of nascent H_2 molecules depending on the formation mechanism and modelling techniques used. Morisset *et al.* [56] investigated H_2 formation *via* the ER mechanism on planar polycyclic aromatic hydrocarbons (PAHs) at low collision temperatures of 5 K. They observed vibrational excitation of newly formed H_2 up to $v = 10$, with the higher vibrational states being more populated. In a later study, the Sidis group found that formation of H_2 on a graphite surface *via* the LH mechanism does not give rise to H_2 in either low vibrational or rotational states [53]. For example, an ER study of two

para-chemisorbed H-atoms of graphite indicates that the average vibrational level of nascent molecules should be $v = 5$ [67]. An investigation of the ER mechanism on graphene predicts similar vibrational excitation, with $\langle v \rangle \sim 4 - 5$, $\langle J \rangle \sim 2 - 4$ [66]. The Sidis group have also studied the LH recombination of physisorbed atoms on graphene, including the collision of nascent molecules with the graphene wall [65]. It was found that nascent molecules have $\langle v \rangle \sim 12 - 14$, $\langle J \rangle \sim 10$ and that collisions result in the conversion of vibrational to rotational energy. Several impacts with the graphene wall are needed to cool the molecule.

These theoretical studies have been conducted using models of 'ideal' grains, and this will affect the applicability of the theoretical results to astrophysical regions in the ISM and also to any laboratory experiments conducted. Nevertheless, the general conclusion from the above theoretical studies is that the formation of H_2 on a dust grain surface is efficient, and that nascent molecules may display significant vibrational and rotational excitation: in other words, formation pumping may occur.

1.5.2 Experimental Studies of Molecular Hydrogen Formation

Laboratory investigations into H_2 formation have yielded a variety of results, both contradictory and in agreement with the theoretical results. Gough and co-workers [15] investigated H_2 formation on carbon surfaces at T = 90 – 300 K, with temperatures much higher than interstellar dust in diffuse and dark clouds. Gough *et al.* analysed the H^- ion yield from dissociative attachment of electrons to $H_2(v, J)$. The H_2 molecules desorbed from the carbon surfaces were found to be highly vibrationally excited up to $v = 7$. However, the degree of vibration was found to be strongly dependent on the temperature of the surface, thus these results may not be relevant to the ISM.

Lemaire and co-workers [70] studied the ro-vibrational excitation of D_2 formed *via* the recombination of D-atoms on a non-porous amorphous solid water (ASW) surface held at T = 8 – 30 K. The experiments involve temperature programmed desorption (TPD) of molecules from the surface. TPD experiments are carried out by dosing the reactant molecules onto a surface, then increasing the temperature of the surface *via* a

linear or non-linear ramp rate. The molecules that desorb during this TPD experiment are detected using a mass spectrometer. Amiaud *et al.* [70] detected nascent D_2 in states $v = 1 - 7$, by scanning the kinetic energy of electrons required to ionize nascent D_2. Congiu *et al.* [73] extended the work of Amiaud *et al.* [70] by showing that D_2 is not formed with $v \geq 2$ on porous ice, hence the molecules are assumed to lose their ro-vibrational excitation *via* collisions with the pore walls. Furthermore, D_2 was neither formed internally excited on non-porous ice nor on porous ice in a regime of high molecular coverage, thus Congiu *et al.* concluded that hydrogen molecules thermalize on the surface of dust grains in dark clouds and no formation pumping occurs. Other work by the Lemaire group has studied the adsorption and desorption processes of H_2, D_2, HD on ASW [70-75] and confirmed the mobility of D-atoms on ASW at 10 K, which implies that recombination of hydrogen atoms and the hydrogenation of species on an interstellar dust grain surface may be efficient [76].

Govers *et al.* [90, 91] studied the adsorption and desorption of H_2 and D_2 and the recombination of H- and D-atoms on a cryodeposit on a liquid helium cooled bolometer. The atoms were found to be mobile down to 3 K and recombination of H-atoms was found to cause desorption of preadsorbed D_2 molecules. Zecho *et al.* [88, 92-98] conducted reactions of H- and D-atoms at T > 2000 K chemisorbed on a graphite surface. The barrier to chemisorption was confirmed and sticking coefficients were determined [88]. The graphite surface was etched to create terrace edges on the planes of graphite, in order to introduce defects onto the surface. Recombination of chemisorbed atoms on the surface was found to be largely independent of the number of defects on the surface, which implies that recombination occurs mainly at the planar surface of the graphite [98].

Pirronello, Vidali and co-workers [21-33] carried out TPD studies of H_2 formation on various surfaces of astrophysical relevance, such as silicate surfaces by using olivine as the dust grain analogue, amorphous carbon surfaces and amorphous water-ice surfaces. On olivine, the Pirronello group found that the recombination efficiency was lower than model-based estimates [26]. However, the recombination efficiency obtained by Pirronello and co-workers could be reconciled with estimates of the recombination efficiency from astrophysical observations and models, if the dust grains are taken to be rougher and larger than those currently defined in the existing

models. By studying HD formation on olivine as a function of surface temperature, Pirronello *et al.* [24] conclude that there are two main regimes of surface coverage by H-atoms that are of astronomical importance, at low surface temperatures. There can be a low coverage or a high coverage that is still less than a monolayer. The high coverage regime exhibited first order desorption kinetics, which means that H_2 molecules will form at low temperatures but will not desorb until that temperature is raised. The low coverage regime exhibited second order kinetics, indicating that the hydrogen atoms remain on the surface as atoms and also stay localized without recombining. The result for the high coverage regime indicates that the binding energy (~4.5 eV) released by the formation of H_2 will not cause the molecule to be desorbed directly into the gas phase, but that the surface may act as a reservoir for a significant amount of energy. In a further study, the Pirronello group also found that the recombination of H_2 is efficient for olivine held at a range of temperatures 6 K < T < 10 K and for carbon surfaces held at a range of temperatures 10 K < T < 20 K [29].

The Pirronello group also investigated H_2 formation on amorphous ice on top of an inert surface [31], using both low and high density ASW. Low density ASW is microporous and has a higher surface area to volume ratio than high density ice. Low density ASW has a density of 0.94 ± 0.03 g cm^{-3} and was obtained by depositing water vapour on an inert surface at 77 K, whereas high density ASW has a density of 1.1 ± 0.1 g cm^{-3} and was obtained by the deposition of water on a substrate at approximately 10 K. It was found that H_2 formation was more efficient on low density ASW but also that the efficiency increases at low surface temperatures, at T = 10 K.

The morphology of the dust grain surface is thought to have a significant influence on H_2 formation. Hornekaer *et al.* [46, 47] carried out TPD studies of molecular hydrogen formation and desorption kinetics on ASW. A large HD TPD signal was obtained from a porous ice surface but little or no signal was obtained from a non-porous surface. These results were attributed to molecules on the non-porous surface desorbing immediately after formation, hence none were retained to be observed during the TPD. On the porous surface, the molecules were thought to be trapped within the pores, where they thermalize with the surface and desorb only when activated by heating during the TPD. Thus internal excitation of nascent molecules would not be expected on porous ice. However, H_2 formed on non-porous surfaces

may be ro-vibrationally excited, if desorption occurs too promptly to allow thermalization with the surface.

Other work by Hornekaer *et al.* [77-80] was carried out on the formation of molecular hydrogen following the chemisorption of D-atoms at T > 2000 K on a graphite surface. Scanning tunnelling microscopy images revealed that there are two distinct dimer adsorption structures of D-atoms on the hexagonal graphite ring. Recombination is only possible when D-atoms are bonded to carbon atoms on opposite corners to each other on the graphite ring [78-80]. Nascent molecular hydrogen formed from the recombination of chemisorbed atoms was found to desorb with significant velocity normal to the surface, with a very broad translational energy distribution, from 0.5 to 3 eV, peaking at ~ 1.3 eV [77].

1.5.3 The UCL Cosmic Dust Experiment

The subject of this thesis is the Cosmic Dust Experiment, which was built by Perry *et al.* [99-101]. It was initially developed to probe the ro-vibrational distribution of H_2 and HD molecules formed on a highly ordered pyrolytic graphite (HOPG) surface below 50 K. Previous work has included the detection of the populations of the ro-vibrational levels $v = 1$, $J = 0 – 4$ and $v = 2$, $J = 0 – 4$ for H_2 and HD. It was found that the average rotational temperature of nascent molecules is much higher than the surface temperature on which they have formed. Chapter 2 explains the set-up of the experiment, the results of which are given in Chapter 3. Chapter 4 extrapolates the experimental results to create a new formation pumping model and investigates whether there is a characteristic signature for formation pumping observable in dark clouds.

1.6 Interstellar Dust Grains

As aforementioned, Charles Messier discovered emission nebulae. His first recorded observation of a nebula was in 1758, of an object he called M1, now often referred to as the Crab Nebula. In 1784, William Herschel was making a study of nebulae, when he discovered there were ‘holes in the sky’. These dark patches are actually due to

dense interstellar clouds, which lie in the line-of-sight between the observer and background stars, causing a phenomenon known as extinction. An example of a dark cloud can be seen below in Figure 1.5. Extinction occurs when starlight is obscured by interstellar dust. Thus Herschel had made the first observations of interstellar dust.

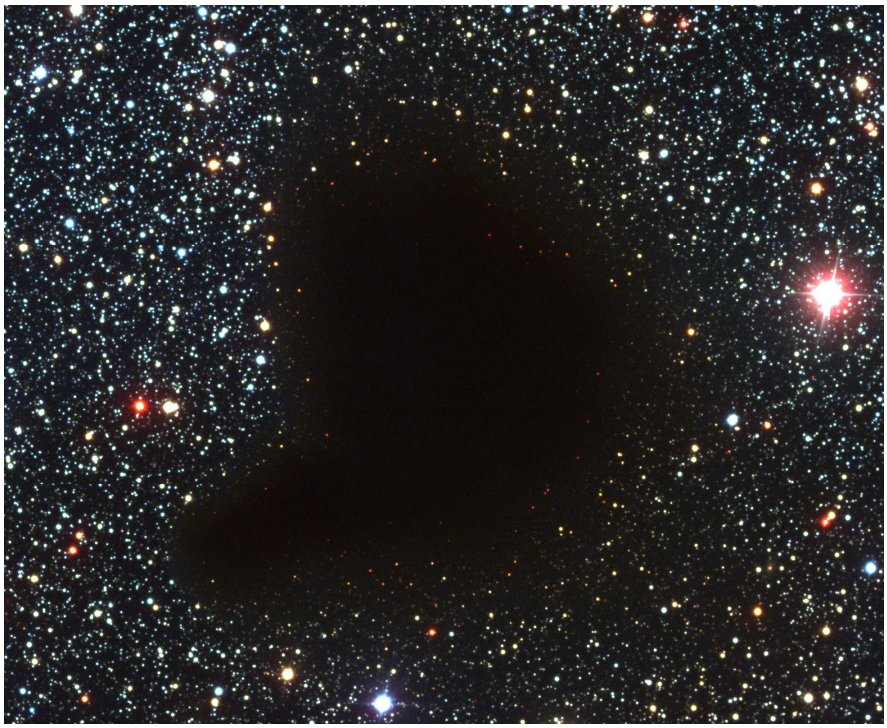

Figure 1.5 The dark cloud Barnard 68, also known as Lynds Dark Nebula 57, about half a light year across and 500 light years away, towards the constellation Ophiucus. The dust particles result in the extinction of the background visible starlight.

Credit: FORS Team, 8.2-meter VLT Antu, ESO. Image taken from Astronomy Picture of the Day [102], http://antwrp.gsfc.nasa.gov/apod/ap090623.html

In diffuse clouds, the surface temperature of the grains is ~15 K [44]. In dense clouds, the grain temperatures are lower, around 5 – 10 K, due to shielding from background photons by the dust and gas. In total, dust grains make up ~ 1% of the mass of the ISM. The dust and gas in interstellar clouds can also be at very different temperatures, with the gas usually being warmer than the dust.

These dust grains play an important role in interstellar chemistry. The formation of molecular hydrogen is catalyzed by dust grains, which provide a third body to take away the binding energy released. It is also thought that other species whose

abundance cannot be explained by gas phase formation, such as CH_3OH, may have formed on dust [103, 104]. As already discussed, the results from astrochemical simulations of H_2 formation in the ISM are extremely dependent on the nature of the dust grains modelled. Not only are the compositon, number density and degree of clumpiness of dust grains in a cloud important, but also their porosity (or 'fluffiness'), dimensions and electromagnetic properties. Furthermore, experimental studies have shown that the composition and morphology of a dust grain affects molecular formation on a dust grain, adsorption and desorption from the dust grain. In the experiments carried out as part of this thesis, a smooth graphite substrate has been used as a dust grain analogue, which has its limitations. The observational evidence concerning the nature of dust grains is described below.

From studying elemental abundances in the interstellar medium surrounding dust grains, and observing which elements are depleted, it is possible to conjecture that the missing atoms are locked in the dust grains [9]. Stars are known to form from the collapse of interstellar clouds, hence the relative abundances of elements in the Sun and other stars should be similar to that of interstellar clouds. However, near the star ζ Ophiuchi some metals, such as Fe, Ca and Ti have abundances much less than expected relative to the Sun. This depletion can be explained if some of the gas in the circumstellar clouds containing these metals cools to form stable solids which can then accrete to form dust grains. Similarly, depletion is also observed for carbon such that the percentage of carbon present in the dust is thought to be high.

The main source of information on the nature of dust grains is provided by the stellar extinction curve, where the optical depth is measured as a function of wavelength, as shown in Figure 1.6. Dust causes the most extinction at wavelengths that correspond to the size of the dust grain particle [105]. Furthermore, as seen by the image of the Iris Nebula in Figure 1.1, dust reflects and scatters light, also at wavelengths comparable to their size. Thus, particle sizes of dust grains can be calculated, by observing the absorption and scattering of UV, optical and IR radiation from dust clouds and by modelling the extinction curve. A wide distribution of dust grain sizes have been determined, ranging from a few nanometres up to around 1 μm [64]. The extinction curve can also give us information on the composition of the grains.

Various dielectric materials have been used in models of the extinction curve. From these models, dust grains are thought to be composed of either carbonaceous material, or silicates or oxides or a combination of all of these. It has been suggested that the bump at 4.6 μm^{-1} in the extinction curve is mainly due to graphite, and Figure 1.6 shows the contribution to the extinction curve expected to be due to graphite [106]. Hence graphite is used in the Cosmic Dust Experiment as an analogue of a dust grain surface.

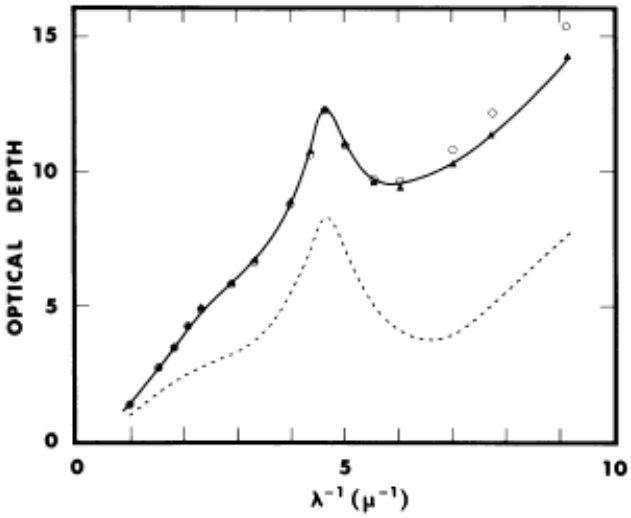

Figure 1.6 Plot of the interstellar extinction curve, taken from Mathis *et al.* [106]. A dotted line shows the proposed contribution of graphite to the curve.

The structure of silicate dust grains has been found to be both amorphous and crystalline from IR observations by the Infrared Space Observatory (ISO) [44, 64]. Dark clouds are seen to polarize starlight. This polarization is due the alignment of grains causing greater extinction in the axis of alignment. The polarization only exists to a few percent since the grains are rotating and their orientations will also be affected by collisions. The degree of polarization suggests that grains are asymmetric by a factor ~2, such that they are ellipsoid in shape, rather like a rugby ball. As alignment of the dust grains are seen to occur, dust grains must be magnetically susceptible due to the presence of iron and/or oxides. It is also thought that some grains must be refractory, and that dust particles are very non-uniform in shape [9]. The dust is thought to contain polycyclic aromatic hydrocarbons (PAHs) [8]. In regions where neutral interstellar gas is heated by star, emission lines characteristic of

PAHs are found at wavelengths between 3 and 11 μm. The conventional interpretations of these findings are that PAHs are excited by UV starlight and then emit whilst cooling.

In dark clouds and hot cores, which are dense regions heated by massive stars, IR spectroscopy has shown that dust grains are surrounded by a mantle of molecular mixed ices (see Figure 1.7). IR absorption features of H_2O, CO, CO_2, CH_3OH and other molecules in the solid phase have been detected by ISO in dense regions [64]. These species take part in chemical reactions on the grain and may undergo processing from cosmic rays and UV photons [103, 107]. Observations of diffuse clouds, however, have shown little or no evidence of ices on the grains, due to the low density of these regions [44, 64].

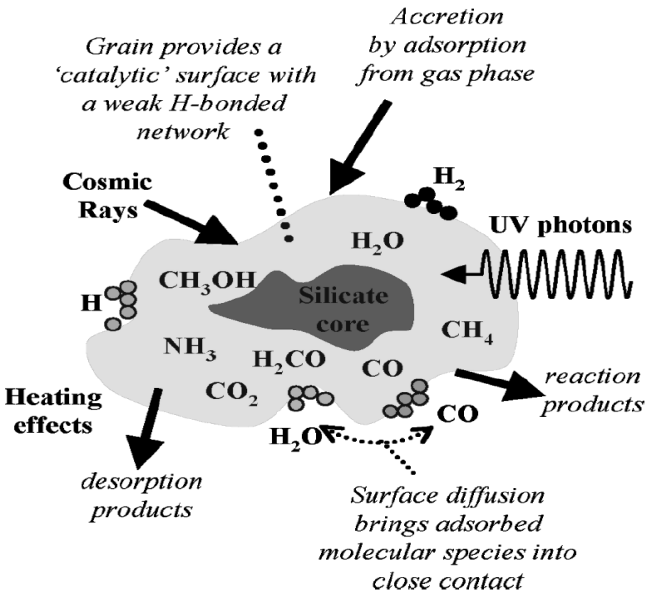

Figure 1.7 Schematic of a dust grain in dense clouds, taken from Fraser *et al.* [103]. The typical energetic processes to which a dust grain is exposed in the ISM are also shown.

1.7 Pumping Mechanisms of Molecular Hydrogen

Observations of H_2 in the ISM, particularly in diffuse and shocked regions, have found the molecule to be populated in highly excited ro-vibrational levels within the ground state. *Copernicus* and FUSE data show that in most diffuse clouds there is substantial population of H_2 in rotational levels up to about $J = 6$ [8]. This pumping is due to UV radiation and is important in both diffuse and translucent regions [108]. UV pumping occurs when H_2 absorbs photons and is excited to the Lyman and Werner bands. Subsequent decay ensues, leading to either the dissociation of the molecule or the population of ro-vibrational levels in the ground state *via* quadrupole transitions in a radiative cascade. In 10 – 15 % of UV absorption events, the molecule will dissociate [109]. The UV pumping mechanism is shown in Figure 1.8 below:

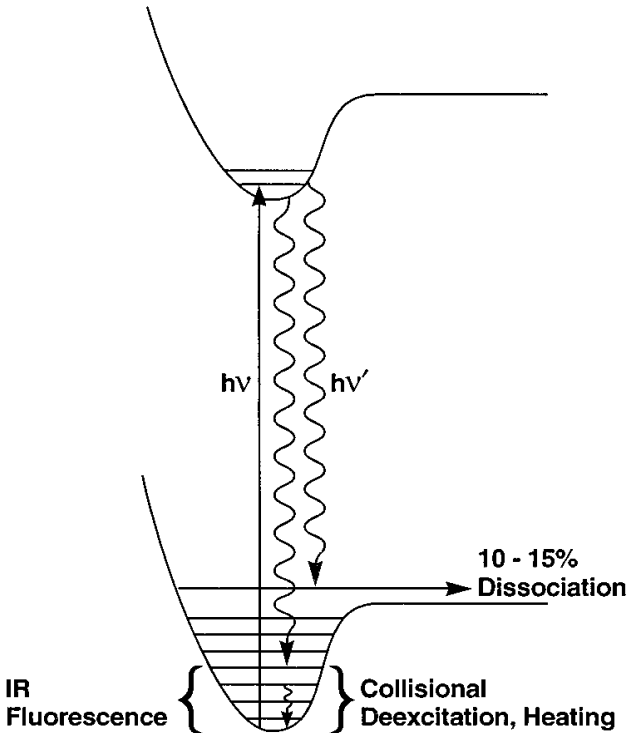

Figure 1.8 The UV pumping mechanism, taken from Hollenbach and Tielens [109].

Other H_2 pumping mechanisms also occur in the ISM. For example, an H_2 molecule can be ro-vibrationally excited by impacts with H-atoms, He and other ortho and para H_2 molecules [110-114]. These thermal collisions are particularly important in shocked regions of the ISM, such as molecular outflows [115]. Also for diffuse

clouds, collisions of H_2 with H-atoms can easily populate the low rotational states within the $v = 0$ level. In dark clouds, UV pumping is negligible due to self-shielding by H_2 and dust. In these dark regions, cosmic rays can cause the ro-vibrational excitation of H_2 [116]. Pumping of the H_2 molecule can occur directly by the primary cosmic ray or *via* excitation due to secondary electrons, which have energy in the range 30 – 36 eV for a cosmic ray proton of 10 – 100 MeV. Other mechanisms to ro-vibrationally excite H_2 include X-ray pumping in XDRs, which are regions where neutral gas is exposed to intense X-rays [117], and of course, formation pumping.

1.7.1 Formation Pumping

In 1976, Black and Dalgarno first realized that ro-vibrational excitation of nascent molecules may contribute to the IR spectrum of H_2 [108]. Hence they created a model of formation pumping in which equipartition of the H-H binding energy released was arbitrarily assumed. Thus the 4.5 eV is split equally between the internal energy of the molecule, its translational energy on desorption from the grain surface, and heat imparted to the grain lattice. Also the internal energy, assumed to be 1.5 eV, is spread with a Boltzmann distribution throughout the ro-vibrational levels, with the ortho-to-para ratio assumed to be 3.

In another model of formation pumping, Draine and Bertoldi [118] proposed a ro-vibrational distribution function that boosts the populations of vibrational states relative to the population of rotational states. The formation temperature is found to be $T = 5 \times 10^4$ K, the ortho-to-para ratio is 2.78 and the mean vibrational and rotational levels are 5.3 and 8.7 respectively in the Draine and Bertoldi formation pumping model.

Classical molecular dynamics and quantum mechanical calculations have been carried out for H_2 formation on surfaces whose chemical compositions are analogous to interstellar dust grains [5, 14, 38, 39, 41, 42, 49, 50, 52-58, 62, 63, 65-69, 83], but the results have been very different, particularly in the predicted vibrational distribution. There have also been experimental studies that confirm the formation of molecular hydrogen in ro-vibrationally excited states [70, 73, 90, 119-121], although some

predict that formation pumping would not occur in dark clouds [73]. The many theoretical and laboratory studies on H_2 formation have already been discussed in Section 1.5.

There have also been some studies which consider the effect of formation pumping on the IR emission spectra of H_2. These studies generate IR spectra in order to obtain a spectral signature of the formation pumping process. Duley and Williams [122] suggested a mechanism which differs from previous proposals in the method of stabilization of the reacting complex [122]. The stabilization energy (~ 0.4 eV) is transferred to a surface band, whose energy is that of the OH stretching vibration. The Duley and Williams model predicts that the H_2 molecule on formation is ejected into the gas vibrationally excited (v ~ 6, 7) but rotationally cool (J = 0, 1). As would be expected, the intensities of v = 6 lines are found to be considerably greater under the Duley and Williams model than in other models, however the fluorescent cascade to the emission was not taken into account to produce the spectra.

Le Bourlot *et al.* [123] generate H_2 spectra for three different formation pumping distributions. The first adopts the equipartion of the binding energy and statistical distribution of the work by Black and Dalgarno [108]. The second postulates that no energy is transferred to translation or to dust lattice modes, so H_2 is formed in its highest vibrational level, v = 14, close to the dissociation threshold, with J = 2 and 3, weighted by the nuclear spin statistics. The third adopts the scheme by Duley and Williams with v ~ 6, 7 [122]. Le Bourlot *et al*. present spectra for pure formation pumping of H_2, also including excitation by secondary electrons from cosmic rays, but do not include UV pumping. They identify spectral lines that may help distinguish between formation pumping models, but find that the spectra are not observable unless there is a high cosmic-ray ionization rate of $\zeta = 10^{-14}$ s^{-1}, rather than the standard rate of $\zeta = 10^{-17}$ s^{-1}.

H_2 spectra were presented by Tine *et al*. [20] based on ER quantum calculations by Farebrother *et al.* [14] and Meijer *et al.* [42]. Tine *et al.* predicted H_2 ro-vibrational emission line intensities for representative points in diffuse and dark interstellar clouds in a chemical steady state, taking into account collisional and UV processes. Takahashi and Uehara [68] investigated the effects of formation pumping on the IR

H_2 emission spectra produced in a collisionless gas. However, other pumping mechanisms were not taken into consideration. Takahashi and Uehara constructed formation pumping models for hydrogen molecules newly formed on icy mantles, carbonaceous and silicate dust, based on classical and quantum theoretical studies of molecular dynamics [14, 42, 57, 62, 63]. For each of these surfaces there were two rotational distributions used: either a sharp distribution, termed Model A, which peaked strongly at the average rotational level; or a less sharp distribution, termed Model B. Both Takahashi and Uehara and Tine *et al.* conclude that spectral lines arising from formation pumping should be detectable. Duley and Williams [4] assert that the most favourable location to detect a formation pumping signature would be from dense, dark, quiescent, star-less cores, where UV pumping is minimized. This is supported by Tine *et al.* [20] who find that the relative emissivities of lines due to formation pumping in dense clouds can be a factor of 500 greater than in diffuse clouds. However, observations of the dark clouds L1512 and L1498 did not yield any detections of spectral lines due to formation pumping. Similary, a study of dark cloud Barnard 68 by Lemaire and Field also resulted in a non-detection [73, 124]. In Chapter 4, an experimentally derived formation pumping model is developed and IR emission spectra of H_2 in dark clouds from 7 different formation pumping models are investigated.

Although there have been no positive detections of formation pumping in dark clouds, a few tentative claims have been made for the observation of formation pumping in diffuse regions. Burton *et al*. [125] ascribe the H_2 6 – 4 O(3) emission line at 1.7326 µm in the diffuse nebula Messier 17 to formation pumping. A marked difference in spatial distribution is observed for the 6 – 4 O(3) line and the 1 – 0 S(1), 2 – 1 S(1) and 1–0S (7) lines in M17, suggesting that the sets of lines are populated by different mechanisms. The spatial distribution and line ratios of the 1 – 0 S(1), 2 – 1 S(1), and 1 – 0 S(7) emission indicate that they are due to UV pumping. Therefore the 6 – 4 O(3) line is not excited by an UV process and is thought to be too high in energy to be thermally populated; hence Burton *et al*. conclude that formation pumping provides a significant component to the flux of the line. This may be the first direct astronomical observational evidence of H_2 formed in the $v = 6$ state. Measurements of over 30 H_2 lines in reflection nebula NGC 2023 by Burton *et al.* [126] were also made prior to the M17 observations. Burton *et al.* suggest that there may be an excess of H_2

molecules in the v = 4 state in NGC 2023, that cannot be accounted for by UV or collisional pumping. However, these results were not conclusive due to signal-to-noise issues.

Wagenblast [127] analysed *Copernicus* observations of the UV spectra of H_2 in states v = 0, J = 5, 6 and 7 towards three diffuse clouds. Wagenblast found that the populations of these states are not consistent with UV pumping. Instead, these rotational states may have been populated by either collisions with H-atoms or by formation pumping into high J states. Wagenblast found that if it is assumed that formation pumping occurs mainly into only two adjacent rotational states within a given vibrational level, then the observed populations may be explained by formation pumping into a rotationally hot state, such that $J \geq 7$, and into a range of vibrational states up to v = 11.

Rosenthal *et al.* [128] observed near- and mid-IR spectra, from 2.4 to 28 µm towards OMC-1 Peak 1 using the Short Wavelength Spectrometer on ISO. This study provided information on the average gas excitation over an unprecedented range. The H_2 v = 0, J = 27 state, which is the highest level detected, appears overpopulated with respect to an extrapolation of the lower energy level populations. Shock models fail by a factor of five to reproduce the v = 0, J = 27 state. It appears that a different mechanism might be populating this level and possibly other high energy levels. Rosenthal *et al.* suggested the presence of gas phase routes for H_2 formation, that preferentially produce H_2 molecules in highly excited ro-vibrational levels. This gas phase route is the associative detachment channel and has already been given in 1.1.

1.8 Chemistry in the Interstellar Medium

Over 150 molecules have been discovered in the ISM to date [129], both in diffuse and in dark clouds. A list of the molecules is provided in Table 1.1. Molecules are of great importance to astronomers because they can be used to probe astrophysical conditions. For example, tracer molecules such as NH_3, HC_5N and CS become excited at high densities only. Therefore emissions from these molecules can be used to infer the density of interstellar gas. Molecular emission and absorption can occur from the

UV to the radio, thus molecules can provide information about gas in a wide range of excitation. Molecules also provide cooling mechanisms through emission, which is vital in reducing the temperature of a dust cloud, facilitating the gravitational collapse required for star formation.

In diffuse clouds, where T ~ 100 K, n_H ~ 100 cm^{-3}, there is not much extinction in the visual or UV wavelengths. The medium is optically thin, hence radiative processes dominate the chemistry. Characteristically, in diffuse clouds, the neutral hydrogen is predominantly atomic and simple molecules exist. Diffuse clouds contain H_2, as the formation mechanism is highly efficient due to heterogeneous catalysis by dust grains. UV photons from starlight can easily initiate photodissociation of the atoms and molecules in diffuse clouds. Species with ionization energy less than that of hydrogen (E_i < 13.6 eV) can be ionized, such as carbon and sulphur, whereas those with higher ionization energies, such as oxygen and nitrogen are found in neutral form, since the higher energy radiation is absorbed by the neutral hydrogen. Simple molecules such as CO, S, S^+, CS, CH_3, NH, CH^+ and C_2H_2 have been observed in diffuse clouds [9]. There is also evidence of much larger molecules in diffuse clouds. Several hundred bands have been found between wavelengths of 443 nm to 1 micron. These diffuse interstellar bands (DIBs) are thought to be carried by species on the order of 100 atoms, but as yet it remains one of the 'big questions' of astrochemistry to unequivocally pinpoint the particular species which have produced the DIBs.

In dark clouds, also called dense clouds as n_H ~ 10^4 cm^{-3}, or molecular clouds because most of the hydrogen is molecular, the dust and H_2 provide so much shielding that the temperature to falls to T ~10 K. The temperature is maintained by the ionization of hydrogen by cosmic rays, which sweep through the ISM at energies of several hundred MeV. The low temperatures of dark clouds result in higher molecule column densities and richer chemistry. Dust grains in dark clouds are covered by films of ice, mostly made up of water and other simple molecules as explained in Section 1.6. Associations of dark molecular clouds can result in the formation of Giant Molecular Clouds (GMCs), which are the largest known objects in the Milky Way Galaxy, containing up to one million solar masses. GMCs are huge reservoirs of galactic matter and are incredibly important as they are the stellar nurseries of the Universe.

2 atoms	3 atoms	4 atoms	5 atoms	6 atoms	7 atoms	≥ 8 atoms
AlF	AlNC	c-C_3H	C_5	C_5H	c-C_2H_4O	C_7H
AlCl	c-SiC_2	l-C_3H	C_4H	C_5N^-	C_6H	CH_2CCHCN
AlO	C_3	C_2CN	C_4H^-	C_2H_4	C_6H^-	CH_3COOH
C_2	C_2H	C_3N	C_4Si	c-H_2C_3O	$CH_2CH(CN)$	H_2C_6
CF^+	C_2O	C_3O	l-C_3H_2	CH_3CN	$CH_2CH(OH)$	$H(CC)_3H$
CH	C_2S	C_3S	c-C_3H_2	CH_3NC	CH_3NH_2	$HC(O)OCH_3$
CH^+	CCP	C_2H_2	CH_2CN	CH_3OH	H_3C-CC-H	H_2C=CH-C(O)H
CN	CH_2	CH_3	CH_2CO	CH_3SH	$HC(O)CH_3$	H_3C-CC-CN
CO	CO_2	HCNO	CH_2NH	$H(CC)_2H$	HCC-CC-CN	$HOCH^2C(O)H$
CO^+	H_3^+	HCCN	CH_4	H_2CCCC		H_2NCH_2CN
CP	HCN	$HCNH^+$	HCC-CN	H_2CCNH		C_8H
CS	HCO	HNCO	HCC-NC	HCC-C(O)H		C_8H^-
CSi	HCO^+	HNCS	HC(O)CN	HC_4N		$(CH_3)_2O$
FeO	HCP	$HOCO^+$	HCOOH	HC_3NH^+		CH_3C_4H
H_2	HCS^+	H_2CO	NHCCC	$HC(O)NH_2$		$CH_3C(O)NH_2$
HCl	HOC^+	H_2CN	NH_2CN	C_5N		CH_3CH_2CN
HF	H_2O	H_2CS	SiH_4			HCC-CC-CC-CN
KCl	H_2S	H_3O^+	H_2COH^+			CH_3CH_2OH
LiH	HNC	NH_3				CH_3CHCH_2
N_2	HNO	SiC_3				$(CH_3)_2CO$
NH	MgCN					$CH_3(CC)_2CN$
NO	MgNC					H_3C-CH_2-C(O)H
NS	N_2H^+					$HOCH_2CH_2OH$
NaCl	N_2O					CH_3C_6H
O_2	NaCN					HCC-CC-CC-CC-CN
OH	NH_2					$HC(O)OCH_2CH_3$
PN	OCN^-					C_6H_6
PO	OCS					$CH_3CH_2CH_2CN$
SH	SiCN					HCC-CC-CC-CC-CC-CN
SiN	SiNC					
SiO	SO_2					
SiS						
SO						
SO^+						

Table 1.1 The molecules observed in the ISM to date, adapted from http://www-691.gsfc.nasa.gov/cosmic.ice.lab/interstellar.htm [129].

When dark clouds collapse to become massive stars, hot core regions are formed as the molecular regions are warmed by starlight. Unlike the bulk of the dark cloud, these hot cores are both dense and warm (T ~ 200-300 K, $n_H \sim 10^7$ cm^{-3}) as well as optically thick, making for a rich chemistry. The high column densities in hot cores allow the detection of molecular species that are scarce in other regions of the ISM. Hot cores contain large molecular species, the abundances of which are a factor of $10^3 - 10^5$ more than in the cold regions of a dark cloud. Hydrogenation of molecular species should occur on the hot core dust grains, eventually leading to the formation of large organic molecules on the grain, such as methanol, ethanol, formic acid and the sugar glycolaldehyde ($HOCH_2CHO$).

1.8.1 The Role of Molecular Hydrogen

Much of the formation of molecules found in the ISM can be explained using gas phase chemistry initiated by cosmic rays. H_2 is ionized by cosmic rays, which leads to the formation of H_3^+ *via* the following reactions, where e^- denotes an electron and c.r. denotes a cosmic ray [1]:

$$H_2 + \text{c.r} \rightarrow H_2^+ + e^- + \text{c.r} \qquad 1.7$$
$$H_2^+ + H_2 \rightarrow H_3^+ + H$$

The low proton affinity of molecular hydrogen means that the H_3^+ ion readily donates H^+ to a large variety of atoms and molecules to give rise to the production of larger molecules. The H_3^+ ion is required for a large number of reactions, for example in reactions with atomic oxygen to form water and the OH radical, which are both found in high abundances:

$$H_3^+ + O \rightarrow OH^+ + H_2 \qquad 1.8$$
$$OH^+ + H_2 \rightarrow H_2O^+ + H$$
$$H_2O^+ + H_2 \rightarrow H_3O^+ + H$$
$$H_3O^+ + e^- \rightarrow OH + 2H$$
$$\rightarrow H_2O + H$$

The second most abundant molecule in the ISM is CO, of major importance in star formation. At low cloud temperatures (10 – 100 K) CO is the most important molecular coolant, radiating excess energy in the millimetre wavelength range. OH can react with C or C^+ to produce CO in the following processes:

$$OH + C \rightarrow CO + H \qquad 1.9$$

or

$$C^+ + OH \rightarrow CO^+ + H \qquad 1.10$$
$$CO^+ + H_2 \rightarrow HCO^+ + H$$
$$HCO^+ + e^- \rightarrow CO + H$$

Simple hydrocarbons, such as CH_2, can also be produced *via* radiative association:

$$H_2 + C^+ \rightarrow CH_2^+ + h\nu \qquad 1.11$$
$$CH_2^+ + H_2 \rightarrow CH_3^+ + H$$
$$CH_3^+ + e^- \rightarrow CH_2 + H$$

Molecular formation in the ISM often proceeds through ion-neutral or neutral-neutral reactions. As the most abundant neutral species, these reactions are of course dominated by hydrogen. Reactive elements such as oxygen, nitrogen, carbon, iron, silicon and sulphur are much more likely to collide with hydrogen in atomic or molecular form rather than with any other species [1].

A reaction is more likely to occur if an atomic species collides with molecular hydrogen rather than atomic hydrogen [1]. Atom-atom interactions occur on a timescale too fast to enable the excess energy on formation of a molecule to be radiated away; hence two atoms readily fall apart without stabilizing as a molecule. In contrast, reactions between H_2 molecules and atoms of other reactive elements, or between any molecule and an H-atom, may be more efficient because rearrangements can occur such that the excess energy is removed as shown in equations 1.12.

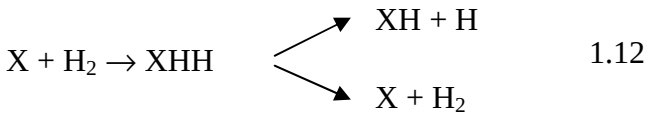

1.12

Therefore, none of the molecules listed in Table 1.1 would be found in the ISM but for the presence of H_2, which initiates all of the chemistry in the ISM and is essential for the synthesis of larger species.

Formation pumping of H_2 could have significant effects on the chemistry of the ISM by increasing the overall energy budget of gas phase reactions. For example, internally excited H_2 is likely to form OH and CH^+ in shocked regions [130]. The formation of the OH radical is much more likely when $O(^3P)$ reacts with H_2 in the v = 3 state rather than with H_2 in the v = 1 state [131, 132]. Furthermore, vibrationally excited H_2 molecules will be easier to ionize than molecules in the ground state, which can lead to an increase in the abundance of the H_3^+ ion [1]. Also, in the very early stages of star formation, the collapse of a molecular cloud may be facilitated by nascent H_2 molecules. If the molecules are formed in excited states, they may undergo ro-vibrational transitions to emit radiation, thereby cooling the cloud and accelerating collapse [42].

H_2 may also affect the chemisty of icy mantles on the surface of dust grains. As the formation of the H-H bond releases energy, heating of the dust grain may take place. Hence, the desorption of volatile molecules from the dust grain surface may occur [4]. Gas phase species are known to ‘freeze-out’ onto the surface of dust grains. In dark clouds, this ice mantle growth is limited by heating from H_2 formation, direct cosmic ray heating and cosmic ray-induced photodesorption [133]. The desorption of only one CO molecule per 100 H_2 formation events is sufficient for H_2 formation to become the dominant mechanism in limiting freeze-out, which is considered a modest requirement [107]. Therefore, the partitioning of the 4.5 eV released during H_2 formation between is key to understanding astrochemistry and can be constrained by studying the ro-vibrational excitation of nascent H_2 molecules.

1.9 Summary

In this chapter, the background to the Cosmic Dust Experiment has been discussed. H_2 is the most abundant molecule in the interstellar medium and has been observed to form efficiently *via* heterogenous catalysis on the surface of dust grains. As yet, there are still many unanswered questions concerning the formation mechanism of H_2.

In particular, it is of great importance to know how the H–H binding energy will be partitioned between internal and translational energy of the nascent molecule and the energy lost to the dust grain surface during formation. Theoretical and experimental studies have shown that this energy partition is strongly dependent on the morphology and chemical composition of dust grains. The UCL Cosmic Dust Experiment has been designed to probe the ro-vibrational distribution of molecular hydrogen formed on surfaces analogous to interstellar dust grains.

The formation of H_2 in ro-vibrational states above $v = 0$, $J = 0, 1$ is known as formation pumping. Other pumping mechanisms such as radiative and collisional pumping also occur in the ISM. Formation pumping will have consequences for the chemistry that occurs in the interstellar medium and may be observable in the ISM.

1.10 References

1. Dyson, J.E. and D.A. Williams, *The Physics of the Interstellar Medium*. 2nd ed. 1997, Bristol: Institute of Physics.

2. Tennyson, J., *Astronomical Spectroscopy*. Imperial College Press Advanced Physics Texts. Vol. 2. 2005, London: Imperial College Press.

3. Duley, W. and D.A. Williams, *Interstellar Chemistry*. 1984, London: Academic Press.

4. Duley, W.W. and D.A. Williams, *The Formation of H-2 on Interstellar Dust*. Monthly Notices of the Royal Astronomical Society, 1993. **260**(1): p. 37-42.

5. Gould, R.J. and E.E. Salpeter, *The Interstellar Abundance of the Hydrogen Molecule. I. Basic Processes*. Astrophysical Journal, 1963. **138**: p. 393-407.

6. Jura, M., *Interstellar Clouds Containing Optically Thin H2*. Astrophysical Journal, 1975. **197**(3): p. 575-580.

7. Nemiroff, R. and J. Bonnell. *Astronomy Picture of the Day, Iris Nebula*. 2005 [cited 25/10/2009]; Available from: http://apod.nasa.gov/apod/ap051229.html.

8. Snow, T.P. and B.J. McCall, *Diffuse atomic and molecular clouds*. Annual Review of Astronomy and Astrophysics, 2006. **44**: p. 367-414.

9. Williams, D.A. and S. Viti, *Recent progress in astrochemistry*. Annual Reports on the Progress of Chemistry, Vol 98, Section C: Physical Chemistry, 2002. **98**: p. 87-120.

10. Nemiroff, R. and J. Bonnell. *Astronomy Picture of the Day, IC1396*. 2005 [cited 25/10/2009]; Available from: http://apod.nasa.gov/apod/ap050930.html.

11. Biham, O., I. Furman, N. Katz, V. Pirronello, and G. Vidali, *H-2 formation on interstellar grains in different physical regimes*. Monthly Notices of the Royal Astronomical Society, 1998. **296**(4): p. 869-872.

12. Carruthers, G.R., *Rocket Observation of Interstellar Molecular Hydrogen*. Astrophysical Journal, 1970. **161**: p. L81-L85.

13. Rogerson, J.B., L. Spitzer, J.F. Drake, K. Dressler, E.B. Jenkins, D.C. Morton, and D.G. York, *Spectrophotometric Results from Copernicus-Satellite .1. Instrumentation and Performance*. Astrophysical Journal, 1973. **181**(3): p. L97-L102.

14. Farebrother, A.J., A.J.H.M. Meijer, D.C. Clary, and A.J. Fisher, *Formation of molecular hydrogen on a graphite surface via an Eley-Rideal mechanism*. Chemical Physics Letters, 2000. **319**(3-4): p. 303-308.

15. Gough, S., C. Schermann, F. Pichou, M. Landau, I. Cadez, and R.I. Hall, *The formation of vibrationally excited hydrogen molecules on carbon surfaces*. Astronomy and Astrophysics, 1996. **305**(2): p. 687-693.

16. Moos, H.W., W.C. Cash, L.L. Cowie, A.F. Davidsen, A.K. Dupree, P.D. Feldman, S.D. Friedman, J.C. Green, R.F. Green, C. Gry, J.B. Hutchings, E.B. Jenkins, J.L. Linsky, R.F. Malina, A.G. Michalitsianos, B.D. Savage, J.M. Shull, O.H.W. Siegmund, T.P. Snow, G. Sonneborn, A. Vidal-Madjar, A.J. Willis, B.E. Woodgate, D.G. York, T.B. Ake, B.G. Andersson, J.P. Andrews, R.H. Barkhouser, L. Bianchi, W.P. Blair, K.R. Brownsberger, A.N. Cha, P. Chayer, S.J. Conard, A.W. Fullerton, G.A. Gaines, R. Grange, M.A. Gummin, G. Hebrard, G.A. Kriss, J.W. Kruk, D. Mark, D.K. McCarthy, C.L. Morbey, R. Murowinski, E.M. Murphy, W.R. Oegerle, R.G. Ohl, C. Oliveira, S.N. Osterman, D.J. Sahnow, M. Saisse, K.R. Sembach, H.A. Weaver, B.Y. Welsh, E. Wilkinson, and W. Zheng, *Overview of the Far Ultraviolet Spectroscopic Explorer Mission*. Astrophysical Journal, 2000. **538**(1): p. L1-L6.

17. Boisse, P., F. Le Petit, E. Rollinde, E. Roueff, G.P. des Forets, B.G. Andersson, C. Gry, and P. Felenbok, *A far UV study of interstellar gas towards HD 34078: High excitation H-2 and small scale structure*. Astronomy & Astrophysics, 2005. **429**(2): p. 509-523.

18. Bell, T.A., E. Roueff, S. Viti, and D.A. Williams, *Molecular line intensities as measures of cloud masses - I. Sensitivity of CO emissions to physical parameter variations*. Monthly Notices of the Royal Astronomical Society, 2006. **371**(4): p. 1865-1872.

19. Hartquist, T.W. and D.A. Williams, *The Chemically Controlled Cosmos*. 1 ed. 1995: Cambridge University Press. 169.

20. Tine, S., D.A. Williams, D.C. Clary, A.J. Farebrother, A.J. Fisher, A. Meijer, J.M.C. Rawlings, and C.J. Davis, *Observational indicators of formation excitation of H-2*. Astrophysics And Space Science, 2003. **288**(3): p. 377-389.

21. Vidali, G., V. Pirronello, C. Liu, and L.Y. Shen, *Experimental studies of chemical reactions on surfaces of astrophysical interest*. Astrophys. Lett. Comm., 1998. **35**(6): p. 423-447.

22. Vidali, G., V. Pirronello, L. Li, J. Roser, G. Manico, E. Congiu, H. Mehl, A. Lederhendler, H.B. Perets, J.R. Brucato, and O. Biham, *Analysis of molecular hydrogen formation on low-temperature surfaces in temperature programmed desorption experiments*. J. Phys. Chem. A, 2007. **111**(49): p. 12611-12619.

23. Vidali, G., L. Li, J.E. Roser, and R. Badman, *Catalytic activity of interstellar grains: Formation of molecular hydrogen on amorphous silicates*. Advances in Space Research, 2009. **43**(8): p. 1291-1298.

24. Pirronello, V., C. Liu, L.Y. Shen, and G. Vidali, *Laboratory synthesis of molecular hydrogen on surfaces of astrophysical interest*. Astrophysical Journal, 1997. **475**(1): p. L69-L72.

25. Pirronello, V., C. Liu, J.E. Roser, and G. Vidali, *Measurements of molecular hydrogen formation on carbonaceous grains*. Astronomy and Astrophysics, 1999. **344**(2): p. 681-686.

26. Pirronello, V., O. Biham, C. Liu, L.O. Shen, and G. Vidali, *Efficiency of molecular hydrogen formation on silicates*. Astrophysical Journal, 1997. **483**(2): p. L131-L134.

27. Perets, H.B., A. Lederhendler, O. Biham, G. Vidali, L. Li, S. Swords, E. Congiu, J. Roser, G. Manico, J.R. Brucato, and V. Pirronello, *Molecular hydrogen formation on amorphous silicates under interstellar conditions*. Astrophysical Journal, 2007. **661**(2): p. L163-L166.

28. Perets, H.B., O. Biham, G. Manico, V. Pirronello, J. Roser, S. Swords, and G. Vidali, *Molecular hydrogen formation on ice under interstellar conditions*. Astrophysical Journal, 2005. **627**(2): p. 850-860.

29. Vidali, G., J.E. Roser, L. Ling, E. Congiu, G. Manico, and V. Pirronello, *The formation of interstellar molecules via reactions on dust grain surfaces*. Faraday Discussions, 2006. **133**: p. 125-135.

30. Roser, J.E., S. Swords, G. Vidali, G. Manico, and V. Pirronello, *Measurement of the kinetic energy of hydrogen molecules desorbing from amorphous water ice*. Astrophysical Journal, 2003. **596**(1): p. L55-L58.

31. Roser, J.E., G. Manico, V. Pirronello, and G. Vidali, *Formation of molecular hydrogen on amorphous water ice: Influence of morphology and ultraviolet exposure*. Astrophysical Journal, 2002. **581**(1): p. 276-284.

32. Manico, G., G. Raguni, V. Pirronello, J.E. Roser, and G. Vidali, *Laboratory measurements of molecular hydrogen formation on amorphous water ice*. Astrophysical Journal, 2001. **548**(2): p. L253-L256.

33. Katz, N., I. Furman, O. Biham, V. Pirronello, and G. Vidali, *Molecular hydrogen formation on astrophysically relevant surfaces*. Astrophysical Journal, 1999. **522**(1): p. 305-312.

34. Biham, O., I. Furman, V. Pirronello, and G. Vidali, *Master equation for hydrogen recombination on grain surfaces*. Astrophysical Journal, 2001. **553**(2): p. 595-603.

35. Biham, O., I. Furman, N. Katz, V. Pirronello, and G. Vidali, *H_2 formation on interstellar grains in different physical regimes*. Monthly Notices of the Royal Astronomical Society, 1998. **296**(4): p. 869-872.

36. Cazaux, S., P. Caselli, V. Cobut, and J. Le Bourlot, *The role of carbon grains in the deuteration of H-2*. Astronomy & Astrophysics, 2008. **483**(2): p. 495-508.

37. Cazaux, S. and M. Spaans, *HD and H-2 formation in low-metallicity dusty gas clouds at high redshift*. Astronomy & Astrophysics, 2009. **496**(2): p. 365-374.

38. Cazaux, S. and A. Tielens, *Molecular hydrogen formation in the interstellar medium*. Astrophysical Journal, 2002. **575**(1): p. L29-L32.

39. Cazaux, S. and A. Tielens, *Formation on grain surfaces*. Astrophysical Journal, 2004. **604**(1): p. 222-237.

40. Habart, E., M. Walmsley, L. Verstraete, S. Cazaux, R. Maiolino, P. Cox, F. Boulanger, and G.P. Des Forets, *Molecular hydrogen*. Space Science Reviews, 2005. **119**(1-4): p. 71-91.

41. Meijer, A., A.J. Farebrother, and D.C. Clary, *Isotope effects in the formation of molecular hydrogen on a graphite surface via an Eley-Rideal mechanism*. J. Phys. Chem. A, 2002. **106**(39): p. 8996-9008.

42. Meijer, A.J.H.M., A.J. Farebrother, D.C. Clary, and A.J. Fisher, *Time-dependent quantum mechanical calculations on the formation of molecular hydrogen on a graphite surface via an Eley-Rideal mechanism*. J. Phys. Chem. A, 2001. **105**(11): p. 2173-2182.

43. Gautier III, T.N., U. Fink, R.R. Treffers, and H.P. Larson, *Detection of Molecular Hydrogen Quadrupole Emission in the Orion Nebula*. Astrophysical Journal, 1976. **207**: p. L129-L133.

44. Greenberg, J.M., *Cosmic dust and our origins*. Surface Science, 2002. **500**(1-3): p. 793-822.

45. Hollenbach, D.J. and E.E. Salpeter, *Surface Recombination of Hydrogen Molecules*. Astrophysical Journal, 1971. **163**: p. 155-164.

46. Hornekaer, L., A. Baurichter, V.V. Petrunin, D. Field, and A.C. Luntz, *Importance of surface morphology in interstellar H-2 formation*. Science, 2003. **302**(5652): p. 1943-1946.

47. Hornekaer, L., A. Baurichter, V.V. Petrunin, A.C. Luntz, B.D. Kay, and A. Al-Halabi, *Influence of surface morphology on D-2 desorption kinetics from amorphous solid water*. J. Chem. Phys., 2005. **122**(12).

48. Kim, Y.H., J. Ree, and H.K. Shin, *Formation of vibrationally excited hydrogen molecules on a graphite surface*. Chemical Physics Letters, 1999. **314**(1-2): p. 1-8.

49. Ree, J., Y.H. Kim, and H.K. Shin, *Dynamics of H-2 formation on a graphite surface*. Chemical Physics Letters, 2002. **353**(5-6): p. 368-378.

50. Meijer, A., A.J. Fisher, and D.C. Clary, *Surface coverage effects on the formation of molecular hydrogen on a graphite surface via an Eley-Rideal mechanism*. J. Phys. Chem. A, 2003. **107**(50): p. 10862-10871.

51. Morisset, S. and A. Allouche, *Quantum dynamic of sticking of a H atom on a graphite surface*. J Chem Phys, 2008. **129**(2): p. 024509.

52. Morisset, S., F. Aguillon, M. Sizun, and V. Sidis, *Wave-packet study of H-2 formation on a graphite surface through the Langmuir-Hinshelwood mechanism*. J. Chem. Phys., 2005. **122**(19): p. art. no.-194702.

53. Morisset, S., F. Aguillon, M. Sizun, and V. Sidis, *Quantum dynamics of H-2 formation on a graphite surface through the Langmuir Hinshelwood mechanism*. J. Chem. Phys., 2004. **121**(13): p. 6493-6501.

54. Morisset, S., F. Aguillon, M. Sizun, and V. Sidis, *Role of surface relaxation in the Eley-Rideal formation of H-2 on a graphite surface*. J. Phys. Chem. A, 2004. **108**(41): p. 8571-8579.

55. Morisset, S., F. Aguillon, M. Sizun, and V. Sidis, *The dynamics of H-2 formation on a graphite surface at low temperature*. Phys. Chem. Chem. Phys., 2003. **5**(3): p. 506-513.

56. Morisset, S., F. Aguillon, M. Sizun, and V. Sidis, *Quantum wavepacket investigation of Eley Rideal formation of H- 2 on a relaxing graphite surface*. Chemical Physics Letters, 2003. **378**(5-6): p. 615-621.

57. Parneix, P. and P. Brechignac, *Molecular dynamics simulation of the H-2 recombination on a graphite surface*. Astronomy and Astrophysics, 1998. **334**(1): p. 363-375.

58. Rutigliano, M., M. Cacciatore, and G.D. Billing, *Hydrogen atom recombination on graphite at 10 K via the Eley- Rideal mechanism*. Chemical Physics Letters, 2001. **340**(1-2): p. 13-20.

59. Sha, X.W., B. Jackson, D. Lemoine, and B. Lepetit, *Quantum studies of H atom trapping on a graphite surface*. J. Chem. Phys., 2005. **122**(1).

60. Sha, X.W., B. Jackson, and D. Lemoine, *Quantum studies of Eley-Rideal reactions between H atoms on a graphite surface*. J. Chem. Phys., 2002. **116**(16): p. 7158-7169.

61. Sha, X.W. and B. Jackson, *First-principles study of the structural and energetic properties of H atoms on a graphite (0001) surface*. Surface Science, 2002. **496**(3): p. 318-330.

62. Takahashi, J., K. Masuda, and M. Nagaoka, *The formation mechanism of molecular hydrogen on icy mantles of interstellar dust*. Monthly Notices of the Royal Astronomical Society, 1999. **306**(1): p. 22-30.

63. Takahashi, J., K. Masuda, and M. Nagaoka, *Product energy distribution of molecular hydrogen formed on icy mantles of interstellar dust*. Astrophysical Journal, 1999. **520**(2): p. 724-731.

64. Williams, D.A. and E. Herbst, *It's a dusty Universe: surface science in space*. Surface Science, 2002. **500**(1-3): p. 823-837.

65. Bachellerie, D., M. Sizun, F. Aguillon, and V. Sidis, *Effects of a Nonrigid Graphene Surface on the LH Associative Desorption of H Atoms and on the Deexcitation of Nascent H-2 Molecules Colliding with Model Walls of Carbonaceous Porous Material*. J. Phys. Chem. A, 2009. **113**(1): p. 108-117.

66. Bachellerie, D., M. Sizun, F. Aguillon, D. Teillet-Billy, N. Rougeau, and V. Sidis, *Unrestricted study of the Eley-Rideal formation of H-2 on graphene using a new multidimensional graphene-H-H potential: role of the substrate*. Phys. Chem. Chem. Phys., 2009. **11**(15): p. 2715-2729.

67. Bachellerie, D., M. Sizun, D. Teillet-Billy, N. Rougeau, and V. Sidis, *Eley-Rideal formation of H-2 involving one of two para-chemisorbed H atoms on a graphite surface*. Chemical Physics Letters, 2007. **448**(4-6): p. 223-227.

68. Takahashi, J. and H. Uehara, *H-2 Emission spectra with new formation pumping models*. Astrophysical Journal, 2001. **561**(2): p. 843-857.

69. Takahashi, J., *The ortho/para ratio of H-2 newly formed on dust grains*. Astrophysical Journal, 2001. **561**(1): p. 254-263.

70. Amiaud, L., F. Dulieu, J.H. Fillion, A. Momeni, and J.L. Lemaire, *Interaction of atomic and molecular deuterium with a nonporous amorphous water ice surface between 8 and 30 K*. J. Chem. Phys., 2007. **127**(14).

71. Amiaud, L., J.H. Fillion, S. Baouche, F. Dulieu, A. Momeni, and J.L. Lemaire, *Interaction of D-2 with H2O amorphous ice studied by temperature-programed desorption experiments*. J. Chem. Phys., 2006. **124**(9).

72. Amiaud, L., A. Momeni, F. Dulieu, J.H. Fillion, E. Matar, and J.L. Lemaire, *Measurement of the adsorption energy difference between ortho- and para-D-2 on an amorphous ice surface*. Physical Review Letters, 2008. **100**(5).

73. Congiu, E., E. Matar, L.E. Kristensen, F. Dulieu, and J.L. Lemaire, *Laboratory evidence for the non-detection of excited nascent H-2 in dark clouds*. Monthly Notices of the Royal Astronomical Society, 2009. **397**(1): p. L96-L100.

74. Dulieu, F., L. Amiaud, S. Baouche, A. Momeni, J.H. Fillion, and J.L. Lemaire, *Isotopic segregation of molecular hydrogen on water ice surface at low temperature*. Chemical Physics Letters, 2005. **404**(1-3): p. 187-191.

75. Fillion, J.H., L. Amiaud, E. Congiu, F. Dulieu, A. Momeni, and J.L. Lemaire, *D-2 desorption kinetics on amorphous solid water: from compact to porous ice films*. Phys. Chem. Chem. Phys., 2009. **11**(21): p. 4396-4402.

76. Matar, E., E. Congiu, F. Dulieu, A. Momeni, and J.L. Lemaire, *Mobility of D atoms on porous amorphous water ice surfaces under interstellar conditions*. Astronomy & Astrophysics, 2008. **492**(1): p. L17-L20.

77. Baouche, S., G. Gamborg, V.V. Petrunin, A.C. Luntz, A. Baurichter, and L. Hornekaer, *High translational energy release in H-2 (D-2) associative desorption from H (D) chemisorbed on C(0001)*. J. Chem. Phys., 2006. **125**(8).

78. Hornekaer, L., E. Rauls, W. Xu, Z. Sljivancanin, R. Otero, I. Stensgaard, E. Laegsgaard, B. Hammer, and F. Besenbacher, *Clustering of chemisorbed H(D) atoms on the graphite (0001) surface due to preferential sticking*. Physical Review Letters, 2006. **97**(18).

79. Hornekaer, L., Z. Sljivancanin, W. Xu, R. Otero, E. Rauls, I. Stensgaard, E. Laegsgaard, B. Hammer, and F. Besenbacher, *Metastable structures and recombination pathways for atomic hydrogen on the graphite (0001) surface*. Physical Review Letters, 2006. **96**(15).

80. Hornekaer, L., W. Xu, R. Otero, E. Laegsgaard, and F. Besenbacher, *Long range orientation of meta-stable atomic hydrogen adsorbate clusters on the graphite(0001) surface*. Chemical Physics Letters, 2007. **446**: p. 237-242.

81. Hollenbach, D. and E.E. Salpeter, *Surface Recombination of Hydrogen Molecules*. Astrophysical Journal, 1971. **163**: p. 155-164.

82. Jackson, B. and D. Lemoine, *Eley-Rideal reactions between H atoms on metal and graphite surfaces: The variation of reactivity with substrate*. J. Chem. Phys., 2001. **114**(1): p. 474-482.

83. Martinazzo, R. and G.F. Tantardini, *Quantum study of Eley-Rideal reaction and collision induced desorption of hydrogen atoms on a graphite surface. I. H-chemisorbed case*. J. Chem. Phys., 2006. **124**(12).

84. Martinazzo, R. and G.F. Tantardini, *Quantum study of Eley-Rideal reaction and collision induced desorption of hydrogen atoms on a graphite surface. II. H-physisorbed case*. J. Chem. Phys., 2006. **124**(12).

85. Kerkeni, B. and D.C. Clary, *Quantum dynamics study of the Langmuir-Hinshelwood H+H recombination mechanism and H-2 formation on a graphene model surface*. Chemical Physics, 2007. **338**(1): p. 1-10.

86. Hollenbach, D. and E.E. Salpeter, *Surface Adsorption of Light gas Atoms*. J. Chem. Phys., 1970. **53**(1): p. 79-86.

87. Jeloaica, L. and V. Sidis, *DFT investigation of the adsorption of atomic hydrogen on a cluster-model graphite surface*. Chemical Physics Letters, 1999. **300**(1-2): p. 157-162.

88. Zecho, T., A. Guttler, X.W. Sha, B. Jackson, and J. Kuppers, *Adsorption of hydrogen and deuterium atoms on the (0001) graphite surface*. J. Chem. Phys., 2002. **117**(18): p. 8486-8492.

89. Goumans, T.P.M., C. Richard, A. Catlow, and W.A. Brown, *Formation of H-2 on an olivine surface: a computational study*. Monthly Notices of the Royal Astronomical Society, 2009. **393**(4): p. 1403-1407.

90. Govers, T.R., L. Mattera, and G. Scoles, *Molecular-Beam Experiments on the Sticking and Accommodation of Molecular-Hydrogen on a Low-Temperature Substrate*. J. Chem. Phys., 1980. **72**(10): p. 5446-5455.

91. Govers, T.R., *H atom data*. http://hal.ccsd.cnrs.fr/ccsd-00004273/en/, 2005.

92. Andree, A., M. Le Lay, T. Zecho, and J. Kupper, *Pair formation and clustering of D on the basal plane of graphite*. Chemical Physics Letters, 2006. **425**(1-3): p. 99-104.

93. Guttler, A., T. Zecho, and J. Kuppers, *Adsorption of D(H) atoms on Ar ion bombarded (0001) graphite surfaces*. Surface Science, 2004. **570**(3): p. 218-226.

94. Guttler, A., T. Zecho, and J. Kuppers, *A LEED and STM study of H(D) adsorption on C(0001) surfaces*. Chemical Physics Letters, 2004. **395**(1-3): p. 171-176.

95. Guttler, A., T. Zecho, and J. Kuppers, *Interaction of H (D) atoms with surfaces of glassy carbon: adsorption, abstraction, and etching*. Carbon, 2004. **42**(2): p. 337-343.

96. Kuppers, J., T. Zecho, and A. Guttler, *Adsorption and abstraction of H and D atoms on the (0001) graphite surface*. Abstracts of Papers of the American Chemical Society, 2003. **225**: p. U633-U633.

97. Zecho, T., A. Guttler, and J. Kuppers, *Suppression of D adsorption and D by H abstraction on graphite (0001) surfaces by adsorbed water*. Chemical Physics Letters, 2003. **370**(3-4): p. 366-370.

98. Zecho, T., A. Guttler, and J. Kuppers, *A TDS study of D adsorption on terraces and terrace edges of graphite (0001) surfaces*. Carbon, 2004. **42**(3): p. 609-617.

99. Perry, J.S.A., *State-Selective Reactions of Cosmic Dust Analogues at Cryogenic Temperatures, Deaprtment of Chemistry*. 2001, University College London: London.

100. Perry, J.S.A., J.M. Gingell, K.A. Newson, J. To, N. Watanabe, and S.D. Price, *An apparatus to determine the rovibrational distribution of molecular hydrogen formed by the heterogeneous recombination of H atoms on cosmic dust analogues*. Measurement Science & Technology, 2002. **13**(9): p. 1414-1424.

101. Perry, J.S.A. and S.D. Price, *Detection of rovibrationally excited H-2 formed through the heterogeneous recombination of H atoms on a cold HOPG surface*. Astrophysics and Space Science, 2003. **285**(3-4): p. 769-776.

102. Nemiroff, R. and J. Bonnell. *Astronomy Picture of the Day, B68*. 2005 [cited 25/10/2009]; Available from: http://antwrp.gsfc.nasa.gov/apod/ap090623.html.

103. Fraser, H.J., M.P. Collings, and M.R.S. McCoustra, *Laboratory surface astrophysics experiment*. Review of Scientific Instruments, 2002. **73**(5): p. 2161-2170.

104. Garrod, R.T., S.L.W. Weaver, and E. Herbst, *Complex chemistry in star-forming regions: An expanded gas-grain warm-up chemical model*. Astrophysical Journal, 2008. **682**(1): p. 283-302.

105. Millar, T.J. and D.A. Williams, *Dust and Chemistry in Astronomy*. 1 ed. Graduate Serier in Astronomy, ed. R.E.W. R J Tayler. 1993: Institute of Physics. 335.

106. Mathis, J.S., W. Rumpl, and K.H. Nordsieck, *Size Distribution of Interstellar Grains*. Astrophysical Journal, 1977. **217**(2): p. 425-433.

107. Williams, D.A., W.A. Brown, S.D. Price, J.M.C. Rawlings, and S. Viti, *Molecules, ices and astronomy*. Astron. Geophys., 2007. **48**(1): p. 25-34.

108. Black, J.H. and A. Dalgarno, *Interstellar H2 - Population Of Excited Rotational States And Infrared Response To Ultraviolet-Radiation*. Astrophysical Journal, 1976. **203**(1): p. 132-142.

109. Hollenbach, D.J. and A. Tielens, *Photodissociation regions in the interstellar medium of galaxies*. Reviews of Modern Physics, 1999. **71**(1): p. 173-230.

110. Flower, D.R., *The rotational excitation of H-2 by H-2*. Monthly Notices of the Royal Astronomical Society, 1998. **297**(1): p. 334-336.

111. Flower, D.R. and E. Roueff, *Vibrational relaxation in H-H-2 collisions*. Journal of Physics B-Atomic Molecular and Optical Physics, 1998. **31**(23): p. L955-L958.

112. Flower, D.R. and E. Roueff, *Rovibrational relaxation in collisions between H-2 molecules: I. Transitions induced by ground state para-H-2*. Journal of Physics B-Atomic Molecular and Optical Physics, 1998. **31**(13): p. 2935-2947.

113. Flower, D.R., E. Roueff, and C.J. Zeippen, *Rovibrational excitation of H-2 molecules by He atoms*. Journal of Physics B-Atomic Molecular and Optical Physics, 1998. **31**(5): p. 1105-1113.

114. Le Bourlot, J., G.P. des Forets, and D.R. Flower, *The cooling of astrophysical media by H-2*. Monthly Notices of the Royal Astronomical Society, 1999. **305**(4): p. 802-810.

115. Le Bourlot, J., G.P. des Forets, D.R. Flower, and S. Cabrit, *New determinations of the critical velocities of C-type shock waves in dense molecular clouds: application to the outflow source in Orion*. Monthly Notices of the Royal Astronomical Society, 2002. **332**(4): p. 985-993.

116. Prasad, S.S. and S.P. Tarafdar, *Uv-Radiation Field inside Dense Clouds - Its Possible Existence and Chemical Implications*. Astrophysical Journal, 1983. **267**(2): p. 603-609.

117. Maloney, P.R., D.J. Hollenbach, and A. Tielens, *X-ray-irradiated molecular gas .1. Physical processes and general results*. Astrophysical Journal, 1996. **466**(1): p. 561-584.

118. Draine, B.T. and F. Bertoldi, *Structure of stationary photodissociation fronts*. Astrophysical Journal, 1996. **468**(1): p. 269-289.

119. Creighan, S.C., J.S.A. Perry, and S.D. Price, *The rovibrational distribution of H-2 and HD formed on a graphite surface at 15-50 K*. J. Chem. Phys., 2006. **124**(11).

120. Islam, F., E.R. Latimer, and S.D. Price, *The formation of vibrationally excited HD from atomic recombination on cold graphite surfaces*. J. Chem. Phys., 2007. **127**: p. 064701-8.

121. Latimer, E.R., F. Islam, and S.D. Price, *Studies of HD formed in excited vibrational states from atomic recombination on cold graphite surfaces*. Chemical Physics Letters, 2008. **455**(4-6): p. 174-177.

122. Duley, W.W. and D.A. Williams, *The Formation of Interstellar H2 on Amorphous Silicate Grains*. Monthly Notices of the Royal Astronomical Society, 1986. **223**(1): p. 177-182.

123. Lebourlot, J., G.P.D. Forets, E. Roueff, A. Dalgarno, and R. Gredel, *Infrared Diagnostics of the Formation of H-2 on Interstellar Dust*. Astrophysical Journal, 1995. **449**(1): p. 178-183.

124. Lemaire, J.L., *Private Communication*. 2008.

125. Burton, M.G., D. Londish, and P. Brand, *Formation pumping of molecular hydrogen in the Messier 17 photodissociation region*. Monthly Notices Of The Royal Astronomical Society, 2002. **333**(4): p. 721-729.

126. Burton, M.G., M. Bulmer, A. Moorhouse, T.R. Geballe, and P. Brand, *Fluorescent Molecular-Hydrogen Line Emission In The Far-Red*. Monthly Notices Of The Royal Astronomical Society, 1992. **257**(1): p. P1-P6.

127. Wagenblast, R., *Interpretation Of The Level Population-Distribution Of Highly Rotationally Excited H-2-Molecules In Diffuse Clouds*. Monthly Notices Of The Royal Astronomical Society, 1992. **259**(1): p. 155-165.

128. Rosenthal, D., F. Bertoldi, and S. Drapatz, *ISO-SWS observations of OMC-1: H-2 and fine structure lines*. Astronomy and Astrophysics, 2000. **356**(2): p. 705-723.

129. Hudson, R. *The Cosmic Ice Laboratory, Interstellar Molecules*. 2009 26/04/2009 [cited 2009 27/10/2009]; Available from: http://www-691.gsfc.nasa.gov/cosmic.ice.lab/interstellar.htm

130. Garrod, R.T., J.M.C. Rawlings, and D.A. Williams, *Chemical effects of H-2 formation excitation*. Astrophysics and Space Science, 2003. **286**(3-4): p. 487-499.

131. Weck, P.F. and N. Balakrishnan, *Dynamics of chemical reactions at cold and ultracold temperatures*. Journal of Physics B-Atomic Molecular and Optical Physics, 2006. **39**(19): p. S1215-S1227.

132. Sultanov, R.A. and N. Balakrishnan, *Oxygen chemistry in the interstellar medium: The effect of vibrational excitation of H-2 in the O(P-3)+H-2 reaction*. Astrophysical Journal, 2005. **629**(1): p. 305-310.

133. Roberts, J.F., J.M.C. Rawlings, S. Viti, and D.A. Williams, *Desorption from interstellar ices*. Monthly Notices of the Royal Astronomical Society, 2007. **382**(2): p. 733-742.

Chapter Two

Experimental Set-up to Study HD Formation

2.1 Overview

In Chapter 1, the formation of molecular hydrogen on interstellar dust grains was discussed. It is currently unclear how the binding energy of 4.5 eV released by H_2 formation is redistributed in the interstellar medium (ISM). The energy may flow into the dust grain surface on which formation occurs, or may be manifest in the ro-vibrational excitation of the nascent H_2 molecule. If the degree of ro-vibrational excitation is high, this may significantly affect the energy budget of chemical reactions in the ISM [1, 2].

The UCL Cosmic Dust Experiment probes the internal ro-vibrational energy distribution of a nascent hydrogen molecule, once it has desorbed from an analogue of an interstellar dust grain surface. This chapter will describe the experimental set-up and method employed in the UCL Cosmic Dust Experiment. The experimental arrangement employed has also been described in detail elsewhere [3-7]. To mimic an interstellar environment, the experiment is carried out *in vacuo*. H- and D-atoms, in separate beams, are transported onto a graphite surface held at 15 K. The atoms recombine to form HD, which desorbs from the surface in a distribution of ro-vibrationally excited states. HD in one particular ro-vibrational state is state-selectively ionized *via* Resonance Enhanced Multi-Photon Ionization spectroscopy (REMPI), using UV photons produced by the laser system. The HD^+ ions are detected by a time-of-flight mass spectrometer (TOFMS). The yield of HD^+ ions is directly

proportional to the population of the HD ro-vibrational state, after some correction factors are included. The process is repeated for HD in many rotational states within each vibrational state to give relative populations of the ro-vibrational states. The experiments carried out within this thesis investigate HD formed in vibrational states $v = 3 – 7$. This thesis follows on from previous work on the design and construction of the Cosmic Dust Experiment [5, 6] and studies of H_2 and HD formed in vibrational states $v = 0 – 2$ using the Cosmic Dust Experiment [3].

2.2 Vacuum Set-up

In order to simulate interstellar conditions as closely as possible, the UCL Cosmic Dust experiment must be conducted under ultra-high vacuum (UHV) conditions. Molecular clouds, the densest interstellar regions, contain ~ 10^{10} hydrogen nuclei m^{-3} which corresponds to a pressure of 10^{-13} Torr [8]. Indeed diffuse clouds, where the effects of H_2 formation are more significant because there is proportionally more atomic hydrogen available, will be even less dense at ~ 10^{7} hydrogen nuclei m^{-3} [8]. However, with the current set-up, a base pressure of only 10^{-10} Torr can be achieved with both atom sources turned off, as is usual for UHV experiments. To attain this low pressure, a vacuum system has been set-up as shown in Figure 2.1. Two vacuum chambers are used, one to house the sources of atomic hydrogen and deuterium which will be referred to as the ‘source chamber’, and the other to house the highly oriented pyrolytic graphite (HOPG) surface, which will be referred to as the ‘target chamber’. These chambers are made of stainless steel and are sealed with conflat flanges. UHV is achieved using turbomolecular pumps, which have a pumping speed of 400 l s^{-1}, backed by two-stage rotary pumps on both chambers, coupled with selective warming of the chamber to return water into the gas phase so it can be pumped away. There is also a titanium sublimation pump (TSP) which can be used to coat a chamber wall with a clean titanium film. Background H_2 molecules adsorb onto the titanium so that they are effectively removed from the system, thus lowering the chamber pressure. A Penning gauge and an ion gauge are used to monitor the pressures in the source and target chambers respectively.

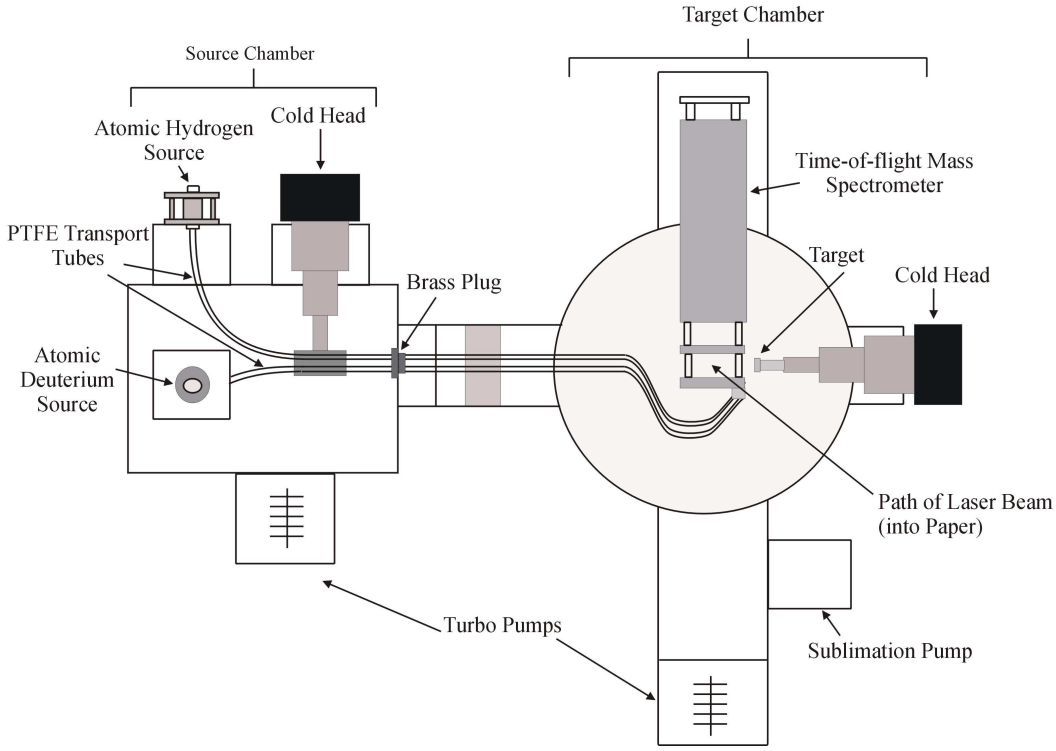

Figure 2.1 Schematic diagram of vacuum chamber set-up (not to scale).

2.3 H-atom and D-atom Sources

It has been shown in other work [3, 4] that the current H-atom source also produces excited H_2 which cannot be clearly distinguished from H_2 formed on the graphite surface. H_2 from the H-atom source cannot be eliminated unless the H-atom flux is reduced below a detectable level. Thus the UCL Cosmic Dust Experiment now studies HD formation using both H- and D-atom sources. For the experiments discussed in this thesis, no ro-vibrationally excited HD has been detected entering the target chamber. Also if either the H- or D-source is turned off, no HD is detected. Therefore, the HD signals must originate from HD formed on the graphite surface. Prior experiments [3, 4], in which the H-atom source did not produce ro-vibrationally excited H_2, achieved by use of a different microwave generator, have shown that the ro-vibrational distribution of nascent HD measured here is very similar to that of nascent H_2. The differences between the isotopologues will be discussed further in Chapter 4.

The H- and D-atom beams are created in separate pyrex glass cells, *via* microwave dissociation of high purity H_2 and D_2 gases. These pyrex cells were passivated before installation by being immersed in ortho-phosphoric acid (H_3PO_4) for over 12 hours, then rinsed in distilled water. This minimizes any recombination on the glass walls of the cell [9]. Copper radiators fit around the pyrex cells to transmit microwave radiation into the molecular gas. This type of atom source was designed by McCullough *et al.* [10, 11]. The H-atom and D-atom sources are supplied with microwaves from the same Sairem generator, with the microwave frequency being 2.45 GHz and the power delivered being 180 W. In order to deliver the microwaves efficiently, it is important to minimize the power reflected back to the generator. A reflected power of less than 10% was achieved by connecting an external reflected power meter to the microwave generator, from which Sucoflex waveguides were connected to either side of the radiator on each source. A photograph of the H-atom source is shown in Figure 2.2.

Figure 2.2 Photograph of the H-atom source.

The sources need to 'warm up' for 2 – 3 days to achieve optimum H and D production; therefore they are left on at all times. It is estimated that the dissociation fraction of the molecular gas is 90% on leaving the source cell [10, 11] and 20% at the graphite surface. Experiments have found the H-atom flux reaching the surface is ~ 10^{13} cm^{-2} s^{-1} [6]. Note that the continuous running of the sources increases the source

chamber pressure to ~ 10^{-6} Torr. The resulting pressure is 10^{-8} – 10^{-7} Torr in the target chamber. However, this pressure increase is due to pure hydrogen atomic or molecular gases, not water vapour, which would be the major contaminant in other laboratory studies conducted at similar pressures. Water vapour would readily form ice covering the graphite surface. As mentioned before, even the standard UHV base pressure of 10^{-10} Torr is still several orders of magnitude higher than typical pressures of the ISM.

Since the sources are never turned off, there is a system of safety trips in place, which may be bypassed if necessary. The safety trips turn off the microwave generator and stop the gas flow to the sources if the pressure in the source chamber reaches $\geq 6 \times 10^{-5}$ Torr or the pressure in the target chamber reaches $\geq 1 \times 10^{-5}$ Torr. The temperature of the pyrex cells must be monitored, not only to avoid the apparatus overheating, but also because recombination of atoms on the glass surface increases with temperature. Heat and light sensors adjacent to the sources also activate the safety trips if the cells rise in temperature above 25 °C or if the brightness of the plasma in the cells falls below a certain threshold.

The atomic beams are carried separately from the sources and piped up to the graphite surface using polytetrafluoroethylene (PTFE) tubing, because PTFE is highly inert and has a very low H_2 recombination efficiency [12]. The atoms leave the pyrex cells *via* a narrow capillary to enter the PTFE tubes of outer diameter 6mm. The 'bottleneck' ensures that the source cells remain at an optimum pressure of 0.5 Torr for maximum dissociation. The H- and D-atom beams collide with the PTFE tubing walls as they are transported, so that the atoms are translationally cooled back to room temperature. The tube passes through an opening from the source chamber to the target chamber. The hole is surrounded by a brass seal to prevent leakage of gas from the source chamber into the target chamber, other than by way of the atom beams. This arrangement allows the two chambers to be differentially pumped; the pressure in the target chamber stays low, at ~ 10^{-8} Torr, whereas the pressure in the source chamber is ~ 10^{-6} Torr to maintain optimum pressure in the discharge cells. The ends of the PTFE tubing are held only 2 mm away from the surface, so that the atom beams do not interact with each other before impacting on the surface. This ensures that vibrationally-excited HD cannot form in the dissociation cells, or in other parts of the

source chamber or the target chamber, because the H- and D-atoms only meet at the target surface.

2.4 Graphite Surface and Cold Head

As discussed in Chapter 1, dust grains in the ISM are likely to be carbonaceous. In order to simulate the dust grain surface to a first approximation, highly oriented pyrolytic graphite (HOPG) has been used for these experiments. HOPG has a very pure, well-ordered and non-porous surface in contrast to the fluffy interstellar dust grains covered by icy mantles. However, it is important to first understand this simple system before investigating more complex configurations of carbonaceous material. Another benefit of using HOPG is that there have been many experimental and theoretical investigations of H_2 formation on graphite which may be compared to our results [13-32].

The HOPG substrate has dimensions 10 mm × 20 mm × 2 mm and a mosaic spread of of 3.5° ± 1.5°. The mosaic spread is a measure of the relative disorder of the atomic layers within the graphite, thus a more ordered sample has a lower value of mosaic spread. The sample was cleaned using the 'scotch-tape method' [33] to expose a fresh layer of graphite before attachment to the target mount. The HOPG is also cleaned prior to each experiment by heating to 500 K, which removes any unwanted adsorbates from the surface [34, 35].

The HOPG target must be close not only to the ends of the PTFE tubing but also to the laser focus (see Figure 2.3). The laser interaction region is 2 cm directly above the surface so that some of the hydrogen molecules desorbing from the substrate will encounter UV photons and be ionized. Any newly formed molecules which do not reach the laser interaction region will not be detected by the TOFMS. When the ends of the PTFE tubing are moved, such that HD molecules form away from the laser interaction region, no HD signals are detected. Hence, any detected molecules do not collide with the chamber walls or other apparatus before ionization.

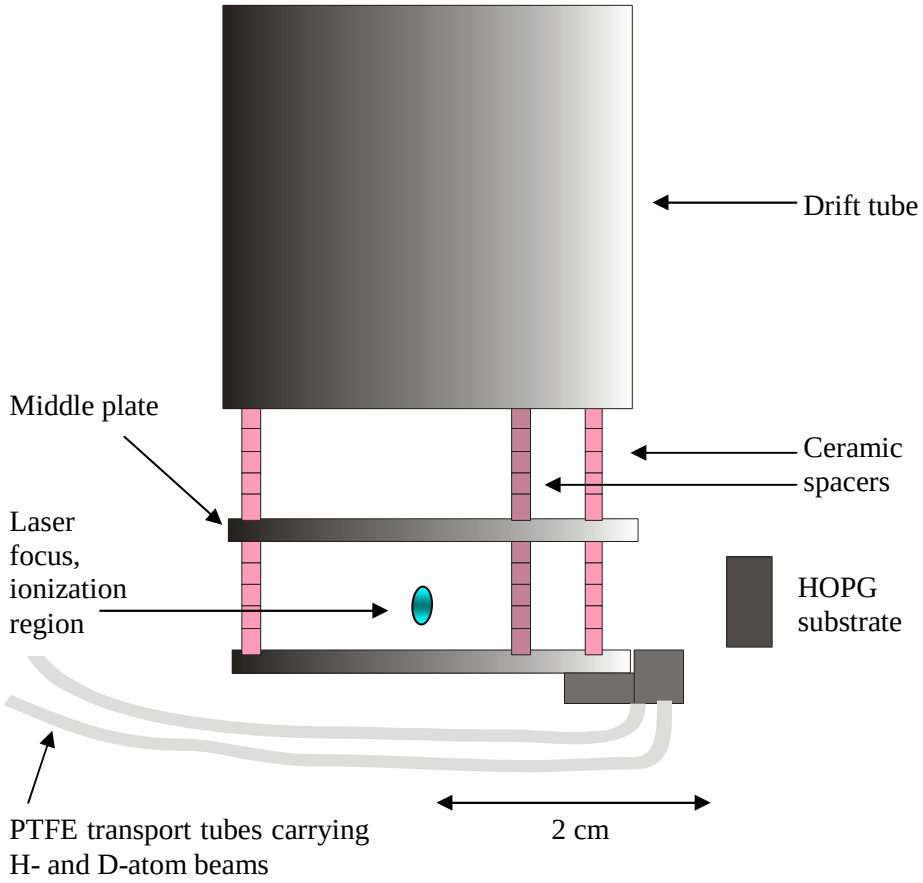

Figure 2.3 Schematic diagram to show the arrangement of the HOPG surface, PTFE tubing, TOFMS and the laser focus, where HD molecules are ionized.

The target mount holds the HOPG substrate and is detachable from the coldhead. The set-up shown in Figure 2.4 is designed to cool any substrate to temperatures of interstellar relevance. At present, the HOPG sample is cooled cryogenically to temperatures of 12 – 15 K by a closed cycle helium compressor driving a two-stage 12 W coldhead, which has a maximum operating temperature of 330 K. The coldhead can achieve temperatures of 9 K from room temperature in approximately 45 minutes, but the sample cannot currently be cooled to T < 10 K due to thermal contact limitations. However this temperature range is perfectly suitable to simulate interstellar dust grains, which typically have temperatures of 10 – 20 K [36, 37].

Thermal conductivity between the coldhead and mount has been optimized by use of a 1 mm thick piece of sapphire. When sapphire is cooled below 50 K, it is a very efficient thermal conductor but when it is heated above 200 K, it is a very poor thermal conductor [38]. Hence the HOPG surface can be cooled to 12 K during the

experiments and also heated to 500 K before each experiment, allowing the coldhead to remain in use during cleaning, without heating above its maximum operating temperature. It is possible to heat the mount above 1000 K, but studies have shown that only 500 K is required to desorb impurities from the surface [35]. The target mount has a tantalum strip heater attached to raise the temperature. An N-type thermocouple measures the temperature of the surface. A silicon thermodiode monitors the temperature of the coldhead. An aluminium radiation shield protects the coldhead and target mount from radiative heating emitted from the chamber to keep the surface temperature stable at T ~ 15 K.

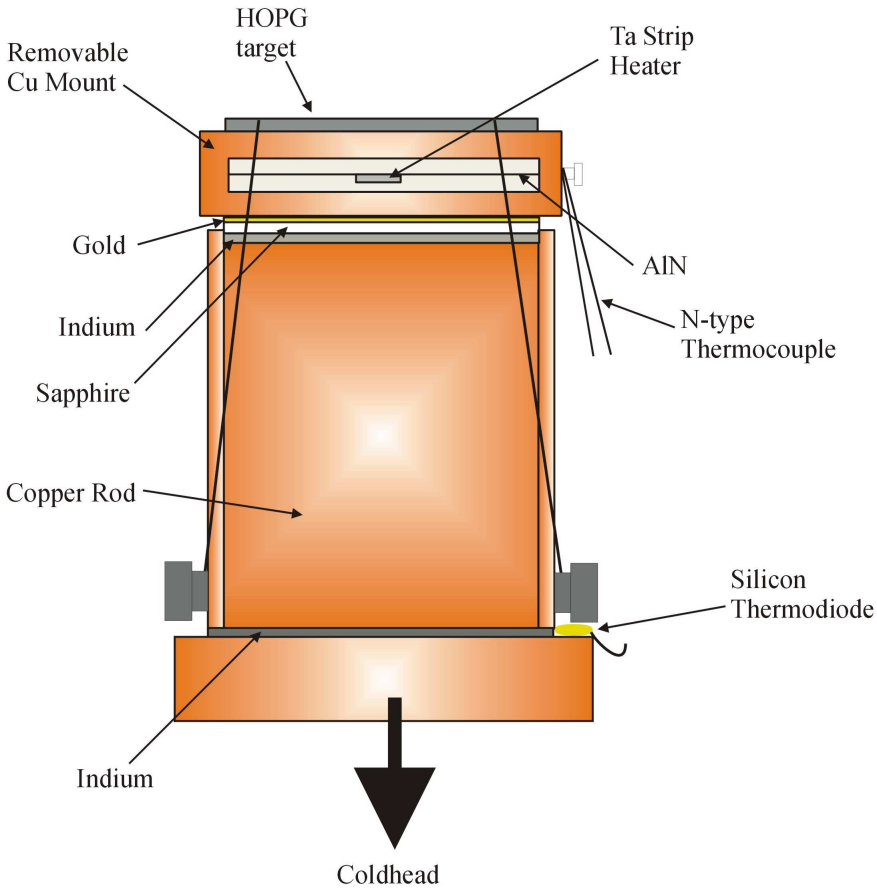

Figure 2.4 Schematic diagram of the HOPG substrate and target mount

2.5 Time-of-Flight Mass Spectrometer

After the HD molecules are ionized in the interaction region of the laser, they are detected by time-of-flight mass spectrometry. A schematic diagram of the TOFMS is shown in Figure 2.5 and follows the basic arrangement of Wiley and McLaren [39]. Advantages of using a TOFMS to detect the HD ions are that it is compact and relatively easy to build, entailing neither complex moving parts nor accurate magnetic fields.

2.5.1 Principles of Mass Spectrometry

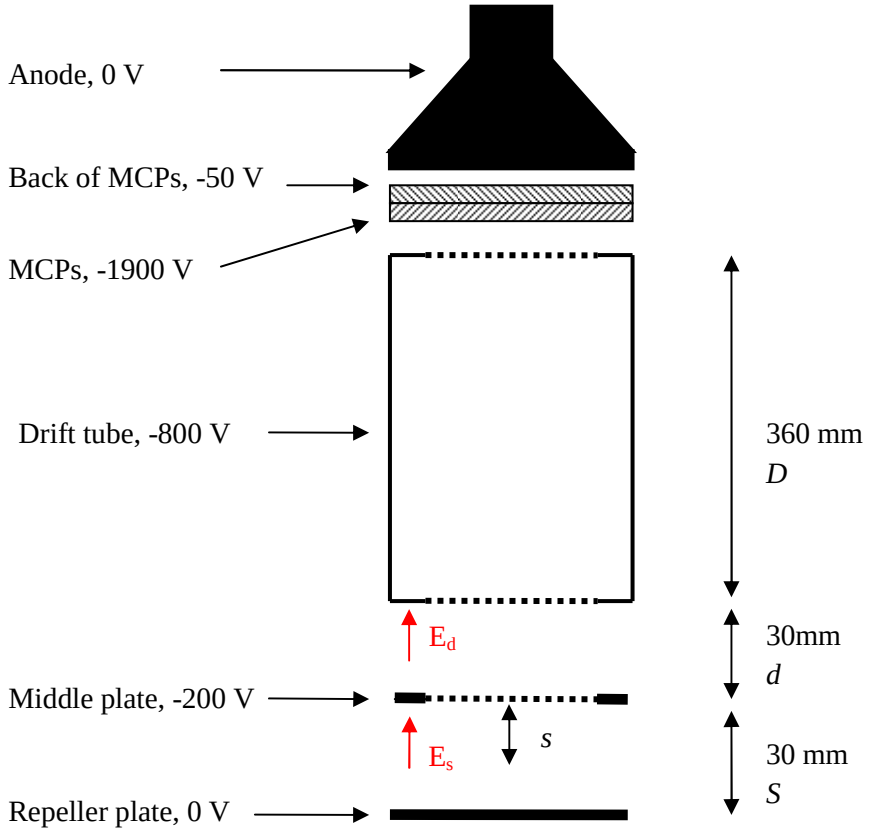

Figure 2.5 Schematic diagram of the time-of-flight mass spectrometer, where D is the length of the drift tube, d is the distance between the middle plate and the drift tube, S is the distance between the repeller and middle plates, E_s is the electric field between the repeller and middle plates, E_d is the electric field between the middle plate and drift tube and *s* is the distance the ion travels to reach the middle plate. The microchannel plates (MCPs) are located at the end of the drift tube.

A TOFMS uses a series of electric fields to accelerate ions. The fields are applied to cations by holding a series of plates and grids at negative voltages, with the repeller

plate and middle plate either side of the ionization region. The repeller plate may be held at a small positive voltage or ground. The fields accelerate ions through grids in the middle plate and into an area of uniform potential called the drift tube or flight tube. At the end of the drift tube is a microchannel plate detector (MCP). A laser pulse marks the start time at which HD molecules are ionized and begin travelling down the drift tube. Ions of different masses will arrive at the MCP at different times. Thus the mass/charge ratio of an ion can be determined by measuring the time of flight of the ion through the drift tube using the equation

$$t = k\sqrt{m} + C \qquad 2.1$$

where t is the time of flight of the ion, m is the mass of the ion, k is a constant relating to the electric fields and dimensions of the spectrometer and C is a constant relating to the electronic timing system. The output of the TOFMS is a mass spectrum of ion counts detected plotted against ion flight times. Constants k and C are determined using calibration experiments, by identifying the species responsible for two peaks in the mass spectrum. Equation 2.1 is derived as shown below:

As an ion of charge q moves a distance, s', through an electric field, E, it acquires an energy, U', given by

$$U' = q\,s'\,E \qquad 2.2$$

Thus the total energy, U, acquired by an ion as it moves from its original position in the ionization region and through the drift tube to be detected by the MCP is

$$U = U_0 + q\,s\,E_s + q\,d\,E_d \qquad 2.3$$

where s is the distance the ion travels to reach the middle plate and d is the distance the ion travels from the middle plate to the drift tube, as shown in Figure 2.5. There are no accelerating fields within the drift tube. The total time of flight of the ion, t, is the sum of the time the ion takes to traverse distances s, d and D, where D is the length of the drift tube such that

$$t = t_s + t_d + t_D \qquad 2.4$$

If v_0 is the initial velocity of the ion, v_s is the ion's velocity after being accelerated through a distance s, and a is the acceleration the ion undergoes due to the electric field, E_s, then Newton's laws of motion state that

$$a = (v_s - v_0) / t_s \qquad 2.5$$

and

$$v_s^2 = v_0^2 + 2 a s \qquad 2.6$$

The above equations can be rearranged to give

$$t_s = \frac{(v_0^2 + 2as)^{\frac{1}{2}} \pm v_0}{a} \qquad 2.7$$

Only the positive root is taken in equation 2.7 because v_s must be positive as positive ions are always accelerated towards the drift tube. The ± arises in front of v_0 as ions will be created with initial velocities both towards and away from the detector.

The initial kinetic energy of the ion U_0 will be of the form

$$U_0 = ½ m v_0^2 \qquad 2.8$$

which may be rearranged to find v_0 and substituted into equation *2.7* to give

$$t_s = \left(\left(\frac{2U_0}{m} + 2as \right)^{\frac{1}{2}} \pm \left(\frac{2U_0}{m} \right)^{\frac{1}{2}} \right) \frac{1}{a} \qquad 2.9$$

Newton's second law asserts that the net force on a particle is proportional to its acceleration, thus

$$F = m a = q E_s \qquad 2.10$$

which implies

$$a = q E_s / m \qquad 2.11$$

Substituting 2.11 into 2.9 gives

$$t_s = \left(\left(\frac{2U_0}{m} + \frac{2sqE_s}{m} \right)^{\frac{1}{2}} \pm \left(\frac{2U_0}{m} \right)^{\frac{1}{2}} \right) \frac{m}{qE_s} \qquad 2.12$$

which can be simplified to

$$t_s = \frac{(2m)^{\frac{1}{2}}}{qE_s} \left((U_0 + sqE_s)^{\frac{1}{2}} \pm (U_0)^{\frac{1}{2}} \right) \qquad 2.13$$

Similarly t_d, the time the ion takes to travel from the middle plate to the drift tube can be derived using

$$t_d = \frac{v_d - v_s}{a_d} \qquad 2.14$$

where v_d is the ions velocity after being accelerated though a distance d and a_d is the acceleration of the ion as it passes through an electric field E_d. As before, v_d is found using

$$v_d^2 = v_s^2 + 2a_d d = v_s^2 + \frac{2dqE_d}{m} \qquad 2.15$$

to yield

$$t_d = \frac{(2m)^{\frac{1}{2}}}{qE_d}\left(U^{\frac{1}{2}} - (U_0 + qsE_s)^{\frac{1}{2}}\right) \qquad 2.16$$

The ions then travel at constant velocity through the drift tube to give

$$t_D = \frac{D}{v_d} = \frac{D}{\left(v_s^2 + \frac{2dqE_d}{m}\right)^{\frac{1}{2}}} \qquad 2.17$$

Substituting 2.6 and 2.8 into 2.17 gives

$$t_D = \frac{D}{\left(\left(\frac{2}{m}\right)(U_0 + sqE_s + dqE_d)\right)^{\frac{1}{2}}} \qquad 2.18$$

Substituting 2.3, this simplifies to

$$t_D = \frac{(2m)^{\frac{1}{2}} D}{2U^{\frac{1}{2}}} \qquad 2.19$$

Thus 2.4 then becomes

$$t = (2m)^{\frac{1}{2}}\left\{\frac{\left((U_0 + sqE_s)^{\frac{1}{2}} \pm (U_0)^{\frac{1}{2}}\right)}{qE_s} + \frac{\left(U^{\frac{1}{2}} - (U_0 + sqE_s)^{\frac{1}{2}}\right)}{qE_d} + \frac{D}{2U^{\frac{1}{2}}}\right\} \qquad 2.20$$

Equation 2.20 shows that the time of flight of the ion is proportional to root of the mass of the ion. The time of flight also depends on the charge on the ion, the dimensions of the TOFMS and the electric fields which are all constant. Additionally, there will be delays from the electronics of the detection system which are independent of the ion trajectory and are constant, such that

$$t = \sqrt{m}\sqrt{2}\left\{\frac{\left((U_0 + sqE_s)^{\frac{1}{2}} \pm (U_0)^{\frac{1}{2}}\right)}{qE_s} + \frac{\left(U^{\frac{1}{2}} - (U_0 + sqE_s)^{\frac{1}{2}}\right)}{qE_d} + \frac{D}{2U^{\frac{1}{2}}}\right\} + C \qquad 2.21$$

Thus, the total time of flight of the ion is of the form $t = k\sqrt{m} + C$.

The analysis above may only be applied if all ions are ejected from the ionization region at the same time. The voltages on the repeller plate may be pulsed to set the ions in motion; however this technique can often lead to ringing due to sudden changes in voltage. The UCL Cosmic Dust experiment avoids this problem by using constant voltages and the ionizing laser is pulsed to create the ions simultaneously. The start of the pulse also activates the electronic detection system of the TOFMS. The pulses from the ionizing laser are 4 ns long during which ions are created. Thus, the ions are produced in packets that have a temporal distribution of at least 4 ns 'wide', which will contribute to the peak width of the mass spectra, on detection by the MCP.

Peak broadening is the spread in the flight times of ions with the same mass-to-charge ratio, so that all ions do not arrive simultaneously to form an infinitely sharp peak in the mass spectrum. It is important to minimize the peak broadening, such that the ions are detected within a narrow time window. This ensures that the flight times of ions with adjacent masses will not overlap. Peak broadening is also dependent on the positions of the ions when they were first created or accelerated. Ions formed further away from the drift tube form at a higher potential, hence have higher kinetic energies and will travel faster down the drift tube. Consequently ions which are formed further away from the drift tube catch up with those ions formed more closely to the drift tube. There will be some focus distance, and thus some flight time, where the ions will draw level with each other, despite their different initial positions, such that the time-of-flight spread is small. This focus distance can be expressed as the distance at which ions with initial position $s = s_0 \pm \frac{1}{2}\delta s$ from the detector pass ions with initial position $s = s_0$. By differentiating equation 2.21 and setting $\left(\frac{dt}{ds}\right)_{s_0} = 0$, we can calculate the electric field required for the ions to arrive coincidently at the particular distance of the detector. The voltages on the plates can then be adjusted so that the

ions arrive coincidently in the region of the detector. Minimizing the peak broadening with respect to the initial positions of the ions is known as space focusing [39]. The UCL Cosmic Dust experiment does not require much space focusing since the HD^+ ions are formed in the very small volume of the laser beam waist.

There is also peak broadening in the mass spectrum due to ions having a range of initial kinetic energies. For example, consider one HD molecule moving towards the drift tube and another HD molecule moving away from the drift tube at the time of ionization. The HD ion initially moving away from the drift tube will be decelerated by the electric fields, come to a halt, then accelerate towards the drift tube. A time lag arises between the two ions, known as the 'turn-around time'. Minimizing this time lag is known as energy focusing [39], and cannot be carried out in the linear TOFMS used in this study. However in this investigation, peak broadening of TOF mass spectra was employed to infer the translational energy of the nascent HD formed on the HOPG surface. Further details on how to calculate an upper limit for the HD translational energy is given in Chapter 3

.

2.5.2 Plates, Flight Tube and Detector

To ensure that ions do not collide with other molecules as they approach the detector, the TOFMS must be *in vacuo*, hence it is housed inside the target chamber. MCPs should be used at pressures $\leq 10^{-5}$ Torr. At higher pressures, MCPs become damaged due to ion impacts producing an excess of electrons and electrical discharges.

A schematic of the TOFMS is shown in Figure 2.5. The repeller and middle plates both have a diameter of 50 mm and are on either side of the laser ionization region. The middle plate is mounted on ceramic spacers 30 mm above the repeller plate and 30 mm below the drift tube, as shown in Figure 2.3 and Figure 2.5. For most experiments conducted in this thesis, there was a fine Ni mesh fixed across the middle plate. This type of grid allows 98% transmission of the ions and is used to keep the electric field uniform throughout the TOFMS. The drift tube is 360 mm long and also has grids at each end. However for some experiments, all grids were removed. The lack of grids, and thus a decrease in field uniformity, did not make any discernable difference to the time-of-flight mass spectra. The spectra did not appear to change

because the ionization region in this experiment is very localized, hence the ions all originate from similar initial positions within the field. Nevertheless, the grids were later replaced for consistency.

As shown in Figure 2.5, the detector consists of MCPs placed directly above the drift tube. The MCP is constructed of tubes, or microchannels, of width 10 μm cut at an angle to the plate. When an ion impacts on the wall of a channel, an electron is released. As the electron travels down the plate, further collisions with the channel walls ensue and liberate a cascade of electrons to form a charge pulse. Over 10^4 electrons are produced per ion impact, which are accelerated 5 mm to the anode by a small voltage. The anode is funnel shaped, with its tapered end attached to a wire. This gradual change in shape avoids any sudden changes in capacitance which can cause electrical interference, known as ringing. The charge pulse is then conducted away by the wire and amplified by a series of electronics described in Section 2.5.3.

The repeller plate is grounded, not held at a positive potential as is common for time-of-flight mass spectrometers. This is so that the repeller plate does not attract any photoelectrons, produced due to reflected light from the laser, which may collide with the plates to release ions. These ions could then be detected and create noise in the mass spectra. The middle plate is held at a voltage of -200 V, the drift tube at -800 V and the MCP at -1900 V. These voltages were determined from experiment for space focusing. The back of the MCP is held at -50 V and the anode is grounded to attract electrons emerging from the MCP.

2.5.3 Electronic Detection System

As previously mentioned, mass spectrometry may only be performed if the ions are formed or ejected from the ionization region simultaneously. HD^+ ions are only created when the laser pulse begins and are immediately accelerated by the electric fields. When the laser pulse is switched on, a ‘start’ signal is sent by the pulse generator to the time-to-digital-converter (TDC), which initiates a ‘look window’. The look window is the period of time, typically 9 μs long, in which ions may impact on the MCP and detection may occur. A ‘stop’ signal is sent to the TDC each time an ion

is detected. A signal to 'end' the look window is also transmitted from the pulse generator to the TDC.

The detection signal, the aforementioned cascade of electrons, travels from the MCP and anode through a system of electronics shown in Figure 2.6. The signal is processed by an impedance matching circuit, a fast pre-amplifier (Ortec VT120) and amplifier (Ortec 573) in order to increase the signal strength. The signal is then received by a constant fraction discriminator (CFD) (Ortec 935) which outputs an electrical pulse that can be read by the TDC as an ion detection. The ion counts from the TDC are then sent *via* a CAMAC/GPIB interface to a computer, which records the number of ions detected and the flight time of each ion. TOF mass spectra and REMPI spectra, which will be explained in detail in Chapter 3, can be calculated by the computer.

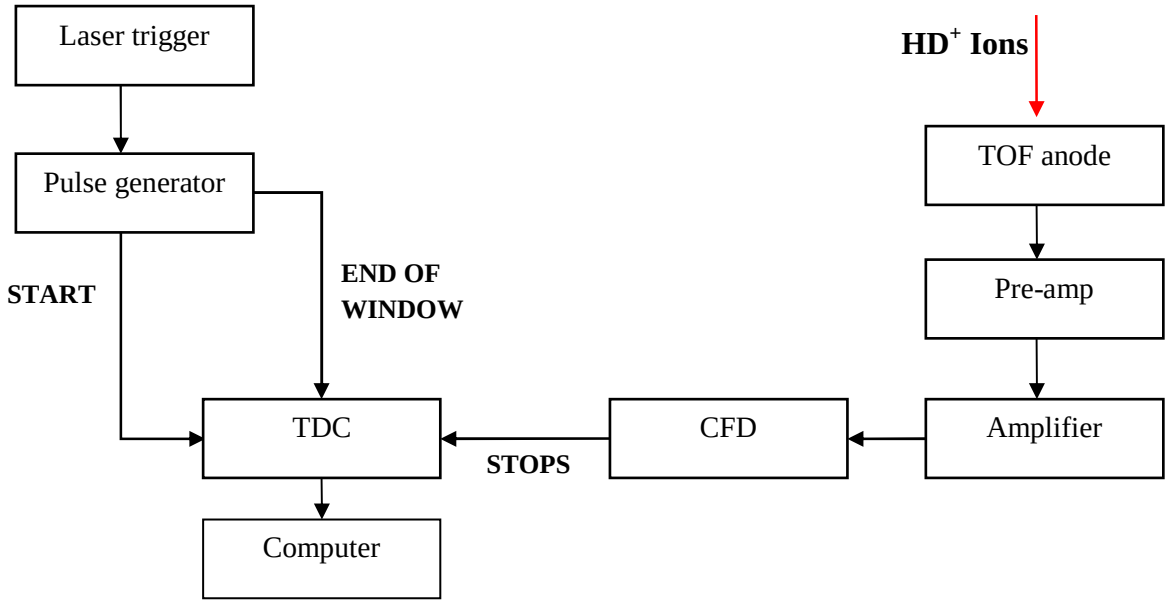

Figure 2.6 Flowchart showing the electronic detection system for the TOFMS.

2.6 The Laser System

UV photons of the required frequency to ionize HD formed in vibrational states $v = 3 – 7$ are generated by a laser system consisting of two different lasers. The primary laser is a pulsed Nd:YAG laser, which produces light that is frequency tripled to pump the Sirah dye laser. The dye laser is tuneable, meaning that it is a source of light

of variable wavelengths. The light from the dye laser is then frequency doubled to give photons of wavelength 210 – 250 nm. The photons are directed into the vacuum chamber using beam-steering optics. These photons are used to state-selectively ionize the nascent HD molecules formed on the HOPG surface *via* REMPI spectroscopy. The HD^+ ions are then detected by the TOFMS. This section on the laser system will describe UV photon generation, beam steering and the use of baffles to minimize reflected light within the vacuum chamber. The principles and methodology of the REMPI technique will be discussed in Section 2.8.

2.6.1 Nd:YAG Laser

The Neodymium: Yttrium Aluminium Garnet laser (Nd:YAG) is a solid state laser. A rod of $Y_3Al_5O_{12}$ contains impurities of Nd^{3+} ions [40]. These Nd^{3+} ions are randomly distributed within the YAG lattice, residing in sites instead of yttrium ions. Gas phase Nd^{3+} ions have many degenerate energy levels, but when surrounded by the YAG crystal lattice, the energy levels are split to remove the degeneracy. This is due to the YAG lattice generating a 'crystal field' around the Nd^{3+} ions. Some transitions, forbidden for gas phase Nd^{3+} ions, become allowed for Nd^{3+} ions in the lattice. The ground and first excited states of the Nd^{3+} ions are split into groups of levels, as shown in Figure 2.7.

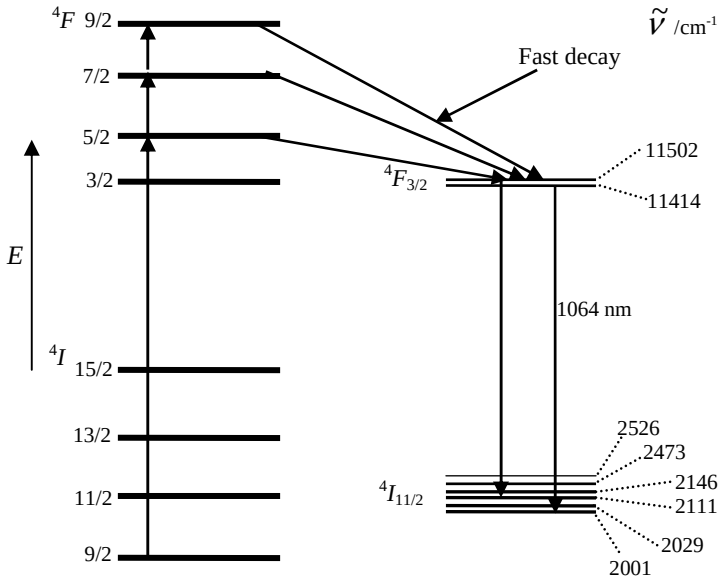

Figure 2.7 Energy level diagram for the transitions in the Nd:YAG laser. $\tilde{\nu}$ is the wavenumber of the particular level, and is given in cm^{-1}.

The groups of energy levels of the Nd^{3+} ion are pumped using two xenon flash-lamps. The Nd^{3+} ions are excited from the ground $^4I_{9/2}$ level to levels above the $^4F_{3/2}$ state. From these higher levels, there is rapid non-radiative decay to the $^4F_{3/2}$ state. Photons are then emitted as the Nd^{3+} ion decays radiatively from the $^4F_{3/2}$ level back to the ground state [41]. The most intense laser transition occurs in the infrared at 1064 nm and is a superposition of the two transitions shown in Figure 2.7. The YAG matrix takes no part in the lasing action.

The laser is forced to produce pulsed laser radiation by use of Q-switching [41, 42]. The intensity of light, and thus energy of the pulses, can also be controlled by this method. The Q-switch is an electro-optic device known as a Pockels cell inserted into the laser cavity. The Q-switch is used to introduce a time-dependent loss in the cavity, measured by the Q-factor. A poor Q-factor means that the cavity conditions are unsuitable for lasing. The Q-switch can be rapidly turned off and on by an electrical signal to the Pockels cell. Whilst the Q-switch is off, the population inversion of the Nd^{3+} ions increases, until the levels are saturated. Thus the longer a Q-switch is turned off, the more intense the resulting laser pulse, until the upper states are saturated. When the Q-switch is turned on, a light wave traverses the cavity to stimulate photon emission and lasing begins. The Nd:YAG pulses at a frequency of 10 Hz with each pulse lasting a duration of 4 – 6 ns. The 1064 nm light is frequency tripled to 355 nm by a potassium di-hydrogen phosphate (KD*P, KH_2PO_4) crystal and a barium borate (BBO, β-BaB_2O_4) crystal. This third harmonic is used to pump the tuneable Sirah dye laser when investigating HD in vibrational states $v = 3 – 7$. A description of higher order frequency generation in non-linear crystals, such as frequency tripling and doubling, phase matching and optical mixing can be found in Section 2.6.3.

For the experiments studying HD in vibrational states $v = 3 – 7$, the 355 nm light pulses typically have energy ~ 300 mJ per pulse, although this is reduced to 100 mJ per pulse by increasing the delay between the Q-switch and the flash lamp pumping in order to conserve the dye in the Sirah laser. For HD in lower vibrational levels, $0 \leq v \leq 2$ which were studied in previous experiments [3, 4], the dye laser was pumped by the 523 nm second harmonic. The pulses at 523 nm were generated *via* energy doubling, with energies typically ~ 400 mJ per pulse.

2.6.2 Tuneable Dye Laser

In order to photoionize HD in a variety of ro-vibrational states, we require a source that can produce photons of a large range of wavelengths. This variable light source is the Sirah dye laser, which is pumped by the 355 nm third harmonic of the Nd:YAG laser described above. Dye lasers consist of an organic dye dissolved in a solvent such as methanol. The dye is excited by the pulses of light from the Nd:YAG laser and fluoresces over a broad wavelength range. An advantage of a dye laser is that it is tuneable over this broad fluorescence wavelength range [41, 42]. This allows us to scan over a range of wavelengths until the ionization signal is found, meaning that photons of the correct wavelength to ionize HD have been generated within the scan.

The Nd:YAG laser light pumps the dye from the ground S_0 state to S_1, the first excited electronic state, or sometimes to the S_2 electronic state, as shown below in Figure 2.8. These are all singlet electronic states.

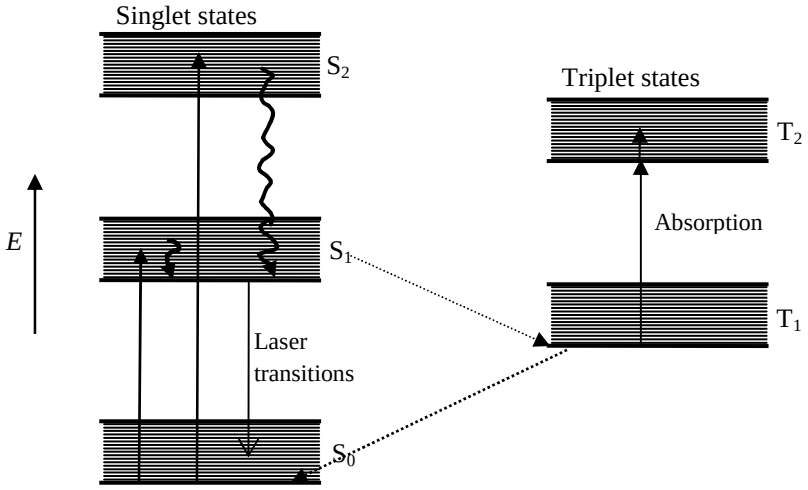

Figure 2.8 Energy level diagram for the transitions in a dye laser.

The excited states decay to the lower ro-vibrational levels of the S_1 state *via* non-radiative collisional relaxation. This leads to a population inversion between the ro-vibrational levels of the S_1 and S_0 states. Due to the ro-vibrational levels within each state being closely spaced, there is the possibility of many transitions; hence fluorescence occurs over a broad wavelength range [41, 42].

There are triplet states in the dye which may also affect the laser action [43]. There may be non-radiative decay from the S_1 to T_1 states, although this transition is quantum mechanically unfavourable. The T_1 state may be pumped to the T_2 state by the same range of frequencies of light that pump the laser transition. Any photons absorbed by this $T_1 \rightarrow T_2$ transition cannot be absorbed in the $S_0 \rightarrow S_1$ transition, which results in a reduction in gain of the laser. This problem can be overcome by pulsing the Nd:YAG light. Time between pulses allows the T_1 state to decay back to the S_0 state; the T_1 level is emptied before excitation to the T_2 level may occur. Pumping pulses of less than 1 μs duration are required to avoid significant population of the T_1 level and appreciable loss in laser gain.

The laser dyes chosen for the experiment depend on the wavelength of light required to ionize HD in a particular ro-vibrational level. Coumarin dyes were used as they produce photons of a large wavelength range of about 440 – 560 nm. These photons are frequency doubled, which will be explained further in Section 2.6.3. The dyes used are shown in Table 2.1, which also includes the dyes used in the laser system for vibrational states $v = 0 – 2$ studied in previous work [3, 4].

v	**Laser dye**	**Wavelength range of dye photons (nm)**	**Laser system**
0	Rhodamine 640 mixed with Rhodamine 610	594 – 629 [4]	YAG doubled, dye tripled
1	Rhodamine 101 (DCM)	607 – 663 [4]	YAG doubled, dye tripled
2	Rhodamine 101 (DCM)	607 – 663 [4]	YAG doubled, dye tripled
3	Coumarin 120 (C 440)	429 – 463 [44]	YAG tripled, dye doubled
4	Coumarin 2 (C 450)	434 – 463 [44]	YAG tripled, dye doubled
5	Coumarin 102 (C 480)	452 – 500 [44]	YAG tripled, dye doubled
6	Coumarin 102 (C 480)	452 – 500 [44]	YAG tripled, dye doubled
7	Coumarin 102 (C 480)	452 – 500 [44]	YAG tripled, dye doubled

Table 2.1 The laser dyes used in the Sirah dye laser, with their alternative names and the range of wavelengths of photons they are able to produce. Also shown is the set-up of the laser system to show if light from the YAG laser or the Sirah dye laser has been energy doubled or tripled by use of the KD*P and BBO crystals.

Coumarin dyes degrade reasonably rapidly through lasing action and need to be changed approximately every two weeks. To slow down the photo-breakdown of the dye, the Nd:YAG laser power is set to 100 mJ per pulse, although greater laser power above 300 mJ per pulse can be employed if necessary. For the Nd:YAG laser at 100 mJ per pulse, the power of the dye laser with Coumarin dyes is about 12 mJ per pulse when the dye is fresh, before doubling.

The dye laser consists of an oscillator, a pre-amplifier and an amplifier, all contained within dye cells. The beam from the Nd:YAG laser is split by use of dichroic mirrors and guided into the different dye cells. The dye cells are made of quartz and contain a flow of laser dye, which is pumped by the light from the Nd:YAG laser. The oscillator and pre-amplifier are contained within the same dye cell, but at different heights within this cell.

The oscillator is tuneable, meaning that photons can be produced at a specified wavelength, given that the appropriate dye has been used in the Sirah laser system. 5% of the Nd:YAG beam is passed through the oscillator cell and the dye fluoresces. The emerging dye light is directed onto the oscillator. A grating with 2400 lines mm^{-1} acts as the back mirror of the oscillator and only reflects and amplifies light at the required wavelength, in a first order reflection. The angle of the grating is computer-adjusted to select the chosen wavelength.

The beam of light leaving the oscillator cavity passes onto the pre-amplifier, which acts to increase the power of the dye beam, but is not a laser cavity itself. The pre-amplifier is housed above the oscillator in the same dye cell, and consists of dye pumped by 10% of the Nd:YAG light. The emerging dye light is then directed to the final amplifier cell, which is pumped by the remaining 85% of the Nd:YAG beam. This is shown by Figure 2.9:

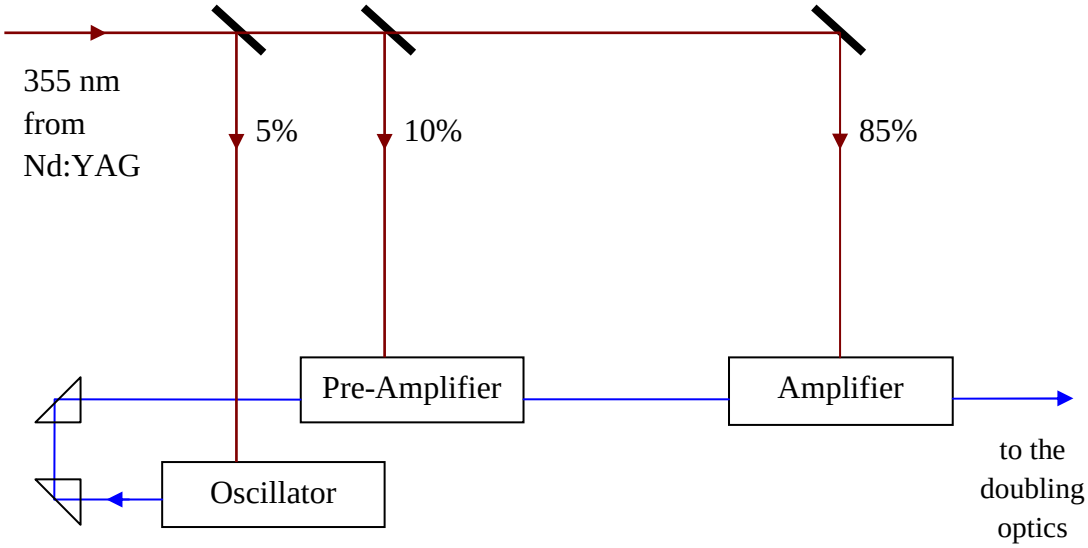

Figure 2.9 Schematic diagram of the Sirah dye laser, pumped by the third harmonic of the Nd:YAG laser, used for studying HD formed in vibrational states $v = 3 – 7$.

In setting up the laser system, it is important to check the alignment of the dye beam and the Nd:YAG beam so that there is good overlap between them. This will ensure than the dye beam has a good shape and is uniform in intensity throughout its cross-section. A uniform beam allows the doubling process to work more effectively and avoids inadvertent burning of parts of the laser system. The spectral linewidth of the dye laser beam is approximately 0.1 cm^{-1} and the beam diameter is 3 – 6 mm.

2.6.3 Frequency Doubling and Tripling

Frequency (or energy) doubling, also called second harmonic generation, is a non-linear optical process [42]. Light from the dye laser can be frequency doubled using either KD*P or BBO (Barium Borate, β-BaB_2O_4) crystals. When the laser light is frequency doubled, the BBO crystal is used to produce photons with wavelength half that of the incident photons. When the laser light is frequency tripled, the KD*P crystal is used to double the light, then this doubled light is frequency mixed with the fundamental light of the original beam in a BBO crystal, to result in photons with a wavelength a third of that of the fundamental photons.

A light beam consists of oscillating electric and magnetic fields. When an external electric field is applied to a crystal by incident laser light, the electrons and atomic nuclei are pulled in opposite directions, resulting in the polarization of the crystal. Electric dipoles are induced *via* this charge separation, with dipole moment μ, which interact with the electric field E as given below. The polarizability of the medium is α.

$$\mu = \alpha E \qquad 2.22$$

The crystals used for frequency doubling and tripling are non-linear media, such that the polarization responds non-linearly with the electric field applied by the incident laser beam. Equation 2.22 is an approximation for weak electric fields and comes from the first term of the power series

$$\mu = \alpha E + \frac{1}{2}\beta E^2 + \frac{1}{6}\gamma E^3 + \ldots \qquad 2.23$$

where β is the hyperpolarizability and γ is the second order hyperpolarizability of the medium.

Thus, as the strength of the electric field increases, non-linear effects arise from the higher order terms in equation 2.23. At any point in the crystal, the variation of the electric field strength with time as the laser passes through the crystal is

$$E = E_0 \sin(2\pi f t) \qquad 2.24$$

where E_0 is the amplitude of oscillation of the laser light and f is the frequency of the incident laser photons. Therefore, as the intensity of the laser light increases, so does the external electric field applied on the crystal and non-linear effects on the vibrations within the crystal lattice become appreciable. Effectively, the higher order terms in equation 2.23 become significant.

The second order term in equation 2.23 contains E^2, which can be expressed

$$E^2 = E_0^2(\sin(2\pi f t))^2 = \frac{1}{2}E_0^2(1-\cos(2\pi 2 f t)) \qquad 2.25$$

Thus the dipole induced in the crystal, μ, will give rise to some photons with frequency $2f$ emerging from the crystal. These photons are known as the second

harmonic light. Only non-centrosymmetric crystals, which have a non-linear response to an applied electric field, can be used for frequency doubling or tripling [41, 42].

Frequency tripling, used to obtain the third harmonic of the Nd:YAG laser light in this work and to obtain the third harmonic of dye laser light in previous work [3, 4], is produced by frequency mixing in a BBO crystal [41, 42]. Two light beams are incident on the BBO mixing crystal: the original fundamental laser light and the second harmonic of the laser light.

For two beams of frequencies f_1 and f_2 and amplitudes E_1 and E_2, the effective strength of the electric field is

$$E = \left(E_1 \sin f_1 t + E_2 \sin f_2 t\right) \qquad 2.26$$

The second order polarization term from equation 2.23 becomes

$$\beta\left(E_1 \sin f_1 t + E_2 \sin f_2 t\right)^2 \qquad 2.27$$

Expanding this term gives

$$\beta\left(E_1^2 \sin^2 f_1 t + E_2^2 \sin^2 f_2 t + 2E_1 E_2 \sin f_1 t \sin f_2 t\right) \qquad 2.28$$

The third term in this expression can be rewritten as

$$E_1 E_2 \beta\left[\cos\left(f_1 - f_2\right)t - \cos\left(f_1 + f_2\right)t\right] \qquad 2.29$$

Therefore, the crystal emits some photons with frequencies f_3 where

$$f_3 = f_1 \pm f_2 \qquad 2.30$$

Hence, when the fundamental light and doubled light are mixed, the third harmonic of the laser light emerges from the crystal. There will also be components in the emergent laser beam of fundamental and doubled light.

Accumulating substantial intensity of the second and third harmonic light can be a problem. The optical properties of doubling and tripling crystals are such that the refractive index of the crystal, and therefore the speed of the light travelling through it, depends on the wavelength of the laser light. If we take the case of second harmonic generation, the doubled light travels through the crystal at different speeds from the fundamental light. The fundamental light generates more frequency doubled photons as it propagates through the crystal, hence the doubled light cannot stay in

phase with itself. This may lead to destructive interference, reducing the power of the doubled light. To overcome this problem, a technique known as phase-matching is used. A direction through the crystal is chosen such that both the fundamental and harmonic light propagate through this direction at the same velocity. Hence, the doubled light does not interfere destructively with itself, and the power of the doubled light is optimized. This phase-matching direction is found by rotating the crystal until maximum doubled light is emitted from the crystal.

The required path through the crystal for phase matching will change with the wavelength of the doubled light. Any deviation from the path means that the beams cannot stay in phase indefinitely, so the crystal position must ensure that both the fundamental and harmonic beams travel exactly along the desired direction. To direct the beam along the desired path, 'look-up' tables are created for the crystal position as a function of wavelength. Look-up tables are set-up for both the doubling and tripling systems. The rotation of a crystal is changed in small steps to find the optimum position of the crystal at which maximum conversion to the harmonic light occurs, at a certain wavelength. The laser is then moved to another wavelength and the optimization process is repeated to find the next optimum position of the crystal until crystal positions have been found for a range of wavelengths. The optimum positions for both the BBO and KD*P crystals are stored as data points in these look-up tables so that the crystal position can be computer-adjusted. The computer fits a line to the data points, incorporating parameters to account for the angle cut and temperature of the crystal, so that the appropriate crystal position between data points can be estimated. During a scan, the computer moves the crystal, mounted on a motor, to the correct position for a given wavelength, as specified by the look-up tables. This means that as the laser scans over a particular wavelength range, the crystals are automatically moved to the position where the phase-matching is maximized.

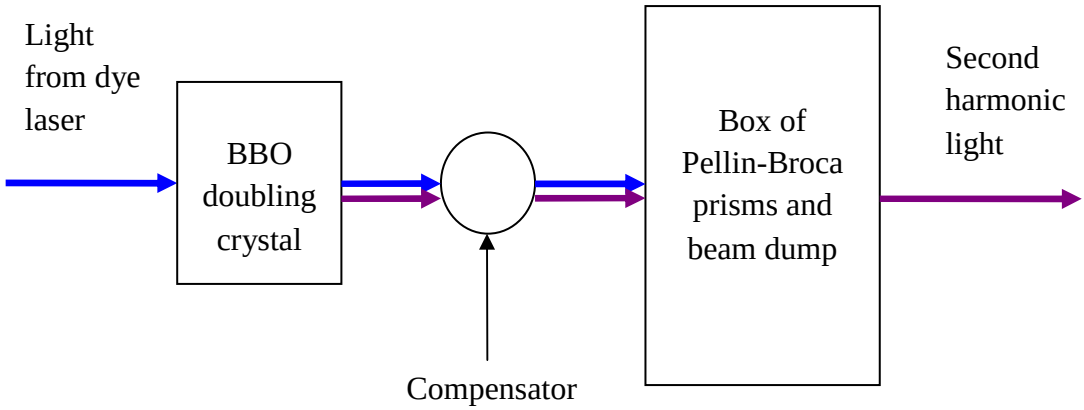

Figure 2.10 Schematic diagram of the set-up for frequency doubling of the dye laser light.

For HD in vibrational states $v = 3 – 7$, the dye laser light is frequency doubled by the series of optics shown in Figure 2.10. Details of the set-up of optics for the tripling of dye laser light, used for HD in vibrational states $v = 0 – 2$, are not provided as part of this study and are given elsewhere [4]. The dye laser light passes through the BBO doubling crystal, which is rotated to the optimum position using the look-up tables, as described above. The refractive indices of the crystals are temperature dependent, thus the BBO doubling crystal is attached to a heater that maintains a constant working temperature at around T ~ 50 °C. After emerging from the doubling crystal, the light then enters a quartz compensator, which compensates the light for any 'beam walk' that may occur as a result of the twist of the doubling crystal. The compensator is also moved according to the same look-up table that controls the BBO crystal position, in order to maintain constant beam position for all wavelengths. As mentioned before, both the fundamental and the doubled light leave the BBO crystal. Any higher order harmonic light is negligible as it does not propagate *via* an appropriate phase-matching pathway. A series of Pellin-Broca prisms is used to separate the fundamental and second harmonic beams. Only the second harmonic light is allowed to leave the prism box. This doubled light typically has energy 1.5 – 2.5 mJ per pulse when the dye has been freshly changed. In order to conserve the dye as long as possible, the Q-switch delay is adjusted to lower the doubled light power to ~ 1 mJ per pulse when REMPI scans are performed.

2.7 Laser Beam Steering and Stray Light Minimization

After generation, the doubled light must travel to the ionization region of the time-of-flight mass spectrometer. The laser beam is directed into the vacuum chamber using two UV-reflecting steering mirrors. The beam must be focused down to an intense spot in order to achieve adequate power for the non-linear REMPI process to occur to a sufficient number of HD molecules for detection. Thus the beam passes through a lens of focal length 30 cm before it enters the vacuum chamber, which focuses the beam into a spot of radius 0.15 mm and area 7.1×10^{-4} cm^2.

As one pulse from the Nd:YAG laser is approximately 4 ns long and has an energy of about 1 mJ, the resulting power density per pulse at the laser focus is

$$\frac{1\times10^{-3}}{7.1\times10^{-4}} \cdot \frac{1}{4\times10^{-9}} = 0.35 \text{ GJ cm}^{-2} \qquad 2.31$$

Given that the Nd:YAG laser pulses at 10 Hz, this power density must be multiplied by 10 Hz to give a time-averaged power density of 3.5 GW cm^{-2}. This value is in good accord with other groups who have carried out REMPI of H_2 [45, 46].

Within the vacuum chamber, scattered laser light can release photoelectrons from the stainless steel chamber walls. These photoelectrons may ionize background HD gas in the chamber, which may be detected by the TOFMS and swamp the HD signal for the REMPI process. To minimize any stray light from the laser beam as it traverses the chamber, conical baffles have been arranged as shown in Figure 2.11. One set of baffles is placed next to the quartz window to immediately surround the laser beam entering the chamber. Attached to the end of the baffles is a copper tube, of diameter 10 mm, which has a roughened inner surface. Any stray light that hits the rough walls of the copper tube will be reflected around inside the copper tube and will not be directed on to the TOFMS ionization region. There is a second set of baffles, attached to a section of PTFE tubing, placed in front of the exit window. This arrangement blocks any back scattered light reflected by the exit window reaching the TOFMS ionization region.

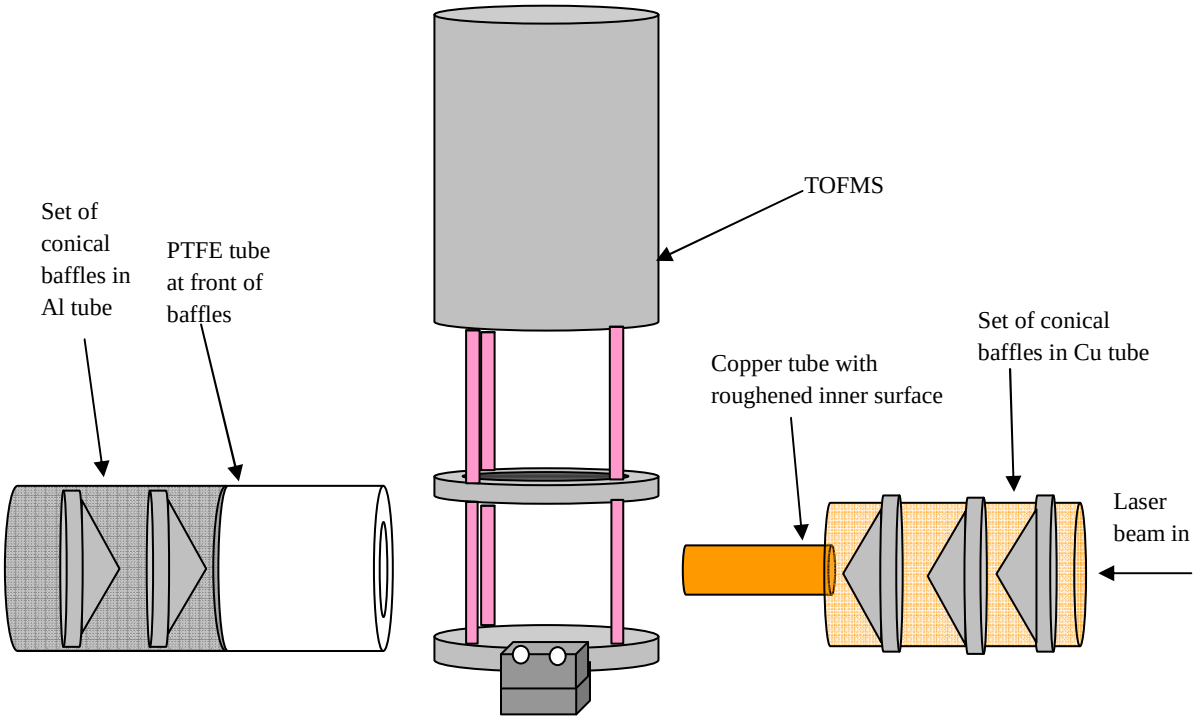

Figure 2.11 Schematic diagram of the set-up of baffles used to minimize stray light within the vacuum chamber.

The laser beam alignment also has a marked effect on the scattered light in the chamber. A badly aligned laser beam results in many stray photons producing photoelectrons, which increase the background counts detected by the TOFMS. In order to measure the background count, the laser is set to produce photons at a wavelength not expected to ionize HD molecules. The TOFMS is used to detect the number of HD^+ ions in a particular period of time, usually about 20 seconds. The alignment of the laser beam through the chamber is then adjusted by manipulating the steering mirrors and the background count is re-measured. This process is repeated until the background count has been minimized by optimizing the laser beam alignment.

2.8 REMPI Spectroscopy

In order to ionize molecules for detection by the TOFMS, the Cosmic Dust Experiment uses Resonance Enhanced Multi-Photon Ionization spectroscopy. In the REMPI process utilized in this study, newly formed HD molecules are ionized from a particular ro-vibrational quantum state (v, J) to form HD^+.

REMPI is a well established spectroscopic technique to ionize molecules in specific ro-vibrational states [45, 47]. REMPI spectroscopy is a two stage process. Firstly, one or more photons are used to excite a molecule to a resonant electronic state. Secondly, the molecule is ionized from this resonant state using more photons. The ions are then detected by a TOFMS. REMPI processes are labelled (A+B) where A corresponds to the number of photons required to excite the molecule to the resonant state and B is the number of photons used to ionize the molecule from the resonant electronic state. Figure 2.12 shows the prototypical transitions involved in (1+1) and (2+1) REMPI schemes.

If more than one photon is used to excite the molecule to the resonant state, the excitation has occurred *via* non-resonant 'virtual' states [48]. A virtual state is not an eigenstate of the molecule and is very short lived, with lifetime ~10^{-15} s. In order for the resonant state to be reached, the virtual states must be populated by A photons within 10^{-15} s. The population of the virtual state can be the rate-limiting step of the REMPI process. The photon density must be sufficiently high for the virtual state to be populated and thus for REMPI to occur. It is not necessary for the A and B photons, or all of the A photons, or all of the B photons, to be of the same frequency as long as the combination of their energies is sufficient to excite the molecule to the resonant state.

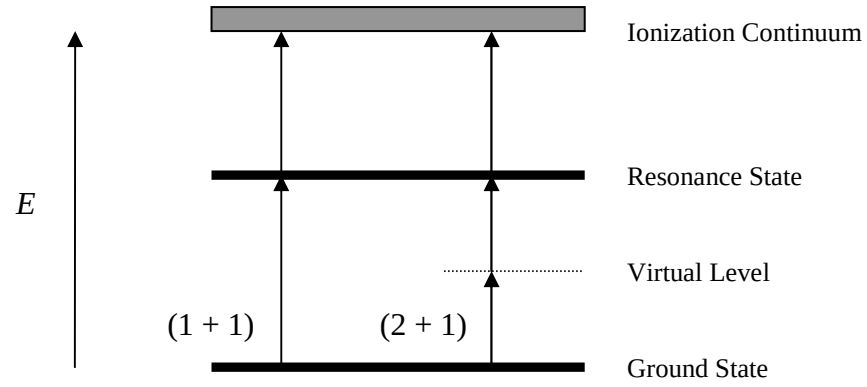

Figure 2.12 The transitions involved in (1+1) and (2+1) REMPI schemes.

To state selectively ionize hydrogen molecules, a (2+1) REMPI scheme is required, shown below in Figure 2.13. Two photons are used to excite the HD molecules from a specific ro-vibrational level in the ground electronic state, $X\ ^1\Sigma_g^+$ (v'', J''), *via* a virtual level to the $E,F\ ^1\Sigma_g^+$ (v', J') resonant electronic state. A third photon then ionizes the HD. The third photon is of the same frequency as the previous two photons, as all the photons originate from the same laser beam, produced by frequency doubling the light of the dye laser as explained in Section 2.6. Ro-vibrational levels in the lower state of a transition are denoted (v'', J'') and the upper state of a transition is denoted (v', J').

As shown in Figure 2.13, two photons are required to excite hydrogen in the ground electronic state to the resonant state; hence the change in the rotational quantum number is $\Delta J = 0, \pm 2$. The Q branch transitions are approximately 30 times stronger than those in the O or S branches [49-51]. Thus, the key step in the REMPI transition employed in the Cosmic Dust Experiment is $X\ ^1\sum_g^+ (v'', J'') \rightarrow E,F\ ^1\sum_g^+ (v', J' = J'')$.

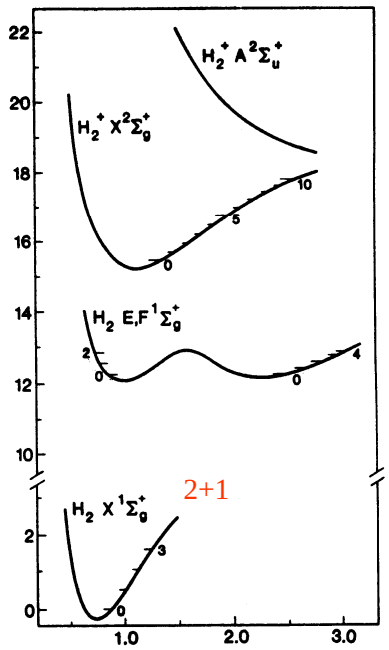

Figure 2.13 The (2+1) REMPI scheme for hydrogen molecules [45].

The wavelengths of the two photons used in the excitation process are such that they each have half the energy required for the transition. The standard spectroscopic equations for electronic, rotational and vibrational energies are used to calculate the wavelengths of the photons required for REMPI transitions.

The energy of a vibrational state above the bottom of the potential well is given by

$$E_v = \left(v+\frac{1}{2}\right)\varpi_e - \left(v+\frac{1}{2}\right)^2 \varpi_e x_e \text{ cm}^{-1} \qquad 2.32$$

The energy of a rotational state above the vibrational state is

$$E_J = \left[B_e - \alpha\left(v+\tfrac{1}{2}\right)\right]J(J+1) - DJ^2(J+1)^2 \text{ cm}^{-1} \qquad 2.33$$

where

E_v is the energy of the vibrational state, vibrational quantum number v,

E_J is the energy of the rotational state, rotational quantum number J,

ϖ_e is the fundamental vibration wavenumber,

x_e is an anharmonicity constant,

B_e is the equilibrium value of the rotational constant B,

α is a vibration-rotation interaction molecular constant,

D is the centrifugal distortion coefficient.

The values of the spectroscopic constants, ϖ_e, x_e, B_e, α and D, are taken from the NIST online database [52] or other literature [53, 54]. The total energy of each state is given by

$$E_{\text{total}} = E_{elec} + E_v + E_J \qquad 2.34$$

where E_{elec} is the electronic state energy.

As aforementioned, the laser photons involved in the REMPI process used in the Cosmic Dust Experiment must cause the transition $X\ ^1\sum_g^+ (v'', J'') \rightarrow E,F\ ^1\sum_g^+ (v', J' = J'')$. An example of the calculated photon wavelengths for HD formed on HOPG in the vibrational state $v = 3$ are shown in Table 2.2 below. In this case, $v'' = 3$ and the E, F vibrational state chosen for the transition is $v' = 1$, because of favourable Franck-Condon Factors between these vibrational states. Franck Condon factors are a measure of the overlap of two vibrational states and indicate the likelihood of a transition occurring between these states.

J″	***v″***	**Wavelength of REMPI photon / nm**	**Wavelength of dye laser photon / nm**
0	3	219.732	439.465
1	3	219.810	439.619
2	3	219.964	439.928
3	3	220.194	440.388
4	3	220.497	440.995
5	3	220.872	441.744
6	3	221.314	442.629
7	3	221.820	443.641
8	3	222.385	444.771
9	3	223.003	446.007
10	3	223.668	447.336

Table 2.2 Calculated photon wavelengths for the transition $X\ ^1\Sigma_g^+ (v'' = 3, J'') \rightarrow E,F\ ^1\Sigma_g^+ (v' = 1, J' = J'')$.

In order to ionize HD, the Sirah dye laser is set to scan over a range of wavelengths until the REMPI transition is found. For example, for HD formed in the (v'' = 3, J'' = 0) state, the dye laser can be set to scan over 439.435 – 439.495 nm, as the dye laser light is frequency doubled to produce the REMPI photons, in steps of 0.003 nm in a 20 step scan. HD^+ ions are detected by the TOFMS when the REMPI transition occurs. This total ion yield is known as the REMPI signal. The laser is set to dwell at each wavelength point for a given accumulation time, in which ions are detected by the TOFMS. The accumulation time depends on the strength of the REMPI signal and can range from 30 s for a strong signal to 320 s for a weak signal.

If there is no REMPI signal for the scan, a different wavelength range is chosen and another scan is performed. The REMPI signal will not necessarily occur at exactly the calculated value. This discrepancy is due to a combination of reasons. Firstly, the inbuilt calibration of the laser is not perfectly accurate and leads to a laser 'offset'. Secondly, there are higher order terms in equations 2.32 and 2.33 which are neglected in the calculation. Hence ranges of wavelengths are typically searched up to 0.5 nm away from the doubled light wavelength value calculated in Table 2.2, until the transition is found.

2.9 Summary

This chapter has described the experimental set-up of the UCL Cosmic Dust Experiment, which has been used to study the formation of HD on an analogue of an interstellar dust grain, namely an HOPG surface held at 15 K. This chapter includes details on how UHV has been achieved and the generation of H- and D-atom beams, which are transported to the HOPG surface. The HOPG surface is cryogenically cooled by a helium cold head and heated by a tantalum strip heater for cleaning. Nascent HD molecules desorb from the HOPG surface and are state-selectively ionized by REMPI spectroscopy. REMPI photons are produced by the laser system. For HD formed in vibrational states v = 3 – 7, the third harmonic from an Nd:YAG laser is used to pump a tuneable dye laser. The beam from the dye laser is then frequency doubled to obtain the REMPI photons. The REMPI photons ionize HD from a particular ro-vibrational state in the ground electronic state *via* a resonant E, F state in a (2+1) REMPI scheme. The HD^+ ions are then detected by the TOFMS. Data

processing of the mass spectra of HD^+ ions is required to calculate the relative populations of the ro-vibrational states of nascent HD. The data analysis procedure and results will be explained in Chapter 3.

2.10 References

1. Garrod, R.T., V. Wakelam, and E. Herbst, *Non-thermal desorption from interstellar dust grains via exothermic surface reactions*. Astronomy & Astrophysics, 2007. **467**(3): p. 1103-1115.

2. Weck, P.F. and N. Balakrishnan, *Dynamics of chemical reactions at cold and ultracold temperatures*. Journal of Physics B-Atomic Molecular and Optical Physics, 2006. **39**(19): p. S1215-S1227.

3. Creighan, S.C., J.S.A. Perry, and S.D. Price, *The rovibrational distribution of H-2 and HD formed on a graphite surface at 15-50 K*. Journal Of Chemical Physics, 2006. **124**(11).

4. Creighan, S.C., *Laboratory Studies of the Formation of Molecular Hydrogen on Surfaces at Cryogenic Temperatures*, *Department of Chemistry*. 2006, University College London: London.

5. Perry, J.S.A., J.M. Gingell, K.A. Newson, J. To, N. Watanabe, and S.D. Price, *An apparatus to determine the rovibrational distribution of molecular hydrogen formed by the heterogeneous recombination of H atoms on cosmic dust analogues*. Meas. Sci. Technol., 2002. **13**(9): p. 1414-1424.

6. Perry, J.S.A. and S.D. Price, *Detection of rovibrationally excited H-2 formed through the heterogeneous recombination of H atoms on a cold HOPG surface*. Astrophysics and Space Science, 2003. **285**(3-4): p. 769-776.

7. Perry, J.S.A., *State-Selective Reactions of Cosmic Dust Analogues at Cryogenic Temperatures*, *Department of Chemistry*. 2001, University College London: London.

8. Dyson, J.E. and D.A. Williams, *The Physics of the Interstellar Medium*. 2nd Edition ed. The Graduate Series in Astronomy, ed. R.J. Tayler and M. Elvis. 1997, Bristol: Institute of Physics Publishing.

9. Donnelly, A., M.P. Hughes, J. Geddes, and H.B. Gilbody, *A Microwave-Discharge Atom Beam Source of High-Intensity*. Meas. Sci. Technol., 1992. **3**(5): p. 528-532.

10. Higgins, D.P., R.W. McCullough, J. Geddes, J.M. Woolsey, M. Schlapp, and H.B. Gilbody, *New Thermal-Energy Sources of H, O, Cl and N Atoms for Material Processing*. Advances in Engineering Materials, 1995. **99-1**: p. 177-183.

11. McCullough, R.W., *Characterisation and Applications of a New Reactive Atom Beam Source*, in *Application of Accelerators in Research and Industry*, J.L. Duggan and I.L. Morgan, Editors. 1997, AIP Press: New York. p. 275-278.

12. Walraven, J.T.M. and I.F. Silvera, *Helium-Temperature Beam Source of Atomic-Hydrogen*. Review of Scientific Instruments, 1982. **53**(8): p. 1167-1181.

13. Jeloaica, L. and V. Sidis, *DFT investigation of the adsorption of atomic hydrogen on a cluster-model graphite surface*. Chemical Physics Letters, 1999. **300**(1-2): p. 157-162.

14. Morisset, S., F. Aguillon, M. Sizun, and V. Sidis, *Quantum dynamics of H-2 formation on a graphite surface through the Langmuir Hinshelwood mechanism*. J. Chem. Phys., 2004. **121**(13): p. 6493-6501.

15. Morisset, S., F. Aguillon, M. Sizun, and V. Sidis, *Wave-packet study of H-2 formation on a graphite surface through the Langmuir-Hinshelwood mechanism*. J. Chem. Phys., 2005. **122**(19): p. art. no.-194702.

16. Sha, X.W. and B. Jackson, *First-principles study of the structural and energetic properties of H atoms on a graphite (0001) surface*. Surface Science, 2002. **496**(3): p. 318-330.

17. Roser, J.E., S. Swords, G. Vidali, G. Manico, and V. Pirronello, *Measurement of the kinetic energy of hydrogen molecules desorbing from amorphous water ice*. Astrophysical Journal, 2003. **596**(1): p. L55-L58.

18. Vidali, G., J.E. Roser, G. Manico, and V. Pirronello, *Laboratory studies of formation of molecules on dust grain analogues under ISM conditions*. Journal of Geophysical Research-Planets, 2004. **109**(E7).

19. Farebrother, A.J., A.J.H.M. Meijer, D.C. Clary, and A.J. Fisher, *Formation of molecular hydrogen on a graphite surface via an Eley-Rideal mechanism*. Chemical Physics Letters, 2000. **319**(3-4): p. 303-308.

20. Jackson, B. and D. Lemoine, *Eley-Rideal reactions between H atoms on metal and graphite surfaces: The variation of reactivity with substrate*. J. Chem. Phys., 2001. **114**(1): p. 474-482.

21. Kim, Y.H., J. Ree, and H.K. Shin, *Formation of vibrationally excited hydrogen molecules on a graphite surface*. Chemical Physics Letters, 1999. **314**(1-2): p. 1-8.

22. Martinazzo, R. and G.F. Tantardini, *Quantum study of Eley-Rideal reaction and collision induced desorption of hydrogen atoms on a graphite surface. I. H-chemisorbed case*. J. Chem. Phys., 2006. **124**(12).

23. Meijer, A., A.J. Farebrother, and D.C. Clary, *Isotope effects in the formation of molecular hydrogen on a graphite surface via an Eley-Rideal mechanism*. J. Phys. Chem. A, 2002. **106**(39): p. 8996-9008.

24. Meijer, A., A.J. Fisher, and D.C. Clary, *Surface coverage effects on the formation of molecular hydrogen on a graphite surface via an Eley-Rideal mechanism*. J. Phys. Chem. A, 2003. **107**(50): p. 10862-10871.

25. Meijer, A.J.H.M., A.J. Farebrother, D.C. Clary, and A.J. Fisher, *Time-dependent quantum mechanical calculations on the formation of molecular hydrogen on a graphite surface via an Eley-Rideal mechanism*. J. Phys. Chem. A, 2001. **105**(11): p. 2173-2182.

26. Morisset, S., F. Aguillon, M. Sizun, and V. Sidis, *The dynamics of H-2 formation on a graphite surface at low temperature*. Phys. Chem. Chem. Phys., 2003. **5**(3): p. 506-513.

27. Morisset, S. and A. Allouche, *Quantum dynamic of sticking of a H atom on a graphite surface*. J Chem Phys, 2008. **129**(2): p. 024509.

28. Parneix, P. and P. Brechignac, *Molecular dynamics simulation of the H-2 recombination on a graphite surface*. Astronomy and Astrophysics, 1998. **334**(1): p. 363-375.

29. Ree, J., Y.H. Kim, and H.K. Shin, *Dynamics of H-2 formation on a graphite surface*. Chemical Physics Letters, 2002. **353**(5-6): p. 368-378.

30. Rutigliano, M., M. Cacciatore, and G.D. Billing, *Hydrogen atom recombination on graphite at 10 K via the Eley- Rideal mechanism*. Chemical Physics Letters, 2001. **340**(1-2): p. 13-20.

31. Sha, X.W., B. Jackson, and D. Lemoine, *Quantum studies of Eley-Rideal reactions between H atoms on a graphite surface*. J. Chem. Phys., 2002. **116**(16): p. 7158-7169.

32. Zecho, T., A. Guttler, X.W. Sha, B. Jackson, and J. Kuppers, *Adsorption of hydrogen and deuterium atoms on the (0001) graphite surface*. J. Chem. Phys., 2002. **117**(18): p. 8486-8492.

33. Zecho, T., A. Guttler, and J. Kuppers, *Suppression of D adsorption and D by H abstraction on graphite (0001) surfaces by adsorbed water*. Chemical Physics Letters, 2003. **370**(3-4): p. 366-370.

34. Bolina, A.S., A.J. Wolff, and W.A. Brown, *Reflection absorption infrared spectroscopy and temperature programmed desorption investigations of the interaction of methanol with a graphite surface*. J. Chem. Phys., 2005. **122**(4): p. 12.

35. Pirronello, V., C. Liu, L.Y. Shen, and G. Vidali, *Laboratory synthesis of molecular hydrogen on surfaces of astrophysical interest*. Astrophysical Journal, 1997. **475**(1): p. L69-L72.

36. Greenberg, J.M., *Cosmic dust and our origins*. Surface Science, 2002. **500**(1-3): p. 793-822.

37. Dyson, J.E. and D.A. Williams, *The Physics of the Interstellar Medium*. 2nd ed. 1997, Bristol: Institute of Physics.

38. Berman, R., E.L. Foster, and J.M. Ziman, *Thermal Conduction in Artificial Sapphire Crystals at Low Temperatures. I. Nearly Perfect Crystals*. Proceedings of the Royal Society A, 1955. **231**(1184): p. 130-144.

39. Wiley, W.C. and I.H. McLaren, *Time-of-Flight Mass Spectrometer with Improved Resolution*. Review of Scientific Instruments, 1955. **26**(12): p. 1150-1157.

40. Demtröder, W., *Laser Spectroscopy Basic Concepts and Instrumentation*. 1981: Springer-Verlag.

41. Hawkes, J. and J. Wilson, *Optoelectronics, an introduction*. 3rd ed. 1998: Prentice Hall Europe.

42. Hawkes, J. and J. Wilson, *Lasers Principles and Applications*. Prentice Hall International Series in Optoelectronics. 1987: Prentice Hall Europe.

43. Banwell, C.N. and E.M. McCash, *Fundamentals of Molecular Spectroscopy*. Vol. 4th. 1994: McGraw-Hill Book Company.

44. Sirah. *Sirah Laser und Plasmatechnik.* [cited 2009; Available from: http://www.sirah.com/.

45. Rinnen, K.D., M.A. Buntine, D.A.V. Kliner, R.N. Zare, and W.M. Huo, *Quantitative-Determination of H_2, HD, and D_2 Internal-State Distributions by (2+1) Resonance-Enhanced Multiphoton Ionization*. J. Chem. Phys., 1991. **95**(1): p. 214-225.

46. Kligler, D.J. and C.K. Rhodes, *Observation of Two-Photon Excitation of the H_2 $E,F\ ^1\Sigma_g^+$ State*. Physical Review Letters, 1978. **40**(5): p. 309-313.

47. Huo, W.M., K.D. Rinnen, and R.N. Zare, *Rotational And Vibrational Effects In The E 1-Sigma-G+-X 1-Sigma-G+ 2-Photon Transitions Of H2, Hd, And D2*. J. Chem. Phys., 1991. **95**(1): p. 205-213.

48. Hollas, J.M., *Modern Spectroscopy*. 4th ed. 2004: John Wiley & Sons Ltd.

49. Kligler, D.J., J. Bokor, and C.K. Rhodes, *Collisional and radiative properties of the H_2 $E,F\ ^1\Sigma_g^+$ state*. Physical Review A, 1980. **21**(2): p. 607-617.

50. Marinero, E.E., R. Vasudev, and R.N. Zare, *The $E,F\ ^1\Sigma_g^+$ Double-Minimum State of Hydrogen - 2-Photon Excitation of Inner and Outer Wells*. J. Chem. Phys., 1983. **78**(2): p. 692-699.

51. Pozgainer, G., K.D. Rendulic, and A. Winkler, *Laser Spectroscopy on Hydrogen Desorbing from Nickel*. Surface Science, 1994. **309**: p. 344-349.

52. Huber, K.P. and G. Herzberg, *Constants of Diatomic Molecules*, in *NIST Standard Reference Database Number 69*, P.J. Linstrom and W.G. Mallard, Editors.

53. Huber, K.P. and G. Herzberg, *Molecular spectra and molecular structure IV: Diatomic molecules*. 1979: Van Nostrand Reinhold Company.

54. Dabrowski, I. and G. Herzberg, *Absorption and Emission-Spectra of Hd in Vacuum Ultraviolet*. Can. J. Phys., 1976. **54**(5): p. 525-567.

Chapter Three

Results of the HD Formation Experiment

3.1 Overview

This chapter will describe the results of the UCL Cosmic Dust Experiment on the formation of HD in vibrational states $v = 3 – 7$. Previous work using the Cosmic Dust Experiment, pertinent to this thesis, will be summarized in Section 3.2. The particular experimental method procedure for the $v = 3 – 7$ experiments will be explained in Section 3.3. After collection, the data needs to be processed, taking into account laser power to obtain the relative rotational populations, which will be explained in Section 3.4.1. Section 3.5 describes the calculations performed to obtain the average rotational temperature within each vibrational state. The ro-vibrational distribution of nascent HD molecules will be discussed in Sections 3.6 – 3.9.

The complete set of UCL data, from all HD ro-vibrational states detected to date, is used to determine the energy partitioning between the internal energy and translational energy of the nascent HD molecule and energy lost to the graphite surface in Sections 3.10 and 3.11. In this chapter, ro-vibrational states within the *X* state, in which the HD is formed, will be denoted (v'', J'') and ro-vibrational states within the *E, F* state used in the REMPI process will be denoted (v', J').

3.2 Previous Work

The UCL Cosmic Dust Experiment was commissioned 10 years ago to study the formation of molecular hydrogen on surfaces analogous to interstellar dust grains. The aim of the experiment is to probe the ro-vibrational distribution of nascent hydrogen molecules using REMPI spectroscopy. H_2 and HD formation on an HOPG surface held at a range of temperatures between 15 K and 50 K has been studied [1-3]. Newly-formed H_2 was detected in the $v'' = 1$, $J'' = 0 – 3$ and $v'' = 2$, $J'' = 0 – 3$ states. Newly-formed HD was detected in the $v'' = 1$, $J'' = 0 – 4$ and the $v'' = 2$, $J'' = 0 – 4$ states. The rotational temperatures for each vibrational state were found to be significantly higher than the surface temperature and are shown in Table 3.1 below:

Molecule	Vibrational state, v''	Rotational states, J''	Surface Temperature / K	Rotational Temperature / K
H_2	1	0 – 3	23	314 ± 9 [1]
		0 – 3	30	214 ± 11 [3]
		0 – 3	50	224 ± 21 [3]
H_2	2	0 – 3	15	364 ± 37 [1]
		0 – 2	23	309 ± 41 [1]
		0 – 3	30	316 ± 41 [1]
		0 – 2	50	345 ± 153 [1]
HD	1	0 – 4	15	265 ± 15 [2]
		0 – 4	27	274 ± 20 [2]
		0 – 4	40	198 ± 13 [2]
		0 – 4	50	283 ± 20 [2]
HD	2	0 – 4	15	286 ± 37 [2]
		0 – 4	27	299 ± 31 [2]
		0 – 4	40	331 ± 37 [2]
		0 – 4	50	345 ± 39 [2]

Table 3.1 Ro-vibrational states and rotational temperatures for nascent H_2 and HD detected in previous work.

A search for HD formed in vibrational state $v'' = 0$ was also made, but was not successful. This was because the observed REMPI signals of HD in $v'' = 0$, $J'' = 0 – 4$ were not necessarily due to nascent HD molecules forming on the surface but were, in fact, dominated by thermally relaxed HD molecules already present within the vacuum chamber. Very high rotational states such as $J'' = 7$ and 8 are not expected to be populated by thermalized HD, thus the REMPI signals for these states should not be swamped by the background gas. However, these states were not detected, indicating that nascent HD does not populate $v'' = 0$, $J'' = 7$ and 8 at a level above the experimental detection limits.

3.3 Detection of HD in $v = 3 – 7$

The experiments carried out in this thesis probed the formation of HD in vibrational states $v'' = 3 – 7$. The $v'' = 3$ and 4 states were detected first, followed by a hiatus of three months, after which the $v'' = 5 – 7$ states were observed. The delay in data collection occurred because of contamination of the vacuum chamber by pump oil due to a power cut, leading to a loss of signal. Also for the higher vibrational states, the values of spectroscopic constants from the NIST database [4] are inadequate to calculate an accurate wavelength for the REMPI photons; thus an alternative source for calculating the energies of the E, F energy levels had to be sought [5]. This calculation is given in Section 3.7.

For the first period of data collection, in which the $v'' = 3$ and 4 states were studied, the pressure in the H_2 source was 0.14 – 0.25 Torr and the pressure in the D_2 source was 0.16 – 0.20 Torr. The target chamber pressure was $1.2 \times 10^{-7} – 2.4 \times 10^{-7}$ Torr. During the collection of the $v'' = 5 – 7$ data, the pressure in the H_2 and D_2 sources was 0.24 – 0.37 Torr and 0.22 – 0.29 Torr respectively. The target chamber pressure for the $v'' = 5 – 7$ experiments was $5.0 \times 10^{-8} – 1.0 \times 10^{-7}$ Torr, marginally lower than for the $v'' = 3$ and 4 experiments, as the chamber had been cleaned and new pumps had been installed. As outlined in Chapter 2, the sources are never switched off, so that H- and D-atoms continuously dose the HOPG surface, which is cooled cryogenically to T = 15 K by the helium coldhead. The surface is cleaned before every REMPI scan by

heating to 500 K to remove any adsorbates on the surface. It takes approximately 45 minutes for the HOPG to cool back down to 15 K.

HD is formed in a distribution of ro-vibrational states (v'', J'') in the X state, but the Cosmic Dust Experiment can only probe the population of one state at a time. HD is state-selectively ionized using laser photons, *via* a resonant E, F (v', J') state. For each v'' value, the most favourable v' state must be determined from Franck-Condon factors. For HD in the X state with v'' = 3, 4, 5, 6, and 7 the resonant E, F states used were v' = 1, 1, 1, 2 and 3 respectively. The FCFs for the $v'' \rightarrow v'$ transitions are shown in Table 3.2. The Q-branch is the most intense rotational transition, and is always used in the REMPI process; hence there is no change in the value of rotational quantum number, so $J' = J''$. The two-photon wavelength is then calculated for the REMPI transition $X\ ^1\sum_g^+\ (v'', J'') \rightarrow E, F\ ^1\sum_g^+\ (v', J' = J'')$ taking into account any possible offsets, such as laser calibration offsets. The dye laser is then set up to perform a scan over this wavelength. When the REMPI transition occurs during the scan, HD^+ ions are formed and detected by the TOFMS: the ion count detected is the REMPI signal. The dye laser wavelength range at which REMPI signals occurred, when first detected, is shown in Table 3.2 below:

v'', J''	v'	FCF	Wavelength range of detected REMPI signals / nm
3, 0 – 6	1	0.182	439.55 – 442.79
4, 0 – 6	1	0.283	455.09 – 458.18
5, 0 – 6	1	0.154	470.83 – 473.70
6, 0 – 4	2	0.242	475.81 – 476.73
7, 0 – 3	3	0.159	481.40 – 482.66

Table 3.2 The ro-vibrational states detected with the resonant E, F state for each vibrational state and Franck-Condon factor for the $v'' \rightarrow v'$ transition. The range of wavelengths of the dye laser at which REMPI signals were detected for each vibrational level is also shown; this is the wavelength of the dye photons before energy doubling by the crystal optics.

As stated in Chapter 2, a look-up table must be created and enabled for each scan, so that the doubling crystal is in the correct position to ensure constant laser power throughout the wavelength range of the scan. A computer program is used for data collection, which enables the TOFMS and the TOFMS counting electronics to communicate with the laser. The laser scans the wavelength range in small incremental steps of 0.003 nm in size. The laser can be set to dwell at each wavelength point for a given accumulation time. The length of accumulation time set depends on the strength of the REMPI signal and ranges from 30 s to 320 s, depending on the strength of the signal.

The yield of HD^+ ions is counted by the electronics associated with the TOFMS, as described in Chapter 2. In order to find the flight time of the HD^+ ions, a mass spectrum is taken with the laser off-resonance. Stray light from the laser beam hits the stainless steel chamber walls and releases photoelectrons. These photoelectrons ionize the background gas in the chamber to form H^+ ions, which can be readily identified in the mass spectrum. The other peaks in the mass spectrum can then be assigned to particular ions such as H_2^+, HD^+ and D_2^+, which are also abundant in the vacuum chamber; thus the flight times of HD^+ ions can be constrained to a finite range from the size of the peak. The TOFMS counting electronics are then set to integrate over the flight times which contain only HD^+ ions. Figure 3.1 shows an on-resonance mass spectrum, taken during a REMPI scan when HD in ro-vibrational state $v'' = 4$, $J''= 1$ was ionized. The H^+ peak appears at approximately 250 ns, H_2^+ at 680 ns, HD^+ at 940 ns and D_2^+ at 1250 ns. The spectral peaks for H^+, H_2^+ and D_2^+ are due to ions created by photoelectrons and are wider than the on-resonance HD^+ peak produced *via* REMPI.

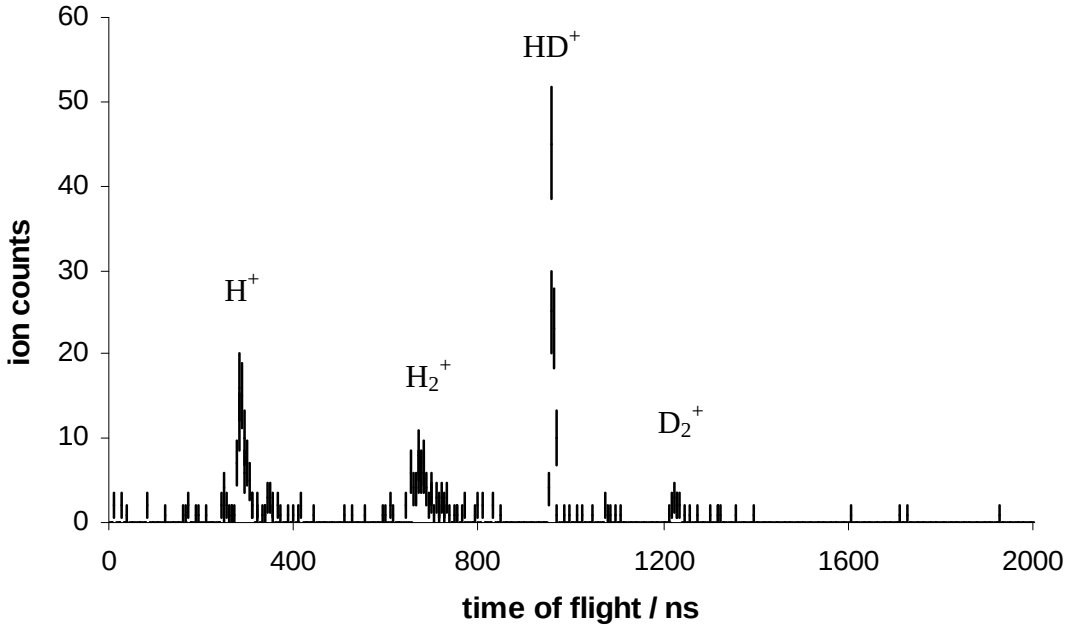

Figure 3.1 On-resonance mass spectrum for HD v'' = 4, J'' = 1, showing the peaks for H^+, H_2^+, HD^+ and D_2^+.

The timing electronics of the TOFMS count each HD^+ ion signal from the detector. However, after one ion is detected, there is a 'dead time' of 50 ns during which another ion cannot be detected. Thus the laser power must be set so that only one ionization event occurs for each laser pulse. The laser start signal repeats at a frequency of 10 Hz, so the laser power is adjusted to fulfil the relationship

$$\textit{Ion counts per wavelength step} \leq 10 \times \textit{accumulation time} \qquad 3.1$$

The output of the data collection computer program is the HD^+ ion counts per wavelength step, as shown in the REMPI spectrum given in Figure 3.2.

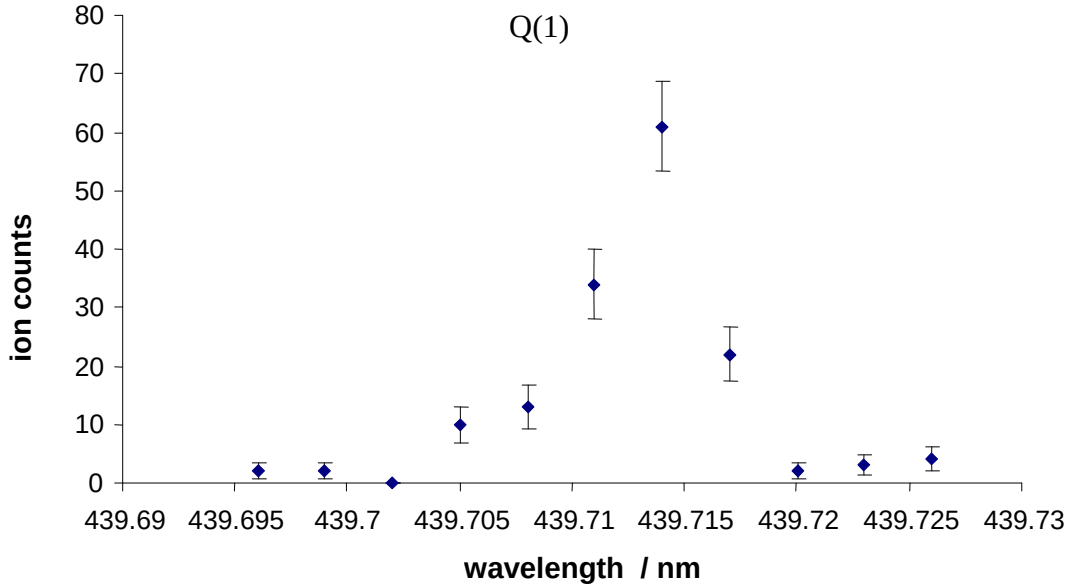

Figure 3.2 REMPI spectrum of HD $v'' = 3$ $J'' = 1$, following the reaction of H- and D-atoms on a HOPG surface held at 15 K. The REMPI transition is $X\ ^1\Sigma_g^+$ $(v'' = 3, J'' = 1) \rightarrow E, F\ X\ ^1\Sigma_g^+$ $(v' = 1, J' = J'')$, which is the Q(1) line. The ion signal is the number of HD^+ ions detected during an accumulation time of 30 s per wavelength step. The error bars are the square root of the ion counts.

The area under the peak in Figure 3.2 can be related to the rotational population of HD formed in one rotational state within a vibrational level. REMPI scans for other rotational states within the same vibrational level are then performed. The first state searched for was the $v'' = 3$, $J'' = 1$ state, as $J'' = 1$ has been found to be the most populated rotational state in previous work [1]. The $J'' = 0$ state was investigated next, followed by states $J'' \geq 2$ in ascending order of J'', until higher rotational states could not be detected. Subsequently higher vibrational states were investigated by the same method. The $v'' = 8$, $J'' = 1$ state was later searched for, but not detected [6]. Searches were made by scanning the dye laser over ranges of wavelengths near the calculated 2-photon wavelength until the REMPI transition was observed. When searching for a REMPI signal, short accumulation times of 30 seconds per wavelength step are used, for as many as 30 wavelength steps. When the REMPI transition is found, it occurs over several wavelength steps, as shown in Figure 3.2. For data collection, to determine the rotational populations, the laser is set to scan over a range with only 10 – 12 wavelength steps, spending 30 s – 320 s per wavelength step, depending on the strength of the REMPI signal. REMPI signals for the $v'' = 4$ level are shown below:

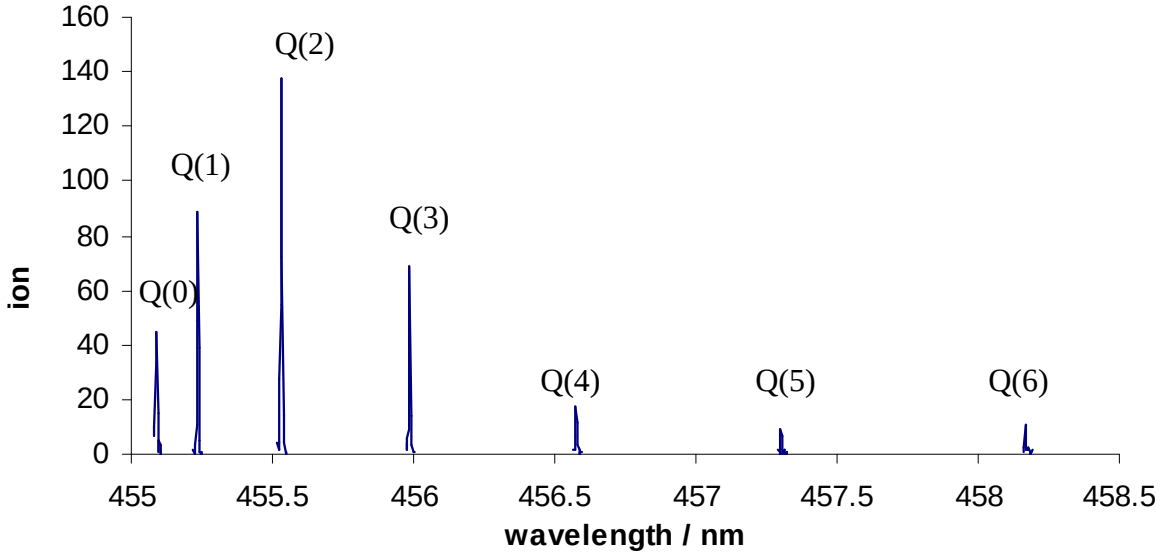

Figure 3.3 REMPI spectra showing the transitions $^1\Sigma_g^+$ X (v'' = 4, J'' = 0 – 6) $\rightarrow$ $^1\Sigma_g^+$ E, F (v' = 1, J' = J''). All the spectra shown are from the Q-branch of the v'' = 4 REMPI transitions. The entire spectrum was not taken at the same time due to the large separation between the rotational lines and the long accumulation times necessary to obtain good signal to noise.

The integrated areas under the REMPI spectra are converted to the relative population of the rotational states by correcting for accumulation time and laser power. The ion signal in a REMPI spectrum is the number of HD^+ ions detected by the TOFMS during the accumulation time. This is scaled to give the number of HD^+ ions expected to be detected in an accumulation time of 60 s. The laser power correction calculation is shown below in Section 3.4.1.

3.4 Data Processing

3.4.1 Relative Rotational Populations

The power of the laser beam is liable to vary from scan to scan and during the course of a scan because the laser dye efficiency is dependent on wavelength. The dye efficiency of Coumarin 480 dependence on wavelength is shown below in Figure 3.4.

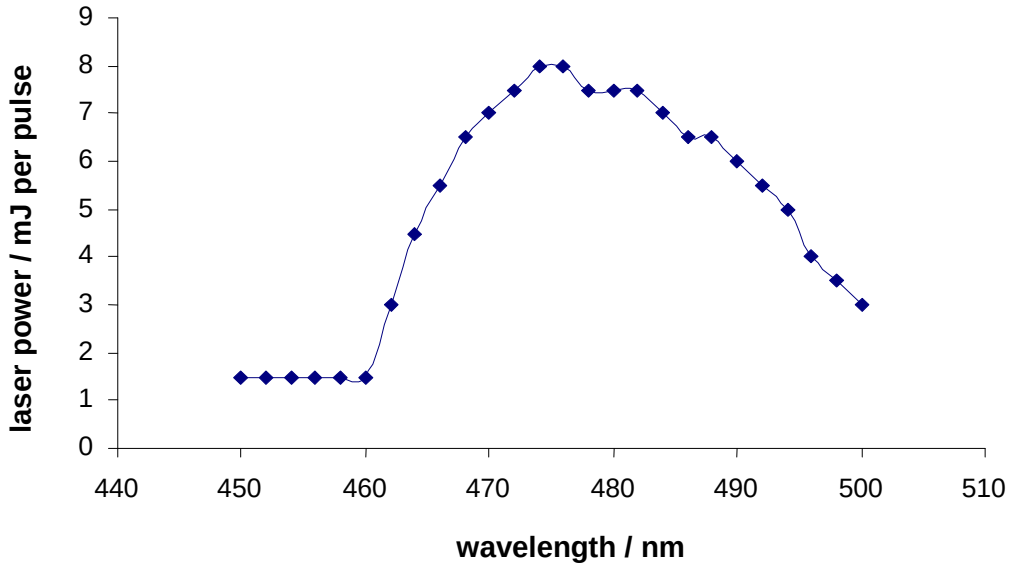

Figure 3.4 The dependence of laser power of the tripled light with wavelength for the dye Coumarin 480, which was used for the $v'' = 5 - 7$ states. A list of the dyes used for each vibrational level is given in Chapter 2, Table 2.1.

The dye also deteriorates with use, as well as varying with wavelength, such that the laser power of the doubled light typically drops by ~ 0.1 mJ per pulse by the end of a laser scan, with even greater drops in power for very long scans. Thus the integrated area under the REMPI peaks must be corrected for laser power. The ion signal strength varies with respect to the laser intensity *via* the power dependence

$$Ion\ signal \propto (laser\ power)^n \qquad 3.2$$

The value of *n*, the laser correction factor, is also transition dependent, thus needs to be calculated for every vibrational state.

To determine the value of *n* in equation 3.2, ion signals from one ro-vibrational state are measured at different values of laser power. A graph of ln(laser power) against ln(ion signal) is plotted, which gives rise to a straight line with a gradient *n*, as shown in Figure 3.5. Within each vibrational level, the rotational state with the strongest REMPI signal is usually used to determine *n*. The strongest rotational states used are typically the $J'' = 1$ or 2 states. The values of *n* for each vibrational level are shown in Table 3.3.

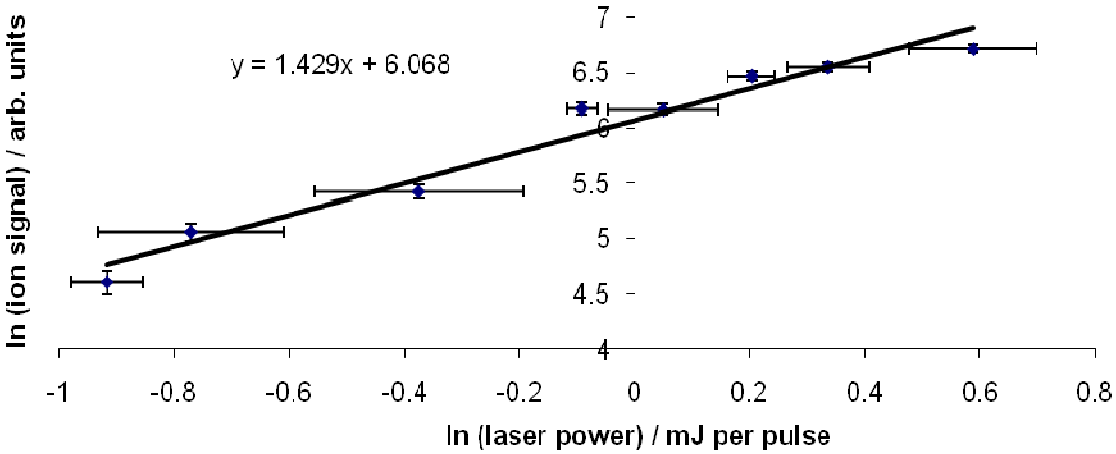

Figure 3.5 Power dependence plot of ln(laser power) against ln(ion signal), taken for REMPI of HD $v'' = 3$ $J'' = 1$ at different values of laser power of the doubled light. The laser power is measured in mJ per pulse, where there are 10 laser pulses per second. The line of best fit, y = 1.4297 x + 6.0684, has a gradient of 1.43, which provides the value of n for all scans with $v'' = 3$. The error bars on the x-axis indicate the drop and fluctuation in laser power during the scan.

Vibrational Level, v''	**Laser Correction Factor, n**
3	1.43 ± 0.11
4	1.62 ± 0.17
5	2.13 ± 0.29
6	2.69 ± 0.32
7	3.32 ± 1.24

Table 3.3 Laser power dependence factor, n, for each vibrational level, v''

As the (2+1) REMPI scheme used in this experiment is a 3-photon process and the ion signal strength depends on laser power as shown in equation 3.2, for a non-saturated process the expected value for the laser correction factor is $n = 3$. If only the one-photon process is saturated, then $n = 2$, and if the 2-photon process is saturated, then $n = 1$ [7, 8]. Furthermore, it is unlikely that the ionization step will be saturated without also saturating the resonance step. For $v'' = 3$ and 4, $n < 2$, thus at least 2 photons are saturated, hence it is probable that the resonance step is saturated. Similarly $v'' = 5$ exhibits some saturation of the resonance step with $n \sim 2$. However, for $v'' = 6$, $n \sim 3$ within error bars, so there seems to be little or no saturation in either step. For $v'' = 7$,

the level of saturation of the REMPI process cannot be inferred from *n* due to the large error bars.

The integrated areas under the REMPI peaks for a set of rotational states within a vibrational level are divided by the laser power raised to the value of *n* for that vibrational level. The corrected areas are then normalized to the $J'' = 0$ state to give the relative populations as shown in Figure 3.8.

3.5 Rotational Temperature

It is possible to create a Boltzmann plot from the relative rotational populations to determine a characteristic rotational temperature for each vibrational level. The Boltzmann distribution describes the population of the rotational levels P_J relative to the population of the $J'' = 0$ state, as shown below:

$$\frac{P_J}{P_0} = g_J(2J+1)\exp\left(-\left(\frac{E_J}{kT}\right)\right) \qquad 3.3$$

where

k is the Boltzmann constant,

J'' is the rotational quantum number,

$E_{J''}$ is the corresponding rotational energy,

T is the temperature and

g_J is the nuclear spin degeneracy, for HD, $g_J = 1$.

Rearranging equation 3.3 gives

$$\frac{E_J}{T} = -k\ln\left(\frac{P_J}{g_J(2J+1)}\right) + k\ln(P_0) \qquad 3.4$$

Equation 3.4 is of the form y = mx + c, therefore plotting $-k\ln\left(\frac{P_J}{g_J(2J+1)}\right)$ *vs.* E_J gives a straight line with gradient 1/T and intercept $k\ln(P_0)$ for rotational states whose population follows a Boltzmann distribution.

The data points will not necessarily fit on the straight line, as the relative populations may deviate from the ideal Boltzmann distribution. If the rotational populations determined from the REMPI peaks are located on the straight line, then the distribution is Boltzmann and the gradient of the line gives the rotational temperature, *T*. A least squares method is used to determine the gradient of the line of best fit to the data.

However, if the Boltzmann plot is non-linear, then the rotational distribution is non-Boltzmann. In this case, the average rotational energy, $\langle E_{rot} \rangle$, is calculated by statistical mechanics:

$$\langle E_{rot} \rangle = \sum_J P_J E_J \qquad 3.5$$

An average rotational temperature $\langle T_{rot} \rangle$ can be calculated from this average rotational energy:

$$\langle T_{rot} \rangle = \frac{\langle E_{rot} \rangle}{k} \qquad 3.6$$

The rotational populations themselves are found using

$$P_J = \frac{I_J}{\sum_J I_J} \qquad 3.7$$

where I_J is the power normalized ion signal detected for rotational state J.

A validation of this method is given in previous work [2], where the REMPI and TOFMS system was used to detect H_2 at room temperature. A Boltzmann plot of the $v'' = 0$, $J'' = 0 - 3$ ro-vibrational populations were found to follow a Boltzmann distribution with $T_{rot} \sim 295$ K, as expected.

3.6 HD Formed in Vibrational States $v'' = 3$ and 4

The results in this section were published in Islam *et al*. 2006 [9]. Nascent HD was detected in vibrational states $v'' = 3$ and 4 following continuous dosing by H- and D-atoms of the HOPG surface held at 15 K. The data was collected over a period of 3 months. The 2-photon wavelength for each REMPI transition was calculated by determining the value of the *X* state and *E, F* state energy levels, using equations 3.8,

3.9, 3.10 and 3.11 below and taking into account predicted offsets. The values of the spectroscopic constants, ϖ_e, x_e, B_e, α and D, were taken from the NIST online database [4], where ϖ_e is the vibrational wavenumber, x_e is the anharmonicity constant, B_e is the equilibrium value of B_v, the rotational constant as a function of the vibrational state, α is the vibration-rotation interaction molecular constant and D is the centrifugal distortion coefficient.

$E_{v,,}$ is the energy of a particular vibrational state, v, and is given by

$$E_v = \left(v + \frac{1}{2}\right)\varpi_e - \left(v + \frac{1}{2}\right)^2 \varpi_e x_e \text{ cm}^{-1} \qquad 3.8$$

E_J is the energy of the rotational state above the vibrational state given by

$$E_J = B_v J(J+1) - DJ^2(J+1)^2 \text{ cm}^{-1} \qquad 3.9$$

where B_v is calculated using

$$B_v = B_e - \alpha\left(v + \tfrac{1}{2}\right) \qquad 3.10$$

The total energy of each state is given by

$$E_{total} = E_{elec} + E_v + E_J \qquad 3.11$$

where E_{elec} is the electronic state energy. The difference in total energy of the *E*, *F* state and the *X* state is then converted to the 2-photon wavelength.

Typically 4 – 12 REMPI spectra were recorded non-sequentially for each ro-vibrational state and the ion signals from these averaged to obtain relative rotational populations with error values, as shown in Figure 3.6:

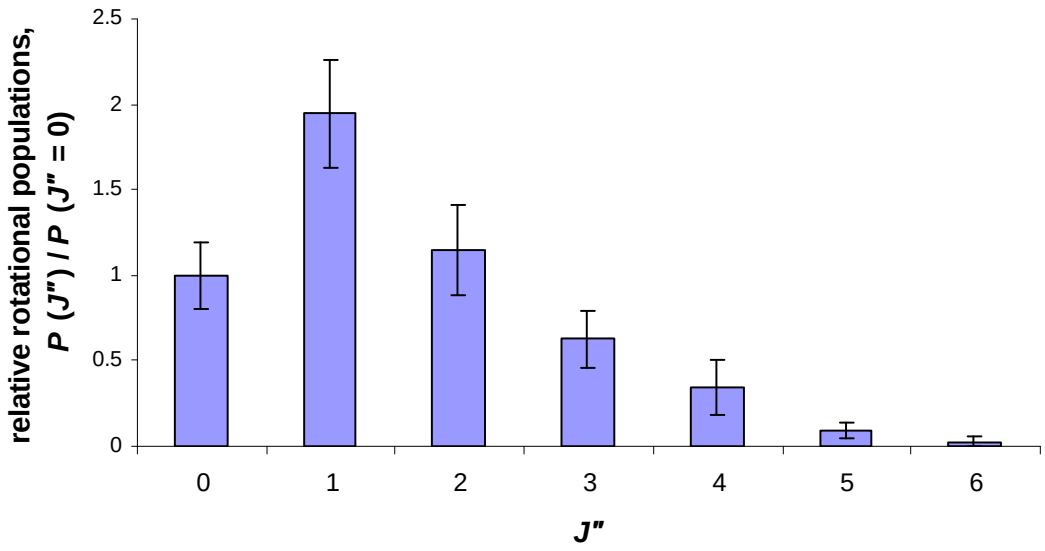

Figure 3.6 Relative rotational populations for HD formed in vibrational level $v'' = 3$. The area under the REMPI peak for each J'' state has been laser power corrected and normalized to the $J'' = 0$ state.

For the $v'' = 3$ level, the most populated rotational state was found to be the $J'' = 1$ state. REMPI signals were detected for rotational states $J'' = 0 – 6$. For strong signals, the signal-to-noise (S/N) values are in excess of 20 and for weak signals, S/N ~ 5. A search was made for states $v'' = 3$, $J'' = 7$ and 8, but no HD^+ ions were detected above the background noise, even at very long accumulation times. The signal-to-noise ratio for this non-detection, at the predicted wavelengths for the $v'' = 3$, $J'' = 7$ and 8 REMPI transitions, was S/N = – 0.2. This implies that either the $v'' = 3$, $J'' = 7$ and 8 states are not populated by nascent HD molecules, or that the population is small enough to be masked by the background counts of the experiment. The background counts are typically 1 – 10 ions in 60 seconds and result from ionization events initiated by photoelectrons. As aforementioned, these photoelectrons are liberated when stray laser light hits the stainless steel chamber walls.

The Boltzmann plot for the $v'' = 3$ state is shown below in Figure 3.7. The rotational temperature was found to be $T_{rot} = 330 \pm 26$ from the gradient of the line of best fit, as described in Section 3.5. The relative rotational populations roughly follow a Boltzmann distribution as the data points are located on the line of best fit, taking into account error bars.

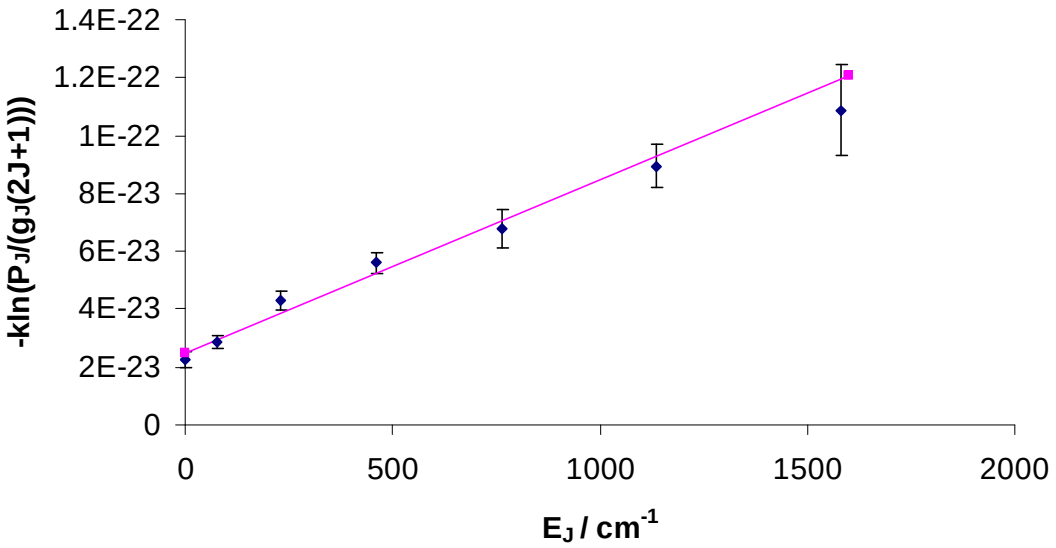

Figure 3.7 Boltzmann plot for the relative rotational populations for HD formed in vibrational level $v'' = 3$ with a weighted least squares fit to the data. The rotational temperature was found to be $T_{rot} = 330 \pm 26$ K.

This procedure was repeated for the $v'' = 4$ level. The areas under the REMPI spectra in Figure 3.3 were corrected for accumulation time and laser power to determine the $v'' = 4$ relative rotational populations, which are shown in Figure 3.8. Again, HD was found to be formed in rotational states $J'' = 0 – 6$ with the most populated rotational state being the $J'' = 1$ state. After Boltzmann analysis, the rotational temperature was found to be $T_{rot} = 368 \pm 22$. The $v'' = 4$ Boltzmann plot is shown in Figure 3.9. Points that lie below the line of best fit shown in Figure 3.9, such as the $J'' = 6$ state, are marginally overpopulated with respect to an ideal Boltzmann distribution with $T_{rot} = 368$. The Boltzmann plot appears non-linear, such that the data points seem to follow a curve, rather than lying on the line of best fit.

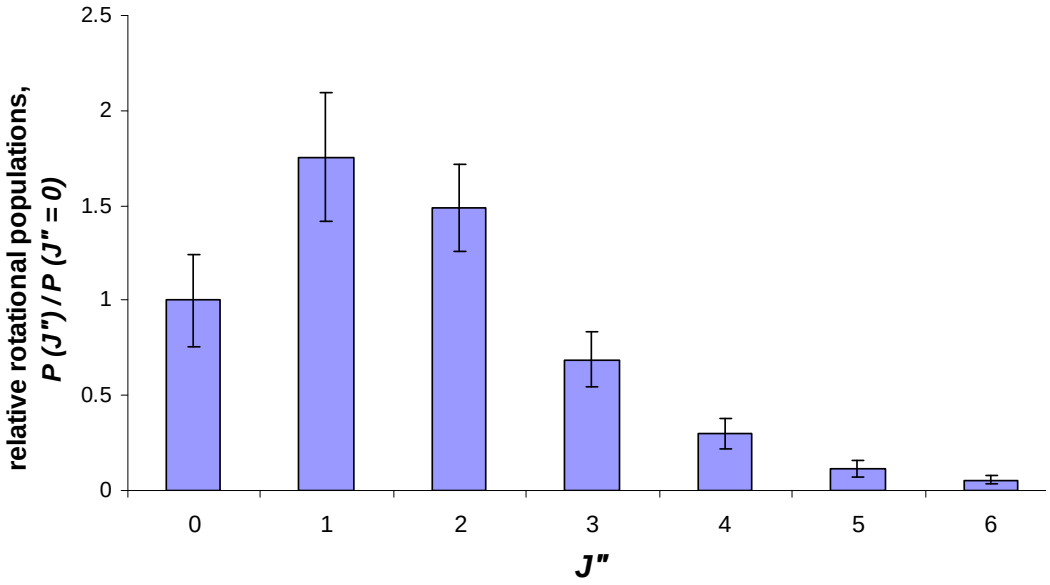

Figure 3.8 Relative rotational populations for HD formed in vibrational level $v'' = 4$. The area under the REMPI peak for each J'' state has been laser power corrected and normalized to the $J'' = 0$ state.

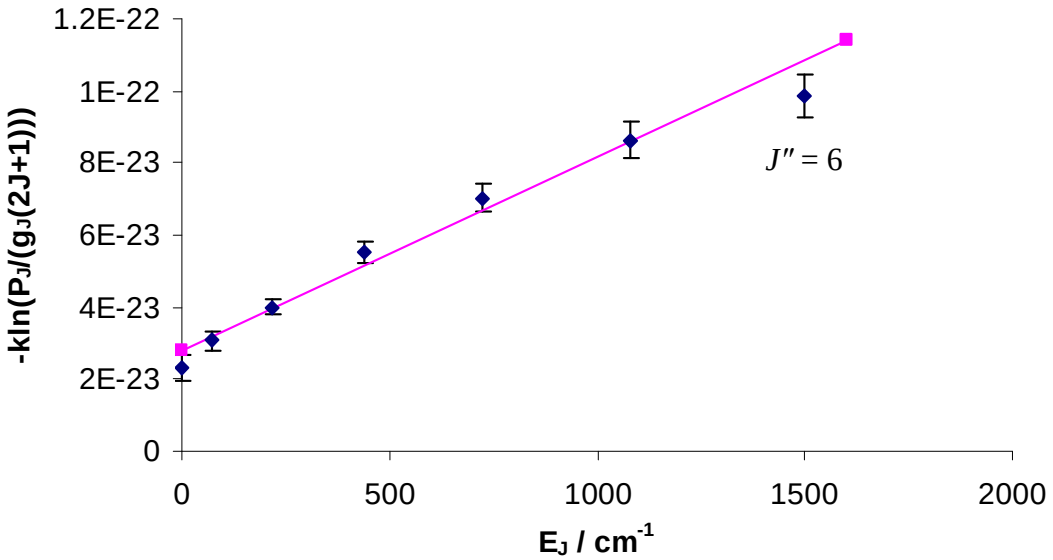

Figure 3.9 Boltzmann plot for the relative rotational populations for HD formed in vibrational level $v'' = 4$ with a weighted least squares fit to the data. The rotational temperature was found to be $T_{rot} = 368 \pm 22$ K.

The rotational populations relative to the $J'' = 0$ state are given in the tables below:

v''	J''	**Relative Population**
3	0	1.00 ± 0.20
	1	1.94 ± 0.32
	2	1.15 ± 0.26
	3	0.63 ± 0.17
	4	0.34 ± 0.16
	5	0.09 ± 0.04
	6	0.03 ± 0.03

Table 3.4 Relative rotational populations for HD formed in $v'' = 3$ on HOPG held at 15 K, normalized to the $v'' = 3$, $J'' = 0$ state

v''	J''	**Relative Population**
4	0	1.00 ± 0.25
	1	1.75 ± 0.34
	2	1.49 ± 0.23
	3	0.69 ± 0.15
	4	0.30 ± 0.08
	5	0.11 ± 0.04
	6	0.05 ± 0.02

Table 3.5 Relative rotational populations for HD formed in $v'' = 4$ on HOPG held at 15 K, normalized to the $v'' = 4$, $J'' = 0$ state

As can be seen in Table 3.4, the $v'' = 3$, $J'' = 6$ state has a relative population of 0.03 ± 0.03, which is effectively negligible, within error bars. Hence, it is unsurprising that higher rotational states were not detected. In order to compare the populations of the $v'' = 3$ and 4 states, the data in Table 3.4 and Table 3.5 was scaled by the Franck-Condon factor of the REMPI transition used to detect each rovibronic state. This is discussed further in Section 3.8.

3.7 HD Formed in Vibrational States $v'' = 5 – 7$

HD formed in the ro-vibrational states $v'' = 5$, 6 and 7 was also detected [10]. This work was conducted after an interval of about 3 months, due to experimental problems. A power cut occurred after the $v'' = 4$ data was taken, which resulted in significant loss in signal. The $v'' = 4$, $J'' = 1$ signal was reduced from 160 ion counts to 27 ion counts for an accumulation time of 60 seconds. It was suspected that the drift tube of the TOFMS had been contaminated, thus the TOFMS was removed from the chamber, dismantled and cleaned. After reassembly and reinstallation of the TOFMS, the REMPI signals returned to their previous strength.

However, despite the cleaning, the $v'' = 5$ signals remained elusive although large ranges of wavelength were searched for a REMPI transition. It transpired that the calculated 2-photon wavelength for the REMPI transition was not accurate, due to the values of the spectroscopic constants involved in equations 3.8, 3.9 and 3.10. Hence, a new method of calculating the energy of the rotational and vibrational levels within the *E, F* state and the *X* state was developed. This involved recalculating the values of $E_{J'}$, $E_{J''}$ and $E_{v''}$ with experimental data taken from Dabrowski and Herzberg [5], as described below.

The constants for the *E, F* state used in the original $v'' = 3$ and 4 calculations are $B_e = 24.568$ cm^{-1} and $D = D_e = 0.0123$ cm^{-1}, where B_e is the equilibrium value of the rotational constant and D is the centrifugal distortion coefficient These values were obtained from the NIST database [4] and are sufficiently accurate for ro-vibrational levels where $v' = 0$, but led to a large range of wavelengths being searched before HD formed in the $v'' = 3$ and 4 states was found, because these states are ionized *via* the $v' = 1$ state. Thus for the $v'' = 5 – 7$ states, which are ionized via the resonant $v' = 1 – 3$ states respectively, experimentally derived constants from Dabrowski and Herzberg [5], shown in Table 3.6, are preferable to NIST data. The values given in this paper are B_v and D_v which are the rotational constant and centrifugal distortion detected for each vibrational state. Equation 3.9 was used to recalculate the rotational energy of the *E, F* state, $E_{J'}$, with the new values of B_v and by setting $D = D_v$.

E, F state, *v′*	B_v (NIST)	B_v	D_v
0	23.924	23.924	0.0123
1	22.636	22.636	0.0118
2	21.348	20.820	0.0830
3	20.060	14.580	0.0997

Table 3.6 Values for B_v and D_v taken from Dabrowski and Herzberg 1975 [5]. The NIST value has been calculated using $B_v = B_e - \alpha\left(v + \frac{1}{2}\right)$, where B_e = 24.568 and α = 1.288. The NIST value for D is D_e = 0.0123, used for all vibrational levels in the *E, F* state [4].

As aforementioned, the NIST data is only sufficiently accurate for the lowest vibrational levels. Therefore the energy of rotational levels within $v'' = 5 - 7$ in the *X* state, $E_{J''}$, also needed to be recalculated using values from Dabrowski and Herzberg [5]. The values of B_v and D_v used for the vibrational levels $v'' = 5 - 7$ in the *X* state are shown below in Table 3.7. The corresponding values from NIST are also shown.

X state, *v″*	B_v (NIST)	B_v	D_v
5	34.732	35.311	0.0228
6	32.746	33.460	0.0221
7	30.760	31.605	0.0219

Table 3.7 Values for B_v and D_v taken from Dabrowski and Herzberg 1975 [5] for the *X* state. The NIST value has been calculated using $B_v = B_e - \alpha\left(v + \frac{1}{2}\right)$, where B_e = 45.655, α = 1.986. The NIST value for D is D_e = 0.026 used for all vibrational levels in the *X* state [4].

Dabrowski and Herzberg also provide the experimentally observed energy levels of all states in the *X* state relative to the $v'' = 0$, $J'' = 0$ state, $E(v'', J'')$, and the energy of the $v'' = 0$, $J'' = 0$ state above the *X* state potential well, E_0. These can be added to calculate $E_{v''}$, the *X* state vibrational energy of the HD molecule, such that

$$E_{v''} = E(v'', J'' = 0) + E_0 \qquad 3.12$$

$E_{v''} + E_{J''}$ can also be obtained directly from the Dabrowski and Herzberg paper by calculating $E(v'', J'') + E_0$.

The vibrational energy of the *E, F* state, $E_{v'}$, is not given in Dabrowski and Herzberg, but the band origins, v_0^{v}, of the vibrational levels are provided. The band origin can be expressed as

$$v_0^{v} = E_{elec,\,E,F} + E_{v'} - (E_{elec,\,X} + E_0) \qquad 3.13$$

The 2-photon wavelength can then be determined by finding the difference in energy, ΔE_{total}, between the ro-vibrational level in the *X* state and the ro-vibrational level in the *E, F* state, such that

$$\Delta E_{total} = (E_{elec,\,E,F} + E_{v'} + E_{J'}) - (E_{elec,\,X} + E_{v''} + E_{J''}) \qquad 3.14$$

where $E_{elec,\,E,F}$ and $E_{elec,\,X}$ are the electronic energy levels of the *E, F* and *X* state respectively. Thus by substituting equations 3.12 and 3.13 into 3.14, we obtain

$$\Delta E_{total} = v_0^{v} + E_{J'} - E(v'', J'' = 0) - E_{J''} \qquad 3.15$$

which can be calculated without using values from NIST.

The wavelength of the dye laser photons required to carry out the REMPI transition is then calculated by doubling the 2-photon wavelength. As can be seen in Table 3.8, which shows the wavelengths of $J'' = 1$ transitions within each vibrational level, the wavelength values calculated using the Dabrowski and Herzberg are more accurate than those using constants from the NIST database for the higher vibrational states.

v''	***v'***	**Wavelength, Observed / nm**	**Wavelength, D&H / nm**	**Δλ, O – D&H / nm**	**Wavelength, NIST / nm**	**Δλ, O - NIST / nm**
3	1	**439.711**	439.838	-0.127	439.619	0.092
4	1	**455.247**	455.389	-0.142	455.001	0.246
5	1	**470.973**	471.135	-0.162	470.482	0.491
6	2	**475.983**	476.132	-0.149	475.142	0.841
7	3	**481.611**	481.790	-0.179	479.780	1.831

Table 3.8 The calculated and observed wavelengths of the dye laser photons, for which the transition $X\ ^1\Sigma_g^+\ (v'', J'' = 1) \rightarrow E, F\ X\ ^1\Sigma_g^+\ (v' = 1, J' = 1)$ occurs. O indicates the laser photon wavelength for an observed REMPI signal, D&H indicates that the Dabrowski and Herzberg constants have been used to calculate the laser photon wavelength and NIST indicates that only NIST constants were employed to calculate the laser photon wavelength. The difference in observed and predicted wavelength is also shown.

The REMPI transitions are much closer to the predicted wavelength for $v'' > 3$, when the predicted wavelength is calculated using the Dabrowski and Herzberg values. Thus HD ion signals are much easier to find using this method. The $v'' = 5 – 7$ states were found in quick succession in a period of 3 weeks. Typically 3 – 6 REMPI spectra were recorded non-sequentially for each ro-vibrational state. As before, the area under these peaks were converted into rotational populations relative to the $J'' = 0$ state within each vibrational level, as shown in Table 3.9. For $v'' = 5$, the rotational states $J'' = 0 – 6$ were detected and signals were noticeably weaker than for the $v'' = 4$ state. This trend continued as the $v'' = 6$ and 7 signals were also subsequently weaker than the $v'' = 5$ signals, such that only the $J'' = 0 – 4$ states could be found for the $v'' = 6$ level and only the $J'' = 0 – 3$ states could be found for the $v'' = 7$ level. The relative vibrational populations will be quantified in Section 3.8. Longer accumulation times were required for these weak signals, such the time spent per wavelength step during the laser scan ranged from 120 s to 320 s. Signal-to-noise values were typically S/N ~ 6 for strong signals and S/N ~ 0.9 for weak signals. Again, higher rotational levels than those detected were searched for, but not found.

The rotational populations relative to the $J' = 0$ state are given in the table below:

v''	J''						
	0	**1**	**2**	**3**	**4**	**5**	**6**
5	1.00 ± 0.15	1.40 ± 0.17	1.96 ± 0.24	0.72 ± 0.11	0.38 ± 0.08	0.09 ± 0.05	0.08 ± 0.05
6	1.00 ± 0.32	2.10 ± 0.47	2.22 ± 0.48	0.59 ± 0.25	0.35 ± 0.19	-	-
7	1.00 ± 0.44	1.88 ± 0.60	1.84 ± 0.56	1.11 ± 0.46	-	-	-

Table 3.9 Relative rotational populations for HD formed in $v' = 5 – 7$ on HOPG held at 15 K, normalized to the $J' = 0$ state within each vibrational level.

Rotational and Boltzmann plots were created for the $v'' = 5 – 7$ states and are shown in Figures 3.10 to 3.15. $J'' = 2$ is the most populated rotational state for $v'' = 5$ and 6, whereas for the lower vibrational levels $v'' \leq 4$, $J'' = 1$ is the most populated. Similarly to the $v'' = 4$ Boltzmann plot, the $v'' = 5$, $J'' = 6$ state is overpopulated with respect to a thermal distribution. In fact, Table 3.9 shows that the population of the $v'' = 5$, $J'' = 6$

state and the $v'' = 5$, $J'' = 5$ state are very similar, which would not be the case for an ideal Boltzmann distribution. However, the populations for these high rotational states are very small, taking into account the errors. The Boltzmann analysis of the $v'' = 6$ and 7 rotational populations indicate that these states are thermally distributed. However, the ion signals for the $v'' = 7$ state were very weak, leading to proportionately large error bars. Also, because the $v'' = 7$ signals were weak, long accumulation times of 320 s per wavelength step were used, resulting in scans which were over 40 minutes long, during which the dye deteriorates significantly. Consequently, there are large laser power fluctuations for the $v'' = 7$ signals. Hence there is a greater degree of uncertainty in the rotational temperature value for $v'' = 7$ than for the other vibrational states. The rotational temperatures were found to be 338 ± 22 K for $v'' = 5$, 266 ± 55 K for $v'' = 6$ and 336 ± 102 K for $v'' = 7$.

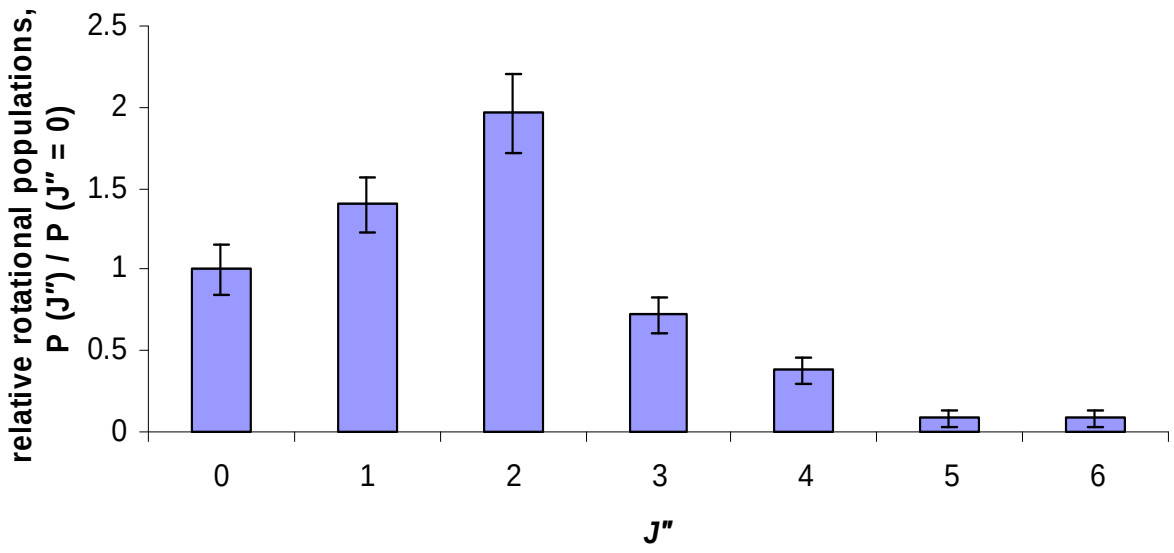

Figure 3.10 Relative rotational populations for HD formed in vibrational level $v'' = 5$. The area under the REMPI peak for each J'' state has been laser power corrected and normalized to the $J'' = 0$ state.

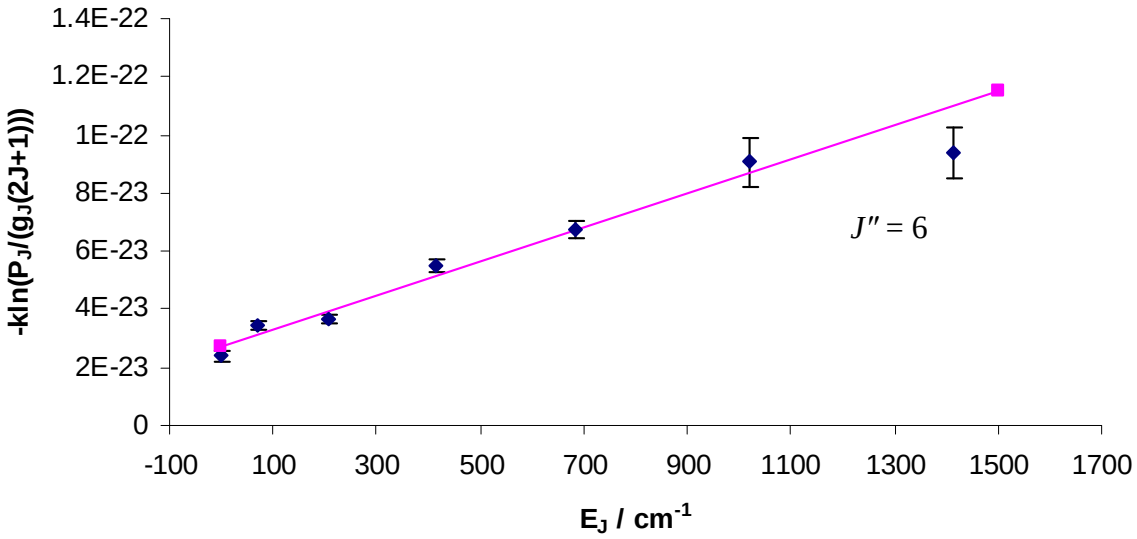

Figure 3.11 Boltzmann plot for the relative rotational populations for HD formed in vibrational level $v'' = 5$ with a weighted least squares fit to the data. The rotational temperature was found to be $T_{rot} = 338 \pm 20$ K.

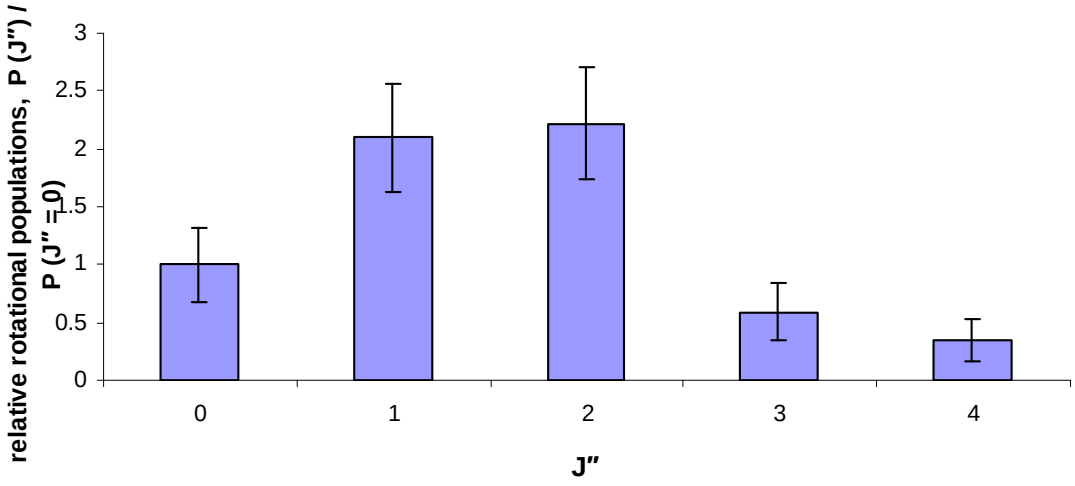

Figure 3.12 Relative rotational populations for HD formed in vibrational level $v'' = 6$. The area under the REMPI peak for each J'' state has been laser power corrected and normalized to the $J'' = 0$ state.

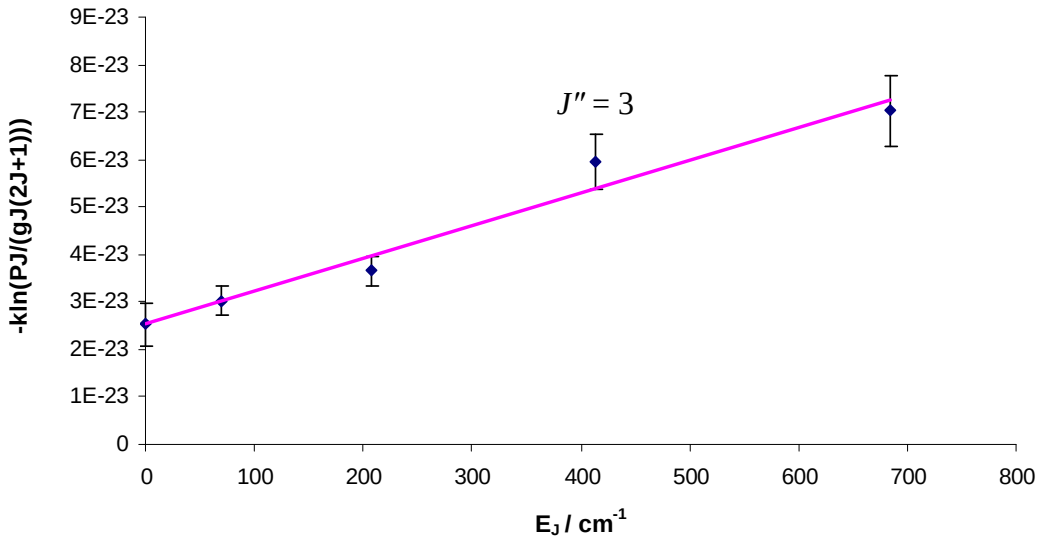

Figure 3.13 Boltzmann plot for the relative rotational populations for HD formed in vibrational level $v'' = 6$ with a weighted least squares fit to the data. The rotational temperature was found to be $T_{rot} = 267 \pm 55$ K.

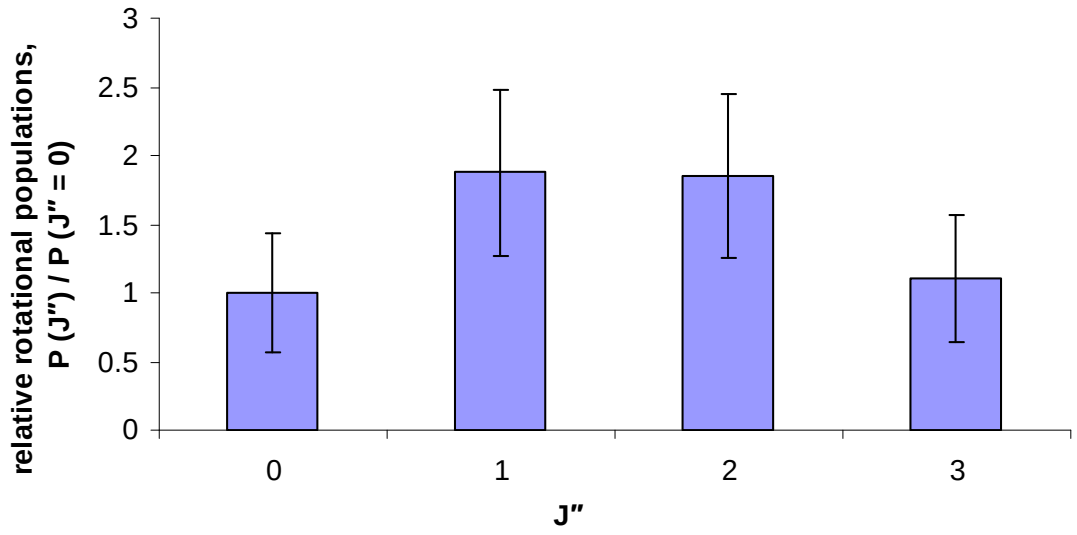

Figure 3.14 Relative rotational populations for HD formed in vibrational level $v'' = 7$. The area under the REMPI peak for each J'' state has been laser power corrected and normalized to the $J'' = 0$ state.

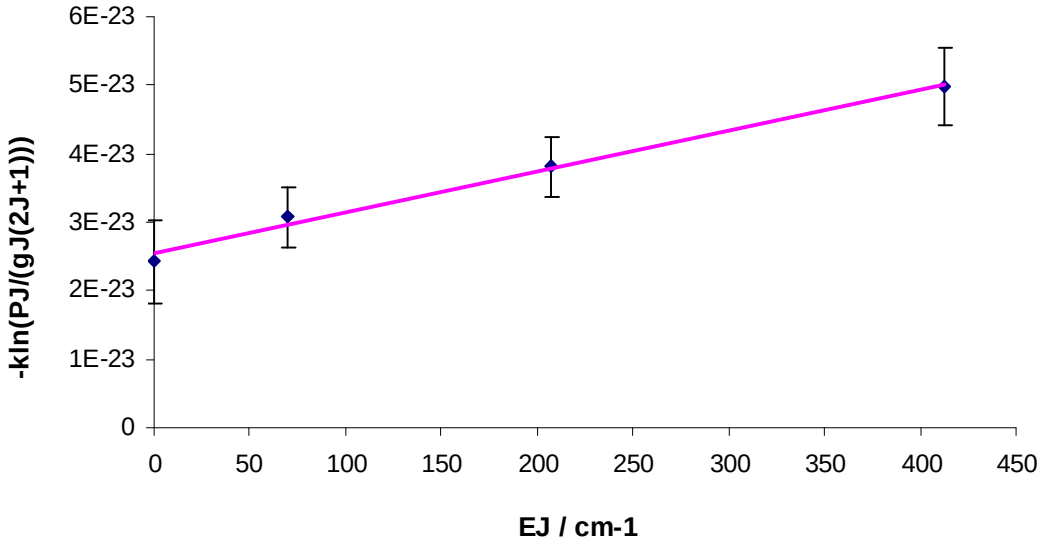

Figure 3.15 Boltzmann plot for the relative rotational populations for HD formed in vibrational level $v'' = 7$ with a weighted least squares fit to the data. The rotational temperature was found to be $T_{rot} = 337 \pm 102$ K.

The rotational temperatures of all the vibrational states investigated by the Cosmic Dust Experiment are tabulated below, including the data for $v'' = 0 - 2$ from previous work [2]. These rotational temperature values are calculated from a weighted least squares fit to the Boltzmann plots and are much higher than the temperature of the HOPG surface for all vibrational levels. It can be seen that the rotational temperature

peaks at $v'' = 4$. The average rotational energy of the states, which is determined from the statistical mechanics calculation described in Section 3.5 is also given. The average rotational energy is a useful alternative measure of the rotational excitation for populations that do not strictly adhere to the Boltzmann distribution, which may be the case for the $v'' = 4$ and 5 rotational populations, where the data points on the Boltzmann plots would be better described by a curve rather than a line of best fit.

States Detected, v'', J''	**Rotational Temperature / K**	**Average Rotational Energy / cm^{-1}**
$v'' = 0$, undetected	-	-
$v'' = 1$, $J'' = 0 – 4$	246 ± 24	177 ± 4
$v'' = 2$, $J'' = 0 – 4$	282 ± 31	180 ± 30
$v'' = 3$, $J'' = 0 – 6$	330 ± 26	213 ± 4
$v'' = 4$, $J'' = 0 – 6$	368 ± 22	217 ± 3
$v'' = 5$, $J'' = 0 – 6$	338 ± 20	224 ± 3
$v'' = 6$, $J'' = 0 – 4$	267 ± 55	163 ± 6
$v'' = 7$, $J'' = 0 – 3$	337 ± 102	147 ± 8

Table 3.10 Rotational temperatures and average rotational energy of HD formed on HOPG at 15 K for all states investigated by the Cosmic Dust Experiment. As previously discussed, the $v'' = 0$ state could not be detected above the background HD in the target chamber.

We can speculate that the data points on the Boltzmann plots in Figure 3.9 and 3.11 do not follow a straight line due to the presence of more than one formation mechanism or different formation sites. However, there is no *a priori* reason for the rotational populations to obey a Boltzmann distribution. However Boltzmann distributions have often, but not always [11] been observed for recombination on metal surfaces. For example, the rotational populations of D_2 formed on an Ni(110) surface has been found to follow a Boltzmann distribution in a study by Winkler [12], with the calculated rotational temperatures being significantly higher than the surface temperature of 180 K. In this study, the rotational temperature was found to decrease with vibrational quantum number, where T_{rot} = 2120 K, 1840 K, 1070 K, and 520 K for the desorbing D_2 molecules in the vibrational states 0, 1, 2, and 3, respectively. Boltzmann rotational distributions were also observed for the formation of D_2 on

Ag(111) by Murphy and Hodgson [13], who found that the rotational temperature was T_{rot} = 550 K, again much higher than the surface temperature of 210 K. Conversely, when studying the formation of H_2 on Pd(100), Schröter *et al.* [14] found that although the rotational populations did obey a Boltzmann distribution, the average rotational temperature of the molecules was lower than that of the surface, with T_{rot} = 281 K from a surface at 570 K

Furthermore, the reverse process to the associative desorption of atoms has been observed, where molecules in a Boltzmann distribution dissociatively adsorb onto a surface [15, 16]. The final state distribution of product molecules from associative desorption can be related to the dynamics of dissociative adsorption by the principle of detailed balance [15]. The principle of detailed balance involves equating the rates of adsorption and desorption for a surface at equilibrium, which allows state-resolved sticking coefficients to be derived from state-resolved desorption data. Thus, it is plausible that HD molecules formed from recombination on a graphite surface have nascent rotational populations following a Boltzmann distribution and that the rotational temperature varies with vibrational level.

The rotational temperatures calculated in Table 3.10 are much higher than the HOPG surface temperature of 15 K. Thus the binding energy of the H- and D-atoms must be converted into rotational energy on recombination. There must be some dynamical origin for the rotational angular momentum, possibly glancing collisions between H- and D-atoms to form HD molecules. The high rotational temperature indicates that the atoms do not thermalize with the surface before recombination. This would rule out the Langmuir-Hinshelwood mechanism, where both the H- and D-atoms undergo physisorption, thermalize with the surface and diffuse across the surface to react. Instead, the hot-atom mechanism, where the H- and D-atoms are bound to the surface but not thermalized, seems more plausible. The Eley-Rideal mechanism, where one atom in the gas phase impacts on the other preadsorbed atom, is unlikely to occur for this experimental set-up as the coverage of atoms on the HOPG surface is expected to be low. Previous work has determined the steady-state coverage of the HOPG surface to be approximately one hundredth of a monolayer [2].

The rotational temperatures shown in Table 3.10 range from 246 K to 368 K, near the value of room temperature, thus we must eliminate the possibility that the HD molecules were involved in collisions before detection. Extensive studies were carried out in previous work [2] to show that it is improbable that the HD molecules were thermalized. When experiments were repeated at half the pressure in the atom cell, and hence at half the pressure in the target chamber, no difference was found in the observed rotational temperature [3]. If the HD molecules collide with other atoms and molecules before detection, then the decrease in pressure would reduce the degree of thermalization and the value of the rotational temperature would be affected, which is not the case. This indicates that the determined rotational temperatures are indicative of the nascent rotational distribution and not of thermalized HD molecules.

3.8 Relative Vibrational Populations

As well as quantifying the rotational distribution within each vibrational level, it would be valuable to quantify the vibrational distribution and calculate relative vibrational populations. To do this, the probability of each REMPI transition must be determined. The rate-determining step of the REMPI process is the transition from a (v'', J'') level in the X state to a (v', J') level in the E, F state, as the efficiency of the non-resonant ionizing step is large. Of course, the excitation step to the resonant E, F state has different probabilities of occurring depending on the states involved, and this is measured by its two-photon transition moment $|M_{fo}|^2$.

Huo *et al.* [17] have calculated $|M_{fo}|^2$ for REMPI transitions of H_2 and HD from different ro-vibrational levels in the X state (v'', J'') *via* E, F ($v' = 0$, $J' = J''$). This work showed that the magnitude of $|M_{fo}|^2$ varies significantly with the vibrational state but is not significantly dependent on the value of J''. For the H_2 transitions, Huo *et al.* [17] compared their calculated $|M_{fo}|^2$ values with the $X \rightarrow E$, F Franck-Condon factors, FCFs, which are a measure of the overlap of two vibrational states. It was found that the probability of a REMPI transition occurring appears to be dominated by the relevant FCF. For HD, we compared the $|M_{fo}|^2$ values of Huo *et al.* [17] with the relevant FCFs as shown in Table 3.11. Again, it appears that the probability of a REMPI transition occurring appears to be dominated by the FCF.

$v'' \rightarrow v'$	$\lvert M_{fo}\rvert^2$	FCF
$0 \rightarrow 0$	6.87	0.12
$1 \rightarrow 0$	22.12	0.31
$2 \rightarrow 0$	28.50	0.33
$3 \rightarrow 0$	19.07	0.18
$4 \rightarrow 0$	7.18	0.053
$5 \rightarrow 0$	1.53	0.0089
$6 \rightarrow 0$	0.18	0.0008

Table 3.11 Two-photon transition moment, $|M_{fo}|^2$, taken from Huo *et al.* [17] and Franck Condon factor, FCF, for the transitions $^1\Sigma_g^+$ *X* (v'', $J'' = 0$) $\rightarrow$ $^1\Sigma_g^+$ *E,F* ($v' = 0$, $J' = J'' = 0$) for $v'' = 0 - 6$.

Huo *et al.* [17] provide the two-photon transition moment for the $v' = 0$ level of the *E, F* state and $v'' = 0 - 6$ of the *X* state. However, the experiments detailed in this thesis involved transitions to the *E, F* states $v' = 1$, 2 and 3 and go up to the $v'' = 7$ level of the *X* state. For the FCFs of the states actually used to obtain data, with their values of v'' and v', see Table 3.2. As aforementioned, the resonant *E, F* states were selected due to their favourable FCFs for the particular $v'' \rightarrow v'$ REMPI transition, because a transition with a high FCF will correspondingly have a high value of $|M_{fo}|^2$ and thus lead to strong, detectable signals. We extend the conclusions from the study Huo *et al.* [17] and assume that the REMPI probability for these transitions is dominated by the relevant FCFs and does not depend strongly on rotational state. Hence, to express the relative rotational populations of all the vibrational states on the same scale, the REMPI signal of all ro-vibrational states must be divided by the Franck-Condon factor of the transition.

Scaling the normalized ion signals of each REMPI transition by the appropriate FCFs gives an indication of the relative ro-vibrational populations as shown in Figure 3.16. The scaled normalized signals are then summed within each vibrational level to give

the total normalized signal for each vibrational state, which indicates the relative vibrational populations, shown in Figure 3.17. The validity of this intercomparison of vibrational states lies in a variety of experimental parameters remaining effectively constant for all sets of data collection. For example, the laser alignment and beam shape, the atom fluxes from the sources and the ion detection efficiency are experimental parameters that change over time. As stated previously, the $v'' = 5 – 7$ data was collected three months after the $v'' = 3$ and 4 data. However, every effort was made to ensure that the experimental conditions were identical for ionization of the $v'' = 3$ and 4 states and the $v'' = 5 – 7$ states. It is important to realize that the TOFMS measures the density of the ionized nascent molecules and this measurement is related to the flux of desorbing HD molecules by the velocity of the ion. Thus, implicit in the intercomparison of ro-vibrational levels, is the assumption that the nascent velocities of HD in all vibrational levels are similar. From the temporal widths of our TOF mass spectra, which are not dependent on the HD vibrational level, we have no reason to assume that there is a difference in velocity of HD in different v'' states. Furthermore, HD in all vibrational states is known to have translational energy under 1.1 eV. This is discussed in Section 3.10.

Also included in Figures 3.16 and 3.17 is $v'' = 1$ and 2 data collected in previous work [1, 2], which has been scaled by the appropriate FCFs using the same methodology described above. Since these data on the lower vibrational states were recorded sometime earlier, although under very similar conditions, there is undoubtedly more uncertainty in the relative vibrational populations we derive. Due to the considerable reconfiguration of the laser system necessary to detect the $v'' = 1$ and 2 states, a remeasurement of the intensities of these vibrationally excited molecules from the surface would be no more accurate than comparing with our previous measurements. For $v'' = 1$ and 2, the YAG light is energy doubled to pump the dye laser and the dye laser light is energy tripled to produce the REMPI photons; whereas for the $v'' = 3 – 7$ states the YAG light is energy tripled to pump the dye laser and the dye laser light is energy doubled to produce the REMPI photons. Further details of the difference in laser configuration for the $v'' = 1$ and 2 states are given in Chapter 2. The magnitude of the laser power and the laser power fluctuations are similar for both laser configurations, therefore the intercomparison of the $v'' = 1$ and 2 states to the $v'' = 3 – 7$ states is still valid, despite the change in laser system.

The ro-vibrational states in the v'' = 0 level cannot be detected due to thermalized HD molecules in the vacuum chamber swamping the REMPI signals as described in Section 3.2. Without the detection of the v'' = 0 state, a Boltzmann plot cannot be constructed for the ro-vibrational populations. The average ro-vibrational energy, calculated using $\langle E \rangle = \sum_{v,J} P_{v,J} E_{v,J}$, is 1.75 eV, where all non-detected states are neglected and the v'' = 0 state ro-vibrational populations have been taken to equal the v'' = 1 state ro-vibrational populations, with $\sum_{v,J} P_{v,J} = 1$. An alternative method is to assume that the populations of the v'' = 0 states are negligible, as well as all non-detected states, which gives an average internal energy of 1.83 eV.

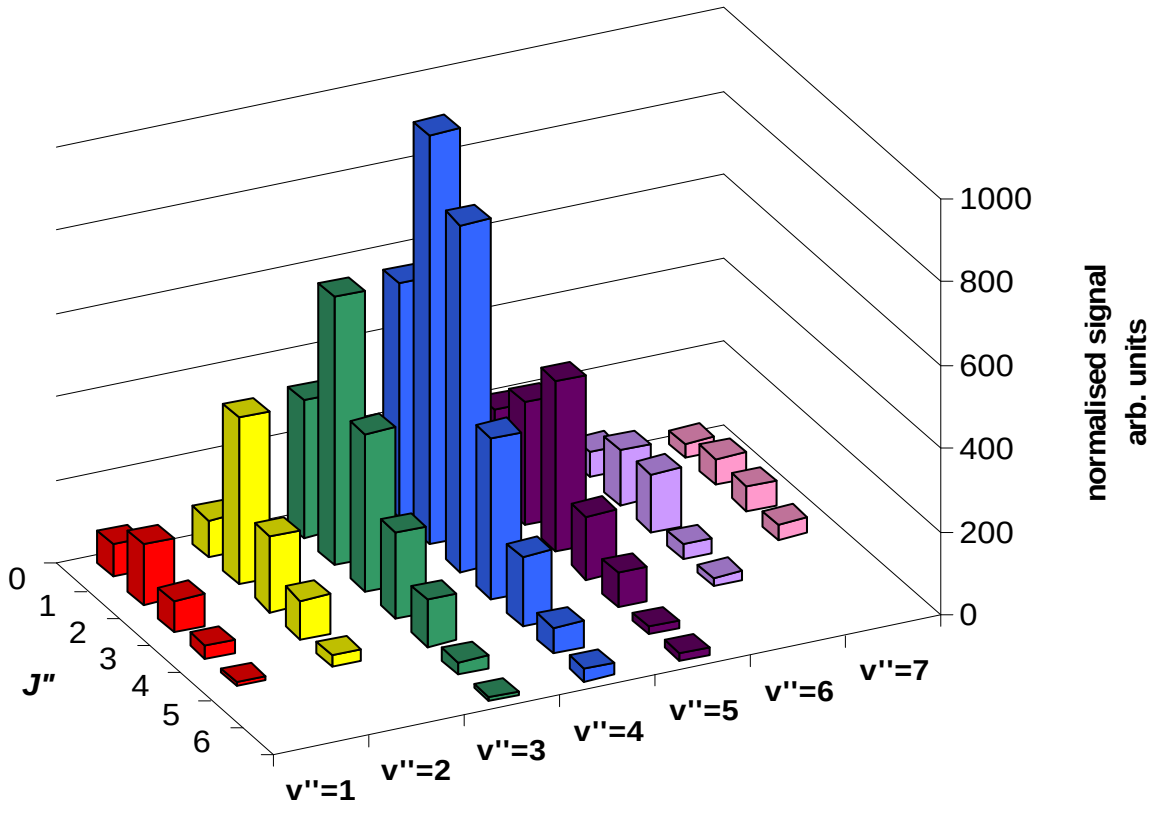

Figure 3.16 Relative ro-vibrational populations for HD formed in vibrational level v'' = 1 – 7 on an HOPG surface held at 15 K. The normalized ion signal has been scaled by the appropriate FCFs as described above.

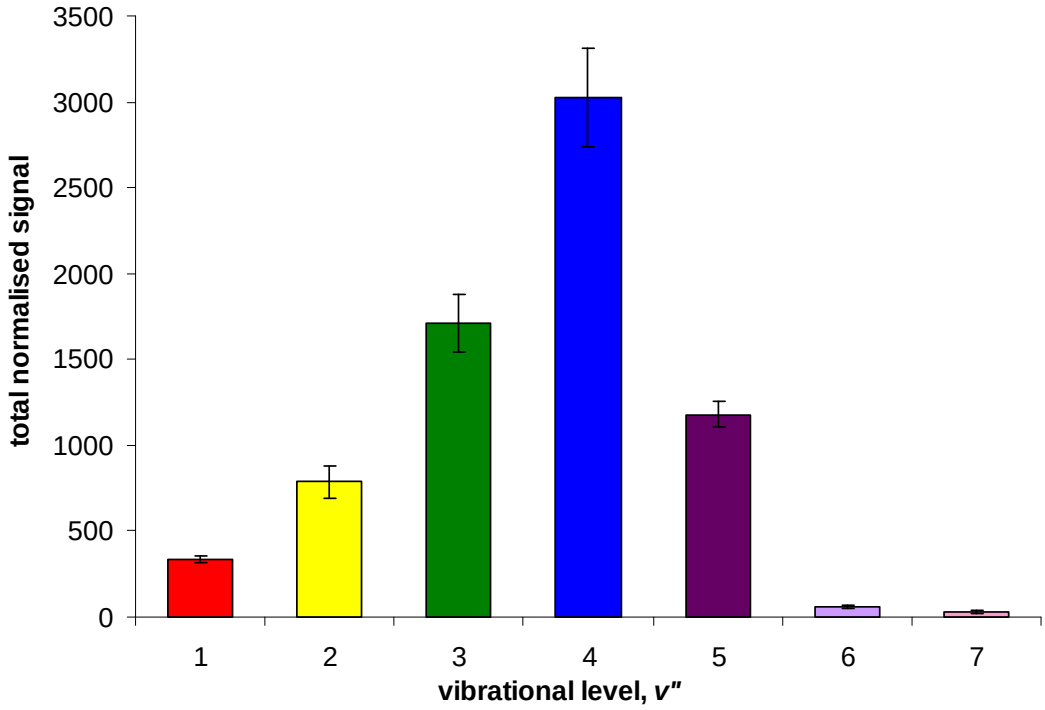

Figure 3.17 Relative vibrational populations for HD formed in vibrational level $v'' = 1 – 7$ on an HOPG surface held at 15 K. The rotational populations have been summed within each vibrational level to obtain this plot.

Figure 3.17 clearly shows that the total vibrational population roughly doubles with vibrational state up to the $v'' = 4$ state, after which there is a decline in the vibrational populations. The raw data of Figure 3.16 and Figure 3.17 are given in Table 3.12 and Table 3.13 respectively below:

v″	***J″***						
	0	**1**	**2**	**3**	**4**	**5**	**6**
1	79 ± 9	144 ± 10	75 ± 10	31 ± 9	9 ± 7	-	-
2	89 ± 26	400 ± 72	180 ± 36	93 ± 29	26 ± 21	-	-
3	330 ± 65	642 ± 105	379 ± 86	207 ± 55	113 ± 53	29 ± 16	8 ± 9
4	560 ± 137	983 ± 190	833 ± 127	387 ± 83	168 ± 46	64 ± 23	30± 13
5	209 ± 31	293 ± 36	411 ± 51	151 ± 23	80 ± 17	18 ± 11	17 ± 11
6	40 ± 13	84 ± 19	88 ± 19	23 ± 10	14 ± 8	-	-
7	33 ± 14	61 ± 20	60 ± 20	36 ± 15	-	-	-

Table 3.12 Relative ro-vibrational populations for HD formed in vibrational level $v'' = 1 – 7$ on an HOPG surface held at 15 K. The normalized ion signal has been scaled by the appropriate FCFs as described above.

Vibrational Level, v''	Total normalized signal
1	**339 ± 20**
2	**788 ± 92**
3	**1708 ± 169**
4	**3025 ± 284**
5	**1179 ± 77**
6	**60 ± 8**
7	**30 ± 5**

Table 3.13 Relative vibrational populations for HD formed in vibrational level $v'' = 1 – 7$ on an HOPG surface held at 15 K. The relative rotational populations in Table 3.12 have been summed within each vibrational level to obtain this plot.

3.9 Consecutive Scans

A series of rapid consecutive scans were carried out in order to check the ro-vibrational populations calculated in Figure 3.16. Three REMPI scans were carried out and averaged for the most abundant J'' state in each v'' state for vibrational levels $v'' = 3 – 7$. The states used were (v'', J'') = (3, 1), (4, 1), (5, 2), (6, 2) and (7, 2). The normalized ion signals were then scaled by the appropriate Franck-Condon factors as described previously in Section 3.8. The population of the one rotational state was then used to scale the population of the other rotational states within each vibrational level to obtain the full ro-vibrational distribution. This allowed data collection to occur over a very short timescale of a few days, enabling experimental conditions to be kept constant. In particular, conducting the scans consecutively facilitates more consistency in laser alignment, beam shape, atom flux and source and target chamber pressure. The ro-vibrational populations obtained the consecutive scans is shown below in Figure 3.18.

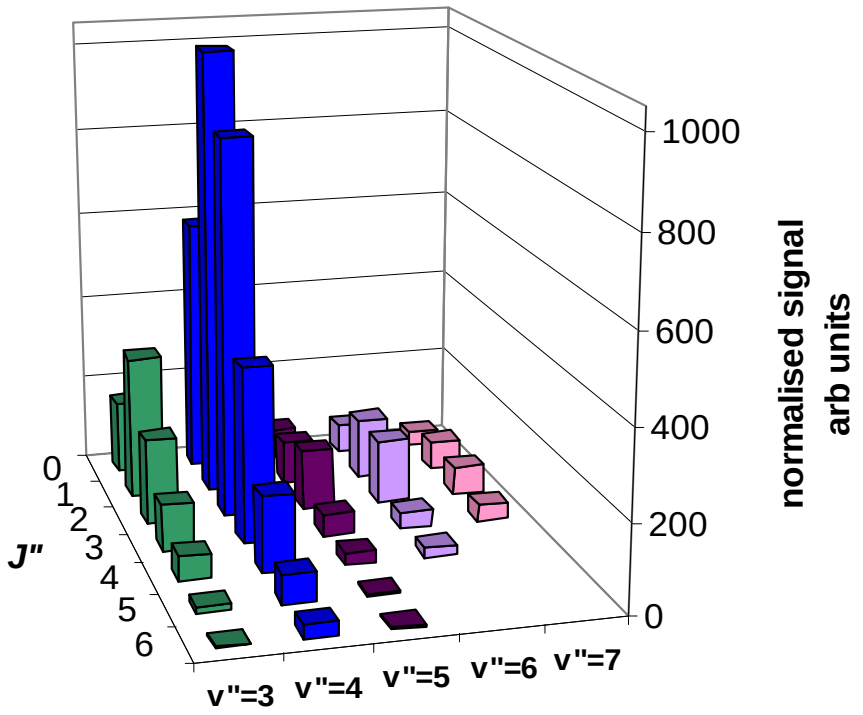

Figure 3.18 Relative ro-vibrational populations for HD formed in vibrational level $v'' = 3 – 7$ on an HOPG surface held at 15 K calculated by conducting consecutive scans of the most populated rotational state in each vibration level, then scaling the rest of the rotational state populations to the most populated rotational state.

Using this methodology of scaling by the consecutive scans, the populations of the $v'' = 3$ and 5 states appear to be reduced in comparison to Figure 3.16, although the $v'' = 4$ states were found to be approximately similar in population for Figure 3.18 and Figure 3.16. When comparing the results of the two methodologies, it was found that the populations of 19 of the 30 detected ro-vibrational levels agree within 1σ; whilst 28 of the 30 levels agree within 3σ. Hence, it seems clear that the data presented in Figures 3.18 and 3.16 sample the same ro-vibrational distribution, within experimental uncertainty.

3.10 Translational Energy

The primary goal of the Cosmic Dust Experiment is to determine the ro-vibrational population distribution of nascent molecular hydrogen forming on the surface of dust grains in the interstellar medium. However, additional information such as the translational, namely kinetic, energy of the nascent hydrogen can also be ascertained from the experiment. This information may have important consequences for the

energy budget of chemical reactions in the interstellar medium. Furthermore, the translational energy and the full ro-vibrational distribution of nascent hydrogen molecules can be used to constrain the energy transferred to the surface during the formation process, as described in Section 3.11.

The translational energy of the HD molecules desorbing from the HOPG surface in the Cosmic Dust Experiment cannot be measured directly with our current TOF mass spectrometer. Nevertheless, the temporal widths of the TOF mass spectra can be used to infer an upper limit to the translational energy in the direction towards the MCP detector, which is perpendicular to the HOPG surface. An example of a TOF mass spectrum is given in Figure 3.1. The temporal widths of the peaks in a TOF mass spectrum depend on many factors. Jitter in the timing electronics and non-uniformity in the electric fields can lead to a spread in the flight times of an ion. Also, if molecules desorb from the surface with non-zero kinetic energy, they have a distribution of velocities in all directions. When these molecules are ionized, they retain their translational energy and the velocity distribution will affect the flight times of the ions, and will, in principle, contribute to the width of the peaks in a TOF mass spectrum.

To illustrate the effect of the velocity distribution on the time-of-flight of ions, consider two ions, which are formed at the same point with the same magnitude of velocity, but travelling in opposite directions. Ion 1 is travelling towards the MCP detector, whereas ion 2 is travelling in the opposite direction, with both motions perpendicular to the HOPG surface. Ion 2 will be decelerated by the electric field in the source region of TOFMS, until it becomes stationary, then accelerated to the same speed as ion 1. Thus ion 2 has been 'turned around' and the motion of the two ions has become identical, except for the time-lag of ion 2. Therefore, there will be a spread in the flight times, δt, of the ions hitting the detector, which is equal to the 'turn-around time'. This turn-around time is equal to twice the time required to decelerate ion 2. If s is the distance required to bring ion 2 to a halt, then

$$U_0 = qsE_s \qquad 3.16$$

where U_0 is the initial kinetic energy of the ions, m is the mass of the ion, q is the charge on the ion and E_s is the electric field in the source region of the TOFMS.

Using the equation of motion and the standard expression for the kinetic energy, *KE*, both given below, where *v*, v_f and v_i are the velocity, final velocity and initial velocity respectively, s_0 is the initial position and *t* is the time:

$$KE = \frac{1}{2}mv^2 \qquad 3.17$$

$$s = s_0 + \frac{1}{2}(v_f + v_i)t \qquad 3.18$$

We obtain δt, the spread in the flight times

$$\delta t = \frac{2(2mU_0)^{\frac{1}{2}}}{qE_s} \qquad 3.19$$

This expression for δt was first given in Wiley and McLaren 1955 [18].

The flight time of an ion with zero initial kinetic energy is known as the thermal flight time, t_{therm}, and lies between the flight time of ion 1 and ion 2:

$$t_{therm} = t_{expt} + \frac{(2mU_0)^{\frac{1}{2}}}{qE_s} \qquad 3.20$$

where t_{expt} is the measured time-of-flight of the ion with initial kinetic energy U_0 in the direction of the detector.

Considering equations 3.16 and 3.17, equation 3.20 can be rearranged to give

$$v_z = -[t_{expt} - t_{therm}]\frac{qE_s}{m} \qquad 3.21$$

where v_z is the velocity of the ion in the direction towards the detector, perpendicular to the surface.

Thus, if the spread in times of flight of ions are due to the initial velocity of the ions only, then v_z can be calculated using equation 3.21. Of course, this cannot be the case for the HD^+ ions involved in the Cosmic Dust Experiment as all TOF mass spectra obtained to date have very similar peak widths for the HD peak. This indicates that the HD peak width is dominated by the instrument function of the TOFMS, not by the translational energy of the HD ions.

However, we can calculate an equivalent value of v_z for our HD peaks, which are approximately 40 ns wide. This value of v_z corresponds to the minimum velocity an ion would have to have in order to cause observable peak broadening. The spread in flight times of the ions δt is 40 ns, the charge, q, on the ion is 1.60×10^{-19} C, the mass of HD is 4.98×10^{-27} kg. The source field, E_s, is $\frac{400}{0.03} = 1.33 \times 10^4$ V m^{-1}, because the separation of the middle and repeller plate is 0.03 m and the voltages on the middle and repeller plates were 400 V and 0 V respectively, when the mass spectrum was taken. As the thermal flight time occurs at the centre of a spectral peak, we can use

$$\left[t_{\text{expt}} - t_{therm}\right] = \frac{\delta t}{2} \qquad 3.22$$

to obtain $v_z = 8.57 \times 10^3$ ms^{-1}. The equivalent translational energy is ~1.1 eV or a translational temperature of $T_{trans} < 12\,800$ K.

Thus, for the HD^+ ions to cause observable broadening in the TOF mass spectra, they must have initial kinetic energies above 1 eV. Hence we assume an approximate upper limit to the translational energy of nascent HD formed on our HOPG surface of 1 eV. This is supported by the findings of Roser *et al.* [19] who monitored the translational temperature of D_2 desorbed in TPD experiments from an amorphous ice surface previously dosed with D-atoms. Roser *et al.* calculate that the kinetic energy of the hydrogen molecules is ~3 meV. Hence, the upper limit of 1 eV derived above may be a considerable overestimate, although it should be noted that the HD^+ ions in consideration are forming on a non-porous HOPG surface, rather than on porous ice, as in the Roser *et al.* study. This is an important difference because molecules desorbing from a porous surface are more likely to get trapped in pores and thus lose their translational energy before escaping the surface.

The installation of a position sensitive detector will allow the translational energy of the HD^+ ions to be calculated more precisely. This is discussed further in Chapter 5.

3.11 The Energy Budget

The upper limit of 1 eV to the translational energy of nascent HD molecules formed on an HOPG surface held at 15 K can be used to partition the 4.48 eV released during the formation of the molecules between various modes. Firstly, there is the internal energy of the HD molecule, consisting of the vibrational and rotational modes which are probed directly by the Cosmic Dust Experiment. Secondly, there is the translational energy of the molecule, which is known to be less than 1 eV. Thirdly, there is energy that is lost to the HOPG surface during formation. There may be important consequences to molecular hydrogen being formed with significant internal excitation. Energy may be emitted from nascent H_2 molecules, providing a cooling mechanism for a molecular cloud in the early stages of star formation. This cooling facilitates the collapse of a cloud to form a star. Also, ro-vibrationally excited hydrogen molecules may have enough energy to overcome the energy barriers to form radicals such as OH and CH^+ in the ISM [20, 21]. Furthermore, highly excited H_2 molecules with $v'' > 4$ may be directly ionized or undergo charge-exchange with H^+ to form H_2^+. H_2^+ can then subsequently react to form H_3^+, an important precursor molecule for much of the chemistry in the ISM, as discussed in Chapter 1. If a significant proportion of the binding energy is deposited into dust grains during the formation of molecular hydrogen in the ISM, then this may cause localized heating of the grain mantle to desorb other molecules [22, 23]. Thus, the energy partition of the binding energy of molecular hydrogen is of great importance to interstellar chemistry.

Using the standard spectroscopic equations given in equations 3.8, 3.9 and 3.10, the energy into the vibrational and rotational modes of a HD molecule can be calculated for each value of v'' and J''. The translational energy upper limit is 1 eV, which corresponds to 22% of 4.48 eV. As aforementioned, it is unlikely that the HD molecules are thermalizing with gas in the vacuum chamber and thereby losing energy to other molecules. Hence, the remainder of the energy is assumed to flow into the HOPG surface. Table 3.14 below details how the binding energy is partitioned for HD molecules in a selection of particular v'', J'' states:

HD State		Energy Distribution, % of 4.48 eV			
v''	J''	Translation	Vibration	Rotation	Surface
1	0	22	15	0	62
1	4	22	15	2	60
2	0	22	25	0	54
2	4	22	25	2	51
3	0	22	34	0	44
3	6	22	34	4	40
4	0	22	42	0	35
4	6	22	42	4	31
5	0	22	50	0	28
5	6	22	50	4	24
6	0	22	58	0	20
6	4	22	58	2	18
7	0	22	65	0	13
7	3	22	65	1	12

Table 3.14 The distribution of the 4.48 eV binding energy into the different modes of a HD molecule. The energy into the vibrational and rotational modes is calculated as described in the text. The upper limit of the translational energy is taken as 22% and the remainder is assumed to be lost to the surface.

As shown in Section 3.8, the average internal energy of the HD molecules is calculated to be 1.83 eV, neglecting the populations of the $v'' = 0$ state and other non-detected ro-vibrational states. This corresponds to 40.9 % of the binding energy being converted into internal energy on average. The internal energy is the sum of the vibrational and rotational modes, with 40.3 % and 0.6 % of the binding energy converted into vibrational and rotational energy respectively. An upper limit of 22 % of the binding energy may be converted to kinetic energy, hence at least 37.1 % of 4.48 eV must be lost to the HOPG surface. As the translational energy may be significantly lower, the energy that flows into the surface may be even higher, up to 59.1 % of the binding energy; the energy imparted to the surface must be 1.66 – 2.65 eV. Thus, there may be heating of interstellar dust grains by the formation of molecular hydrogen. Of course, in the ISM, molecular hydrogen is mainly in the form of H_2. For H_2, the internal energy is expected to be marginally higher than for HD, as

the energy levels are more spaced out within the potential well, therefore the energy that flows into the surface during the formation process may be less for H_2 than for HD. This is discussed further in Chapter 4. If states with $v'' \geq 8$ are significantly populated, the internal energy of nascent hydrogen molecules will be much higher and very little energy will be lost to the dust grain during formation. However, we feel this is unlikely due to the sharp decline in population with progressive vibrational state for states with $v'' \geq 4$.

3.12 Discussion

In this section we will discuss the results presented above in conjunction with other studies relevant to the formation of molecular hydrogen on surfaces analogous to interstellar dust grains. Both theoretical and experimental work will be discussed. For astronomical implications of H_2 formation and observations of formation pumping, see Chapter 4 and Chapter 1.

3.12.1 Comparison of Results to Theoretical Studies

Theoretical studies of the heterogeneous recombination of hydrogen atoms have mainly focused on the Eley-Rideal (ER) mechanism [24-39] because this mechanism is easier to model than the Langmuir-Hinshelwood (LH) mechanism [40-43]. As described in Chapter 1, the ER mechanism consists of an incident atom in the gas phase colliding with a preadsorbed atom on the surface; whereas in the LH mechanism, both atoms reach equilibrium with the surface, then diffuse together and react. The ER mechanism is more straightforward in modelling terms because there is only one atom bonded to the surface, and this atom is localized. Most ER studies consider the preadsorbed atom to be chemisorbed to the surface [26, 36, 44, 45] although a few consider physisorbed atoms [37, 46]. The ER studies have been discussed in Chapter 1 and predict a variety of different ro-vibrational distributions for nascent molecular hydrogen. Most studies are in agreement with our results in that ro-vibrational excitation of nascent molecules is predicted, but the amount of vibrational energy predicted is inconsistent. In the most recent study to date, Bachellerie *et al.* [35] studied the ER mechanism whereby a gaseous H-atom reacts

with a chemisorbed H-atom on graphene. The graphene sheet is allowed to pucker out on adsorption of an H-atom. Bachellerie *et al.* predict similar internal excitation to our observations, with $\langle v'' \rangle = 5 - 4$ and $\langle J'' \rangle = 2 - 4$. The work by Meijer *et al.* [28], which involves a time-dependent wave packet method to study the formation of H_2 on graphite, predicts that the $v'' = 3 - 5$ states will be most populated, as is observed by our experiments. Conversely, Meijer *et al*. also predict high rotational excitation, with $J'' = 8 - 11$ being the most populated, in contrast to our experimental results, where $J'' = 1$ and 2 are the most populated rotational states. The trajectory calculations of Kim *et al.* [47] study the recombination of hydrogen atoms on graphite grains in the limits of strong and weak interactions between the atoms and the grain surface. For the strong gas-grain interactions, where chemisorption dominates, the ro-vibrational distribution spans $v'' = 0 - 4$ and peaks at $J'' = 0$, thus is similar to our results. Other than the study by Kim *et al.* [47], the rotational excitation detected by the Cosmic Dust Experiment is much lower than predicted by theory.

However, the comparison of ER models of molecular hydrogen formation may not be appropriate to the results of the Cosmic Dust Experiment. This is because our incident atoms are at room temperature, with an equivalent energy of ~ 26 meV, and thus do not have sufficient energy to chemisorb to the graphite surface, assuming chemistry at defects is unimportant. A barrier to chemisorption was first derived theoretically by Jeloica and Sidis [48] and later confirmed experimentally by Zecho *et al.* [49] to be 0.2 eV. The chemisorption barrier also implies that the LH mechanism dominates H_2 formation in diffuse and dark clouds, where the interstellar gas has very low temperatures of 10 – 100 K [50]. Furthermore, as previous work has calculated that the coverage of the HOPG surface in the Cosmic Dust Experiment is much less than a monolayer [2], a gas phase atom is unlikely to impact on a preadsorbed atom, hence ER reactions do not dominate the HD formation process.

Morisset *et al.* [40, 41] have studied the LH mechanism using quantum dynamical calculations of H-atoms physisorbed on a graphite surface and predict that the formation of molecular hydrogen is efficient at 15 K, which has been confirmed by our experimental results. Morisset *et al.* [41] found that nascent H_2 molecules are likely to be highly vibrationally excited, with the most populated states being $v'' \sim 12$, $J'' \sim 10$ for incident atoms at energies 10 – 50 meV. Thus this study predicts higher ro-

vibrational excitation than observed by the Cosmic Dust Experiment. Nevertheless, the Morisset *et al.* study is in accordance with our results in that at least some ro-vibrational excitation is expected and the population of the ro-vibrational states increase with v'' and J''above $v'' = 0$ to peak at some higher v'', J'' state. Morisset *et al.* explain this phenomenon in the following way: The H_2 molecules trapped on the graphite surface will rotate and vibrate. The rotational and vibrational motions in the z axis are hindered by the surface, where the z axis is perpendicular to the plane of the surface. When the rotational and vibrational motions of the molecule are hindered, the molecule may desorb rapidly; hence molecules with more motion in the z direction have the greatest probability of desorption. When $v'' = 0$, the motion of the molecule is directed along the z axis, thus these states dissociate back to atoms. As v'' increases, the vibrational motion becomes more parallel to the surface and consequently the lifetime of the H_2-graphite complex increases with v''. Morisset *et al.* found that the ro-vibrational populations, explicitly the reaction probability to form particular ro-vibrational states, are dependent on the lifetime of the H_2-graphite complex. Hence, the population of the ro-vibrational states increase with v'' above $v'' = 0$.

Bachellerie *et al.* [43] modelled a non-rigid graphene sheet as an interstellar surface on which physisorbed H-atoms recombined *via* the LH mechanism. The desorbing H_2 molecules were then allowed to undergo collisions with the graphene, acting as pore walls within the grain. The results were similar to the Morisset *et al.* study [41] in that the nascent molecules have high ro-vibrational excitation, with $v'' \sim 12 - 14$, $J'' \sim 10$. It was found that typically only ~ 0.05 eV is imparted to the surface during formation, which is in contrast to the 1.66 – 2.65 eV calculated from our experimental results in Section 3.11. If a nascent H_2 molecule collides with the graphene walls, it may be reflected or trapped onto the surface. Most collisions result in reflections, as only 7 % of H_2 molecules get trapped at T = 200 K. For the reflected molecules, there is significant conversion of the vibrational energy to rotational energy with each subsequent impact. After 10 – 15 impacts, the rotational distribution is extended from $5 < J'' < 20$ upward by 5 to 10 quanta, whilst the vibrational distribution is cooled from $5 < v'' < 15$ down to $0 < v'' < 10$. On average, 0.03 eV is converted to translational energy and 0.05 – 0.06 eV flows into the surface per impact event. After 12 ps, H_2 molecules typically undergo 12 impacts with reflections and 6 impacts with trapping, such that 56% of molecules are reflected and 44% are trapped. This suggests

that our results, where the vibrational distribution peaks at $v'' = 4$, may be explained if the nascent HD molecules undergo collisions before being ionized by the REMPI photons. However, this is unlikely to be the case as HOPG is non-porous, hence molecules will not collide with pore walls. Also, as discussed previously, the HD molecules detected in our experiment have not thermalized with background gas in the chamber. Furthermore, the Bachellerie *et al.* models predict high rotational states after collisions, in contrast to the low rotational excitation detected by the Cosmic Dust Experiment.

Work on the LH mechanism by Kerkeni and Clary [42] has also been conducted. Although this study predicts less internal energy of nascent hydrogen molecules than the Bachellerie *et al.* [43] and Morisset *et al.* [40, 41] LH studies, with the distribution peaking at $v'' \sim 8$, the degree of ro-vibrational excitation is still a little higher than observed in our investigations. Thus, in general, theoretical models of the formation of molecular hydrogen *via* the LH pathway predict higher ro-vibrational excitation than observed by the Cosmic Dust Experiment. This may be due to defects in the HOPG surface used in the experiment. Defects may affect the ro-vibrational distribution of a nascent molecule as they allow atoms to chemisorb, hence bond more strongly with the graphite surface. Thus more energy may be lost to the surface, reducing the internal energy of a nascent hydrogen molecule [46]. As a consequence of a defected surface, the formation of HD in the Cosmic Dust Experiment may not be completely dominated by the LH mechanism. Instead there may be contributions from the ER mechanism, where defects facilitate chemisorption.

In general, ER studies often predict vibrational excitation [24-39] less than or comparable to that observed by the Cosmic Dust Experiment, whereas the LH studies usually predict more internal energy [40-43]. Hence, it is also probable that the formation mechanism occurring in our experiment lies between the two extremes of ER and LH, whereby at least one of the H or D-atoms are trapped on the HOPG surface and diffuses across the surface to react with another atom and at least one of the atoms is not thermalized by the surface. This is known as the ‘hot atom’ mechanism, which has not yet been studied in detail, so there are no predicted internal energies of nascent molecules formed *via* this mechanism to date. As described in Section 3.7, the rotational temperatures calculated for all vibrational levels detected

are much greater than the HOPG surface temperature. It is possible that the high rotational temperatures are due to incident atoms not being thermalized with the surface before recombination. This scenario favours the hot atom mechanism, where at least one of the atoms is not thermalized with the surface, over the LH process, where both atoms are in equilibrium with the surface.

Undoubtedly it is the formation process, whether it is dominated by the ER, LH or the hot atom mechanisms or a combination of these, that determines the energy partition between internal and translational energy of nascent molecules and the energy imparted to the HOPG surface during formation. The results presented in this thesis confirm experimentally that nascent hydrogen molecules are ro-vibrationally excited, as predicted by theory.

3.12.2 Comparison of Results to Experimental Studies

Govers *et al.* [51] used bolometry to determine the sticking probabilities of H-atoms on a 4 K surface. From this data, the rate of H-atom recombination as a function of surface coverage was determined. It was also found that when the surface was pre-dosed with D_2 molecules, the recombination of H-atoms liberated D_2 molecules from the surface. There are two possible pathways for the desorption of the D_2 molecules: either a proportion of the H-H binding energy may have flowed into the surface during recombination to cause localized heating of the surface and desorb D_2 molecules, or, nascent H_2 collided with D_2 molecules to liberate them from the surface. Both these pathways result in a reduction of the internal energy of nascent H_2. On average, it was found that at least one D_2 molecule is desorbed per recombination event, although it is assumed that this number will be a function of the coverage. In light of this study, we must examine the possibility that a significant fraction of the HD molecules desorbing from the HOPG surface in the Cosmic Dust Experiment may not be nascent molecules, but instead arise from “secondary” desorption events. It is feasible that the HD molecules may be nascent molecules that have undergone impacts with other molecules on the surface before desorption, or they may be pre-formed HD molecules liberated by nascent HD molecules. However, previous work [1, 2] employing a kinetic model and data supplied by Govers *et al.* [51, 52] has

shown that the coverage on our HOPG surface is dominated by hydrogen molecules in the chamber, not by HD formed from the reaction atoms on the surface. The coverage has been found to be very low: approximately 1 % of a monolayer. Hence, under these low coverage conditions, the HD molecules detected in the Cosmic Dust Experiment are assumed to be nascent molecules, which desorb from the surface without collisions with preadsorbates.

Govers *et al.* [51] have shown that H-atoms are mobile on a surface with temperatures as low as 4 K, which implies H_2 formation is efficient at very low temperatures. This agrees with our experimental results, which could not be obtained if HD formation were not efficient on HOPG at 15 K. However, the results of both our work and the study by Govers *et al.* are somewhat in contrast to the work of the Pirronello group [19, 53-77]. This group uses temperature-programmed desorption (TPD) experiments to study the formation of molecular hydrogen on amorphous carbon, silicate and water ice surfaces at 5 – 20 K. In some of the Pirronello experiments [68], the detection of HD is attempted during dosing of the surface by H and D in order to investigate the 'prompt' reaction of the atoms. HD is also detected after dosing, during the heating stage of the TPD, in order to study the 'delayed' reaction. It was found that the prompt reaction is weak for surfaces at low temperatures such as 15 K, in disagreement with our results. Pirronello and co-workers have also suggested that the recombination process is thermally activated; hence the delayed reaction is efficient at temperatures as low as 8 K. However, it must be noted that the surfaces used by Pirronello *et al.* [68] are mostly amorphous surfaces; whereas the Cosmic Dust Experiment employs non-porous and well-ordered HOPG. Hence, the prompt reaction is probable on HOPG, but may be less likely to occur if nascent molecules thermalize in pores. This thermalization has been shown to occur by TPD studies of the reactivity of H- and D-atoms on amorphous water surfaces [19, 78]. Significantly reduced HD signals for the delayed reaction were observed when a non-porous water surface, was irradiated with H- and D-atoms. The reduction in signal indicated that on a non-porous surface, the nascent molecules are lost promptly to the gas phase during dosing, before the heating cycle. Thus it is likely that such promptly desorbing molecules will be detected in our continuous dosing experiments on non-porous HOPG.

Also, the flux of incident atoms on the surface in the Pirronello experiments are 10^{12} atoms cm^2 s^{-1}, which is a factor of 10 lower than for the Cosmic Dust Experiments, hence the Pirronello results may be applicable to a different energy regime than our experiments. The Pirronello group [68] suggest that at low coverages, the principal formation process is the LH mechanism, but at high coverages approaching a monolayer, the hot atom mechanism dominates. Again we can compare this to our results, where we estimate we have coverage of 1 % of a monolayer, but have a much higher flux of incident H-atoms on the surface. Therefore, the hot atom mechanism seems the most likely pathway to HD formation, unless defects play a significant role.

Pirronello and co-workers [54] constructed kinetic models from their H- and D-atom TPD experiments. It was determined that 40 % of the nascent HD molecules reside on the surface for significant timescales before desorption. The residence time must be at least comparable with the timescale of a TPD experiment. This indicates that a considerable amount of the energy released upon formation of the H–D bond must flow into the surface before desorption. This result in accordance with the energy partition calculations in Section 3.11, where it was determined that at least 37.1 % of the H-D binding energy must be imparted to the HOPG surface.

As previously discussed, there is a 0.2 eV barrier to chemisorptions [33, 48, 49] on graphite surfaces, which arises from carbon atoms having to pucker out of the graphite sheet to bond with incident hydrogen atoms. Hence for the Cosmic Dust Experiment, where the incident H- and D-atoms are at ~300 K, chemisorption is improbable unless the formation mechanism is dominated by reactions at defects. TPD of an etched graphite surface irradiated by H-atoms at 2000 K was conducted by Zecho *et al.* [49]. The high temperature of the H-atoms allowed them to overcome the 0.2 eV barrier and chemisorb to the surface. The etched surface created terrace edges on the graphite surface, namely defects. Zecho *et al.* found that atoms bond more strongly at the defects. However, there was minimal change in the recombination of chemisorbed atoms with the density of terrace edges on the graphite surface, implying that the formation process was dominated by conventional sites on the planar surface. Hydrogen atoms adsorbed at terrace edges were found to desorb primarily in the form of hydrocarbons, rather than molecular hydrogen. However, these results may not apply to the Cosmic Dust Experiment due to the much lower energy of the incident H-

and D-atoms than in the Zecho experiments. Thus it is still feasible that defects dominate the reaction of hydrogen atoms at low temperatures, facilitating chemisorption and the ER formation mechanism.

Hornekaer *et al.* [79] studied the formation of molecular hydrogen on graphite surfaces using scanning tunnelling microscopy (STM) in conjunction with TPD studies. Atomic beams at 2200 K were used to chemisorb D-atoms onto the graphite surface. The STM images showed that the deuterium on the graphite had two different characteristic structures: one with pairs of D-atoms adjacent on the graphite ring, known as the *ortho* configuration; and the other with pairs of D-atoms bonded to opposite carbon atoms of the graphite ring, known as the *para* configuration. Hornekaer *et al.* [79] showed that the recombination of D-atoms occurs *via* the *para* structure. A subsequent study [80] used laser assisted associative desorption in tandem with TPD techniques and time-of-flight measurements to identify the velocity distributions of chemisorbed H_2 and D_2 desorbing from graphite at different angles to the surface. The average translational energy of H_2 and D_2 moving normal to the surface was found to be 1.3 eV, leaving about 60% of the desorption energy to be converted to ro-vibrational excitation of the molecule or flow into the surface. Again these results are for chemisorbed hydrogen atoms and are in a different energy regime to the H- and D-atoms in the Cosmic Dust Experiment, thus the results may not be comparable. Nevertheless, in Section 3.10, the translational energy of the HD molecules was found to be less than 1.1 eV. In general, we have observed energy transfer to the surface and also significant internal excitation of the nascent molecules, in agreement with the experiments of the Hornekaer group. In another study, Hornekaer *et al.* [81] also investigated the formation of molecular hydrogen on amorphous and non-porous water-ice surfaces using TPD. They found that HD formed on porous amorphous solid water (ASW) had totally thermalized with the surface before desorption; whereas nascent molecules desorbed promptly from non-porous surfaces. Internal excitation is expected for those rapidly desorbing molecules, as they have not had sufficient time to impart a significant proportion of the binding energy to the surface. Our observation of ro-vibrationally excited HD molecules desorbing from non-porous HOPG is in accord with these results, indicating that the HD has not fully thermalized with the surface. Thus the rotational temperatures

determined in Table 3.10 are significantly higher than 15 K, the temperature of the HOPG surface.

Using REMPI spectroscopy, Yabushita *et al.* [82, 83] detected H_2 in ro-vibrational states $v'' = 0 – 5$, $J'' = 0 – 17$ from the 157 nm photodissociation of a porous ASW surface at 100 K. Two distinct formation mechanisms were identified. Firstly, endothermic abstraction of an H-atom from H_2O by another H-atom liberated by photolysis, which produced vibrationally cold nascent H_2 mostly in the $v'' = 0$ state with translational energy $T_{trans} = 100$ K. Secondly, the recombination of two H-atoms, which yielded H_2 molecules with a highly excited vibrational distribution and non-Boltzmann rotational population distributions in states $v'' \geq 2$. This is in general accord with the results of the Cosmic Dust Experiment, although it must be noted that the H-atoms in our experiment are not produced from the pholoysis of water-ice and H_2 is formed not on ASW, but on a non-porous graphite surface. Yabushita *et al*. found that the H_2 formed from recombination of H-atoms exhibited translational energy distributions with $T_{trans} = 1800$ K and $T_{trans} = 110$ K, well below the upper limit of $T_{trans} < 12\,800$ K calculated in Section 3.10. Yabushita *et al*. attributed the two characteristic translational energies to the formation of H_2 in different regions of the ice. The ER mechanism was found to dominate the recombination reaction near the top of the surface, whereby a preadsorbed, thermalized H-atom encounters a phtotoproduced H-atom. A nascent H_2 molecule near the surface can easily escape without losing its translational energy. The recombination reaction is more likely to occur within micropores in the bulk of the ASW, rather than close to the ice surface – vacuum interface. H_2 molecules will collide many times with the ASW surface walls before desorption, hence their translational energies thermalize to that of the bulk. Yabushita *et al*. also expect the H_2 formation reaction and subsequent energy release to lead to the simultaneous desorption of water molecules.

Gough *et al.* [84] developed a new technique to study the H^- ion yield produced by the reaction of H_2 in different ro-vibrational states with electrons *via* dissociative attachment. H_2 formation on carbon surfaces at $T = 90 – 300$ K was investigated. H_2 was detected in vibrational states up to $v = 7$, in general agreement with our experimental results, although it must be noted that the carbon surfaces used by

Gough *et al.* were at much higher temperatures than the HOPG at 15 K used by the Cosmic Dust Experiment, thus the formation mechanisms may not be comparable.

The ro-vibrational excitation of D_2 formed *via* the recombination of D-atoms on a non-porous amorphous solid water (NP ASW) held at 8 – 30 K was studied by Lemaire and co-workers [85] using TPD. The recombination and desorption occurred during the irradiation stage of the TPD experiment, hence the prompt reaction occurs for NP ASW. This is in accordance with the Cosmic Dust Experiment, where the prompt reaction is observed on HOPG. Amiaud *et al.* [85] detected nascent D_2 in states $v'' = 1 – 7$, by scanning the kinetic energy of electrons required to ionize the D_2 desorbing from their surface. In the apparatus used by the Lemaire group, the kinetic energy of the electrons that ionize D_2 molecules can be tuned in steps of 0.1 eV. The D_2^- ions are then detected by QMS. Thus it was possible to discriminate between ground state D_2 molecules with an ionization threshold of 15.46 eV and excited D_2 molecules, which have their ionization threshold lowered by internal excitation. However, this does not mean that states $v'' > 7$ are not populated, as these states are more difficult to detect due to the sensitivity of detection decreasing rapidly with the energy of the ionizing electron. Most recently, Congiu *et al.* [86] extended the work of Amiaud *et al.* [85] by showing that D_2 is not formed in vibrationally excited states with $v'' \geq 2$ on porous ice surfaces. They also found that degree of internal excitation of D_2 to be significantly reduced on both non-porous and on porous water ice in a regime of high molecular coverage, as is the case in dark molecular clouds, which will be discussed further in Chapter 4. The results of the Lemaire group do not provide a quantitative comparison of the vibrational distribution between $v'' = 1 – 7$. Nevertheless, their work is further confirmation of our results with the Cosmic Dust Experiment that molecular hydrogen is formed in vibrationally excited states, at least on non-porous surfaces at low coverages. Perhaps the similarity between the two experiments implies that formation of hydrogen molecules on HOPG and NP ASW are similar, or that internal excitation of nascent hydrogen molecules does not significantly depend on the chemical composition of the surface, given a non-porous surface.

3.13 Summary

HD formed on a HOPG surface held at 15 K was detected using REMPI in the $v'' = 3 – 7$ vibrational levels, with 4 – 7 rotational states detected within each vibrational level, such that a total of 30 ro-vibrational states were detected. The complete ro-vibrational distribution was estimated by scaling the REMPI signals by the Franck-Condon factor of the REMPI transition. The most populated vibrational level was found to be $v'' = 4$. The most populated rotational states were found to be $J'' = 1$ or 2 depending on the vibrational level. The ro-vibrational distribution peaks at $v'' = 4$, $J'' = 1$. The rotational temperatures were calculated to be significantly higher than the temperature of the HOPG surface, implying that the HD molecules were not thermalized with the surface. The average internal energy of the HD molecules, neglecting undetected states, was found to be 1.83 eV. An upper limit of 1.1 eV to the translational energy was derived. This implies that 37.1 – 59.1 % of the binding energy flows into the HOPG surface.

3.14 References

1. Creighan, S.C., J.S.A. Perry, and S.D. Price, *The rovibrational distribution of H-2 and HD formed on a graphite surface at 15-50 K*. J. Chem. Phys., 2006. **124**(11).

2. Creighan, S.C., *Laboratory Studies of the Formation of Molecular Hydrogen on Surfaces at Cryogenic Temperatures, Department of Chemistry*. 2006, University College London: London.

3. Perry, J.S.A. and S.D. Price, *Detection of rovibrationally excited H-2 formed through the heterogeneous recombination of H atoms on a cold HOPG surface*. Astrophysics and Space Science, 2003. **285**(3-4): p. 769-776.

4. Huber, K.P. and G. Herzberg, *Constants of Diatomic Molecules*, in *NIST Standard Reference Database Number 69*, P.J. Linstrom and W.G. Mallard, Editors.

5. Dabrowski, I. and G. Herzberg, *Absorption and Emission-Spectra of Hd in Vacuum Ultraviolet*. Can. J. Phys., 1976. **54**(5): p. 525-567.

6. Price, S., *Private Communication*. 2009.

7. Rinnen, K.D., M.A. Buntine, D.A.V. Kliner, R.N. Zare, and W.M. Huo, *Quantitative-Determination of H_2, HD, and D_2 Internal-State Distributions by (2+1) Resonance-Enhanced Multiphoton Ionization*. J. Chem. Phys., 1991. **95**(1): p. 214-225.

8. Pozgainer, G., L. Windholz, and A. Winkler, *Rovibrational State-Specific Detection of Desorbing Hydrogen Molecules Using Multiphoton Ionization (Rempi)*. Meas. Sci. Technol., 1994. **5**(8): p. 947-953.

9. Islam, F., E.R. Latimer, and S.D. Price, *The formation of vibrationally excited HD from atomic recombination on cold graphite surfaces*. J. Chem. Phys., 2007. **127**: p. 064701-8.

10. Latimer, E.R., F. Islam, and S.D. Price, *Studies of HD formed in excited vibrational states from atomic recombination on cold graphite surfaces*. Chemical Physics Letters, 2008. **455**(4-6): p. 174-177.

11. Kubiak, G.D., G.O. Sitz, and R.N. Zare, *Recombinative Desorption Dynamics - Molecular-Hydrogen from Cu(110) and Cu(111)*. Journal of Chemical Physics, 1985. **83**(5): p. 2538-2551.

12. Winkler, A., *Interaction of atomic hydrogen with metal surfaces*. Applied Physics A-Materials Science and Processing, 1998. **67**(6): p. 637-644.

13. Murphy, M.J. and A. Hodgson, *Internal state distributions for D-2 recombinative desorption from Ag(111)*. Surface Science, 1996. **368**: p. 55-60.

14. Schroter, L., R. David, and H. Zacharias, *Laser Spectroscopy of Hydrogen Desorption from Pd(100)*. Journal of Vacuum Science & Technology a-Vacuum Surfaces and Films, 1991. **9**(3): p. 1712-1718.

15. Hodgson, A., *State resolved desorption measurements as a probe of surface reactions*. Prog. Surf. Sci., 2000. **63**(1-2): p. 1-61.

16. Rettner, C.T., E.K. Schweizer, and C.B. Mullins, *Desorption and Trapping of Argon at a 2h-W(100) Surface and a Test of the Applicability of Detailed Balance to a Nonequilibrium System*. J. Chem. Phys., 1989. **90**(7): p. 3800-3813.

17. Huo, W.M., K.D. Rinnen, and R.N. Zare, *Rotational And Vibrational Effects In The E 1-Sigma-G+-X 1-Sigma-G+ 2-Photon Transitions Of H2, Hd, And D2*. J. Chem. Phys., 1991. **95**(1): p. 205-213.

18. Wiley, W.C. and I.H. McLaren, *Time-of-Flight Mass Spectrometer with Improved Resolution*. Review of Scientific Instruments, 1955. **26**(12): p. 1150-1157.

19. Roser, J.E., S. Swords, G. Vidali, G. Manico, and V. Pirronello, *Measurement of the kinetic energy of hydrogen molecules desorbing from amorphous water ice*. Astrophysical Journal, 2003. **596**(1): p. L55-L58.

20. Weck, P.F. and N. Balakrishnan, *Dynamics of chemical reactions at cold and ultracold temperatures*. Journal of Physics B-Atomic Molecular and Optical Physics, 2006. **39**(19): p. S1215-S1227.

21. Garrod, R.T., J.M.C. Rawlings, and D.A. Williams, *Chemical effects of H-2 formation excitation*. Astrophysics and Space Science, 2003. **286**(3-4): p. 487-499.

22. Roberts, J.F., J.M.C. Rawlings, S. Viti, and D.A. Williams, *Desorption from interstellar ices*. Monthly Notices of the Royal Astronomical Society, 2007. **382**(2): p. 733-742.

23. Williams, D.A., W.A. Brown, S.D. Price, J.M.C. Rawlings, and S. Viti, *Molecules, ices and astronomy*. Astron. Geophys., 2007. **48**(1): p. 25-34.

24. Farebrother, A.J., A.J.H.M. Meijer, D.C. Clary, and A.J. Fisher, *Formation of molecular hydrogen on a graphite surface via an Eley-Rideal mechanism*. Chemical Physics Letters, 2000. **319**(3-4): p. 303-308.

25. Jackson, B. and D. Lemoine, *Eley-Rideal reactions between H atoms on metal and graphite surfaces: The variation of reactivity with substrate*. J. Chem. Phys., 2001. **114**(1): p. 474-482.

26. Martinazzo, R. and G.F. Tantardini, *Quantum study of Eley-Rideal reaction and collision induced desorption of hydrogen atoms on a graphite surface. I. H-chemisorbed case*. J. Chem. Phys., 2006. **124**(12).

27. Meijer, A., A.J. Farebrother, and D.C. Clary, *Isotope effects in the formation of molecular hydrogen on a graphite surface via an Eley-Rideal mechanism*. J. Phys. Chem. A, 2002. **106**(39): p. 8996-9008.

28. Meijer, A., A.J. Fisher, and D.C. Clary, *Surface coverage effects on the formation of molecular hydrogen on a graphite surface via an Eley-Rideal mechanism*. J. Phys. Chem. A, 2003. **107**(50): p. 10862-10871.

29. Meijer, A.J.H.M., A.J. Farebrother, D.C. Clary, and A.J. Fisher, *Time-dependent quantum mechanical calculations on the formation of molecular hydrogen on a graphite surface via an Eley-Rideal mechanism*. J. Phys. Chem. A, 2001. **105**(11): p. 2173-2182.

30. Morisset, S., F. Aguillon, M. Sizun, and V. Sidis, *Quantum wavepacket investigation of Eley Rideal formation of H- 2 on a relaxing graphite surface*. Chemical Physics Letters, 2003. **378**(5-6): p. 615-621.

31. Morisset, S., F. Aguillon, M. Sizun, and V. Sidis, *Role of surface relaxation in the Eley-Rideal formation of H-2 on a graphite surface*. J. Phys. Chem. A, 2004. **108**(41): p. 8571-8579.

32. Rettner, C.T. and D.J. Auerbach, *Dynamics of the formation of HD from D(H) atoms colliding with H(D)/Cu(111): A model study of an Eley-Rideal reaction*. Surface Science, 1996. **358**(1-3): p. 602-608.

33. Rutigliano, M., M. Cacciatore, and G.D. Billing, *Hydrogen atom recombination on graphite at 10 K via the Eley- Rideal mechanism*. Chemical Physics Letters, 2001. **340**(1-2): p. 13-20.

34. Sha, X.W., B. Jackson, and D. Lemoine, *Quantum studies of Eley-Rideal reactions between H atoms on a graphite surface*. J. Chem. Phys., 2002. **116**(16): p. 7158-7169.

35. Bachellerie, D., M. Sizun, F. Aguillon, D. Teillet-Billy, N. Rougeau, and V. Sidis, *Unrestricted study of the Eley-Rideal formation of H-2 on graphene using a new multidimensional graphene-H-H potential: role of the substrate*. Phys. Chem. Chem. Phys., 2009. **11**(15): p. 2715-2729.

36. Bachellerie, D., M. Sizun, D. Teillet-Billy, N. Rougeau, and V. Sidis, *Eley-Rideal formation of H-2 involving one of two para-chemisorbed H atoms on a graphite surface*. Chemical Physics Letters, 2007. **448**(4-6): p. 223-227.

37. Martinazzo, R. and G.F. Tantardini, *Quantum study of Eley-Rideal reaction and collision induced desorption of hydrogen atoms on a graphite surface. II. H-physisorbed case*. J. Chem. Phys., 2006. **124**(12).

38. Meijer, A., A.J. Farebrother, D.C. Clary, and A.J. Fisher, *Time-dependent quantum mechanical calculations on the formation of molecular hydrogen on a graphite surface via an Eley-Rideal mechanism*. J. Phys. Chem. A, 2001. **105**(11): p. 2173-2182.

39. Farebrother, A.J., A. Meijer, D.C. Clary, and A.J. Fisher, *Formation of molecular hydrogen on a graphite surface via an Eley-Rideal mechanism*. Chemical Physics Letters, 2000. **319**(3-4): p. 303-308.

40. Morisset, S., F. Aguillon, M. Sizun, and V. Sidis, *Quantum dynamics of H-2 formation on a graphite surface through the Langmuir Hinshelwood mechanism*. J. Chem. Phys., 2004. **121**(13): p. 6493-6501.

41. Morisset, S., F. Aguillon, M. Sizun, and V. Sidis, *Wave-packet study of H-2 formation on a graphite surface through the Langmuir-Hinshelwood mechanism*. J. Chem. Phys., 2005. **122**(19): p. art. no.-194702.

42. Kerkeni, B. and D.C. Clary, *Quantum dynamics study of the Langmuir-Hinshelwood H+H recombination mechanism and H-2 formation on a graphene model surface*. Chemical Physics, 2007. **338**(1): p. 1-10.

43. Bachellerie, D., M. Sizun, F. Aguillon, and V. Sidis, *Effects of a Nonrigid Graphene Surface on the LH Associative Desorption of H Atoms and on the Deexcitation of Nascent H-2 Molecules Colliding with Model Walls of Carbonaceous Porous Material*. J. Phys. Chem. A, 2009. **113**(1): p. 108-117.

44. Ree, J., Y.H. Kim, and H.K. Shin, *Reactions of gas-phase atomic hydrogen with chemisorbed hydrogen on a graphite surface*. Bulletin of the Korean Chemical Society, 2007. **28**(4): p. 635-646.

45. Cacciatore, M. and M. Rutigliano. *The semiclassical and quantum-classical approaches to elementary surface processes: dissociative chemisorption and atom recombination on surfaces*. in *Meeting on Molecular and Nanodynamics - From Atoms to Biomolecules*. 2007. La Sapienza, ITALY.

46. Goumans, T.P.M., C. Richard, A. Catlow, and W.A. Brown, *Formation of H-2 on an olivine surface: a computational study*. Monthly Notices of the Royal Astronomical Society, 2009. **393**(4): p. 1403-1407.

47. Kim, Y.H., J. Ree, and H.K. Shin, *Formation of vibrationally excited hydrogen molecules on a graphite surface*. Chemical Physics Letters, 1999. **314**(1-2): p. 1-8.

48. Jeloaica, L. and V. Sidis, *DFT investigation of the adsorption of atomic hydrogen on a cluster-model graphite surface*. Chemical Physics Letters, 1999. **300**(1-2): p. 157-162.

49. Zecho, T., A. Guttler, X.W. Sha, B. Jackson, and J. Kuppers, *Adsorption of hydrogen and deuterium atoms on the (0001) graphite surface*. J. Chem. Phys., 2002. **117**(18): p. 8486-8492.

50. Dyson, J.E. and D.A. Williams, *The Physics of the Interstellar Medium*. 2nd ed. 1997, Bristol: Institute of Physics.

51. Govers, T.R., L. Mattera, and G. Scoles, *Molecular-Beam Experiments on the Sticking and Accommodation of Molecular-Hydrogen on a Low-Temperature Substrate*. J. Chem. Phys., 1980. **72**(10): p. 5446-5455.

52. Govers, T.R., *H atom data*. http://hal.ccsd.cnrs.fr/ccsd-00004273/en/, 2005.

53. Biham, O., I. Furman, N. Katz, V. Pirronello, and G. Vidali, *H_2 formation on interstellar grains in different physical regimes*. Monthly Notices of the Royal Astronomical Society, 1998. **296**(4): p. 869-872.

54. Katz, N., I. Furman, O. Biham, V. Pirronello, and G. Vidali, *Molecular hydrogen formation on astrophysically relevant surfaces*. Astrophysical Journal, 1999. **522**(1): p. 305-312.

55. Manico, G., G. Raguni, V. Pirronello, J.E. Roser, and G. Vidali, *Laboratory measurements of molecular hydrogen formation on amorphous water ice*. Astrophysical Journal, 2001. **548**(2): p. L253-L256.

56. Perets, H.B., O. Biham, G. Manico, V. Pirronello, J. Roser, S. Swords, and G. Vidali, *Molecular hydrogen formation on ice under interstellar conditions*. Astrophysical Journal, 2005. **627**(2): p. 850-860.

57. Pirronello, V., O. Biham, C. Liu, L.O. Shen, and G. Vidali, *Efficiency of molecular hydrogen formation on silicates*. Astrophysical Journal, 1997. **483**(2): p. L131-L134.

58. Pirronello, V., C. Liu, J.E. Roser, and G. Vidali, *Measurements of molecular hydrogen formation on carbonaceous grains*. Astronomy and Astrophysics, 1999. **344**(2): p. 681-686.

59. Pirronello, V., C. Liu, L.Y. Shen, and G. Vidali, *Laboratory synthesis of molecular hydrogen on surfaces of astrophysical interest*. Astrophysical Journal, 1997. **475**(1): p. L69-L72.

60. Roser, J.E., G. Manico, V. Pirronello, and G. Vidali, *Formation of molecular hydrogen on amorphous water ice: Influence of morphology and ultraviolet exposure*. Astrophysical Journal, 2002. **581**(1): p. 276-284.

61. Roser, J.E., G. Vidali, G. Manico, and V. Pirronello, *Formation of carbon dioxide by surface reactions on ices in the interstellar medium*. Astrophysical Journal, 2001. **555**(1): p. L61-L64.

62. Vidali, G., V. Pirronello, C. Liu, and L.Y. Shen, *Experimental studies of chemical reactions on surfaces of astrophysical interest*. Astrophys. Lett. Comm., 1998. **35**(6): p. 423-447.

63. Vidali, G., J.E. Roser, G. Manico, and V. Pirronello, *Laboratory studies of formation of molecules on dust grain analogues under ISM conditions*. Journal of Geophysical Research-Planets, 2004. **109**(E7).

64. Vidali, G., J.E. Roser, G. Manico, and V. Pirronello, *Experimental study of the formation of molecular hydrogen and carbon dioxide on dust grain analogues*, in *Space Life Sciences: Steps toward Origin(S) of Life*. 2004. p. 6-13.

65. Vidali, G., V. Pirronello, L. Li, J. Roser, G. Manico, E. Congiu, H. Mehl, A. Lederhendler, H.B. Perets, J.R. Brucato, and O. Biham, *Analysis of molecular hydrogen formation on low-temperature surfaces in temperature programmed desorption experiments*. J. Phys. Chem. A, 2007. **111**(49): p. 12611-12619.

66. Pirronello, V., G. Manico, E. Congiu, G. Vidali, A. Insolia, and R. Caruso. *The Galactic Interstellar Medium: An overview*. in *Cosmic Ray International Seminar on UHECR - Status and Perspectives*. 2006. Catania, ITALY.

67. Perets, H.B., A. Lederhendler, O. Biham, G. Vidali, L. Li, S. Swords, E. Congiu, J. Roser, G. Manico, J.R. Brucato, and V. Pirronello, *Molecular hydrogen formation on amorphous silicates under interstellar conditions*. Astrophysical Journal, 2007. **661**(2): p. L163-L166.

68. Vidali, G., J.E. Roser, L. Ling, E. Congiu, G. Manico, and V. Pirronello, *The formation of interstellar molecules via reactions on dust grain surfaces*. Faraday Discussions, 2006. **133**: p. 125-135.

69. Pirronello, V., O. Biham, G. Manico, J.E. Roser, and G. Vidali. *Laboratory studies of molecular hydrogen formation on surfaces of astrophysical interest*. in *International Conference on H(2) in Space*. 1999. Paris, France.

70. Biham, O., I. Furman, V. Pirronello, and G. Vidali, *Master equation for hydrogen recombination on grain surfaces*. Astrophysical Journal, 2001. **553**(2): p. 595-603.

71. Pirronello, V., G. Manico, J. Roser, and G. Vidali. *Dust chemistry in the laboratory*. in *4th Cologne-Bonn-Zermatt Symposium on the Dense Interstellar Medium in Galaxies*. 2003. Zermatt, SWITZERLAND.

72. Pirronello, V., O. Biham, G. Manico, G. Raguni, J.E. Roser, and G. Vidali. *Experimental and theoretical studies of surface reactios on solids and in conditions relevant in space*. in *Workshop on Molecules in Space and in the Laboratory*. 1999. Cagliari, Italy.

73. Biham, O., I. Furman, N. Katz, V. Pirronello, and G. Vidali, *H-2 formation on interstellar grains in different physical regimes*. Monthly Notices of the Royal Astronomical Society, 1998. **296**(4): p. 869-872.

74. Pirronello, V. and D. Averna, *Production of Molecular-Hydrogen by Cosmic-Rays in Interstellar Clouds - a Relevant Process*. Astronomy and Astrophysics, 1988. **196**(1-2): p. 201-206.

75. Pirronello, V., *On the Mechanism of H-2 Formation in the Interstellar-Medium*. Iau Symposia, 1987(120): p. 167-169.

76. Vidali, G., J.E. Roser, G. Manico, and V. Pirronello. *Experimental study of the formation of molecular hydrogen and carbon dioxide on dust grain analogues*. in *2nd World Space Congress/34th COSPAR Scientific Assembly*. 2002. Houston, Texas.

77. Roser, J.E., G. Vidali, G. Manico, and V. Pirronello. *Formation of molecular hydrogen on amorphous water ice*. in *Conference on Chemistry as a Diagnostic of Star Formation*. 2002. Waterloo, CANADA.

78. Hornekaer, L., A. Baurichter, V.V. Petrunin, A.C. Luntz, B.D. Kay, and A. Al-Halabi, *Influence of surface morphology on D-2 desorption kinetics from amorphous solid water*. J. Chem. Phys., 2005. **122**(12).

79. Hornekaer, L., Z. Sljivancanin, W. Xu, R. Otero, E. Rauls, I. Stensgaard, E. Laegsgaard, B. Hammer, and F. Besenbacher, *Metastable structures and recombination pathways for atomic hydrogen on the graphite (0001) surface*. Physical Review Letters, 2006. **96**(15).

80. Hornekaer, L., W. Xu, R. Otero, E. Laegsgaard, and F. Besenbacher, *Long range orientation of meta-stable atomic hydrogen adsorbate clusters on the graphite(0001) surface*. Chemical Physics Letters, 2007. **446**: p. 237-242.

81. Hornekaer, L., A. Baurichter, V.V. Petrunin, D. Field, and A.C. Luntz, *Importance of surface morphology in interstellar H-2 formation*. Science, 2003. **302**(5652): p. 1943-1946.

82. Yabushita, A., T. Hama, D. Iida, N. Kawanaka, M. Kawasaki, N. Watanabe, M.N.R. Ashfold, and H.P. Loock, *Measurements of energy partitioning in H-2 formation by photolysis of amorphous water ice*. Astrophysical Journal Letters, 2008. **682**(1): p. L69-L72.

83. Yabushita, A., T. Hama, D. Iida, N. Kawanaka, M. Kawasaki, N. Watanabe, M.N.R. Ashfold, and H.P. Loock, *Release of hydrogen molecules from the photodissociation of amorphous solid water and polycrystalline ice at 157 and 193 nm*. J. Chem. Phys., 2008. **129**(4).

84. Gough, S., C. Schermann, F. Pichou, M. Landau, I. Cadez, and R.I. Hall, *The formation of vibrationally excited hydrogen molecules on carbon surfaces*. Astronomy and Astrophysics, 1996. **305**(2): p. 687-693.

85. Amiaud, L., F. Dulieu, J.H. Fillion, A. Momeni, and J.L. Lemaire, *Interaction of atomic and molecular deuterium with a nonporous amorphous water ice surface between 8 and 30 K*. J. Chem. Phys., 2007. **127**(14).

86. Congiu, E., E. Matar, L.E. Kristensen, F. Dulieu, and J.L. Lemaire, *Laboratory evidence for the non-detection of excited nascent H-2 in dark clouds*. Monthly Notices of the Royal Astronomical Society, 2009. **397**(1): p. L96-L100.

Chapter Four

Modelling the Formation Pumping of Molecular Hydrogen in Interstellar Dark Clouds

4.1 Overview

There have been numerous studies [1-9] that predict H_2 to be formed in highly excited ro-vibrational states in the interstellar medium. This excitation of nascent molecules, namely formation pumping, may be observable in the IR emission spectra of H_2. This chapter describes a new formation pumping model derived from the results of the UCL Cosmic Dust Experiment. The ro-vibrational distribution of nascent HD is extrapolated to give the new UCL H_2 formation pumping model in Section 4.2.

H_2 emission spectra from 0.5 – 5 μm have been generated incorporating the new UCL H_2 formation pumping model. A radiative transfer code written by Silvia Casu and Cesare Cecchi-Pestellini of Cagliari Observatory was used to calculate the H_2 level populations and subsequent emission spectra and is described in Section 4.3. The internal energy of H_2 is redistributed if the molecule undergoes collisions and excitations in the interstellar gas. In other words, formation pumping competes with other pumping mechanisms to ro-vibrationally excite H_2 molecules. Pumping mechanisms taken into account by the radiative transfer code to calculate the H_2 level distribution include ultraviolet (UV) absorption, radiative decay, collisional excitation and de-excitation as well as formation pumping.

To avoid excitation by UV radiation from starlight, we have studied H_2 in dark interstellar clouds. As explained in Chapter 1, Duley and Williams [10] assert that the most favourable location to detect formation pumping would be from dense, dark, quiescent, star-less cores, where UV pumping is minimized. This is supported by Tine *et al.* [9] who state that the relative emissivities of lines due to formation pumping in dense clouds can be a factor of 500 greater than in diffuse clouds. The purpose of this chapter is to discuss the characteristics of a formation pumping signature in the IR emission of H_2 in dark clouds. Thus in Section 4.4, we present H_2 emission spectra for dark clouds at a variety of different densities, temperatures, electron and proton fractions generated using the new UCL formation pumping model.

The radiative transfer code also has the capability to incorporate other formation pumping models [11-13] to calculate the H_2 level distribution. Section 4.5 compares H_2 spectra generated using the new UCL formation pumping model with H_2 spectra generated using the previously postulated formation pumping models. All previous models have been based purely on theoretical calculations and are described in more detail in Chapter 1. This is the first investigation to generate H_2 emission spectra using an experimentally-derived formation pumping model.

Section 4.6 explains the use of a chemical model to corroborate and explain the results of the radiative transfer code. In Section 4.7, the validity of the UCL formation pumping model is examined and put in the context of other studies. Astrophysical implications and observational evidence of formation pumping are discussed.

4.2 Extrapolation of HD Experimental Data to H_2

Previous studies carried out by the UCL Cosmic Dust Experiment [14, 15] investigated both H_2 and HD formation. However, currently the experiment probes HD preferentially to H_2 because it is easier to determine that the nascent molecules have come directly from the surface with HD detection. There is a significant amount of undissociated H_2 originating from the H-atom source, thus H_2 signals have to be carefully monitored for contributions from thermally excited H_2. Likewise, we do not investigate D_2 because there is a significant amount of D_2 in the D-atom beam. Perry

et al. [16] showed that no ro-vibrationally excited H_2 emerged from the ends of the PTFE transport tubing, once the beam was cooled by use of an aluminium channel. Thus, accurate H_2 data could be obtained, albeit with difficulty and painstaking rigour. Studies of v = 1 and 2 for the isotopic species revealed very similar flux densities and rotational distributions for both HD and H_2 molecules [14] . Therefore we feel it is fair to extrapolate the HD v = 3 – 7 data to obtain an approximate ro-vibrational distribution of nascent H_2.

There are a number of considerations to take into account when adapting the HD data to H_2. The HD rotational populations deviate from the Boltzmann distribution in the vibrational states v = 3 – 7 detected in this work, as shown in Chapter 3. This deviation would not be reflected by merely assuming that HD and H_2 were formed at similar rotational temperatures, as was found by Creighan *et al.* [14]. In fact, all deviation from the Boltzmann distribution would be lost in assuming a definitive rotational temperature. Therefore the relative populations for HD must be scaled by the appropriate nuclear spin statistical weight g_N to convert them to relative populations of H_2. Most studies find the ortho-to-para ratio of H_2 formation in space to be ~3 [12, 17]. Thus we have taken g_N = 1 or 3 for even-J and odd-J respectively to retain any deviation from the Boltzmann distribution in our data.

Nascent HD in the v = 0 state could not be detected by REMPI. The signal from surface formation is swamped by background counts of ro-vibrationally relaxed HD already in the chamber. However, H_2 emission spectra cannot be produced without the inclusion of the v = 0 states. As a modest estimate of the internal excitation of H_2, we have taken a rough upper limit of the v = 0 states: We set the v = 0 populations to be equal to the populations of the v = 1 states (see Figure 4.1) such that $P_{v,J} = P_{0,J} = P_{1,J}$ for all J states. Since this is an arbitrary choice, H_2 emission spectra have been generated with the v = 0 states both significantly more and less populated than expected by a factor of 2. The sensitivity of the H_2 spectra to the error in the population of the v = 0 states is discussed further in Section 4.4.7. The relative populations $P_{v,J}$ of all the states are then normalized to obtain $\delta_{v,J}$ the fraction of H_2 formed on grain surfaces that leaves the grain in level v, J, such that $\sum_{v,J} \delta_{v,J} = 1$. The standard population distribution of H_2 we have used throughout this paper is

shown in Figure 4.1. Henceforth, we refer to this ro-vibrational distribution as the UCL formation pumping model (model **u**).

By scaling the ro-vibrational populations from HD to H_2, it must be noted that although the ro-vibrational distribution has been preserved, the average energy of the molecule has been marginally increased. This change in internal energy is due to the energy levels of H_2 being more spaced out within the potential well because H_2 is lighter than HD. In Chapter 3, the average ro-vibrational energy was found to be 1.75 eV. In this calculation, all non-detected states with $v > 7$ were neglected and the $v = 0$ state ro-vibrational populations were taken to equal the $v = 1$ state ro-vibrational populations. However, an H_2 molecule with a 'corresponding' ro-vibrational distribution has <E> = 1.95 eV.

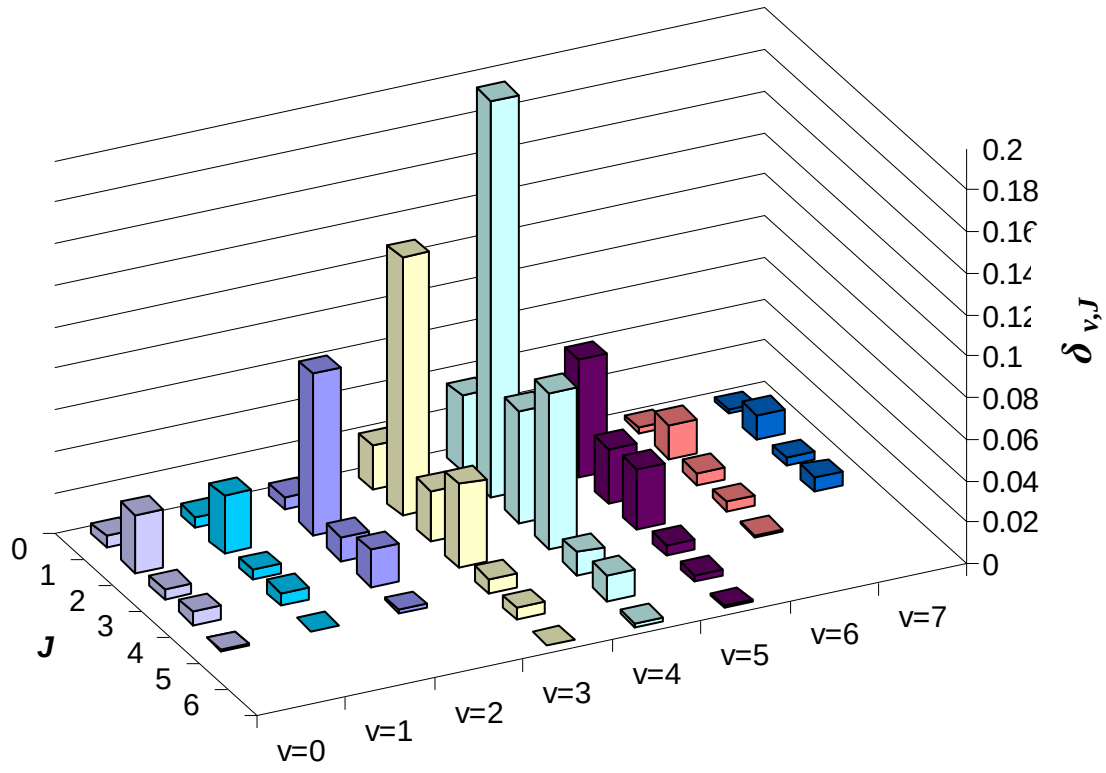

Figure 4.1 The standard UCL formation pumping model. These relative ro-vibrational populations for H_2 are extrapolated from the distribution determined in Chapter 2 by assuming an ortho-to-para ratio of 3 and choosing $P_{v,J} = P_{0,J} = P_{1,J}$. The relative populations have been normalized to obtain $\delta_{v,J}$ the fraction of H_2 formed on grain surfaces that leaves the grain in level v, J.

4.3 The Radiative Transfer Code

The radiative transfer code was written by Casu and Cecchi-Pestellini of Cagliari Observatory and has been previously used to study H_2 formation pumping [18, 19] and H_2 excitation in turbulent molecular clouds [20]. Interstellar cloud parameters and formation pumping models can be specified by changing input files to calculate the ro-vibrational level populations of H_2. The H_2 emission spectrum is then calculated for wavelengths between 0.5 – 5 μm for a specified telescope instrument resolution.

4.3.1 H_2 Ro-Vibrational Level Populations

Casu and Cecchi-Pestellini have constructed models to calculate the H_2 level distribution expected in a thermally and radiatively excited gas. The approach is similar to those developed by Sternberg and Dalgarno [21] and Draine and Bertoldi [12]. The code computes the N populations n_i for each ro-vibrational level $i = v, J$ at statistical equilibrium. The populations of the ro-vibrational levels, n_i, are solutions to the set of algebraic equations

$$n_i\{\sum_{j<i}(A_{ij}+C_{ij}+W_{ij})+\sum_{j>i}(C_{ij}+W_{ij})+\beta_i+\zeta+D_i\} = \sum_{j>i} n_j(A_{ji}+C_{ji}+W_{ji})+Rn_H n_1\delta_i+\kappa_i n_- n_1 \qquad 4.1$$

In equation 4.1, W_{ij} are the excitation rates from the level i to level j *via* UV pumping to electronically excited states, A_{ij} are the Einstein coefficients for spontaneous radiative decay, C_{ij} are the temperature dependent collisional rates, β_i is the rate of photodissociation out of the level i, and D_i is the rate of additional destruction processes, such as collisional dissociation and ionization. The cosmic ray destruction rate is denoted by ζ. The last two terms in the r.h.s. of equation 4.1 describe the formation of H_2 *via* grain catalysis and gas phase associative detachment respectively and are described in more detail below. The number density of hydrogen nuclei, the number density of neutral atomic hydrogen, H, and the number density of hydrogen anions, H^-, are n_H, n_1 and n_- respectively. A standard formation rate, $R = 3 \times 10^{-17}$ cm^3 s^{-1} [22] has been used. In equation 4.1, δ_i is the fraction of H_2 formed on grain surfaces that leaves the grain in level i, while n_- is the abundance of negative

hydrogen ions. The final term on the RHS of equation 4.1, where κ_i is the formation rate of H_2 *via* associative detachment, concerns gas phase formation of H_2 through $H^-$and is discussed later. The radiative transfer code solves equation 4.1 for N = 300 bound states of H_2, with $J \leq 30$. The highest lying state is v, J = (3, 27) at about 52,000 K above the ground state. The level populations are subject to the normalization conditions $\sum_{v,J} n_{v,J} = n_2$ and $n_H = n_1 + 2n_2$ where n_2 is the number density of molecular hydrogen, H_2.

The radiative transfer code includes inelastic collisions with H, He, and ortho and para-H_2, with fully quantum mechanical calculations of collisional rates given in studies by Flower *et al.* [23-27]. For levels where quantum calculations are not available, the extrapolation scheme for the H-H_2 rate collisions provided by Le Bourlot and co-workers in their code for photon-dominated regions (PDRs) has been adopted [28]. For all other collisional partners when quantum calculations are lacking, the collision scheme put forward by Tine *et al*. [29] has been employed. Energy levels, transition and dissociation probabilities for electronic transitions have been published by Abgrall *et al*. [30-33]. Extra data, covering levels up to J = 25, was provided by Abgrall [34]. Quadrupole radiative decays and energies of ro-vibrational levels of the ground electronic state were taken from Wolniewicz *et al.* [35]. All radiation induced processes have been computed taking into account dust extinction, which has been assumed to follow the mean galactic interstellar extinction curve.

In the present study, for all formation pumping models except the UCL formation pumping models (**u**) the assumed molecular hydrogen formation model is given by

$$\delta_{v,J} = C^{-1} g_N f_1(v, J) \exp[-f_2(\Delta E_{v,J}, T_f)] \qquad 4.2$$

where $C = \sum_{v,J} \delta_{v,J}$ is a normalization constant, and $\Delta E_{v,J}$ is the energy in K of level v, J referred to the ground state. The nuclear spin statistic weight has value g_N = 1 for even-J and g_N = 3 for odd-J. The shape functions f_1 and f_2 depend on the specified formation model **b**, **d**, **i**, **c**, **s**, or **m**.

We consider several surface formation pumping models:

(**u**) The UCL formation pumping model, where $\delta_{v,J}$ is taken directly from extrapolation of HD experiments [14, 36, 37], as shown by Figure 4.1.

(**b**) The acquired internal energy, E_{int}, is statistically distributed among the energy levels: $f_1 = 2J + 1$ and $f_2 = \Delta E_{v,J} / T_f$. By setting the formation temperature T_f = 9,000 K (E_{int} ~ 1.5 eV), the model proposed by Black and Dalgarno [11] is recovered, although any value of formation temperature may be inputted into the radiative transfer code;

(**d**) To enhance the populations of high v states with respect to high J states, formation pumping functions with $f_1 = v + 1$ and $f_2 = \Delta E_{v,J} / T_f$ are also investigated; this class of formation models with T_f = 50,000 K provides the pumping profile suggested by Draine and Bertoldi [12]. Again, any value of formation temperature may be inputted into the radiative transfer code;

(**i, c, s**) The three ro-vibrational population distributions for H_2 newly formed on icy mantles (**i**), carbonaceous dust (**c**), and silicate dust (**s**) given by Takahashi and Uehara model A [13];

(**m**) A minimal H_2 formation pumping model which limits the ro-vibrational distribution to the lowest possible levels v, J = (0, 0) and (0, 1) in the ratio 1:3. This represents the 'no formation pumping' case.

The radiative transfer code also includes gas phase H_2 formation *via* the associative detachment mechanism involving atomic hydrogen and the negative ion H^-. This gas phase formation channel can be switched on or off as required in addition to the formation pumping models **u**, **b**, **d**, **i**, **c**, **s**, **m**, so that the models can be run in surface formation mode only or in both surface and gas phase formation mode. The gas phase formation channel was added to the code to study the presence of H_2 in very high rotational states which were observed by Rosenthal *et al.* [38].

H^- is formed principally by radiative association

$$H + e \rightarrow H^- + h\nu \qquad 4.3$$

and is destroyed by the associative detachment channel

$$H^- + H \rightarrow H_2 + e \qquad 4.4$$

The abundance of the H^- ion is limited by the electron fraction x_e in the cloud. At equilibrium, where $\kappa_{AD} = \sum_i \kappa_i$ is the total rate of associative detachment:

$$\kappa_{AD} n_i = k_i x_e n_H \qquad 4.5$$

The surface-to-gas formation ratio is thus given by $R / k_- x_e \approx (T/300)^{1/2} x_e^{-1}$, where $k_- = 5.57 \times 10^{-17} (300/T)^{1/2}$ cm^3 s^{-1} is the reaction velocity of the radiative association to produce H^- [39].

Since $x_e < 10^{-3}$ for interstellar clouds [40], the recombination of H-atoms adsorbed onto grains produces much more H_2 than any gas phase process. The associative detachment channel can be important under particular conditions, such as during the recombination epoch in the early universe [41], or in the transition zone of gaseous nebulae [42]. Associative detachment might be much more efficient if the formation of H_2 in space proceeds according to the model proposed by Field [43], who conjectures that efficient production of H^- may take place on dust surfaces *via* attachment of weakly bound electrons to adsorbed H-atoms. The radiative transfer code scales the associative detachment reaction to the dust surface production rate, which in turn artificially increases the H^- abundance, n_-, such that $n_- = R n_H / \kappa_{AD}$. The associative detachment reaction produces H_2 molecules preferentially in highly excited ro-vibrational levels, which then cascade towards the ground vibrational state by quadrupole radiative transitions. Rate coefficients are used to calculate the populations of the ro-vibrational levels *v, J* by associative detachment of H and H^-, which were computed by Launay, Le Dourneuf and Zeippen [44] by means of resonant scattering theory.

4.3.2 Generating H_2 Emission Spectra

Once the level populations are calculated, H_2 emission spectra can be generated. The cloud is assumed to be a plane-parallel slab of constant density, n_H, and kinetic temperature T. The cloud is single-sided, illuminated by a normally incident UV radiation field. The incident UV field intensity is assumed to be the UV field scaling parameter, χ, times the Draine estimate [45] of the mean interstellar radiation field in the same manner as Sternberg and Dalgarno [21]. The attenuation of the field due to dust extinction is computed using the analytical solution to the transport equation in plane-parallel geometry given in Flannery *et al.* [46]. The predicted IR emission spectra are obtained by integrating the emissivities along the line of sight, and convolving with a Gaussian profile with line width of 5×10^{-5} μm, as this approximately corresponds to the instrument resolution of state-of-the-art echelle spectrometers used by current ground based telescopes such as the Phoenix instrument on the Gemini telescope, which has a resolution of 50 000 – 80 000 for near-IR wavelengths 1 – 5 μm [47]. H_2 emission spectra have been produced using Gaussian profile line widths of 1×10^{-2} μm, 5×10^{-3} μm, 9×10^{-4} μm, 8×10^{-5} μm as well as for 5×10^{-5} μm which roughly correspond to resolutions of 250, 500, 2 800, 32 000 and 50 000 respectively.

To minimize the effect of the UV field, simulations of dark clouds have been run. Dark clouds were chosen as a consequence of the suggestion by Duley and Williams [10] and Tine *et al.* [9] that quiescent, dense clouds with no UV pumping are the regions of the ISM best suited to detect formation pumping. Dark clouds of density $n_H = 10^3 – 10^6$ cm^{-3} with column density $N(H_2) = 4.8 \times 10^{21} – 1.6 \times 10^{23}$ cm^{-2}, and temperatures ranging from T = 10 – 500 K have been investigated. The results are summarized in Section 4.4 and 4.5. A table of the main parameters varied in the radiative transfer code is shown in Table 4.1.

Formation Pumping Model	**u**	**b**	**d**	**i**	**c**	**s**	**m**
Formation mode	Surface only				Surface and gas phase		
Density	A $N(H_2) = 4.8 \times 10^{21}$ cm^{-2}, $n_H = 1 \times 10^3$ cm^{-3}		B $N(H_2) = 1.6 \times 10^{22}$ cm^{-2}, $n_H = 1 \times 10^4$ cm^{-3}		C $N(H_2) = 8.0 \times 10^{22}$ cm^{-2}, $n_H = 1 \times 10^5$ cm^{-3}		D $N(H_2) = 1.6 \times 10^{23}$ cm^{-2}, $n_H = 1 \times 10^6$ cm^{-3}
Temperature, T	10 K		50 K		100 K		500 K
Resolution, Δλ	5×10^{-5} μm	8×10^{-5} μm		9×10^{-4} μm	5×10^{-3} μm		1×10^{-2} μm
Electron fraction, x_e	1×10^{-8}		1×10^{-6}		1×10^{-4}		
Proton fraction, x_{H+}	1×10^{-8}		1×10^{-6}		1×10^{-4}		
UV field scaling, χ	0.5		1		2		4

Table 4.1 The main parameters changed in the radiative transfer code to generate H_2 emission spectra. Dark clouds of density types A, B, C and D have $A_V \sim 3$, 10, 50 and 100 mag respectively using $N_H \sim 1.6 \times 10^{21}$ cm^{-2} mag^{-1} × A_V [48].

The complete grid of spectra exploring the entire parameter space would consist of 40320 models. Therefore, we have only run a selection of models, which includes all the formation pumping models, **u**, **b**, **d**, **i**, **c**, **s**, and **m**, in surface and gas phase formation mode at density $n_H = 1 \times 10^6$ cm^{-3} (cloud type D) and temperature 10 K, with proton fraction and electron fraction both equal to 1×10^{-4}. A number of other combinations of parameters have been run to check the results are consistent. The total number of spectra which have been generated to date is over 200. For clouds with temperature T ≥ 30 K, we have incorporated three rate coefficients for ortho-para conversions provided by Sun and Dalgarno [49] for gas at temperatures T = 30 K – 1000 K. These conversions are the excitation of the $J = 0$ level to the $J = 1$, 3 levels and the excitation of the $J = 1$ level to the $J = 2$ level, in the $v = 0$ state, by impacts

with atomic hydrogen. For T < 30 K, the rate coefficients for ortho-para conversions are taken from Flower *et al.* [26].

4.4 H_2 Spectra for the UCL Formation Pumping Model

In this section we will consider the H_2 spectra generated using UCL experimental data, namely those using formation pumping model **u** only. An intercomparison of all the models follows in Section 4.5.

The spectrum with all the 'default' parameters is shown below in Figure 4.2. This spectrum is for the UCL formation pumping model (**u**), where only the surface formation mode is permitted, for a dark cloud with density $n_H = 1 \times 10^6$ cm^{-3} and column density N(H_2) = 1.6×10^{22} cm^{-2}, temperature T = 10 K, electron fraction $x_e = 1 \times 10^{-4}$, proton fraction $x_{H+} = 1 \times 10^{-4}$, with the standard UV field ($\chi = 1$). The spectrum has been convolved with a Gaussian profile with line width of $\Delta\lambda = 5 \times 10^{-5}$ μm. Most of the strong emission lines are in the wavelength range 1 – 3 μm. Strong lines include 4 – 2 O(3) at 1.51 μm, 2 – 1 O(3) at 2.97 μm, 2 – 1 O(2) at 2.79 μm and 1 – 0 Q(1) at 2.41 μm, in order of line strength.

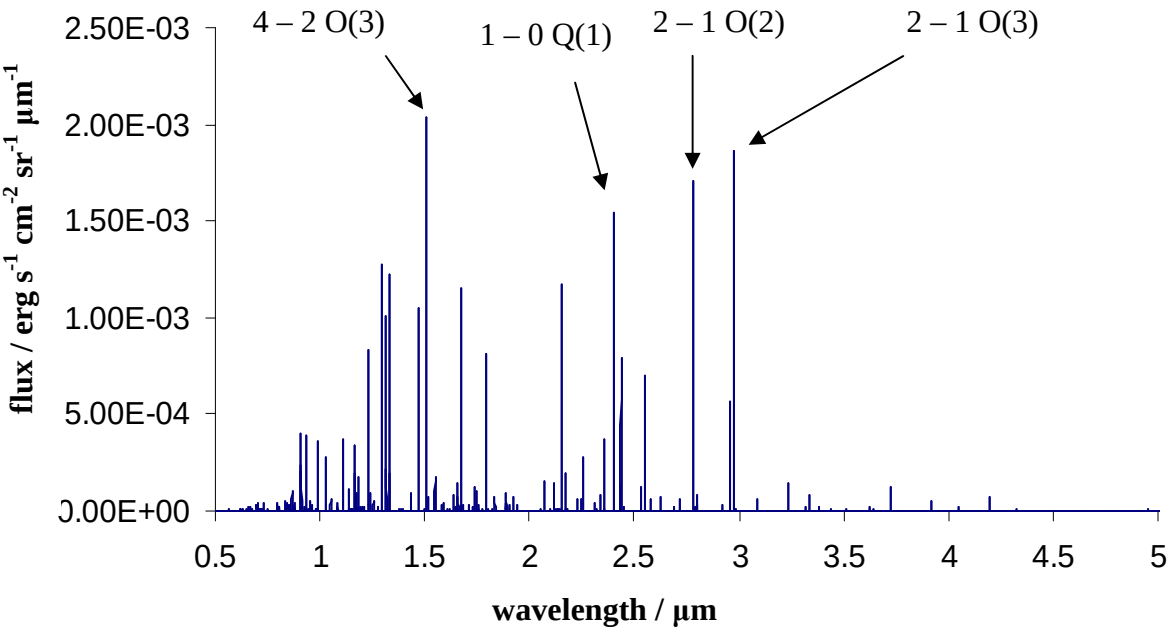

Figure 4.2 H_2 spectrum generated using the UCL formation pumping model (**u**) at resolution $\Delta\lambda = 5 \times 10^{-5}$ μm, for dark clouds with parameters density $n_H = 1 \times 10^6$ cm^{-3} and column density N(H_2) = 1.6×10^{23} cm^{-2}, temperature T = 10 K, electron fraction $x_e = 1 \times 10^{-4}$, proton fraction $x_{H+} = 1 \times 10^{-4}$, with the standard UV field ($\chi = 1$).

4.4.1 Effects of Cloud Density

Figure 4.3 shows spectra generated for dark clouds of increasing density of temperature 10 K, using the UCL formation pumping model and keeping all other parameters at the default values used in Figure 4.2. Cloud A, with density n_H = 1 × 10^3 cm^{-3} has column density N(H_2) = 4.8 × 10^{21} cm^{-2}, chosen so that A_V ~ 3 mag, assuming that in dark clouds most of the hydrogen nuclei are in the form of molecules and that 1 mag corresponds to ~1.6 × 10^{21} cm^{-1} [48]; cloud B with density n_H = 1 × 10^4 cm^{-3} has column density N(H_2) = 1.6 × 10^{22} cm^{-2}, chosen so that A_V ~ 10 mag; cloud C with density n_H = 1 × 10^5 cm^{-3} has column density N(H_2) = 8.0 × 10^{22} cm^{-2} chosen so that A_V ~ 50 mag; and cloud D with density n_H = 1 × 10^6 cm^{-3} has column density N(H_2) = 1.6 × 10^{23} cm^{-2} chosen so that A_V ~ 100 mag. To more easily compare the spectra, the plots are superimposed in Figure 4.4.

From Figure 4.3 and Figure 4.4, it is apparent that the line flux increases with cloud density and the shapes of the spectra do not change dramatically with cloud density. Nevertheless, there are some changes in the shape of the spectra which may be analysed by considering the ratios of particular lines within a spectrum, in particular the line flux ratio between the 2 – 1 O(3) line at 2.97 μm and the 2 – 1 O(2) line at 2.79 μm. This ratio is 0.984, 0.827, 0.911 and 1.09 for clouds A, B, C and D respectively and does not change consistently with increasing cloud density or increasing column density, as can be seen in Figure 4.5. The formation pumping component to the lines should increase with cloud density, as more atomic hydrogen is available for the formation reaction. The fact that the 2 – 1 O(3) line 'wins out' over the 2 – 1 O(2) line at the highest densities is in accordance with the formation pumping distribution shown in Figure 4.1: the 2 – 1 O(3) line has a greater flux at high densities than the 2 – 1 O(2) line because there is more excitation into the v = 2, J = 1 state than into the v = 2, J = 0 state during formation, specifically, $\delta_{2,1} > \delta_{2,0}$.

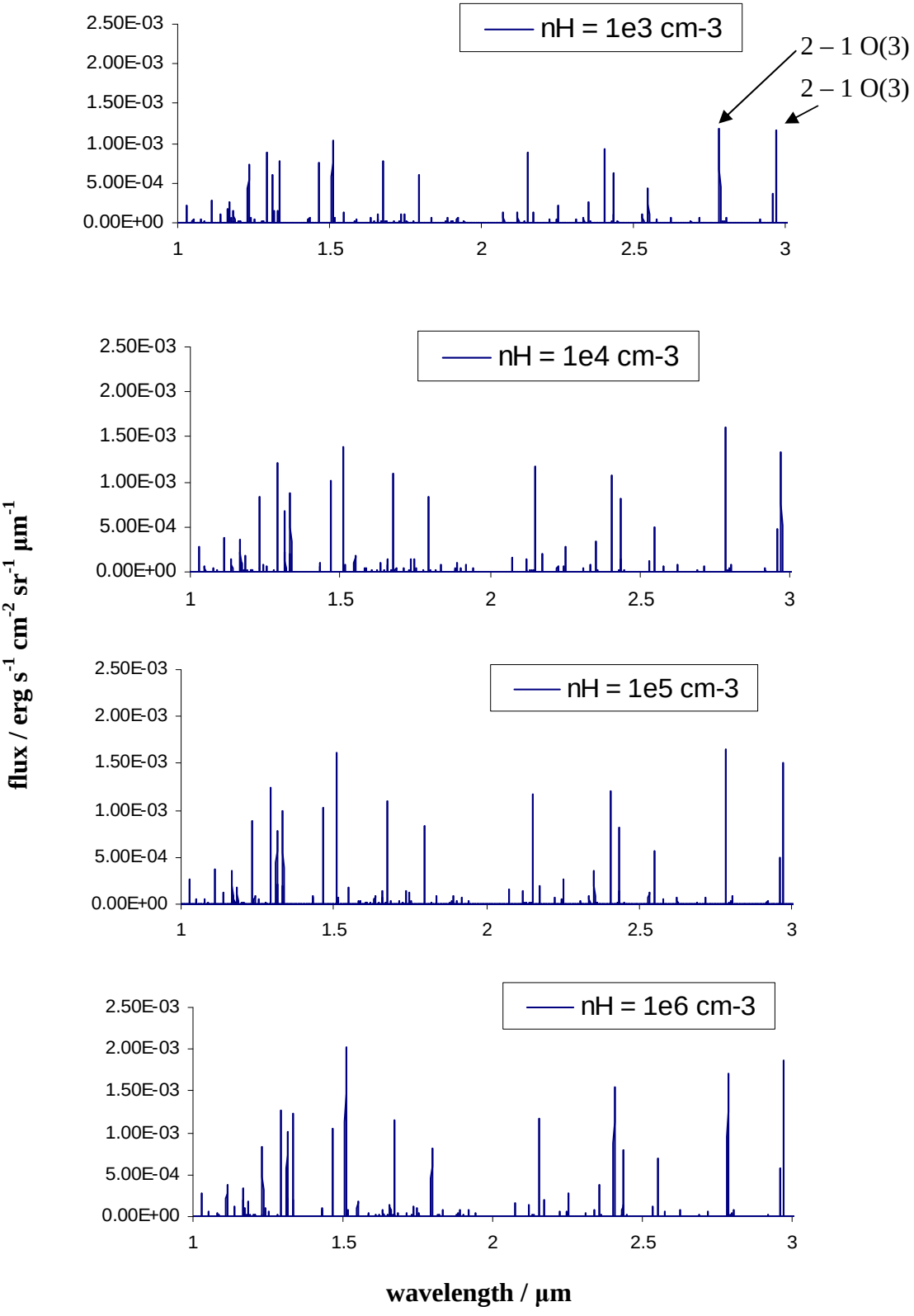

Figure 4.3 H_2 spectra generated using the UCL formation pumping model (**u**) for dark clouds of increasing density and column density at T = 10 K.

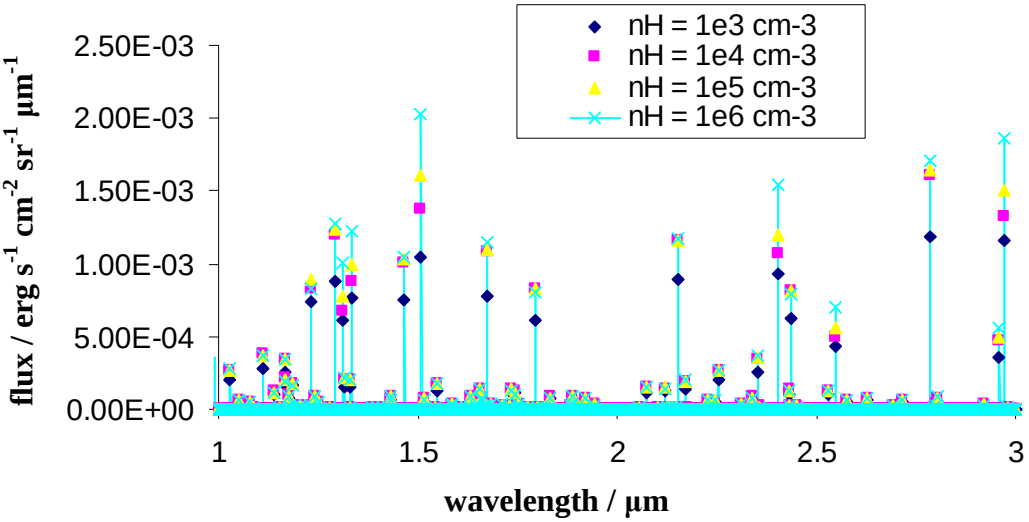

Figure 4.4 Superimposed plots of H_2 spectra generated using the UCL formation pumping model (**u**) for dark clouds of increasing density and column density.

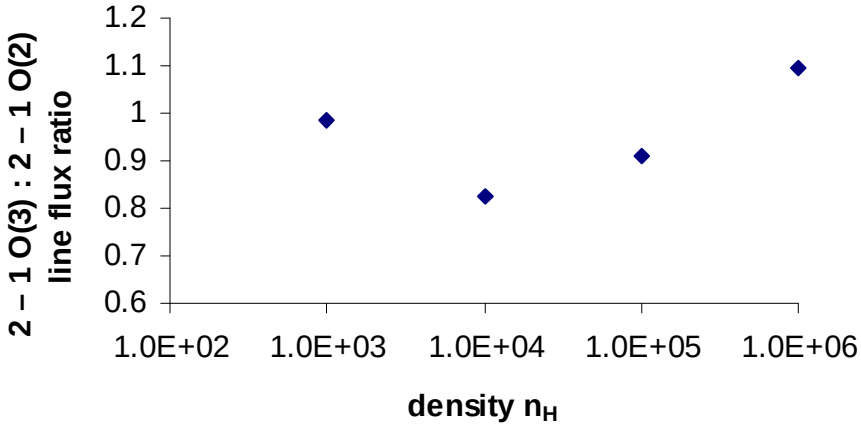

Figure 4.5 Line flux ratio of the 2 – 1 O(3) line at 2.97 µm and the 2 – 1 O(2) line at 2.79 µm against cloud density n_H plotted on a logarithmic scale.

In general, the line fluxes do not scale linearly with cloud density or column density, as can be seen in Figure 4.4. Although cloud D is a factor of 100 more dense than cloud B and has 10 times the column density, the flux magnitudes of lines from cloud D are not even twice as large as those from cloud B. A possible explanation for this phenomenon is that in dark clouds, there is not sufficient atomic hydrogen available to take part in H_2 formation, such that n_1 does not scale with n_H. Due to shielding by dust, UV photons do not penetrate the bulk of dark clouds, hence H_2 destruction is minimized and can only occur through processes such as cosmic ray ionization and

chemical destruction mechanisms. The radiative transfer code does not take chemical destruction of H_2 molecules, by reaction with other species, into account. Therefore, although the density of hydrogen nuclei and column density of H_2 are significantly increasing from cloud B to cloud D, the increase in atomic hydrogen abundance calculated by the code may be relatively small. The majority of the hydrogen in dark clouds is in the form of thermalized molecules, which do not produce significant emission because they already occupy the lowest ro-vibrational levels. To verify that there is only a small increase in atomic hydrogen abundance with n_H in dark clouds, in accordance with Figure 4.4, a chemical model has been used to calculate the fractional abundance of H-atoms in clouds of density types A, B, C and D. A chemical model was used to confirm that there is no significant production of H-atoms through chemical channels, which are neglected by the radiative transfer code. This is explained further in Section 4.6.

H_2 emission spectra increase in line strength, but again do not scale linearly with cloud density for clouds at higher temperatures, as shown in Figure 4.6, Figure 4.7, and Figure 4.8 below. Again this is thought to be due to the H-atom abundance not scaling with the cloud density and the thermalization of most of the H_2 molecules. In Figure 4.8, a strong line at 2.41 μm appears for $n_H = 1 \times 10^6$ cm^{-3}. This is the 1 – 0 Q(1) line and is ascribed to collisional pumping.

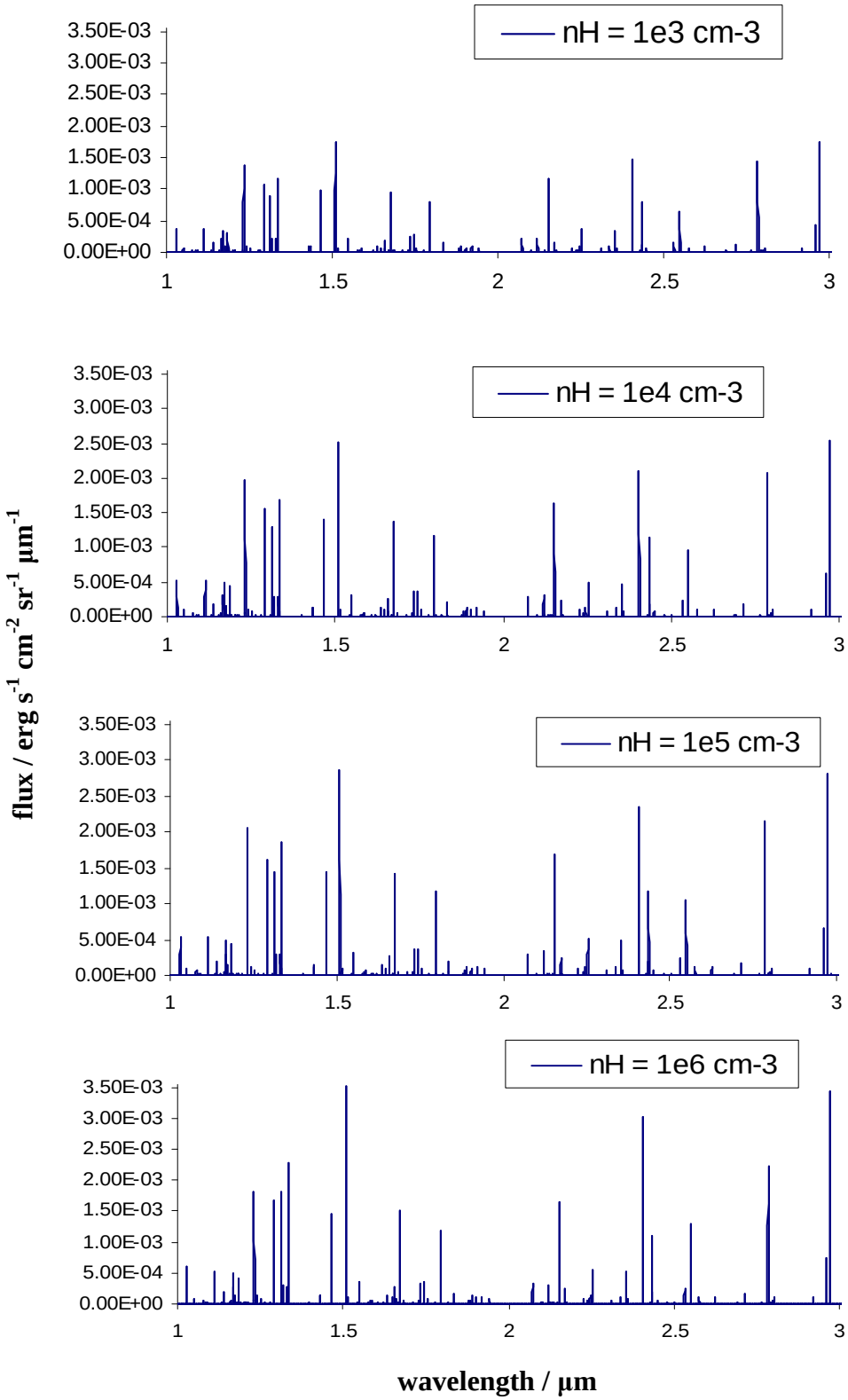

Figure 4.6 H_2 spectra generated using the UCL formation pumping model (**u**) for dark clouds of increasing density and column density at T = 50 K.

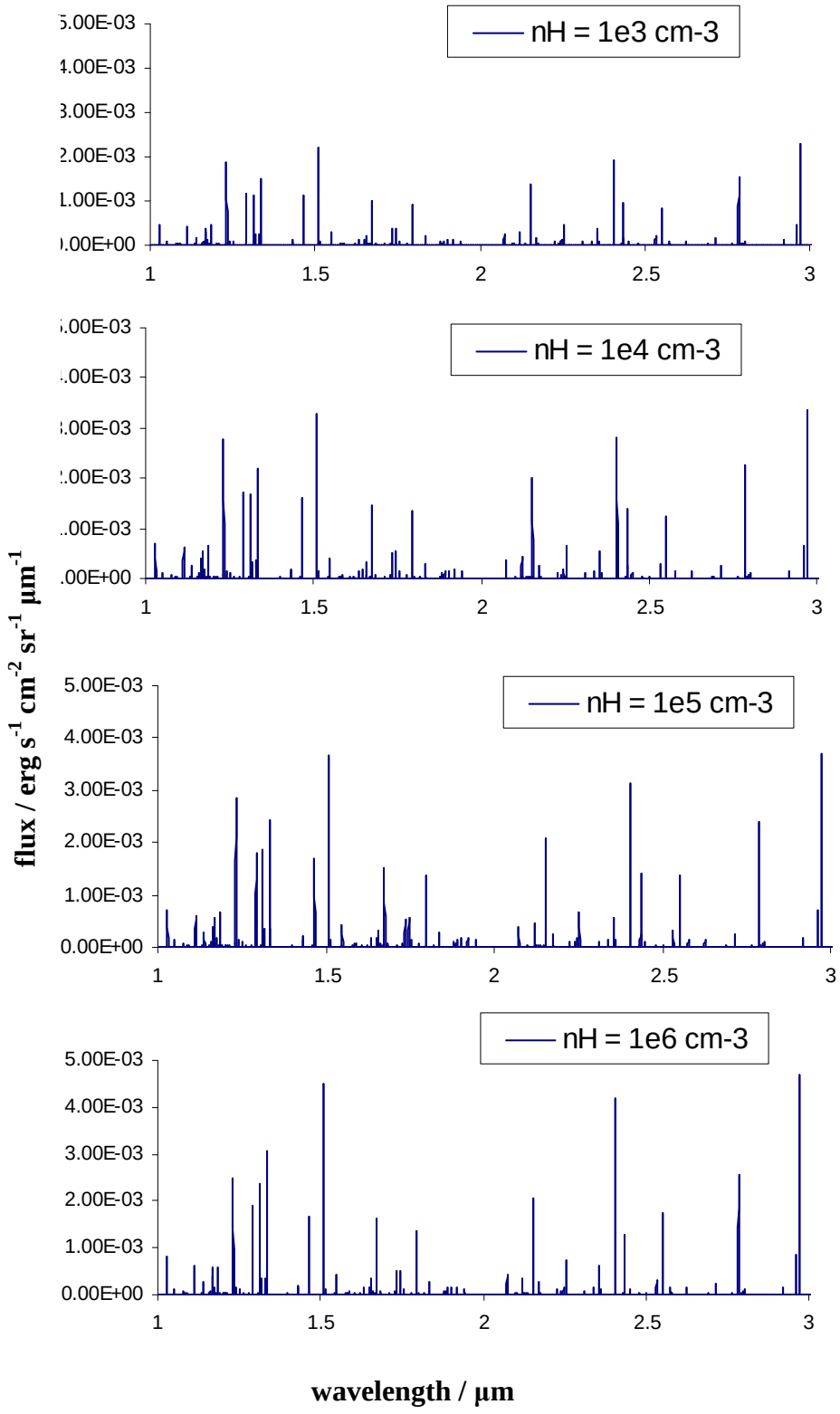

Figure 4.7 H_2 spectra generated using the UCL formation pumping model (**u**) for dark clouds of increasing density and column density at T = 100 K.

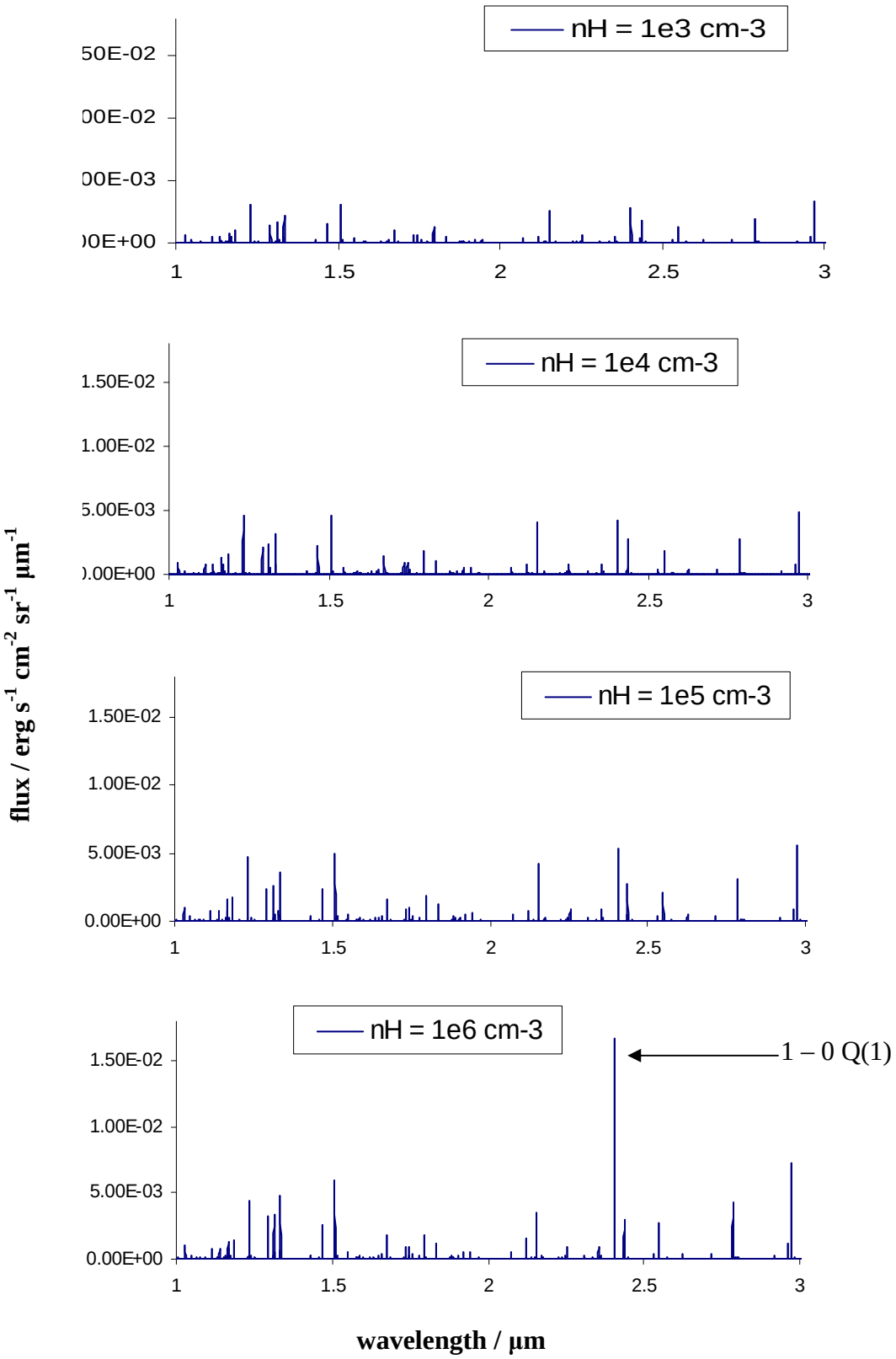

Figure 4.8 H_2 spectra generated using the UCL formation pumping model (**u**) for dark clouds of increasing density and column density at T = 500 K.

4.4.2 Effects of Cloud Temperature

The same spectra in Section 4.4.1 can be re-plotted to show the effect of increasing the temperature of a dark cloud at a specific density. For spectra with T ≥ 50 K, the radiative transfer code includes ortho-para conversions studied by Sun and Dalgarno [49] rather than by Flower *et al.* [26]. However, when the Flower *et al.* values are used for clouds with T ≥ 50 K, there is no significant change to the H_2 emission spectra.

For interstellar dark clouds, the line flux strength increases steadily, although not linearly, with temperature. As the temperature rises, more collisional pumping occurs. As before, the shape of the H_2 spectrum does not greatly alter as the temperature of a cloud is increased, but there are small changes in line ratio, which can be seen in Figure 4.9. For the most dense clouds, with $n_H = 1 \times 10^6$ cm^{-3}, there is a sharp increase in strength for the 1 – 0 Q(1) line between 100 – 500 K. This sharp rise in line strength is due to thermal excitation of H_2 to the $v = 1$, $J = 1$ level.

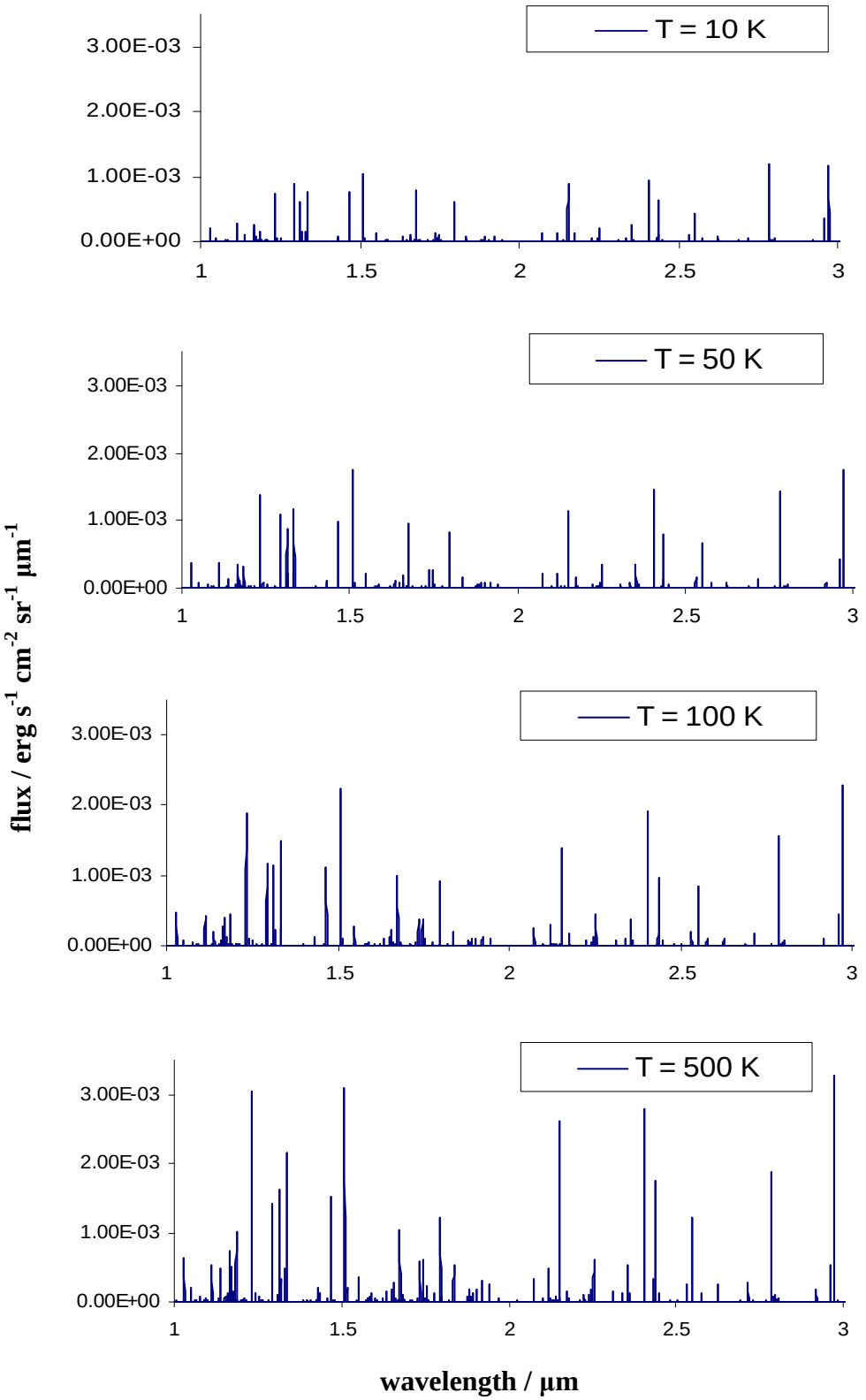

Figure 4.9 H_2 spectra generated for dark cloud A, with $n_H = 1 \times 10^3$ cm^{-3} and N(H_2) = 4.8 × 10^{21} cm^{-2}, using the UCL formation pumping model (**u**) at increasing temperatures.

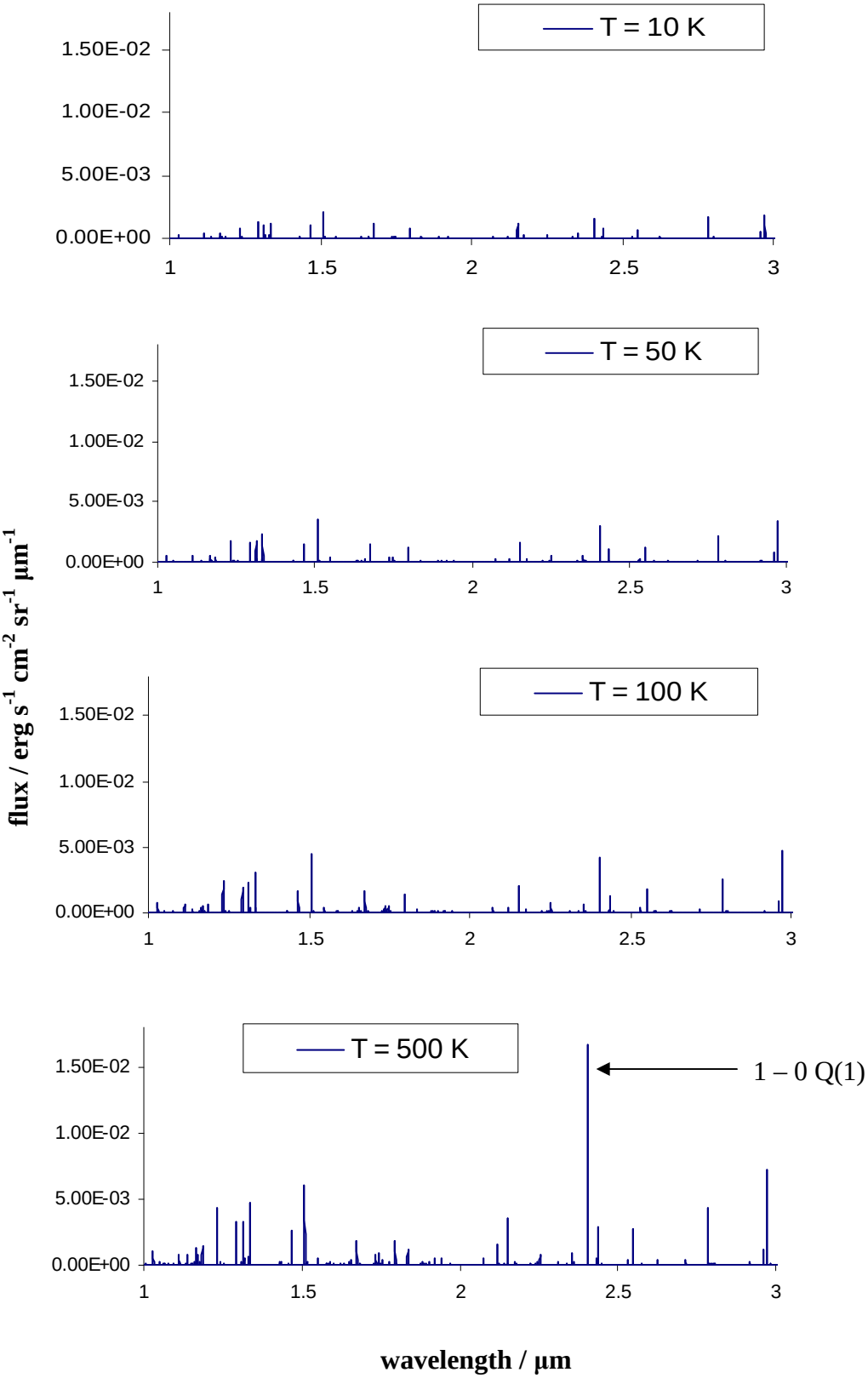

Figure 4.10 H_2 spectra generated for dark cloud D, with $n_H = 1 \times 10^6$ cm^{-3} and N(H_2) = 1.6×10^{23} cm^{-2}, using the UCL formation pumping model (**u**) at increasing temperatures.

4.4.3 Effects of UV Field

The UV radiation permeating the dark cloud can be increased in strength by use of the UV field scaling parameter in the radiative transfer code. Figure 4.11 shows that the line strengths of H_2 emission spectra are linearly dependent on the UV field, due to ro-vibrational excitation of H_2 by UV photons. Quite simply, Figure 4.11 illustrates the effect of UV pumping in the dark clouds investigated. However, it should be noted that the increase in UV field scaling factor from χ = 0.5 to χ = 4 is insufficient to liberate a significant number of H-atoms *via* photodissociation of H_2 molecules in such dense cloud; the UV field is weak such that the clouds remain 'dark'. Therefore it is unlikely that UV excitation plays an important role in formation pumping in dark clouds.

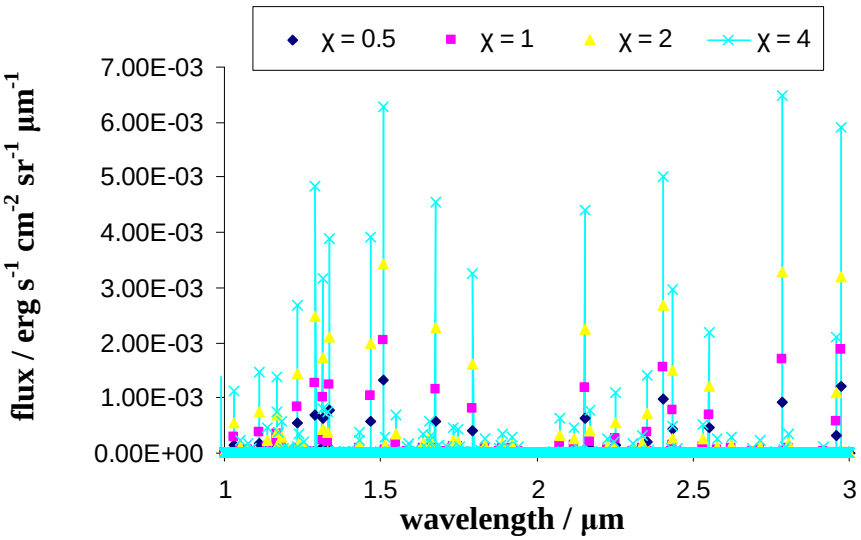

Figure 4.11 H_2 spectra generated using the UCL formation pumping model (**u**) for dark clouds of density $n_H = 1 \times 10^6$ cm^{-3} and temperature T = 10 K, with different UV field scaling parameter, χ = 0.5, 1, 2 and 4.

4.4.4 Effects of Gas Phase Formation

The gas phase H_2 formation channel *via* the associative detachment mechanism involving atomic hydrogen and the negative ion H^- has also been studied. There is negligible difference between spectra when the gas phase formation channels are turned on, as is shown by Figure 4.12. The spectral line strengths are identical to within 0.25%. This is because the overwhelming majority of H_2 formation in dark clouds proceeds *via* surface reactions, thus the gas phase channel is unimportant. As

described in Chapter 1, this gas phase formation pumping route may be more important for shocked regions rather than for quiescent dark clouds, as was found by observations of OMC-1 Peak 1 by Rosenthal *et al.* [38].

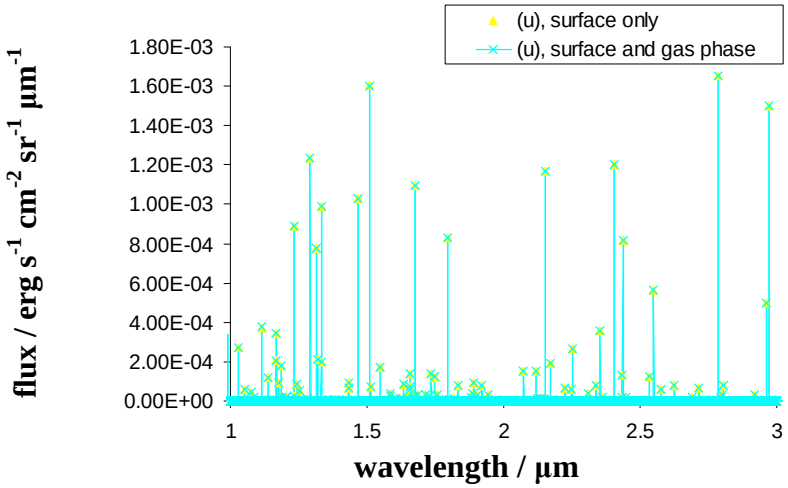

Figure 4.12 H_2 spectra generated using the UCL formation pumping model (**u**) for dark clouds of density n_H = 1 × 10^5 cm^{-3} and temperature T = 10 K, in surface formation only mode and in surface and gas phase formation mode.

4.4.5 Effects of Electron Fraction

The electron fraction parameter has negligible effect on the H_2 emission spectra as shown in Figure 4.13. Spectra generated using x_e = 1 × 10^{-8}, 1 × 10^{-6} and 1 × 10^{-4} for dark clouds at temperature T = 10 K and density n_H = 1 × 10^6 cm^{-3} are similar to within 0.01%.

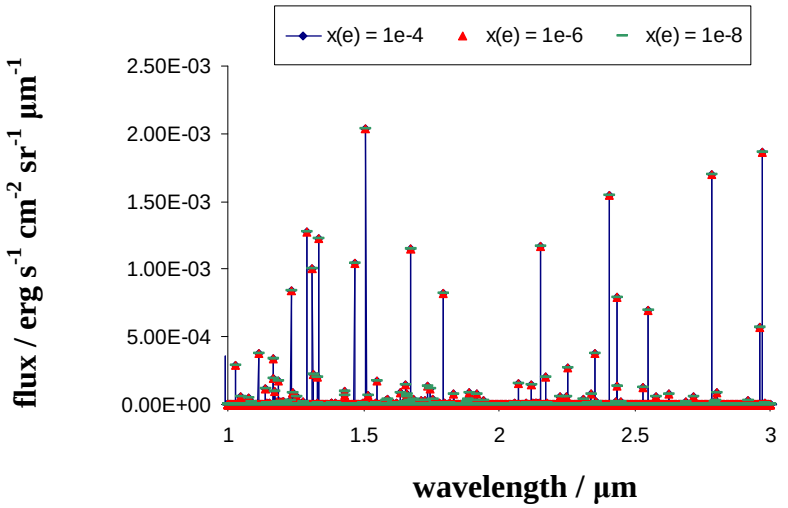

Figure 4.13 H_2 spectra generated using the UCL formation pumping model (**u**) for dark clouds of density n_H = 1 × 10^6 cm^{-3} and temperature T = 10 K, changing the electron fraction x_e = 1 × 10^{-4}, 1 × 10^{-6} and 1 × 10^{-8}.

4.4.6 Effects of Proton Fraction

There is a noticeable difference in H_2 spectra for interstellar dark clouds with varying proton fractions, which have been varied independently of the electron fraction. Clouds with relatively higher proton fractions have marginally lower line fluxes. This is because protons collide with H_2 molecules and provide a de-excitation mechanism, so that the gas is more thermalized. In Figure 4.14, the spectral line strengths for a dark cloud with density $n_H = 1 \times 10^6$ cm^{-3} and temperature T = 10 K but with different values of x_{H+} are similar to within 10%.

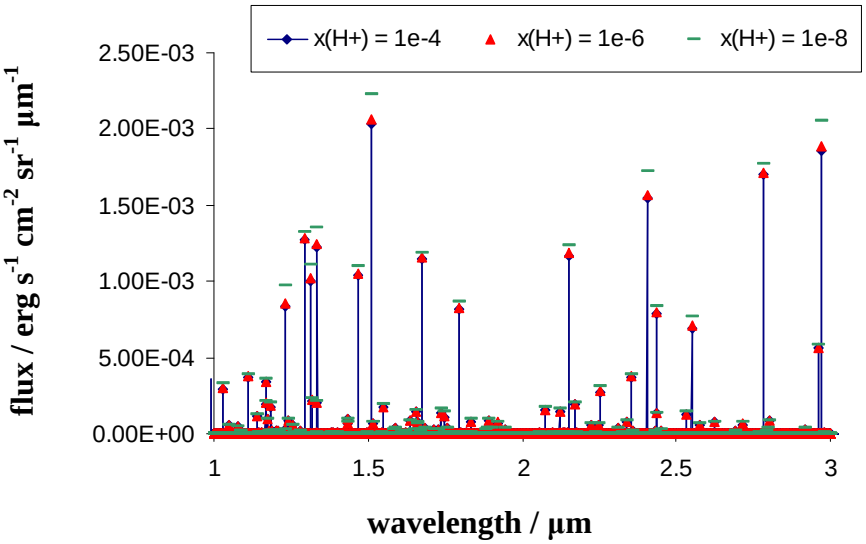

Figure 4.14 H_2 spectra generated using the UCL formation pumping model (**u**) for dark clouds of density $n_H = 1 \times 10^6$ cm^{-3} and temperature T = 10 K, changing the electron fraction $x_{H+} = 1 \times 10^{-4}$, 1×10^{-6} and 1×10^{-8}.

4.4.7 Effects of Changing the $v = 0$ Populations

The experimental results obtained for the formation of HD on graphite described the ro-vibrational level populations for vibrational states $v = 1 - 7$ [14, 36, 37]. As described in Section 4.2, the distribution for HD was extrapolated to create the ro-vibrational level distribution of nascent H_2. The HD level populations were scaled by the appropriate nuclear spin statistical weight g_N to convert them to relative populations of H_2. Data for the $v = 0$ state could not be obtained due to the presence of background HD in the ground state, thus the $v = 0$ level populations were estimated. The $v = 0$ level populations were taken to be equal to the $v = 1$ level populations, such

that $P_{v,J} = P_{0,J} = P_{1,J}$ for all J states detected. This is slightly over-estimating the $v = 0$ populations, as Figure 4.1 shows that lower vibrational states are less populated than higher vibrational levels, for $1 < v < 4$. This vibrational scheme was adopted as a 'lower limit' to the total excitation, in order to take a modest estimate of the amount of formation pumping. As there is more uncertainty in the population of the $v = 0$ levels than for the other vibrational states, H_2 spectra has been generated for a distribution where the $v = 0$ levels are twice as populated as the $v = 1$ levels (model $\mathbf{u_2}$) and for a distribution where the $v = 0$ levels are half as populated as the $v = 1$ levels (model $\mathbf{u_{0.5}}$). Figure 4.15 shows that changing the population of the $v = 0$ levels in the UCL formation pumping models makes only a marginal difference to line strengths. For a dark cloud at density $n_H = 1 \times 10^6$ cm^{-3} and temperature T = 10 K, the spectra generated using models $\mathbf{u_{0.5}}$, $\mathbf{u}$ and $\mathbf{u_2}$ are similar to within 4%.

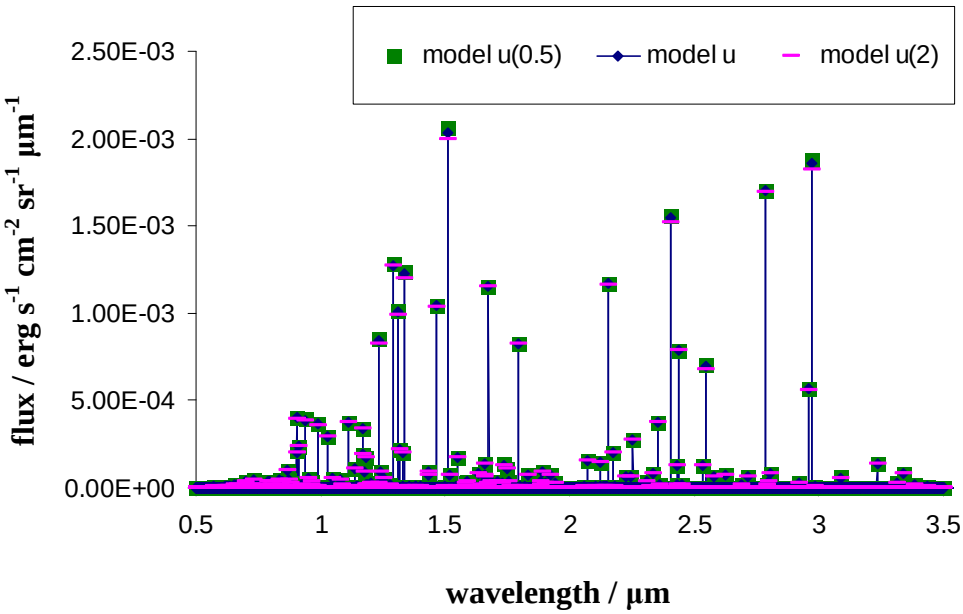

Figure 4.15 H_2 spectra generated for dark clouds of density $n_H = 1 \times 10^6$ cm^{-3} and temperature T = 10 K, changing the population of the $v = 0$ levels in the UCL formation pumping model.

4.4.8 Effects of Telescope Resolution

H_2 spectra can be generated for any instrument resolution required. IR spectra are presented below for a dark cloud of density $n_H = 1 \times 10^6$ cm^{-3} and temperature T = 10 K generated by convolving with different Gaussian line widths, Δλ. Corresponding instrument resolutions for spectra at ~ 2.5 μm are 250, 2800 and 50 000 for Δλ = 0.01 μm, 9×10^{-4} μm and 5×10^{-5} μm respectively.

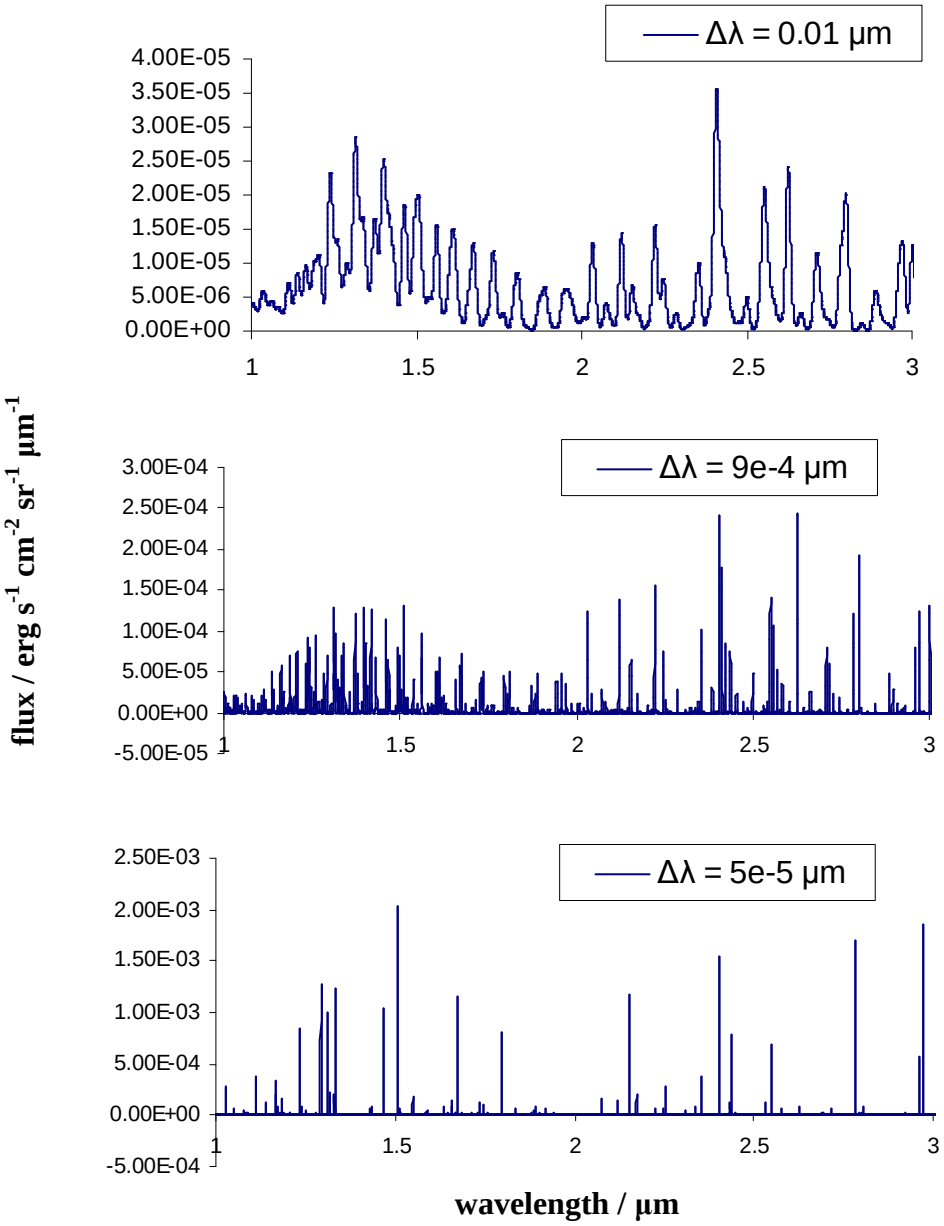

Figure 4.16 H_2 spectra for a dark cloud of density $n_H = 1 \times 10^6$ cm^{-3} and temperature T = 10 K, using the UCL formation pumping model (**u**). The spectra has been generated by convolving with Gaussian line widths of Δλ = 0.01 μm, 9×10^{-4} μm and 5×10^{-5} μm.

4.5 Comparison of Formation Pumping Models

The aim of this study is to find a signature for formation pumping. This signature would be some feature in the H_2 emission spectra due to the formation pumping mechanism only, rather than UV or collisional pumping. We also seek to identify the optimum conditions to distinguish between formation pumping models.

H_2 spectra for the 7 different formation pumping models are presented in Figure 4.17 below:

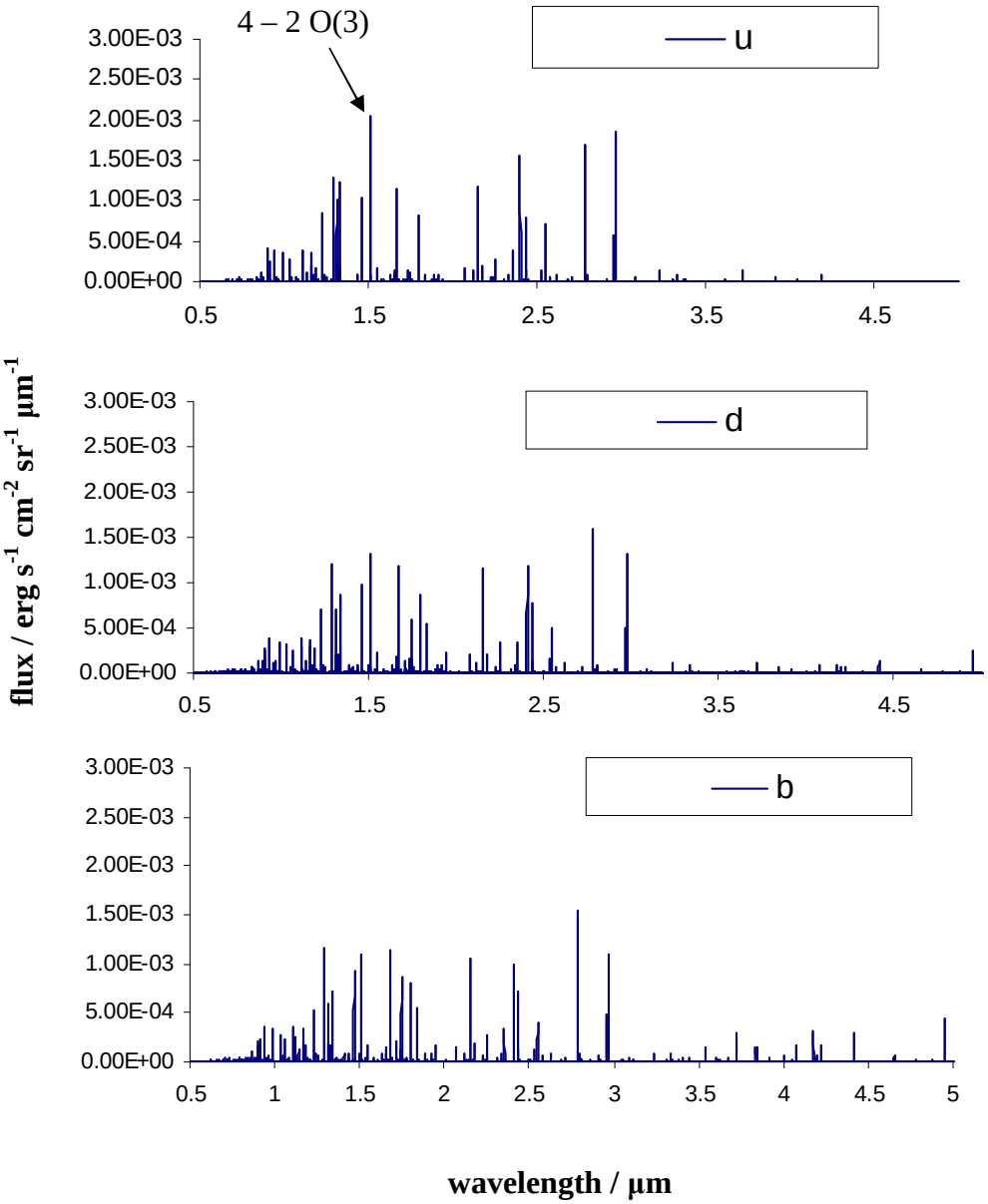

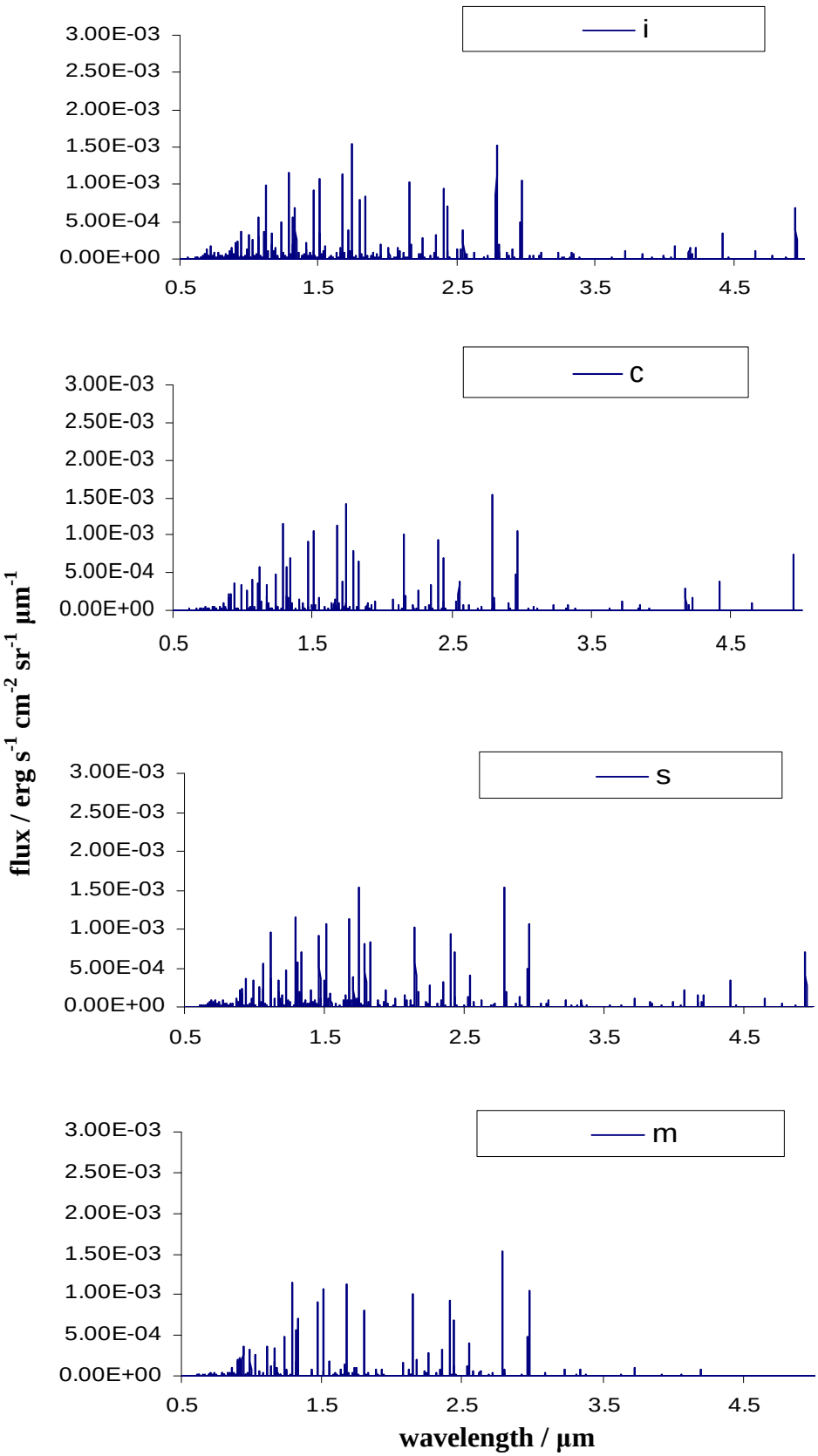

Figure 4.17 H_2 spectra for a dark cloud of density $n_H = 1 \times 10^6$ cm^{-3} and temperature T = 10 K, using the 7 formation pumping models.

Most of the models produce emission spectra where the majority of strong lines fall in the wavelength region λ = 1 – 3 μm, therefore this would be the best wavelength region in which to search for evidence of formation pumping. To obtain an observational signature of a formation pumping model, one must compare the H_2 spectra generated using the model to the H_2 spectra generated using model **m**, the minimum pumping model, as shown in Figure 4.18 below:

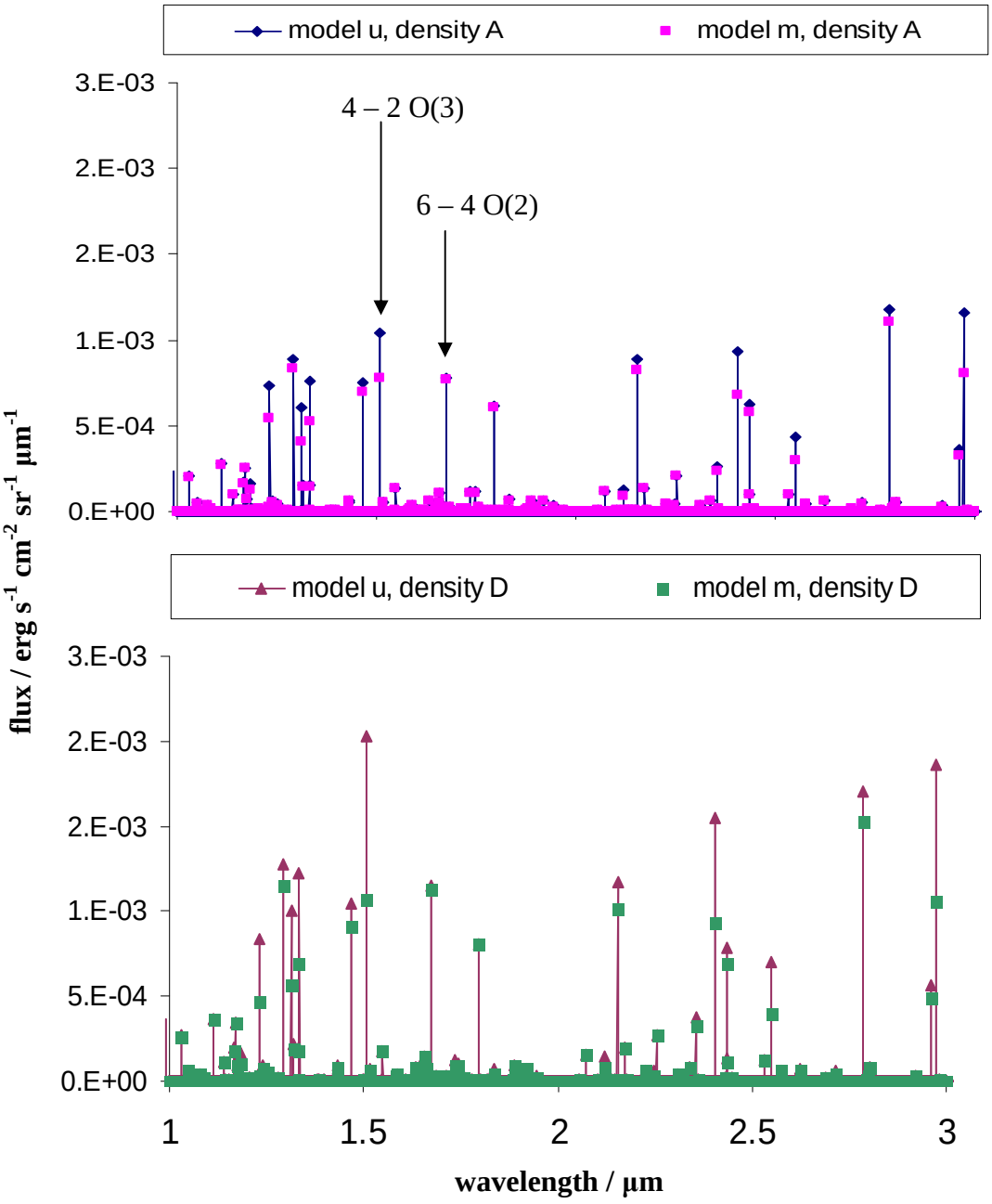

Figure 4.18 Superimposed H_2 spectra for model **u** and model **m** for cloud A and D at densities $n_H = 1 \times 10^3$ and 1×10^6 cm^{-3} respectively, at temperature T = 10 K.

In Figure 4.18, the UCL formation pumping model (**u**) is compared to the minimum formation pumping case (**m**) for clouds of density 1×10^3 cm^{-3} and 1×10^6 cm^{-3}. Formation pumping could be identified by comparing adjacent line strengths of the spectra for model **u** and model **m**. For example, if both the 4 – 2 O(3) line at 1.509 μm and the 6 – 4 O(2) line at 1.6745 μm were observed, and their flux ratio was found to be ~ 2 for dark clouds with density $n_H = 1 \times 10^6$ cm^{-3}, this would be a positive detection of the UCL formation pumping model. However, if the line strengths are approximately equal at such a high density, then it would suggest that model **u** is incorrect and there is no formation pumping into the $v = 4$, $J = 1$ level.

The UCL formation pumping model has characteristic spectra because, unlike most formation pumping models, it does not predict the population of high rotational states. As shown in Figure 4.19 and Figure 4.20, the UCL formation pumping model does not predict a strong line at 1.747 μm, whereas most formation pumping models do predict a significant flux at this wavelength. This is the 1 – 0 S(7) line, which originates in the $v = 1$, $J = 9$ level. The UCL formation pumping model does not predict rotational states with $J > 4$ in the $v = 1$ state to be significantly populated. In Figure 4.19 for clouds with $n_H = 1 \times 10^6$ cm^{-3}, models **d**, **b**, **i**, **c** and **s** all predict line fluxes $> 5 \times 10^{-4}$ erg cm^{-2} sr^{-1} s^{-1} μm^{-1} at 1.747 μm, whereas models **u** and **m** predict line fluxes of 3.7×10^{-6} and 2.5×10^{-6} erg cm^{-2} sr^{-1} s^{-1} μm^{-1} respectively. Note that model **m** is the minimum formation pumping model, where nascent H_2 is formed in the two lowest ro-vibrational states, so this model cannot populate high rotational states. Furthermore, H_2 is unlikely to be excited to high rotational levels, such as $J = 9$, from collisional pumping only [9], thus the 1 – 0 S(7) line will not have significant flux for models **m** and **u**. Therefore, observations of the 1 – 0 S(7) line in a quiescent dark cloud may be able to constrain the formation pumping mechanism. If the line is detected and found to have flux $\geq 5 \times 10^{-4}$ erg cm^{-2} sr^{-1} s^{-1} μm^{-1}, then H_2 must be populated in high rotational levels by formation pumping. If the line is not detected, or found to be weak with flux ~ 10^{-6} erg cm^{-2} sr^{-1} s^{-1} μm^{-1}, then either there is no formation pumping (**m**) or the UCL formation pumping model (**u**) may be the correct pumping scheme. Astronomical observations of H_2 spectra are discussed further in Section 4.7.

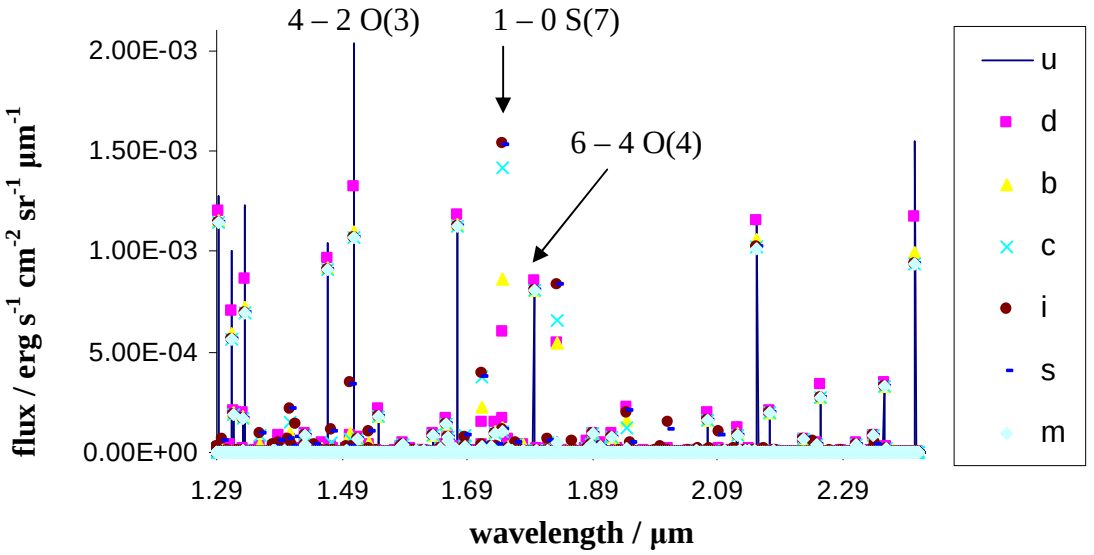

Figure 4.19 Superimposed H_2 spectra for all formation pumping models for a cloud of density $n_H = 1 \times 10^6$ cm^{-3} and temperature T = 10 K.

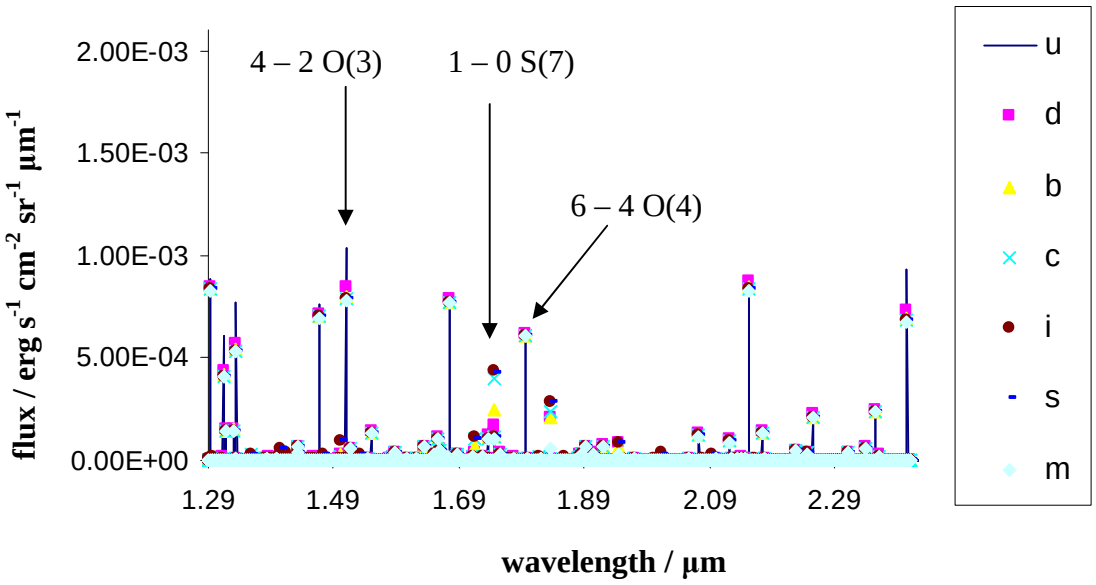

Figure 4.20 Superimposed H_2 spectra for all formation pumping models for a cloud of density $n_H = 1 \times 10^3$ cm^{-3} and temperature T = 10 K.

When there is mimimum formation pumping and model **m** is used in the radiative transfer code, nascent H_2 molecules are formed at the lowest ro-vibrational levels possible (v, J) = (0, 0) and (0, 1). Therefore, all other levels are populated by other pumping mechanisms, mainly by collisional excitation. From Figure 4.21 it is apparent that the spectra for model **m** do not scale linearly with N(H_2). This indicates that the cloud is thermalizing, which means that the impacts between particles are so frequent that much of the H_2 gas is collisionally de-excited to the lowest ro-vibrational levels and so cannot contribute to the IR emission. Denser clouds are more

thermalized, such that above a certain density ($n_H \geq 1 \times 10^5$ cm^{-3}), there will be no significant increase in line strength of the H_2 spectra.

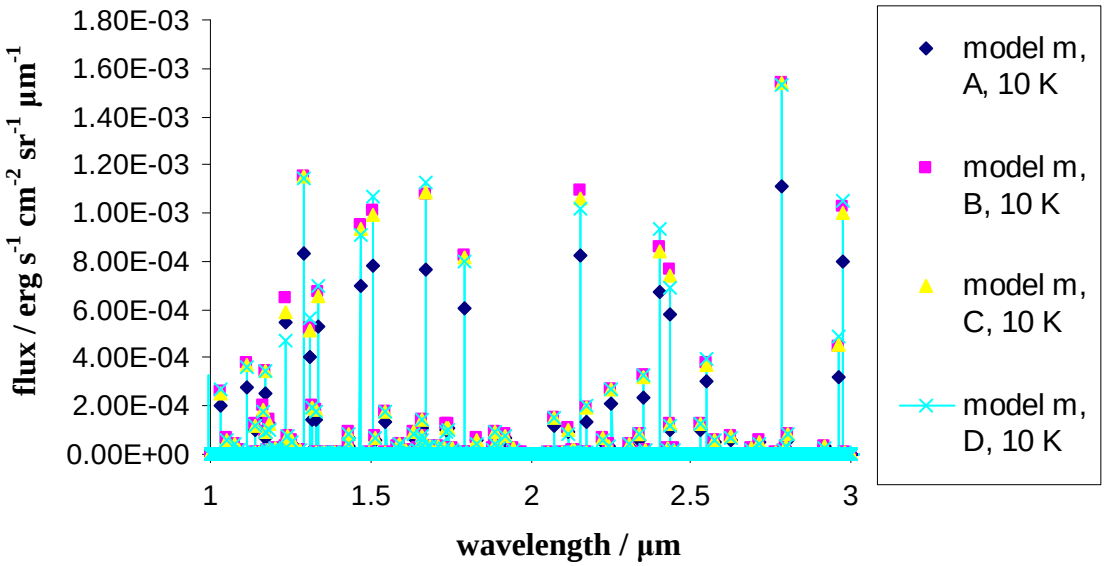

Figure 4.21 Superimposed H_2 spectra for minimum formation pumping, model m, for a clouds of density A ($n_H = 1 \times 10^3$ cm^{-3}, N(H_2) = 4.8×10^{21} cm^{-2}), B ($n_H = 1 \times 10^4$ cm^{-3}, N(H_2) = 1.6×10^{23} cm^{-2}), C ($n_H = 1 \times 10^5$ cm^{-3}, N(H_2) = 8.0×10^{22} cm^{-2}), D ($n_H = 1 \times 10^6$ cm^{-3}, N(H_2) = 1.6×10^{23} cm^{-2}), at temperature T = 10 K.

Changing the parameter space for models **d, b, i, c, s** and **m** yields similar results to changing the parameter space for the UCL formation pumping model. Increasing the cloud temperature increases the line flux, although of course the relationship is not linear. Lines such as 1 – 0 Q(1) increase in strength proportionately more than lines such as 1 – 0 S(7) with cloud temperature. This is because the 1 – 0 Q(1) line has a much greater collisional component than the 1 – 0 S(7) line. The proton fraction makes a small but noticeable change to the line strengths, whereas the electron fraction has a negligible effect on the H_2 emission spectra. The effects of the helium fraction, extinction factor R_V, gas-to-dust ratio and cosmic ionization rate on the H_2 emission spectra produced by the different formation pumping models have not yet been fully investigated.

4.6 Chemical Modelling of Hydrogen Abundance

The radiative transfer code written by Casu and Cecchi-Pestellini [18, 20] described in Section 4.3 includes H_2 destruction mechanisms such as photodissociation and photoionization, collisional dissociation and ionization and cosmic ray ionization. The bulk of a dark cloud is not penetrated by UV photons; hence the H-atom abundance is predicted to be low by the radiative transfer code, because only collisional dissociation and cosmic ray destruction processes are taken into account to liberate H-atoms.

However, the radiative transfer code neglects the destruction of H_2 leading to the production of H-atoms *via* chemical reactions. To investigate chemical destruction of H_2 independently of the radiative transfer code, some calculations have been carried out by use of a chemical model, known as UCL_CHEM 1999, which was developed by Viti and Williams [50]. The model uses a network of gas phase and surface reactions taken from the UMIST RATE06 and RATE99 database [51, 52] to calculate the abundances of chemical species in interstellar environments. Included in the code are 119 gas-phase species and 39 surface species interacting in 1728 chemical reactions. For this study, time-dependent, single-point calculations were performed for clouds of different density and visual magnitude. The cloud starts from a medium in atomic form with initial fractional abundances 1.0, 0.075, 4.45×10^{-4}, 1.79×10^{-4}, 8.52×10^{-5}, 1.43×10^{-6} and 5.12×10^{-6} for H, He, O, C, N, S and Mg respectively to match the findings of Sofia and Meyer [53]. The chemical model was run for dark clouds of constant density and temperature for 1 Myr. During this time, atoms and molecules react in the gas phase such that species are formed and destroyed and also deplete onto grain surfaces. Surface chemistry included in the model consists of the conversion of a fraction of CO to CH_3OH (methanol) and hydrogenation of adsorbates whenever possible. The advantage of this approach is that the mantle composition is derived self-consistently by the chemical model and is not assumed.

The chemical model was used to obtain the fractional abundance of H-atoms, x_1 for dark clouds at 10 K. Cloud densities used were $n_H = 1 \times 10^3$, 1×10^4, 1×10^5 and 1×10^6 cm^{-3} as these are the values for which H_2 spectra have been generated. In order to study the chemistry as a function of depth along the cloud, the chemical model was

run at A_V = 3, 5, 7, 10, 50 and 100 mag. This is because the edges of the cloud are translucent and UV radiation photolyzes H_2 molecules to increase the abundance of hydrogen atoms. Therefore, the atomic abundance may be a function of depth within an interstellar cloud, as well as dependent on the density of the cloud.

Species abundances, and hence the network of chemical reactions, are dependent on the amount of freeze-out occurring in the dark cloud. Freeze-out is the depletion of gaseous molecules such as CO, N_2 and O_2, which are believed to be formed in the gas phase but adsorb onto the grain surface [54, 55]. UCL_CHEM 1999 models freeze-out using a parameter, fr, that can be varied from 0 – 1. After 1 Myr, any species that can freeze-out onto the dust grains will have done so. The freeze-out parameter was chosen for each density of dark cloud so that the percentage of CO frozen out onto the grains was consistent with observations of dark clouds, as CO is a good tracer of H_2 [56]. The values for the freeze out parameter used for each density, along with the resulting percentage of CO frozen out onto grains are shown below in Table 4.2:

n_H	1×10^3 cm^{-3}	1×10^4 cm^{-3}	1×10^5 cm^{-3}	1×10^6 cm^{-3}
fr	0.5	0.5	0.05	0.01
CO on grains	6.3 %	45 %	62 %	88 %

Table 4.2 The freeze-out parameter used in the chemical model for dark clouds of different density.

In this study, UCL_CHEM 1999 has been used to provide x_1, the fractional abundance of H-atoms in dense clouds. The abundance of atomic hydrogen and molecular hydrogen, n_1 and n_2 respectively, are then calculated using $x_1 = n_1 / n_H$ and $n_H = n_1 + 2n_2$. The results are shown in Table 4.3.

n_H (cm^{-3})	A_V (mag)	x_1	n_2 (cm^{-3})	n_1 (cm^{-3})
1×10^3	1	6.586×10^{-2}	4.671×10^2	65.860
1×10^3	3	6.586×10^{-2}	4.671×10^2	65.860
1×10^3	5	6.586×10^{-2}	4.671×10^2	65.860
1×10^3	7	6.586×10^{-2}	4.671×10^2	65.860
1×10^3	10	6.586×10^{-2}	4.671×10^2	65.860
1×10^3	50	6.586×10^{-2}	4.671×10^2	65.860
1×10^3	100	6.586×10^{-2}	4.671×10^2	65.860
1×10^4	1	4.186×10^{-5}	5.000×10^3	0.419
1×10^4	3	3.687×10^{-5}	5.000×10^3	0.369
1×10^4	5	3.656×10^{-5}	5.000×10^3	0.366
1×10^4	7	3.639×10^{-5}	5.000×10^3	0.364
1×10^4	10	3.630×10^{-5}	5.000×10^3	0.363
1×10^4	50	3.630×10^{-5}	5.000×10^3	0.363
1×10^4	100	3.630×10^{-5}	5.000×10^3	0.363
1×10^5	1	5.518×10^{-6}	5.000×10^4	0.552
1×10^5	3	3.562×10^{-6}	5.000×10^4	0.356
1×10^5	5	3.534×10^{-6}	5.000×10^4	0.353
1×10^5	7	3.476×10^{-6}	5.000×10^4	0.348
1×10^5	10	3.439×10^{-6}	5.000×10^4	0.344
1×10^5	50	3.436×10^{-6}	5.000×10^4	0.344
1×10^5	100	3.436×10^{-6}	5.000×10^4	0.344
1×10^6	1	4.703×10^{-7}	5.000×10^5	0.470
1×10^6	3	3.689×10^{-7}	5.000×10^5	0.369
1×10^6	5	3.622×10^{-7}	5.000×10^5	0.362
1×10^6	7	3.473×10^{-7}	5.000×10^5	0.347
1×10^6	10	3.412×10^{-7}	5.000×10^5	0.341
1×10^6	50	3.408×10^{-7}	5.000×10^5	0.341
1×10^6	100	3.408×10^{-7}	5.000×10^5	0.341

Table 4.3 The abundances of atomic and molecular hydrogen in dark clouds of density $n_H = 1 \times 10^3$, 1×10^4, 1×10^5 and 1×10^6 cm^{-3} as a function of depth within the cloud.

As can be seen from Table 4.3, there is a slight decrease in H-atom density (n_1) with depth for dark clouds of density $n_H \geq 1 \times 10^4$ cm^{-3}. The higher atomic abundance is due to the outer layers of the cloud being penetrated by UV radiation, leading to photolysis of H_2 molecules. There is shielding of UV radiation by the dust in the denser clouds, hence the atomic abundance decreases with increasing A_V. A more

surprising result is that the H-atom abundance does not increase with density for clouds with $n_H \geq 1 \times 10^4$ cm^{-3}. In fact, the least dense dark cloud ($n_H = 1 \times 10^3$ cm^{-3}) is found to have the highest H-atom abundance. This confirms that chemical destruction routes would not increase the H-atom abundance for dark clouds. Hence the radiative transfer code does not underestimate the H-atom abundance. As a continuation of this work, these H-atom abundances determined by UCL_CHEM 1999 could be incorporated into the Casu and Cecchi-Pestellini radiative transfer code, which will be discussed further in Chapter 5.

4.7 Discussion

The radiative transfer code has been used extensively by Casu and Cecchi-Pestellini [18-20]. The main uncertainties that arise in the code are from the collisional rate coefficients. In this work, the radiative transfer code has been modified by incorporating the new UCL formation pumping model (**u**). As this model is derived from experiments, there are only 45 ro-vibrational levels included in model **u**. It is possible that some other ro-vibrational levels are populated, but are below the detection limit of the Cosmic Dust Experiment. The advantage of the theoretical formation pumping models (**d, b, i, c, s, m**) is that they provide a continuous distribution of level populations. The $v = 0$ level populations, not detectable with the Cosmic Dust Experiment, were estimated to be equal to the $v = 1$ level populations. As shown in Section 4.4.7, the H_2 spectra are widely unaffected by the error in the $v = 0$ level populations.

The Cosmic Dust Experiment probes the ro-vibrational distribution of HD by measuring the flux density of HD^+ ions detected by a time-of-flight mass spectrometer. The flux density of HD^+ ions is related to the flux of the nascent HD molecules by the velocity of the ions. Therefore, the ro-vibrational distribution described by Figure 4.1 only holds if the velocities of the HD^+ ions are similar. Accurate measurements of the translational energy as a function of ro-vibrational state are essential in corroborating this formation pumping model. Currently, it is known that the translational energy of all HD^+ ions must be below 0.9 eV, for HD formed in any detected ro-vibrational state. This value has been calculated from analysis of the time-of-flight mass spectra, as described in Chapter 3. Nevertheless, a position

sensitive detector has been installed to further constrain the translational energy of molecules in each ro-vibrational state (see Chapter 5).

The incident atom beams were at room temperature for the HD experiments. Interstellar gas is typically much cooler. However, this discrepancy in temperatures is small in comparison to the energies involved in vibrational transitions, so there should be minimal effect on the ro-vibrational distribution. Each atomic source provides a flux of ~10^{12} – 10^{13} atoms cm^{-2} s^{-1} onto the surface [16]. Experimental pressures are much higher than in the interstellar medium and it is possible that this affects our results. The flux of HD molecules desorbing from the surface is also very high, relative to the interstellar medium. Nevertheless, it is unlikely that the nascent HD molecules interact with each other on the surface or on desorption from the surface, thereby causing a redistribution of the internal energy. Thermalization is unlikely because the surface coverage is estimated to be only a few percent of a monolayer for the Cosmic Dust Experiment [14, 57]. Work by Congiu *et al.*[58] suggests that at such a low coverage, desorbing hydrogen molecules do not thermalize with other molecular species resident on the surface, as discussed later.

The Cosmic Dust Experiment uses a highly-oriented pyrolytic graphite (HOPG) surface, whereas interstellar dust grains are likely to be porous. Thus H_2 forming on interstellar dust grains may be trapped in pores and lose excitation *via* collisions with pore walls [59-62]. Therefore, it is possible that only a small percentage of H_2 molecules may leave an interstellar dust grain retaining their ro-vibrational excitation. In this case, the most accurate formation pumping model may be one where there is very little ro-vibrational excitation, such as model **m** rather than model **u**.

The HOPG surface is made of carbon, but dust grains in a particular dark cloud may be composed of silicates. For a dark cloud with silicate dust, the Takahashi and Uehara model (**s**) could be used to generate H_2 spectra, which predicts significant formation pumping into the v = 7 level [13]. The Takahashi and Uehara model for carbonaceous grains (**c**) predicts that H_2 formed on carbonaceous surfaces has less internal energy, with v = 2 to be the most populated state. However, in contrast to the Takahashi and Uehara work, a recent study by Goumans *et al.* [63] suggests that nascent H_2 is actually less ro-vibrationally excited if it forms on olivine rather than on

graphite. Furthermore, the results of the Cosmic Dust experiment have shown that v = 4, not v = 2, is the most populated level for molecular hydrogen formed on a carbonaceous surface. As discussed in Chapter 1, there are many different theoretical formation pumping models with no prevailing consensus, hence more laboratory experiments and astronomical observations are needed to constrain the models.

4.7.1 Observations of Formation Pumping

The Congiu *et al.* study [58] provides both experimental data and dark cloud observations. Congiu *et al.* confirmed experimentally that D_2 formed on non-porous water-ice desorbs in states $2 \leq v \leq 7$ but D_2 formed on porous ice does not desorb with significant vibrational excitation. Unlike the Cosmic Dust experiment, vibrational states with $v > 7$ and rotational states could not be probed and the population distribution of the vibrational states could not be quantified. A full comparison with the Takahashi and Uehara model for icy mantles (**i**) cannot be made because model **i** predicts a ro-vibrational distribution which peaks at the v = 8 level. Congiu *et al.* also found that nascent hydrogen molecules will thermalize with other adsorbates for both porous and non-porous surfaces if the coverage reaches a saturation of ~ 1.8×10^{14} molecules cm^{-2}. Hence there should be minimal formation pumping for H_2 formed in the icy dust mantles of dark clouds, irrespective of surface morphology, as dust grain surface coverages are 1.5×10^{14} − 2×10^{14} molecules cm^{-2} for dark clouds. Again, this indicates that model **m** may be a more appropriate formation pumping model than model **u** or model **i** for interstellar dark clouds. Congiu *et al.* [58] report that observations of Lynds Dark Cloud 57 (or Barnard 68) were made by Lemaire and Field [64] in 2001 at ESO-VLT using the ISAAC instrument in spectroscopic mode using the K-band. Despite an integration time of 5 hours, no H_2 emission was detected, hence formation pumping was not observed. Congiu *et al.* assert that this non-detection demonstrates that either that the emission line intensities put forward by Tine *et al.* [9] are not correct or that formation pumping does not occur due to de-excitation of the H_2 molecule on the grain surface.

As aforementioned, Duley and Williams [10] and Tine *et al.* [9] consider dense, dark clouds as the ideal interstellar regions in which to observe formation pumping. Tine *et*

al. [9] used theoretical calculations of H_2 formation on a graphite surface *via* the Eley-Rideal mechanism to generate H_2 spectra. UV and collisional pumping processes, as well as formation pumping, were incorporated. Tine *et al.* [9] found that H_2 formation pumping should be evident for both diffuse and dark clouds and that the relative emissivities of lines due to formation pumping in dark clouds can be a factor of 500 greater than in diffuse clouds. However, when observations of Lynds Dark Cloud 1512 and Lynds Dark Cloud 1498 were made for the 1 – 4 S(4–9) lines from 1.47 – 2.03 μm using the CGS4 spectrometer on UKIRT, no H_2 spectra were detected. The total on-source time was 49′ and 85′ for L1498 and L1512 respectively. The 3σ upper limit to the non-detection signal for an integration time of 85′ was found to correspond to a line strength of 3.6×10^{-20} W m^{-2}. This upper limit is just above the predicted line strengths of $\sim 3 \times 10^{-20}$ W m^{-2} $arcsec^{-2}$ assuming a pixel size of 1 $arcsec^2$. Co-addition of the signal from the 100 rows may improve the S/N by a factor of ~ 10, assuming that the emission is uniformly distributed along the slit. This co-addition has not yet been performed. Takahashi and Uehara [13] also predict that spectral lines due to formation pumping should be detectable for clouds with density $n_H = 1 \times 10^3$ cm^{-3} using the Subaru-IRCS K-band echelle for an exposure time of 8 hrs. However, no observations have yet been conducted to corroborate the work by Takahashi and Uehara.

In the Casu and Cecci-Pestellini radiative transfer code models, the H-atom abundance increases with cloud density, although this is not a linear relationship. The higher H-atom abundance boosts the formation pumping mechanism. Therefore, lines in the spectra which have a significant formation pumping component, such as the 1 – 0 Q(7) line for models **d, b, c, i** and **s** or the 4 – 2 O(3) line for model **u**, increase in flux when the density of a cloud is increased. By comparing Figure 4.19 and Figure 4.20, it is apparent that that these formation pumping lines increase in strength with cloud density at a greater rate than the lines mainly due to collisional excitation, such as the 6 – 4 O(4) line at 1.796 μm. In the spectra presented in this chapter, the formation pumping lines are strongest for the densest clouds, where the H-atom abundance is the greatest. It is also easier to differentiate between formation pumping models using stronger lines for detection and fitting purposes. Consequently, the spectra generated by the radiative transfer model indicate that the best dark clouds to search for a formation pumping signature would be the densest of the dark clouds, in

accordance with work by Tine *et al*. [9]. However, it is not conclusive that dark clouds would display greater IR emission from formation pumping than diffuse clouds, thus H_2 in dark clouds may not be observable: as aforementioned, dark clouds may not exhibit formation pumping at all, as Congiu *et al.* [58] find that nascent molecular hydrogen may undergo de-excitation on the icy mantles of dark clouds. The results from the radiative transfer model show that the H_2 line flux is dependent on the H-atom abundance and the results from the chemical model confirm that H-atom abundances in dark clouds are very low and drop significantly for clouds of density $n_H \geq 1 \times 10^4$ cm^{-3}. In other words, dark clouds may not be the ideal region in which to search for a signature of formation pumping because the hydrogen is mostly molecular and H abundances are low.

Furthermore, the lines in the spectra presented in this chapter have fluxes ~ 10^{-3} erg cm^{-2} sr^{-1} s^{-1} μm^{-1} for dark clouds of density $n_H = 1 \times 10^3 - 1 \times 10^6$ cm^{-3}, generated by convolving with a Gaussian profile with line width of 5×10^{-5} μm. This corresponds to a surface brightness of ~ 2×10^{-21} W m^{-2} arcsec^{-2}, which is more than 10 times lower than the predicted value of Tine *et al.* [9]. For the UKIRT CGS4 echelle instrument, the 3σ30min sensitivity at 1.6 μm, near the 4 – 2 O(3) line, is 8×10^{-20} W m^{-2} pixel^{-1}. The resolution of the echelle is 37 000 and pixel size is ~ 1 arcsec^2. Therefore, it would take over 500 hours to detect one line from the H_2 spectra presented in this chapter. Hence, the non-detection of a formation pumping signal from observations of dark clouds L1498, L1512 [9] and B68 [58] is unsurprising.

Identifying formation pumping by means of diffuse cloud observations is non-trivial due to the prevalence of UV pumping. In diffuse clouds there is less shielding of the radiation field by dust than for the denser, dark clouds. UV photons can excite H_2 to some higher electronic state, which then decays to ro-vibrational levels in the *X* state *via* a radiative cascade [11]. UV pumping dominates the population of ro-vibrational levels accessible *via* this pathway, although there may be some formation pumping component to the lines. Observations of the diffuse nebula, Messier 17, have detected the H_2 6 – 4 O(3) emission line at 1.7326 μm. This line has been ascribed to formation pumping by Burton *et al.* [65]. Observationally, a marked difference in spatial distribution was observed for the 6 – 4 O(3) line and 1 – 0 S(1), 2 – 1 S(1), 1 – 0 S(7) lines in M17 suggesting that these emission processes are not the result of the same

excitation mechanisms. The topology and line intensity ratios of the 1 – 0 S(1), 2 – 1 S(1), 1 – 0 S(7) lines suggest that they are due to UV pumping. Due to the differences in emission topology, Burton *et al.* conclude that at least some component of the 6 – 4 O(3) line is not due to UV pumping. They estimate that the UV pumping component of the line in the steady-state regions of M17 is ~ 20 %, with ~ 80 % being ascribed to formation pumping. This detection may be the first direct astronomical observational evidence for formation pumping of H_2 into the $v = 6$ level. However, the 6 – 4 O(3) line is not predicted to be strong by any of the formation pumping models **u, d, b, c, i, s** or **m**, although it must be noted that these spectra have been generated for dark, not diffuse clouds, hence the excitation mechanisms may be very different. Neither do Tine *et al.* [9] nor Takahashi and Uehara [13] predict a strong 6 – 4 O(3) line for their formation pumping spectra. This throws some doubt on the classification of the 6 – 4 O(3) emission as a formation pumping line. It is possible that the Burton *et al.* spectra may integrate regions exposed to different excitation sources, leading to unexpected changes in spatial distribution of the spectral line strengths.

In an earlier study, Burton *et al.* [66] also observed the reflection nebula NGC 2023, which is also a diffuse medium. An excess of emission of H_2 in the $v = 4$ states was detected, which was found to be too great to be due to UV pumping alone. Burton *et al.* speculate that this excess of molecules in $v = 4$ was evidence of formation pumping, but signal-to-noise considerations meant that the results were not definitive. However, it is worth noting that the H_2 spectra presented in this chapter also show that lines originating form the $v = 4$ ro-vibrational states are some of the strongest in dark clouds.

Wagenblast detected H_2 in states $v = 0$, $J = 0 – 7$ in diffuse clouds [67]. From comparison with UV models, Wagenblast found that the populations of the $J = 5$, 6, and 7 levels were not consistent with UV pumping. Instead, these rotational states may have been populated by either collisions with H-atoms or by formation pumping of H_2 into high J states. The UCL model (**u**) does not predict significant formation pumping into these high rotational states. However, the Cosmic Dust experiment has not yet searched for nascent molecules in rotational states with J greater than 9. It is feasible that such states could be populated if the rotational distribution of newly-formed hydrogen is bimodal.

Indirect observation of formation pumping may also be possible through astrochemical and astrophysical effects. For example, Garrod *et al.* [68] find that the presence of internally excited H_2 may lead to the formation of free radicals such as OH and CH^+, particularly in shocked regions. This is supported by the work of Weck and Balakrishnan [69], who find that at 100 K, the reaction of $O(^3P) + H_2$ ($v = 3$) to form OH is 11 orders of magnitude higher than for the reaction of $O(^3P) + H_2$ ($v = 0$). Furthermore, vibrationally excited H_2 molecules will be easier to ionize than molecules in the vibrational ground state [70], thus there will be consequences for interstellar chemistry. Specifically, H_2 may undergo charge exchange with H^+, first forming H_2^+ then subsequently forming an H_3^+ ion [71]. As discussed in Chapter 1, H_3^+ is a very important molecule in the ISM and is a precursor for species such as H_2O. Also, the release of the H-H binding energy during formation may lead to localized heating of the molecular cloud. A study by Roberts *et al.* [72] has shown that if only one CO molecule is desorbed per 100 H_2 formation events, this is sufficient to affect freeze-out onto grains, hence limit the depletion of gaseous CO in dark clouds.

4.8 Summary

A new H_2 formation pumping model that is derived from HD formation experiments has been developed. We have characterized the H_2 emission spectra that arise from this formation pumping model. The spectra were generated using a radiative transfer code for dark clouds and the effects of varying astrophysical parameters were investigated. H_2 IR emission was found to increase non-linearly with cloud density and temperature. Both the gas phase formation route of associative detachment and the electron fraction were found to have negligible effect on the spectra of dark clouds. Varying the proton fraction from $x_{H+} = 10^{-4} – 10^{-8}$ was only found to change the spectral line strengths by less than 10 %.

The new UCL formation pumping model was then compared to other established theoretically derived formation pumping models. If the spectra can be detected, then observations of the 1 – 0 S(7) line may help distinguish between the UCL formation

pumping model and most other formation pumping models because the UCL formation pumping model (**u**) does not populate high rotational states. The 1 – 0 S(7) line is expected to be significantly stronger for models **d, b, i, c,** and **s** than for model **u** and for the case of no formation pumping, model **m**. Another way of obtaining a signature of formation pumping is to compare line strength ratios. For clouds of density $n_H = 1 \times 10^6$ cm^{-3} at temperature T = 10 K, model **u** predicts that the strongest line will be the 4 – 2 O(3) line at 1.509 μm.

The H_2 spectral line fluxes depend on the abundance of hydrogen atoms within the dark cloud. The H_2 spectra do not scale linearly with N(H_2). This is because in dark clouds, the H-atom abundances are low, due to the lack of photodissociation of H_2 by UV radiation. A chemical model has been used to eliminate the possibility that there are extra channels of H_2 destruction to augment the H-atom abundance. The chemical model found that the H-atom abundance drops for to $n_1 \sim 0.4$ cm^{-3} for clouds with densities $n_H \geq 10^4$ cm^{-3}, hence there is no increase in H-atom abundance due to chemical destruction routes. Furthermore, the fluxes of the spectral lines presented in this chapter are ~ 10^{-3} erg cm^{-2} sr^{-1} s^{-1} μm^{-1}, generated by convolving with a Gaussian profile with line width of $\Delta\lambda = 5 \times 10^{-5}$ μm. Observation of one line is estimated to require over 500 hours of integration time with the CGS4 echelle instrument on UKIRT. Thus detections of H_2 spectra in dark clouds are probably not viable with current ground based telescopes, which may explain the non-detections of Lemaire and Field [64] and Tine et al. [9].

4.9 References

1. Gough, S., C. Schermann, F. Pichou, M. Landau, I. Cadez, and R.I. Hall, *The formation of vibrationally excited hydrogen molecules on carbon surfaces*. Astronomy and Astrophysics, 1996. **305**(2): p. 687-693.

2. Kim, Y.H., J. Ree, and H.K. Shin, *Formation of vibrationally excited hydrogen molecules on a graphite surface*. Chemical Physics Letters, 1999. **314**(1-2): p. 1-8.

3. Martinazzo, R. and G.F. Tantardini, *Quantum study of Eley-Rideal reaction and collision induced desorption of hydrogen atoms on a graphite surface. I. H-chemisorbed case*. J. Chem. Phys., 2006. **124**(12).

4. Meijer, A.J.H.M., A.J. Farebrother, D.C. Clary, and A.J. Fisher, *Time-dependent quantum mechanical calculations on the formation of molecular hydrogen on a graphite surface via an Eley-Rideal mechanism*. J. Phys. Chem. A, 2001. **105**(11): p. 2173-2182.

5. Morisset, S., F. Aguillon, M. Sizun, and V. Sidis, *The dynamics of H-2 formation on a graphite surface at low temperature*. Phys. Chem. Chem. Phys., 2003. **5**(3): p. 506-513.

6. Ree, J., Y.H. Kim, and H.K. Shin, *Dynamics of H-2 formation on a graphite surface*. Chemical Physics Letters, 2002. **353**(5-6): p. 368-378.

7. Rutigliano, M., M. Cacciatore, and G.D. Billing, *Hydrogen atom recombination on graphite at 10 K via the Eley- Rideal mechanism*. Chemical Physics Letters, 2001. **340**(1-2): p. 13-20.

8. Takahashi, J., K. Masuda, and M. Nagaoka, *Product energy distribution of molecular hydrogen formed on icy mantles of interstellar dust*. Astrophysical Journal, 1999. **520**(2): p. 724-731.

9. Tine, S., D.A. Williams, D.C. Clary, A.J. Farebrother, A.J. Fisher, A. Meijer, J.M.C. Rawlings, and C.J. Davis, *Observational indicators of formation excitation of H-2*. Astrophysics And Space Science, 2003. **288**(3): p. 377-389.

10. Duley, W.W. and D.A. Williams, *The Formation of H-2 on Interstellar Dust*. Monthly Notices of the Royal Astronomical Society, 1993. **260**(1): p. 37-42.

11. Black, J.H. and A. Dalgarno, *Interstellar H2 - Population Of Excited Rotational States And Infrared Response To Ultraviolet-Radiation*. Astrophysical Journal, 1976. **203**(1): p. 132-142.

12. Draine, B.T. and F. Bertoldi, *Structure of stationary photodissociation fronts*. Astrophysical Journal, 1996. **468**(1): p. 269-289.

13. Takahashi, J. and H. Uehara, *H-2 Emission spectra with new formation pumping models*. Astrophysical Journal, 2001. **561**(2): p. 843-857.

14. Creighan, S.C., J.S.A. Perry, and S.D. Price, *The rovibrational distribution of H-2 and HD formed on a graphite surface at 15-50 K*. J. Chem. Phys., 2006. **124**(11).

15. Perry, J.S.A. and S.D. Price, *Detection of rovibrationally excited H-2 formed through the heterogeneous recombination of H atoms on a cold HOPG surface*. Astrophysics and Space Science, 2003. **285**(3-4): p. 769-776.

16. Perry, J.S.A., J.M. Gingell, K.A. Newson, J. To, N. Watanabe, and S.D. Price, *An apparatus to determine the rovibrational distribution of molecular hydrogen formed by the heterogeneous recombination of H atoms on cosmic dust analogues*. Meas. Sci. Technol., 2002. **13**(9): p. 1414-1424.

17. Takahashi, J., *The ortho/para ratio of H-2 newly formed on dust grains*. Astrophysical Journal, 2001. **561**(1): p. 254-263.

18. Casu, S. and C. Cecchi-Pestellini, *Retrieving physical conditions from interstellar H2 emission lines: a non linear fitting technique*. Journal of Physics: Conference Series, 2005. **6**: p. 191.

19. Casu, S. and C. Cecchi-Pestellini. *The role of formation pumping in the excitation of very high rotational states of molecular hydrogen*. in *Conference on the Dusty and Molecular Universe*. 2004. Paris, FRANCE: Esa Publications Division C/O Estec.

20. Cecchi-Pestellini, C., S. Casu, and A. Dalgarno, *H-2 excitation in turbulent interstellar clouds*. Monthly Notices of the Royal Astronomical Society, 2005. **364**(4): p. 1309-1314.

21. Sternberg, A. and A. Dalgarno, *The Infrared Response of Molecular-Hydrogen Gas to Ultraviolet-Radiation - High-Density Regions*. Astrophysical Journal, 1989. **338**(1): p. 197-233.

22. Jura, M., *Interstellar Clouds Containing Optically Thin H2*. Astrophysical Journal, 1975. **197**(3): p. 575-580.

23. Flower, D.R., *The rotational excitation of H-2 by H-2*. Monthly Notices of the Royal Astronomical Society, 1998. **297**(1): p. 334-336.

24. Flower, D.R. and E. Roueff, *Vibrational relaxation in H-H-2 collisions*. Journal of Physics B-Atomic Molecular and Optical Physics, 1998. **31**(23): p. L955-L958.

25. Flower, D.R. and E. Roueff, *Rovibrational relaxation in collisions between H-2 molecules: I. Transitions induced by ground state para-H-2*. Journal of Physics B-Atomic Molecular and Optical Physics, 1998. **31**(13): p. 2935-2947.

26. Flower, D.R., E. Roueff, and C.J. Zeippen, *Rovibrational excitation of H-2 molecules by He atoms*. Journal of Physics B-Atomic Molecular and Optical Physics, 1998. **31**(5): p. 1105-1113.

27. Le Bourlot, J., G.P. des Forets, and D.R. Flower, *The cooling of astrophysical media by H-2*. Monthly Notices of the Royal Astronomical Society, 1999. **305**(4): p. 802-810.

28. Le Bourlot, J. 2005.

29. Tine, S., S. Lepp, R. Gredel, and A. Dalgarno, *Infrared response of H-2 to X-rays in dense clouds*. Astrophysical Journal, 1997. **481**(1): p. 282-295.

30. Abgrall, H., J. Lebourlot, G.P. Desforets, E. Roueff, D.R. Flower, and L. Heck, *Photodissociation of H-2 and the H/H-2 Transition in Interstellar Clouds*. Astronomy and Astrophysics, 1992. **253**(2): p. 525-536.

31. Abgrall, H., E. Roueff, and I. Drira, *Total transition probability and spontaneous radiative dissociation of B, C, B ' and D states of molecular hydrogen*. Astron. Astrophys. Suppl. Ser., 2000. **141**(2): p. 297-300.

32. Abgrall, H., E. Roueff, F. Launay, J.Y. Roncin, and J.L. Subtil, *Table of the Lyman Band System of Molecular-Hydrogen*. Astron. Astrophys. Suppl. Ser., 1993. **101**(2): p. 273-321.

33. Abgrall, H., E. Roueff, F. Launay, J.Y. Roncin, and J.L. Subtil, *Table of the Werner Band System of Molecular-Hydrogen*. Astron. Astrophys. Suppl. Ser., 1993. **101**(2): p. 323-362.

34. Abgrall, H. 2002.

35. Wolniewicz, L., I. Simbotin, and A. Dalgarno, *Quadrupole transition probabilities for the excited rovibrational states of H-2*. Astrophys. J. Suppl. Ser., 1998. **115**(2): p. 293-313.

36. Islam, F., E.R. Latimer, and S.D. Price, *The formation of vibrationally excited HD from atomic recombination on cold graphite surfaces*. J. Chem. Phys., 2007. **127**: p. 064701-8.

37. Latimer, E.R., F. Islam, and S.D. Price, *Studies of HD formed in excited vibrational states from atomic recombination on cold graphite surfaces*. Chemical Physics Letters, 2008. **455**(4-6): p. 174-177.

38. Rosenthal, D., F. Bertoldi, and S. Drapatz, *ISO-SWS observations of OMC-1: H-2 and fine structure lines*. Astronomy and Astrophysics, 2000. **356**(2): p. 705-723.

39. Millar, T.J., P.R.A. Farquhar, and K. Willacy, *The UMIST database for astrochemistry 1995*. Astron. Astrophys. Suppl. Ser., 1997. **121**(1): p. 139-185.

40. McCall, B.J., K.H. Hinkle, T.R. Geballe, G.H. Moriarty-Schieven, N.J. Evans, K. Kawaguchi, S. Takano, V.V. Smith, and T. Oka, *Observations of H-3(+) in the diffuse interstellar medium*. Astrophysical Journal, 2002. **567**(1): p. 391-406.

41. Lepp, S., P.C. Stancil, and A. Dalgarno, *Atomic and molecular processes in the early Universe*. Journal of Physics B-Atomic Molecular and Optical Physics, 2002. **35**(10): p. R57-R80.

42. Cecchi-Pestellini, C. and A. Dalgarno, *Emission of HeH+ in Nebulae*. Astrophysical Journal, 1993. **413**(2): p. 611-618.

43. Field, D., *H-2 formation in space: a negative ion route?* Astronomy & Astrophysics, 2000. **362**(2): p. 774-779.

44. Launay, J.M., M. Ledourneuf, and C.J. Zeippen, *The H+H--Reversible-H2(V,J)+E- Reaction - a Consistent Description of the Associative Detachment and Dissociative Attachment Processes Using the Resonant Scattering-Theory*. Astronomy and Astrophysics, 1991. **252**(2): p. 842-852.

45. Draine, B.T., *Photo-Electric Heating of Inter-Stellar Gas*. Astrophys. J. Suppl. Ser., 1978. **36**(4): p. 595-619.

46. Flannery, B.P., W. Roberge, and G.B. Rybicki, *The Penetration of Diffuse Ultraviolet-Radiation into Inter-Stellar Clouds*. Astrophysical Journal, 1980. **236**(2): p. 598-608.

47. Hinkle, K., R. Joyce, N. Sharp, and J. Valenti. *Phoenix: Operation and performance of a cryogenic high-resolution 1-5 micron infrared spectrograph*. in *Conference on Optical and IR Telescope Instrumentation and Detectors*. 2000. Munich, Germany: Spie-Int Soc Optical Engineering.

48. Snow, T.P. and B.J. McCall, *Diffuse atomic and molecular clouds*. Annual Review of Astronomy and Astrophysics, 2006. **44**: p. 367-414.

49. Sun, Y. and A. Dalgarno, *Rotational-Excitation of H-2 in Collision with H*. Astrophysical Journal, 1994. **427**(2): p. 1053-1056.

50. Viti, S. and D.A. Williams, *Time-dependent evaporation of icy mantles in hot cores*. Monthly Notices of the Royal Astronomical Society, 1999. **305**(4): p. 755-762.

51. Woodall, J., M. Agundez, A.J. Markwick-Kemper, and T.J. Millar, *The UMIST database for astrochemistry 2006*. Astronomy & Astrophysics, 2007. **466**(3): p. 1197-U203.

52. Le Teuff, Y.H., T.J. Millar, and A.J. Markwick, *The UMIST database for astrochemistry 1999*. Astron. Astrophys. Suppl. Ser., 2000. **146**(1): p. 157-168.

53. Sofia, U.J. and D.M. Meyer, *Interstellar abundance standards revisited*. Astrophysical Journal, 2001. **554**(2): p. L221-L224.

54. Rawlings, J.M.C., T.W. Hartquist, K.M. Menten, and D.A. Williams, *Direct Diagnosis of Infall in Collapsing Protostars .1. the Theoretical Identification of Molecular-Species with Broad Velocity Distributions*. Monthly Notices of the Royal Astronomical Society, 1992. **255**(3): p. 471-485.

55. Collings, M.P., M.A. Anderson, R. Chen, J.W. Dever, S. Viti, D.A. Williams, and M.R.S. McCoustra, *A laboratory survey of the thermal desorption of astrophysically relevant molecules*. Monthly Notices of the Royal Astronomical Society, 2004. **354**(4): p. 1133-1140.

56. Carolan, P.B., M.P. Redman, E. Keto, and J.M.C. Rawlings, *CO abundances in a protostellar cloud: freeze-out and desorption in the envelope and outflow of L483*. Monthly Notices of the Royal Astronomical Society, 2008. **383**(2): p. 705-712.

57. Creighan, S.C., *Laboratory Studies of the Formation of Molecular Hydrogen on Surfaces at Cryogenic Temperatures, Department of Chemistry*. 2006, University College London: London.

58. Congiu, E., E. Matar, L.E. Kristensen, F. Dulieu, and J.L. Lemaire, *Laboratory evidence for the non-detection of excited nascent H-2 in dark clouds*. Monthly Notices of the Royal Astronomical Society, 2009. **397**(1): p. L96-L100.

59. Perets, H.B. and O. Biham, *Molecular hydrogen formation on porous dust grains*. Monthly Notices of the Royal Astronomical Society, 2006. **365**(3): p. 801-806.

60. Hornekaer, L., A. Baurichter, V.V. Petrunin, A.C. Luntz, B.D. Kay, and A. Al-Halabi, *Influence of surface morphology on D-2 desorption kinetics from amorphous solid water*. J. Chem. Phys., 2005. **122**(12).

61. Perets, H.B., O. Biham, G. Manico, V. Pirronello, J. Roser, S. Swords, and G. Vidali, *Molecular hydrogen formation on ice under interstellar conditions.* Astrophysical Journal, 2005. **627**(2): p. 850-860.

62. Yabushita, A., T. Hama, D. Iida, N. Kawanaka, M. Kawasaki, N. Watanabe, M.N.R. Ashfold, and H.P. Loock, *Release of hydrogen molecules from the photodissociation of amorphous solid water and polycrystalline ice at 157 and 193 nm*. J. Chem. Phys., 2008. **129**(4).

63. Goumans, T.P.M., C. Richard, A. Catlow, and W.A. Brown, *Formation of H-2 on an olivine surface: a computational study*. Monthly Notices of the Royal Astronomical Society, 2009. **393**(4): p. 1403-1407.

64. Lemaire, J.L., *Private Communication*. 2008.

65. Burton, M.G., D. Londish, and P. Brand, *Formation pumping of molecular hydrogen in the Messier 17 photodissociation region*. Monthly Notices Of The Royal Astronomical Society, 2002. **333**(4): p. 721-729.

66. Burton, M.G., M. Bulmer, A. Moorhouse, T.R. Geballe, and P. Brand, *Fluorescent Molecular-Hydrogen Line Emission In The Far-Red*. Monthly Notices Of The Royal Astronomical Society, 1992. **257**(1): p. P1-P6.

67. Wagenblast, R., *Interpretation Of The Level Population-Distribution Of Highly Rotationally Excited H-2-Molecules In Diffuse Clouds*. Monthly Notices Of The Royal Astronomical Society, 1992. **259**(1): p. 155-165.

68. Garrod, R.T., J.M.C. Rawlings, and D.A. Williams, *Chemical effects of H-2 formation excitation*. Astrophysics and Space Science, 2003. **286**(3-4): p. 487-499.

69. Weck, P.F. and N. Balakrishnan, *Dynamics of chemical reactions at cold and ultracold temperatures*. Journal of Physics B-Atomic Molecular and Optical Physics, 2006. **39**(19): p. S1215-S1227.

70. Dyson, J.E. and D.A. Williams, *The Physics of the Interstellar Medium*. 2nd ed. 1997, Bristol: Institute of Physics.

71. Meijer, A., A.J. Farebrother, D.C. Clary, and A.J. Fisher, *Time-dependent quantum mechanical calculations on the formation of molecular hydrogen on a graphite surface via an Eley-Rideal mechanism*. J. Phys. Chem. A, 2001. **105**(11): p. 2173-2182.

72. Roberts, J.F., J.M.C. Rawlings, S. Viti, and D.A. Williams, *Desorption from interstellar ices*. Monthly Notices of the Royal Astronomical Society, 2007. **382**(2): p. 733-742.

Chapter Five

Conclusions and Further Work

This thesis has described the use of the Cosmic Dust Experiment to probe the ro-vibrational distribution of HD formed on highly–oriented pyrolytic graphite (HOPG) held at 15 K. The results of the experiment were extrapolated to create a new formation pumping model for H_2. The observability of formation pumping in dark clouds was investigated using a radiative transfer model, with a chemical model used in conjunction to perform checks. The conclusions of these studies and the astrophysical implications on H_2 formation in the interstellar medium (ISM) are presented in Section 5.1. This chapter will also outline the next stages for the UCL Cosmic Dust Experiment and the further work that may be carried out by means of the radiative transfer and chemical models in Section 5.2. It should be noted that some of the changes listed in Section 5.2.1 on the Cosmic Dust Experiment have already been made, although all the changes were implemented after the data presented in Chapter 3 were taken.

5.1 Conclusions

At the outset of this thesis, we posed a number of questions that are of importance in the field of astrochemistry. What is the formation mechanism for the recombination of H-atoms on an interstellar dust grain? Is the nascent H_2 molecule formed with significant internal and kinetic energy and can it be detected? Does the formation process cause heating of the dust grain?

Firstly, let us tackle the question of the formation mechanism. The Cosmic Dust Experiment conditions most closely resemble that of diffuse clouds, where the grain surface is relatively bare and the gas is mostly atomic. Important differences between regions of the ISM and the Cosmic Dust Experiment are the surface coverage, temperature of the gas, grain morphology and the chemical composition of the surface. Therefore, in order to extrapolate our results, a working theoretical model of the experiment should be developed which can be used to probe the effects of interstellar conditions. We must understand fully the formation mechanism that occurs on the HOPG surface and apply this knowledge to the more complex environment of the ISM. As described in Chapter 1, there are three possible formation recombination mechanisms to form molecular hydrogen: the Eley-Rideal (ER) mechanism where one gas phase atom impacts on a surface bound atom; the Langmuir-Hinshelwood (LH) mechanism where both atoms are bound and fully thermalized with the surface; and the hot atom (HA) mechanism where both atoms are bound to the surface but at least one atom is not fully thermalized.

The coverage of the HOPG surface in the Cosmic Dust Experiment is much less than a monolayer [1, 2]. Therefore, a gas phase atom is unlikely to impact on a preadsorbed atom on the HOPG surface. Thus, ER reactions do not dominate HD formation and recombination proceeds *via* the LH or the HA mechanisms. For the Cosmic Dust Experiment, where the surface is held at 15 K and the temperature of the incident H- and D-atoms is T ~ 300 K, atoms and molecules are physisorbed to the surface because there is a barrier to chemisorption. Nevertheless, it is still possible that atoms chemisorb at defects. However, a strong chemical bond is likely to impede the mobility of an atom on the surface of the HOPG, such that chemisorbed atoms form molecules *via* an ER process. Thus it is improbable that defects dominate HD formation in the Cosmic Dust Experiment, as the ER mechanism is unfavourable at low coverages. By the same argument, chemisorption (at defects or otherwise) is unlikely to dominate H_2 formation in diffuse and dark clouds where the interstellar gas has low temperatures of T ~ 10 – 100 K [3]. Dust grains in diffuse clouds are bare; whereas in dark clouds, although the grains are covered by ice mantles, the gas is mostly molecular. Subsequently, surface coverage by H-atoms is low in these clouds and ER reactions are improbable. Chemisorption is required in hot regions of the ISM, such as in photodissociation regions (PDRs) around massive stars, to

increase the residence time of H-atoms on a dust grain surface in order for recombination to occur [4]. Hot atoms in PDRs of temperature T ~ 1000 K [5] are too energetic to bind to a dust grain surface by physisorption. Therefore in the ISM, the ER mechanism is important in PDRs and other hot regions only.

From coverage considerations, the formation mechanism in the Cosmic Dust Experiment must follow an LH or HA process, where the atoms diffuse across the surface to react. No thermal activation is required in order to obtain HD signals, implying that the atoms are highly mobile on the HOPG surface. This is supported by the sequential dosing experiments of H + D recombination on amorphous solid water-ice (ASW) conducted by Hornekaer *et al.* [6], where H and D atoms are also found to be react *via* the LH or HA mechanism and be highly mobile on ASW held at temperatures down to 8 K. As the H- and D-atoms are at room temperature in both experiments, physisorption occurs on both ASW and HOPG surfaces; therefore it is probable that the recombination mechanism should be similar. Studies of molecular hydrogen formation on silicates have also confirmed the physisorption and mobility of adsorbed H- and D-atoms [7]. Thus H-atoms are mobile on dust grains in interstellar regions of low gas temperature and recombination follows an LH or HA mechanism given low surface coverage, widely independent of the chemical nature of the dust grain.

As shown in Table 3.10, the rotational temperatures of the nascent HD molecules are 246 K < T_{rot} < 368 K, which is much higher than the HOPG surface temperature of 15 K. As the temperature of the atomic beam is T ~ 300 K, the high rotational temperatures may suggest that the atoms have not fully thermalized with the HOPG surface before recombination. The reaction is more likely to proceed *via* the HA mechanism, where at least one of the atoms is not fully thermalized with the surface, rather than the LH mechanism. However, this result may be coverage dependent and therefore may not hold for the extremely low gas pressures in the ISM, although it must be noted that repeating experiments with the atom beams at half-pressure has no discernible effect on the rotational excitation of nascent HD. It is unclear whether H-atoms in the interstellar medium have a longer time to thermalize with the dust grain surface before encountering another H-atom for recombination. Therefore, the LH mechanism may still be important in interstellar regions.

We now try to answer the next question: is the nascent H_2 molecule formed with significant internal and kinetic energy and can it be detected? According to the results of the Cosmic Dust Experiment, hydrogen molecules are indeed formed with significant internal energy, with the ro-vibrational distribution of nascent HD peaking at $v = 4$, as presented in Figure 3.16. However, the experiment can only provide an upper limit to the kinetic energy of nascent HD. As explained above, the internal excitation may be dependent on the length of time that atoms are accommodated on the surface before recombination, thus the ro-vibrational excitation of interstellar H_2 may peak at $v < 4$ due to the low gas pressures in the ISM. There may also be some isotope effects on the ro-vibrational distribution [8], as the Cosmic Dust Experiment investigates HD formation rather than H_2 formation. However, earlier work by Creighan *et al.* [2] has shown that there is no discernible difference in level populations for H_2 and HD formed in vibrational states $v = 1$ and 2. A more important factor is the dust grain morphology, in particular the porosity of the surface. Both bare and icy grains may exhibit a microporous structure [9-11]. Although atoms are mobile on porous grains [6, 12, 13] and recombination is efficient [6, 14-16], the nascent hydrogen molecules are found to thermalize in the pores, losing kinetic and internal energy [6, 16]. Therefore, although the H_2 molecule may originally form with ro-vibrational excitation, collisions with pore walls may mean that there is no apparent formation pumping of molecules which have escaped the grain surface.

In the case of no formation pumping, the most likely ro-vibrational distribution of nascent H_2 molecules is the population of the lowest possible levels $v, J = (0, 0)$ and $(0, 1)$ in the ratio 1:3 as described by model **m** in Chapter 4. For H_2 spectra in dark clouds generated for model **m**, see Figures 4.17 and 4.18. By use of the Casu and Cecchi-Pestellini radiative transfer code, characteristic spectra have been generated for different formation pumping mechanisms. However, limits in telescope sensitivity mean that the H_2 spectra presented in Chapter 4 are currently undetectable, regardless of the degree of formation pumping. The reasons for this are twofold. Firstly, as discussed in Chapter 1, H_2 IR emission occurs *via* quadrupole transitions which are very weak; H_2 is known to be difficult to detect, hence CO is often used instead to calculate the densities of molecular gas [17]. Secondly, although the abundance of H_2 is extremely high in dark clouds, very few of these molecules are ro-vibrationally

excited due to formation pumping; there is comparatively little recombination in dark clouds. The H_2 formation rate is dependent on the number of H-atoms, n_1, and the density of the dust grains. The density of dust is known to be proportional to n_H throughout the Galaxy [3]. Checks carried out using the chemical model UCL_CHEM 1999 have shown that the abundance of atomic hydrogen drops to $n_1 \sim 0.4$ atoms cm^{-3} in dark clouds with $n_H \geq 10^4$ cm^{-3}. The transition regime between diffuse and dark clouds, namely translucent clouds, have $n_1 = 66$ cm^{-3} and $n_H = 10^3$ cm^{-3} as shown in Table 4.3, so should exhibit a greater H_2 formation rate than dark clouds and be relatively free from UV pumping in comparison to diffuse clouds. Hence from the results presented in this thesis, it seems unlikely that a formation pumping signal could be observed in dark clouds, with translucent clouds being a more favourable alternative.

The final question posed at the outset of this thesis concerns the heating of the dust grain by H_2 formation. It has long been suggested that the release of the H_2 binding energy may liberate volatiles from the grain surface [18]. Astrochemical modelling by Roberts *et al.* [10, 19] has shown that grain heating may have a significant impact on CO abundances if only one CO molecule desorbs each time 100 H_2 molecules are formed. In fact, desorption of adsorbates on dust grains resulting from H_2 formation is known to occur: data by Govers *et al.* [20, 21] indicates that on average at least one D_2 molecule is desorbed per H-atom recombination event. Also, observations of the Taurus dark cloud imply that the sticking efficiency of CO is lower than expected by theoretical models due to desorption of CO by H_2 formation [22]. The results of the Cosmic Dust Experiment are that on average at least 40 % of the binding energy, namely 1.66 – 2.65 eV, is imparted to the surface during HD formation. However, if this much energy were transferred efficiently to volatiles in the dust mantle during H_2 formation, then > 20 molecules could be desorbed per recombination event, thereby preventing any build-up of ices in dark clouds [19]. Thus, desorptive heating of volatiles by H_2 formation is known to be inefficient. The thermal conductivity of dust grains is unclear, although dust grain size, density and chemical compositon are known to affect how the energy spreads through the phonon bath of the surface [18]. Furthermore, as explained previously, on porous grains, the internal and kinetic energy of H_2 molecules will transfer to the pore walls *via* repeated collisions, thus it is probable that most of the H_2 formation energy is lost to dust grains in the ISM.

5.2 Further Work

5.2.1 On the Cosmic Dust Experiment

There is still more work to be done on the formation mechanism of HD in the Cosmic Dust Experiment. In order to further constrain the upper limit of ~ 1 eV determined in Chapter 3 for the translational energy of nascent HD molecules, a position-sensitive detector (PSD) has been installed. PSDs have been employed in many experiments to investigate the dynamics of both unimolecular and bimolecular reactions of molecular dications [23]. As explained in Chapter 2, the nascent HD molecules must be ionized *via* REMPI in order to be detected. The translational energy of an HD^+ ion can be determined quantitatively using the PSD, which consists of a position-sensitive microchannel plate (MCP) and a time-of-flight mass spectrometer (TOFMS). A schematic of this arrangement is shown in Figure 5.1. The trajectory of the ion through the drift tube of the TOFMS is used to calculate the translational energy. Stationary ions travel straight through the drift tube, whilst ions with some kinetic energy have anisotropically distributed velocities, hence they will travel to different places on the MCP of the PSD. The *x* and *y* positions of impact of the HD^+ ion on the MCP can be established, hence the velocity of the ion can be determined.

H_2 is by far the most abundant molecule and is the precursor for most of the chemistry in the ISM. Therefore, the energy budget of many reactions in the interstellar medium could be clarified when both the translational and ro-vibrational excitation of H_2 are known [24-26]. As already discussed, when HD is formed by heterogeneous catalysis on an HOPG surface, the released binding energy is partitioned between internal and kinetic energy of the molecule and heat lost to the surface. The average internal excitation of the HD molecule has been determined to be ~1.83 eV, neglecting the populations of the $v'' = 0$ state and other non-detected ro-vibrational states. Therefore, the value of the translational energy determined using the PSD could then be utilized to determine the amount of heat lost to the HOPG surface during the HD formation process. More knowledge of the grain heating process would help elucidate problems relating to the growth of icy mantles on dust grains in the ISM [10, 18, 19, 22].

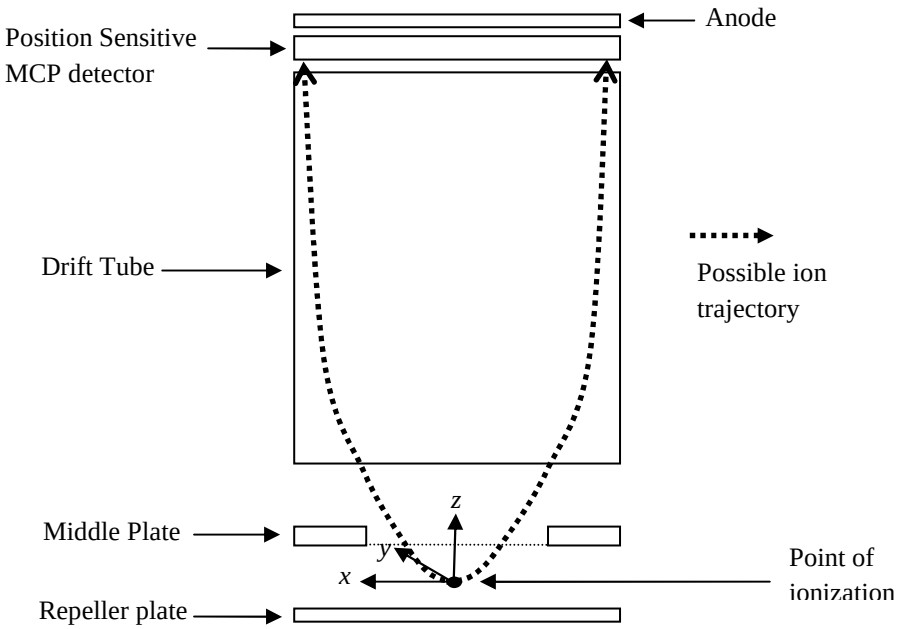

Figure 5.1 Schematic diagram to show the possible trajectory of ions in the TOFMS with PS MCP detector installed.

To further simulate the conditions of the ISM, where typical temperatures of the gas are T ~ 100 K in diffuse clouds and T ~ 10 K in dark clouds [9, 11, 27, 28], a method of cooling the H- and D-atoms has been employed. Cooling of the atoms has been achieved by piping the atomic beams through an aluminium block attached to the helium cold head directly before the atoms impinge on the HOPG. The current set-up of the experiment cools the atomic beams to T = 45 K.

Although no new data has been taken as yet, we can speculate on the effects of cold atoms on the formation mechanism. Cold atoms may have higher sticking probabilities and longer residence times on the HOPG surface, thus may attain a greater degree of thermalization with the 15 K surface. Therefore, the recombination process may become marginally more like the LH mechanism at low atom beam temperatures. Technically, if there is no effect on the ro-vibrational excitation of nascent molecules as a result of reducing the atomic temperature, then this indicates that the molecules thermalize with the surface using both cool (45 K) and warm (~300 K) atoms. Thus the recombination process occurs *via* the LH mechanism. However, the change in temperature of the atoms corresponds to an energy of only ~ 22 meV.

HD levels (v, J) = (4, 1), (4, 0) and (3, 1) have energies of 1.911 eV, 1.902 eV, and 1.529 eV respectively. Therefore, it is unlikely that such a small change in atomic temperature could affect the vibrational distribution of the HD molecule, although a reduction in rotational excitation is feasible. Indeed theoretical work by Kerkeni and Clary [29] shows no strong effect on the ro-vibrational excitation of nascent H_2 with H-atom translational energy.

As described in Chapter 1, interstellar dust grains are very different from an HOPG surface. Interstellar dust may consist of silicates and oxides as well as carbonaceous material. Thus other interstellar dust grain analogue surfaces such as olivine, a mixture of Mg_2SiO_4 and Fe_2SiO_4, could be investigated. There have been many experimental studies of molecular hydrogen formation on olivine [30, 31] which could be compared to the results of the UCL Cosmic Dust Experiment. It has also been predicted that H_2 formed on olivine should exhibit less internal excitation than H_2 formed on graphite [32]. Hence, we would expect HD formed on olivine to be less ro-vibrationally excited than HD formed on HOPG, with the vibrational distribution peaking at $v < 4$. Similarly ASW surfaces could also be investigated. Particular comparison could be made with the work of Amiaud *et al*. [33], which has shown that molecular hydrogen is formed on non-porous ASW in vibrational states $v = 1 - 7$, although the ro-vibrational distribution could not be determined and no other vibrational states could be probed outside this range. The results of Amiaud *et al.* could be quantified using the Cosmic Dust Experiment.

5.2.2 On H_2 Spectra

There are many parameters in the Casu and Cecchi-Pestellini radiative transfer code that may be varied and sensitivity tests should be carried out for as many parameters as possible. In particular, the cosmic-ray ionization rate, ζ, should be investigated, as work by Le Bourlot *et al.* [34] has shown that cosmic rays can produce observable H_2 spectra if $\zeta = 10^{-14}$ s^{-1}. In accordance with the work in this thesis, Le Bourlot *et al.* find that H_2 spectra generated with the standard cosmic-ray ionization rate of $\zeta = 10^{-17}$ s^{-1} are not observable in dark clouds. An increase in cosmic rays liberates H-atoms, thus is expected to significantly boost the formation pumping signal. Other parameters

not yet investigated due to time constraints include helium fraction, total-to-selective extinction ratio and gas-to-dust ratio.

In Chapter 4, it was calculated that the line strengths of the H_2 spectra generated using the Casu and Cecci-Pestellini radiative transfer code are not strong enough to be detectable in dark clouds. The non-detection from the observations of Tine *et al.* [35] in dark cloud Lynds 1512 give an upper limit for the spectral line strength of 3.6×10^{-20} W m^{-2}, which is more than 10 times greater than the value predicted in this work using the Casu and Cecci-Pestellini code. Tine *et al.* assert that co-addition of their observations could boost the signal-to-noise by ~ 10, hence this co-addition should be carried out. If the new H_2 spectra are correct, then co-addition should not result in detection of formation pumping, but the upper limit of the spectral line strengths will at least be further constrained.

The study could also be extended to diffuse clouds and compared to the extensive observations of OMC Peak-1 made by Rosenthal *et al.* [36] from 2.4 to 28 μm, which were used to calculate H_2 ro-vibrational level populations up to $v = 4$. Although the detection of formation pumping in dark clouds may be beyond the limits of the current telescope sensitivity, studies of diffuse and translucent regions may prove more fruitful. The formation rate of H_2 may be greater in these regions as the abundance of H-atoms is expected to be ~ 10 – 100 cm^{-3} in diffuse atomic clouds [37]. The abundance of H-atoms in diffuse clouds could be predicted using UCL_CHEM 1999. The H-atom abundance could then be set to the correct value in the radiative transfer code, thereby taking into consideration chemical channels; thus H_2 spectra could be generated for diffuse clouds. However, diffuse regions are more easily penetrated by the UV field, resulting in significant UV pumping, hence any H_2 spectra would be more difficult to interpret.

5.3 Summary

The Cosmic Dust Experiment probes the ro-vibrational distribution of HD formed *via* heterogeneous recombination of H- and D-atoms on an HOPG surface held at 15 K, under ultrahigh vacuum conditions. This state-of-the-art experiment has confirmed

that HD is formed with significant internal excitation, at least on a non-porous surface. The recombination process is thought to follow the HA or the LH mechanism. The complete ro-vibrational population distribution of HD has been presented in this thesis, which peaks at the $v = 4$, $J = 1$ state. A radiative transfer code, written by Casu and Cecchi-Pestellini was employed to generate H_2 spectra, which may be used to distinguish between formation pumping mechanisms. However, the rate of H_2 formation in dark clouds is thought to be slow due to low atomic abundances, thus the H_2 spectra are too weak to be observed.

This chapter has also described how the study of formation pumping may be extended by means of the radiative transfer code and UCL_CHEM 1999. Existing observations could also be employed to constrain the upper limit of the line flux of H_2 spectra in dark clouds. The Cosmic Dust Experiment will continue to probe HD formation by utilizing cold atom beams at 45 K. The use of the new PSD should also allow a complete investigation of the energetics of nascent HD. Thus, the Cosmic Dust Experiment could clarify many issues of significance in modern astrochemistry.

5.4 References

1. Creighan, S.C., *Laboratory Studies of the Formation of Molecular Hydrogen on Surfaces at Cryogenic Temperatures, Department of Chemistry*. 2006, University College London: London.

2. Creighan, S.C., J.S.A. Perry, and S.D. Price, *The rovibrational distribution of H-2 and HD formed on a graphite surface at 15-50 K*. J. Chem. Phys., 2006. **124**(11).

3. Dyson, J.E. and D.A. Williams, *The Physics of the Interstellar Medium*. 2nd ed. 1997, Bristol: Institute of Physics.

4. Baouche, S., G. Gamborg, V.V. Petrunin, A.C. Luntz, A. Baurichter, and L. Hornekaer, *High translational energy release in H-2 (D-2) associative desorption from H (D) chemisorbed on C(0001)*. J. Chem. Phys., 2006. **125**(8).

5. Williams, D.A. and S. Viti, *Recent progress in astrochemistry*. Annual Reports on the Progress of Chemistry, Vol 98, Section C: Physical Chemistry, 2002. **98**: p. 87-120.

6. Hornekaer, L., A. Baurichter, V.V. Petrunin, D. Field, and A.C. Luntz, *Importance of surface morphology in interstellar H-2 formation*. Science, 2003. **302**(5652): p. 1943-1946.

7. Vidali, G., L. Li, J.E. Roser, and R. Badman, *Catalytic activity of interstellar grains: Formation of molecular hydrogen on amorphous silicates.* Advances in Space Research, 2009. **43**(8): p. 1291-1298.

8. Meijer, A., A.J. Farebrother, and D.C. Clary, *Isotope effects in the formation of molecular hydrogen on a graphite surface via an Eley-Rideal mechanism*. J. Phys. Chem. A, 2002. **106**(39): p. 8996-9008.

9. Greenberg, J.M., *Cosmic dust and our origins*. Surface Science, 2002. **500**(1-3): p. 793-822.

10. Williams, D.A., W.A. Brown, S.D. Price, J.M.C. Rawlings, and S. Viti, *Molecules, ices and astronomy*. Astron. Geophys., 2007. **48**(1): p. 25-34.

11. Williams, D.A. and E. Herbst, *It's a dusty Universe: surface science in space*. Surface Science, 2002. **500**(1-3): p. 823-837.

12. Matar, E., E. Congiu, F. Dulieu, A. Momeni, and J.L. Lemaire, *Mobility of D atoms on porous amorphous water ice surfaces under interstellar conditions*. Astronomy & Astrophysics, 2008. **492**(1): p. L17-L20.

13. Al-Halabi, A. and E.F. Van Dishoeck, *Hydrogen adsorption and diffusion on amorphous solid water ice*. Monthly Notices of the Royal Astronomical Society, 2007. **382**(4): p. 1648-1656.

14. Perets, H.B., O. Biham, G. Manico, V. Pirronello, J. Roser, S. Swords, and G. Vidali, *Molecular hydrogen formation on ice under interstellar conditions.* Astrophysical Journal, 2005. **627**(2): p. 850-860.

15. Perets, H.B., A. Lederhendler, O. Biham, G. Vidali, L. Li, S. Swords, E. Congiu, J. Roser, G. Manico, J.R. Brucato, and V. Pirronello, *Molecular hydrogen formation on amorphous silicates under interstellar conditions.* Astrophysical Journal, 2007. **661**(2): p. L163-L166.

16. Congiu, E., E. Matar, L.E. Kristensen, F. Dulieu, and J.L. Lemaire, *Laboratory evidence for the non-detection of excited nascent H-2 in dark clouds*. Monthly Notices of the Royal Astronomical Society, 2009. **397**(1): p. L96-L100.

17. Bell, T.A., E. Roueff, S. Viti, and D.A. Williams, *Molecular line intensities as measures of cloud masses - I. Sensitivity of CO emissions to physical parameter variations*. Monthly Notices of the Royal Astronomical Society, 2006. **371**(4): p. 1865-1872.

18. Allen, M. and G.W. Robinson, *Formation of Molecules on Small Interstellar Grains*. Astrophysical Journal, 1975. **195**(1): p. 81-90.

19. Roberts, J.F., J.M.C. Rawlings, S. Viti, and D.A. Williams, *Desorption from interstellar ices*. Monthly Notices of the Royal Astronomical Society, 2007. **382**(2): p. 733-742.

20. Govers, T.R., L. Mattera, and G. Scoles, *Molecular-Beam Experiments on the Sticking and Accommodation of Molecular-Hydrogen on a Low-Temperature Substrate*. J. Chem. Phys., 1980. **72**(10): p. 5446-5455.

21. Govers, T.R., *H atom data*. http://hal.ccsd.cnrs.fr/ccsd-00004273/en/, 2005.

22. Duley, W.W. and R.G. Smith, *The Formation of Condensates on Dust in Interstellar Clouds*. Astrophysical Journal, 1995. **450**(1): p. 179-182.

23. Hu, W.P., S.M. Harper, and S.D. Price, *A position-sensitive coincidence spectrometer to image the kinematics of the bimolecular reactions of molecular dications*. Meas. Sci. Technol., 2002. **13**(10): p. 1512-1522.

24. Weck, P.F. and N. Balakrishnan, *Dynamics of chemical reactions at cold and ultracold temperatures*. Journal of Physics B-Atomic Molecular and Optical Physics, 2006. **39**(19): p. S1215-S1227.

25. Sultanov, R.A. and N. Balakrishnan, *Oxygen chemistry in the interstellar medium: The effect of vibrational excitation of H-2 in the O(P-3)+H-2 reaction*. Astrophysical Journal, 2005. **629**(1): p. 305-310.

26. Garrod, R.T., J.M.C. Rawlings, and D.A. Williams, *Chemical effects of H-2 formation excitation*. Astrophysics and Space Science, 2003. **286**(3-4): p. 487-499.

27. Duley, W.W. and D.A. Williams, *Interstellar Chemistry*. London ed. 1984: Academic Press.

28. Dyson, J.E. and D.A. Williams, *The Physics of the Interstellar Medium*. 2 ed. 1997: Institute of Physics publishing. 165.

29. Kerkeni, B. and D.C. Clary, *Quantum dynamics study of the Langmuir-Hinshelwood H+H recombination mechanism and H-2 formation on a graphene model surface*. Chemical Physics, 2007. **338**(1): p. 1-10.

30. Pirronello, V., O. Biham, C. Liu, L.O. Shen, and G. Vidali, *Efficiency of molecular hydrogen formation on silicates*. Astrophysical Journal, 1997. **483**(2): p. L131-L134.

31. Pirronello, V., C. Liu, L.Y. Shen, and G. Vidali, *Laboratory synthesis of molecular hydrogen on surfaces of astrophysical interest*. Astrophysical Journal, 1997. **475**(1): p. L69-L72.

32. Goumans, T.P.M., C. Richard, A. Catlow, and W.A. Brown, *Formation of H-2 on an olivine surface: a computational study*. Monthly Notices of the Royal Astronomical Society, 2009. **393**(4): p. 1403-1407.

33. Amiaud, L., F. Dulieu, J.H. Fillion, A. Momeni, and J.L. Lemaire, *Interaction of atomic and molecular deuterium with a nonporous amorphous water ice surface between 8 and 30 K*. J. Chem. Phys., 2007. **127**(14).

34. Lebourlot, J., G.P.D. Forets, E. Roueff, A. Dalgarno, and R. Gredel, *Infrared Diagnostics of the Formation of H-2 on Interstellar Dust*. Astrophysical Journal, 1995. **449**(1): p. 178-183.

35. Tine, S., D.A. Williams, D.C. Clary, A.J. Farebrother, A.J. Fisher, A. Meijer, J.M.C. Rawlings, and C.J. Davis, *Observational indicators of formation excitation of H-2*. Astrophysics And Space Science, 2003. **288**(3): p. 377-389.

36. Rosenthal, D., F. Bertoldi, and S. Drapatz, *ISO-SWS observations of OMC-1: H-2 and fine structure lines*. Astronomy and Astrophysics, 2000. **356**(2): p. 705-723.

37. Snow, T.P. and B.J. McCall, *Diffuse atomic and molecular clouds*. Annual Review of Astronomy and Astrophysics, 2006. **44**: p. 367-414.

Acknowledgements

At the end of my life as a graduate student at UCL, I find that somehow this thesis is complete and that four years have flown by in a blur of toil and turmoil, but above all, in great joy. The writer Harlan Ellison once said that “The two most common elements in the Universe are hydrogen and stupidity”. It has been my pleasure to have spent my time carrying out scientific research on hydrogen and its role in the Universe. I hope that this thesis goes a little way on reducing the total amount of stupidity in the Universe and throws some light on the complex topic of molecular hydrogen formation.

Of course, I could not have carried out this work without my three wise mentors: I am most indebted to Stephen Price for his excellent supervision. I hope he has by now overcome the shock of acquiring a student with no knowledge of the existence of Allen keys. I must also thank my astrophysics supervisor, Serena Viti, for her invaluable support and instruction in computer modelling and astronomy. Assistance and advice from Wendy Brown was always generously given throughout my PhD, even though I spent only a few months under her tutelage. Thank you all so much!

I owe a great deal to all my friends and colleagues at UCL, who have helped me in countless ways in my studies and in the important task of distracting me when required. I convey my apologies to all my office mates for my incessant chatter and bouts of singing. Particular thanks go to Davy Adriaens, Zainab Awad, Estelle Bayet, Tom Bell, Silvia Casu, Helen

Christie, Susan Creighan, Eduardo Cypriano, Harpreet Dhanoa, John Edridge, Jo Fabbri, Sam Farrens, Fedor Goumans, Emily Hall, Simon-John King, Iraklis Konstantopoulos, Elspeth Latimer, Anais Rassat, Claire Ricketts, Julia Roberts, Fab Sidoli, Daniel Stone, Magda Vasta, Michael Ward, Roger Wesson, Mark Westmoquette, Will Whyatt, Angela Wolff and Nick Wright. I must also thank Cesare Cecchi-Pestellini and David Williams for their advice. It has been my privilege to belong to such a vibrant place as UCL and I will always look back at this time with great affection.

This thesis would have been written more slowly without the intermittent prodding of Hannah Jameel, and I am grateful for her practical sense and tenacious understanding of my idiosyncrasies. Similarly, I owe the preservation of my sanity to Sofia Ismail and Harshini Katugampola; I know that with you three I can always be myself and that you will always listen. Thanks also to Candice Teo, Mark Murrant, Elisabeth Kerner and Deborah Mairs, on whom I know I can rely, even if I don't see them very often. I would like to thank all my dear friends, both old and new, for their support during the course of my studies.

Finally, I am unable to express my gratitude and love to my family, to whom I owe everything. Credit goes to my nephews, Iftee and Irfan, for hours of entertainment. Thanks Mum, for always looking after me and being an amazing mother. Thanks Dad, for always being so wise, so kind and so heroic. I cherish you both more than you will ever know. To Ben Colkett, that wondrous being without whom life would be impossible, I send my eternal love. Thanks for persevering with me when I am ridiculous and for helping me with every aspect of my life. I could not have done this without you.

Farahjabeen Islam,
London,
16th March 2010.